Universidade do Minho
Escola de Engenharia

Fernando Gabriel Machado de Oliveira

Biofunctionalization of titanium surfaces for dental implants: osteogenic, anti-microbial and tribocorrosion resistant surfaces

March, 2015

Universidade do Minho
Escola de Engenharia

Fernando Gabriel Machado de Oliveira

Biofunctionalization of titanium surfaces for dental implants: osteogenic, anti-microbial and tribocorrosion resistant surfaces

PhD thesis in
Biomedical Engineering

Trabalho efectuado sob a orientação do
Supervisor:
Professor Doutor Luis Augusto Sousa Marques da Rocha
Co-supervisor:
Professora Doutora Mariana Contente Rangel Henriques

March, 2015

STATEMENT OF INTEGRITY

I hereby declare having conducted my thesis with integrity. I confirm that I have not used plagiarism or any form of falsification of results in the process of the thesis elaboration.

I further declare that I have fully acknowledged the Code of Ethical Conduct of the University of Minho.

Universidade do Minho, ___/___/_____

Full name: Fernando Gabriel Machado de Oliveira

Signature: _____

Acknowledgements

To my supervisor, Prof. Luis Augusto Rocha, for the support, guidance and scientific teachings throughout the project. For the given opportunities to develop this work in a multicultural and multidisciplinary environment across the world. For the motivation and friendship in key moments of this journey.

To Profª. Mariana Henriques for the valuable work discussions and for always facilitating the access to experimental conditions at DEB-UM.

To Prof. Takao Hanawa and all his team at the IBB-Tokyo, for the remarkable kindness and sympathy in welcoming me in their extraordinary city. For the full availability of experimental conditions and precious mentoring during my stay at the laboratories of IBB-Tokyo.

To Prof. Jean-Pierre Celis and Prof. Pierre Ponthiaux for sharing their broad knowledge during work discussions, providing important ideas for the course of the project and the analysis of experimental results.

To Prof. Carlos Alberto Achete and all his team at INMETRO, Rio de Janeiro, for the availability of experimental conditions and the scientific discussions for the development of an important part of this work.

To Prof. Carlos Roberto Grandini and Prof. Paulo Noronha Lisboa Filho from UNESP-Bauru for the kind reception in Bauru and the access to their laboratories at UNESP.

To Prof. Rodrigo Oliveira from USP-Bauru, for providing full access to experimental conditions for biological experiments at CIP-FOB, and the important insights about biological-related topics of this work.

To my beautiful and bright colleagues of journey, Helena Cruz, Maria João Runa and Sofia Alves for the friendship and exchange of opinions.

To several friends and colleagues from all the institutions that I have been privileged to work and which provided significant assistance for the outcomes of this work. To know:

Profª Ana Maria Pinto, Alexandra Alves, Fatih Toptan, Sónia Costa, Sónia Ferreira and Edith Ariza from Universidade do Minho, Guimarães, Portugal.

Ana Ribeiro, Bráulio Archanjo, Cristol Gouveia, Gerónimo Perez, Joyce Araújo, Andrea Campos, Alexei Kuznetsov and Márcia Maru from INMETRO, Rio de Janeiro, Brazil.

Tsutsumi-sensei, Nakano-san and Tanaka-san from IBB, Tokyo, Japan.

Cintia Tokuhara from Faculdade de Odontologia de Bauru, USP. Bruna Costa, Luciana Trino and all the members of the Laboratory of Anelasticity and Biomaterials from UNESP, Bauru, Brazil.

Special thanks to Denise Lefol, Ana Lúcia Roselino (Naná) and Jeferson Moreto for their love and friendship.

A great thank you, for my close family: my parents, Jorge, Manuela and my beloved niece, Rita.

Finally, I would like to acknowledge the financial support provided by the Portuguese Foundation for Science and Technology – FCT Portugal, through grant SFRH/BD/70857/2010.

FCT Fundação para a Ciência e a Tecnologia
MINISTÉRIO DA EDUCAÇÃO E CIÊNCIA

POPH QUALIFICAR É CRESCER.
QREN QUADRO DE REFERÊNCIA ESTRATÉGICO NACIONAL PORTUGAL 2007.2013
GOVERNO DA REPÚBLICA PORTUGUESA
UNIÃO EUROPEIA Fundo Social Europeu

Biofunctionalization of titanium surfaces for dental implants: osteogenic, anti-microbial and tribocorrosion resistant surfaces

Abstract

The rise of the worldwide dental implant market constantly increases the concerns regarding the quality, efficiency and lifetime of dental implants. Titanium based materials have shown proven ability for application in this field, essentially due to their adequate mechanical properties, corrosion behavior and biocompatibility. However, and despite the high success rates associated with dental implants, failures still continue to occur.

Among the problems affecting the performance of dental implants, one can find: lack of osteointegration, propensity for bacterial colonization and corrosion/tribocorrosion processes. All these aspects are highly dependent on the surface properties of the implant. Ideally, implant surfaces should simultaneously promote adhesion of osteoblasts and inhibit the colonization by unwanted microorganisms. Furthermore, it is also necessary to minimize combined actions between corrosion and wear (tribocorrosion) that can cause degradation of the implant surface and ultimately lead to its failure.

This thesis presents an approach to develop multifunctional titanium oxide surfaces with excellent tribocorrosion performance, while promoting a bio-selective behavior between the adhesion of osteoblastic cells and the minimization of bacterial colonization. For that purpose, surface modification of titanium by Micro-Arc Oxidation was performed, allowing the formation of a thick, adherent and porous titanium oxide structure with incorporated bioactive elements such as calcium, phosphorous, magnesium and zinc.

A detailed characterization of the surfaces provided important insights for the understanding of the mechanisms of film formation. Moreover, the results allowed the correlation between chemical/structural properties of the oxide, and their effect on biological and tribocorrosion mechanisms. The surfaces developed in this work presented excellent tribocorrosion resistance, good interactions with osteoblastic cells, and promising antimicrobial properties.

Bio-funcionalização de superfícies de titânio para implantes dentários: superfícies com propriedades osteogénicas, anti-microbianas e resistentes à tribocorrosão

Resumo

O crescimento do mercado mundial de implantes dentários cria condições para um maior desenvolvimento deste tipo de restaurações e uma crescente exigência em relação à qualidade, eficiência e tempo de vida dos implantes. Materiais à base de titânio mostraram ao longo do tempo que possuem uma eficácia comprovada para uso em implantes devido às suas boas propriedades mecânicas, comportamento à corrosão e biocompatibilidade. No entanto, apesar da elevada taxa de sucesso, são ainda reportadas algumas falhas em sistemas de implantes.

Entre os problemas que afetam a performance dos implantes podem encontrar-se: a falta de osseointegração, a possibilidade de colonização bacteriana e também processos de corrosão e tribocorrosão. A superfície do implante é um fator transversal, que influencia todos estes aspetos. Idealmente, esta deverá promover a adesão de células ósseas ao mesmo tempo que minimiza a colonização e proliferação de microrganismos prejudiciais. Além disso, deverá também minimizar processos de tribocorrosão (ação simultânea de mecanismos de corrosão e desgaste mecânico) que podem causar a degradação do implante e potencialmente levar à sua falha.

Esta tese apresenta uma solução para o desenvolvimento de superfícies multifuncionais de óxido de titânio com excelente resistência à tribocorrosão e um comportamento bio-seletivo através da promoção da adesão de células ósseas e diminuição da atividade bacteriana. Para este fim, a modificação superficial do titânio foi conseguida através da técnica eletroquímica de anodização, permitindo a formação de um filme de óxido de titânio com uma estrutura porosa e dopado com elementos bioativos, como cálcio, fósforo, magnésio e zinco.

Uma caracterização detalhada das superfícies produzidas, permitiu obter informação essencial para a compreensão dos mecanismos de formação do filme. Adicionalmente, os resultados permitiram ainda correlacionar as propriedades químicas e estruturais dos filmes com o comportamento biológico e os mecanismos de tribocorrosão identificados. As superfícies desenvolvidas neste trabalho apresentam uma excelente resistência à tribocorrosão, boa interação com células ósseas e ainda propriedades antibacterianas promissoras.

Table of Contents

List of Figures

- Chapter 2

- Chapter 3

- Chapter 4

- Chapter 5

- Chapter 6

List of Tables

Biofunctionalization of titanium surfaces for dental implants

Chapter 0

Structure of the Thesis

Chapter 0. Structure of the Thesis

For a better understanding and reading experience of this document, hereby is an extended outline, explaining the organization of the chapter structure and the main focus for each section. Being so:

Chapter 1 presents an introductory rationalization about the reason for the development of this work. The present state of affairs of the dental implant industry is referred, and the possible improvements to the actual situation represent the main motivation for this work. According to this, the initial objectives of this project are described.

Chapter 2 contains a comprehensive state-of-the-art review about the most important topics discussed along the thesis. It contains information about biological, corrosion and tribocorrosion issues that are known to be important for biomedical materials. Generic guidelines of each phenomenon are presented as well as some different surface modification solutions found in literature to overcome each concern. Special emphasis is given to titanium materials and the particular surface modification procedure (Micro-Arc Oxidation) used in this work.

The outcomes of this work are compiled in the form of four scientific papers (already published or for publication in international journals) from chapter 3 to chapter 6.

The first publication in **chapter 3** concerns the use of micro-arc-oxidation to produce titanium oxide layers with incorporated bioactive elements (calcium and phosphorous). The tribocorrosion behavior of each condition was correlated with the process parameters and chemical/structural characteristics of the oxides. The tribocorrosion performance of each group of samples was the discriminating criterion used to select the conditions for the upcoming work.

In **chapter 4**, the previously produced samples referred in chapter 3 were tested for their biological behavior in contact with human osteoblast cultures and also a brief investigation on the early gene and cytokine production was performed. A meticulous characterization of the surface, based on the chemical and structural properties of the oxide, was used to understand the successful biological performance and identify the main causes for preferential osteoblast adhesion and spreading in modified titanium surfaces.

The paper presented in **chapter 5** represents an upgraded surface modification method with the addition of magnesium to the previous surfaces containing calcium and phosphorous. The effects of this addition were, to a great extent, responsible for an improved tribocorrosion performance, when compared to the previous treatment conditions. Additionally, this paper

proposes mechanisms for oxide growth and tribocorrosion behavior, based on a detailed characterization of the surfaces before and after tribocorrosion studies.

Following the results obtained in the preceding chapter, the work presented in **chapter 6** relates to the addition of zinc oxide nanoparticles to the previously produced surfaces. The chemical and structural changes induced by the incorporation of zinc oxide nanoparticles are explored. Finally, an integrated approach involving osteogenic, antibacterial and tribocorrosion studies is performed and evaluated.

Following the series of four papers, **chapter 7** includes a general discussion and connecting points between the works. Some final considerations are presented to summarize the outcomes of this project.

To conclude, **chapter 8** presents a few suggestions and future perspectives that could be of interest for the further development of studies in this area.

Biofunctionalization of titanium surfaces for dental implants

Chapter 1

Introduction, Motivation and Objectives

Chapter 1. Introduction, Motivation and Objectives

Losing a tooth...

It's not unlikely to occur. In fact, data from the American Association of Oral and Maxillofacial Surgeons state that 69% of persons aged between 35 and 44 had lost at least one tooth. For people over 74 years old, 26% have lost all permanent teeth. [1]

When a person looses a tooth or teeth, weather due to trauma or periodontal diseases, dental implants are a popular option to replace the missing tooth/teeth and provide a definitive, if successful, solution for the problem. Dental implants are defined as artificial tooth roots, placed in the bone, allowing the installation of a dental prosthesis, restoring masticatory functions and resembling the aesthetics of pre-existing natural teeth [1].

Dental implants are continuously increasing in popularity over the last few years due to the constant increase in life expectancy and higher concerns about oral hygiene and aesthetics. Also, the recent advances in dental technology are producing more attractive and efficient solutions to convince patients to opt for a dental implant. Over the last decades, the worldwide dental implant market has been on the rise, and this trend is yet expected to prolong over the next years with a global yearly growth rate of 10 % from US$ 3.4 billion in 2011, to reach values around US$ 6.6 billion in 2018 [2].

A study from 2009 documented close to 150 dental implant companies worldwide, producing hundreds of different implant systems [3]. The diversity of designs and geometric properties of implants (different diameters, lengths, type of threads) provides the dentists with a wide range of options to choose the best solution that fits each clinical situation. On the other hand, the discussion about the optimal surface characteristics does not generate a consensus. Dental companies and researchers all over the world reveal great concern and growing efforts to develop new implant surfaces, resulting in the continuous release of new patented implant systems, year after year. These advances in surface modification of metallic materials acknowledge the important role of the surface properties as a crucial parameter influencing the behavior of dental implants.

The development of better materials for implantology, demands the cooperation between dentists, scientists and engineers. Everyone involved in the creation of a new medical device is motivated by the hope to increase the quality of life of the patients asking for a treatment. This means, in the case of dental implantology, less invasive surgeries, less pain, state-of-the-art

[1] http://myoms.org/procedures/dental-implant-surgery

materials, with a long life-span, minimizing the need for revision surgeries and ultimately pursuit the complete elimination of failures. Altogether, not only the scientists and engineers should understand the details of implantation processes and possible failure causes, but also dentists should be aware of the new advances in medical technology and the constant development of new surfaces for dental implants.

When talking about modern dental implantology, one name cannot be left untold. Per-Ingvar Branemark (1929–2014) was the father of the modern dental implant, when he discovered that titanium could not only be tolerated by the human body, but also integrate and become strongly embedded in the bone, in a concept that he referred to as "osseointegration" [4, 5]. His revolutionary ideas led to the successful application of titanium in dental implants since the 1960's [6]. In 1965, the first dental implant was inserted in a human patient. Gösta Larsson, who was born with a deformed jaw, received four implants that would work without problems until his death, 41 years later, in 2006. Branemark's second patient, Sven Johansson, received implants in 1967, and is up to this date the person who has had functional oral implants for the longest time in history.

From the first implants placed by Per-Ingvar Branemark, dental implant surfaces went through a great evolution. Current dental implant solutions offer a wide range of surfaces involving several different processing technologies [7-9]. The surface of an implant represents the interface with the biological environment, affecting the biological response of the host. For this reason, most surface modification techniques applied to dental implants aim the improvement of osseointegration and reducing the healing time of the implant after surgery, allowing the loading of the prosthesis with oral forces with safety, and as soon as possible.

The actual market for dental implants presents great variety of surface properties, which can arguably be divided in three main groups: [8]

1) Machined or turned surfaces represent the first and simplest type of implant one can get, and are rarely used nowadays. The only surface features are caused by the instruments during the mechanical processing of the implant;
2) Grit-blasted (sandblasted) and/or Acid-etched surfaces are perhaps the most common type of surfaces available in the market. These can be produced by blasting the surface of the implant with micro sized particles of silica, alumina, titanium oxide or calcium phosphates. This allows the control over the size of the cavities created in the surface, but can leave some blasting particles contaminating the surface. Normally, a cleaning procedure involving

sonication and acid etching is performed after the blasting to remove the particles. Acid etching can also be performed alone, as a treatment to control the surface roughness at micro and nanometer scales. Like the grit-blasting technique, it provides homogeneous levels of roughness and an increase in active area for the adhesion of bone cells. Whether using blasting or acid etching techniques alone or combined, the resulting surface morphology is very similar.

3) A third group of surfaces can include several advanced treatments to improve key properties of the implant through the creation of surface layers with altered chemical composition, topography, surface energy, wettability or crystalline structures presenting an extensive range of superficial properties. Among the different processing techniques employed, one can find: plasma spraying, laser ablation, fluoride treatments or anodization.

Despite the advances in dental materials technology, and the improvement in the success rate of implants, there are still unsolved questions about the way these new surfaces are improving the behavior of the implants. Furthermore, the cases of failed implants keep happening, which shows that there is still room for improvement in the field [10].

Among the problems affecting dental implants, poor osseointegration is the one receiving more attention from literature and dental companies. However there are more reasons leading to failures of implants. There are innumerous sources of bacteria that can colonize and proliferate through the surface of an implant and interfere in the osseointegration process, causing infections in the peri-implant area [11].

Ideally, the implant surface should be capable of simultaneously promote the adhesion of osteoblastic cells and inhibit the colonization by microorganisms. But although most of the dental implant companies pay a great amount of attention to the osteoblastic functions, they do not show much concern with the microbial colonization.

Besides these two aspects, a third issue is gathering the attention of the scientific and dental communities: the degradation of the surface by means of corrosion and wear (tribocorrosion) processes during and after the implantation surgery appears as a threat to the quality of implant systems. Corrosion of metallic implants cause the release of metal ions to the surrounding environment and the micromovements between the implant and bone can cause the degradation of the surface and the release of wear debris to the peri-implant area [12].

Hence, the main **objectives** of this work were the development and characterization of new bio-multifunctional titanium oxide-based surfaces for dental implants. Surface modification of commercially pure titanium grade 2 was performed, in an attempt to achieve highly bioactive surfaces with antimicrobial properties and tribocorrosion resistant behavior.

Electrochemical based techniques, with focus on Micro-Arc Oxidation (MAO), were used to create thick, adherent and porous titanium oxide films doped with bioactive elements. A detailed characterization of the surfaces in terms of topography, crystalline structure, chemical composition, biological behavior and tribocorrosion performance was executed.

The first task of the project was the creation of titanium oxide layers doped with bioactive elements by electrochemical technique. Several parameters were tested, in order to achieve the best surface properties to follow the study, and the further incorporation of additional bioactive species like Mg and ZnO nanoparticles was performed only in selected conditions based on a detailed characterization. The surface characterization was also the basis to suggest a formation mechanism for the oxide films containing Ca, P and Mg.

After the surface modification steps on titanium, the work was oriented towards the characterization of the tribocorrosion behavior under simulated oral environment conditions.

Finally the biological behavior of the newly developed surfaces was tested in terms of cytotoxicity and adhesion/proliferation of osteoblastic cells.

Furthermore, the possible antibacterial efficiency of the incorporated elements was evaluated by antibacterial tests against oral bacteria.

References

[1] C.A. Babbush, J.A. Hahn, J.T. Krauser, and J.L. Rosenlicht. Dental Implants: The Art and Science. Elsevier Health Sciences, **2010**.

[2] Global boom in dental implants. *British Dental Journal*, 214(5): 219-219, **2013**. doi:10.1038/sj.bdj.2013.232

[3] A. Jokstad, M. Esposito, M.G. Grusovin, P. Coulthard, H. Worthington, and B.E. Pætursson. Implant dentistry: a technology assessment. in *Osseointegration and Dental Implants*. Wiley-Blackwell, **2009**.

[4] P.I. Branemark, R. Adell, U. Breine, B.O. Hansson, J. Lindstrom, and A. Ohlsson. Intra-osseous anchorage of dental prostheses: I. Experimental studies. *Scandinavian Journal of Plastic and Reconstructive Surgery*, 3(2): 81-100, **1969**.

[5] P.I. Branemark. Osseointegration and its experimental background. *The Journal of Prosthetic Dentistry*, 50(3): 399-410, **1983**.

[6] R. Adell, U. Lekholm, B. Rockler, and P.I. Brånemark. A 15-year study of osseointegrated implants in the treatment of the edentulous jaw. *International Journal of Oral Surgery*, 10(6): 387-416, **1981**.

[7] P.G. Coelho, J.M. Granjeiro, G.E. Romanos, M. Suzuki, N.R.F. Silva, G. Cardaropoli, V.P. Thompson, and J.E. Lemons. Basic research methods and current trends of dental implant surfaces. *Journal of Biomedical Materials Research Part B: Applied Biomaterials*, 88B(2): 579-596, **2009**.

[8] C.N. Elias. Factors affecting the success of dental implants. in *Implant Dentistry - A Rapidly Evolving Practice*. InTech, **2011**.

[9] T. Hanawa. Research and development of metals for medical devices based on clinical needs. *Science and Technology of Advanced Materials*, 13(6): 64102-64116, **2012**.

[10] P. Hujoel, W. Becker, and B. Becker. Monitoring failure rates of commercial implant brands; Substantial equivalence in question? *Clinical Oral Implants Research*, 24(7): 725-729, **2013**.

[11] K.G. Neoh, X. Hu, D. Zheng, and E.T. Kang. Balancing osteoblast functions and bacterial adhesion on functionalized titanium surfaces. *Biomaterials*, 33(10): 2813-2822, **2012**.

[12] M.T. Mathew, P. Srinivasa Pai, R. Pourzal, A. Fischer, and M.A. Wimmer. Significance of tribocorrosion in biomedical applications: Overview and current status. *Advances in Tribology*, 2009: 250986, **2009**.

Biofunctionalization of titanium surfaces for dental implants

Chapter 2

State of the Art

Chapter 2. State of the Art

Over 80% of all implant devices are metals [1]. For implant applications, metallic materials can outperform ceramics and polymers due to their strength, toughness and durability. But the weakness of any artificial material is that they don't possess any intrinsic biological functions. Scientific research and development of new metallic materials for implantology is constantly aiming at the perfection of mechanical performance and surface properties which will influence the mechanical and biological compatibility.

Titanium is one of the most used materials in implantology, and especially in the dental field. Its use is not limited to the commercially pure grades, but also a large amount of titanium alloys have been developed to enhance the mechanical properties of metallic implants, such as decreasing the Young's modulus, improving tensile and fatigue strength, fracture toughness or wear resistance. Ti6Al4V is the most common titanium alloy used in medicine, however other alloying elements like Mo, Nb, Zr and Ta are being intensely studied for this purposes [1, 2].

1. Titanium and Surface modifications

For around half a century, titanium has been successfully used in dentistry as an implant material. Along the way, the surface of dental implants has evolved from simple machined pieces to highly advanced surfaces, overcoming biological, mechanical and electrochemical concerns.

1.1. Improvement of biological behavior

1.1.1. Roughness and topography

There is still controversy around the ideal surface features of a dental implant, and some of the most discussed parameters are roughness and topography. It is widely accepted for several years that a moderate degree of micro-roughness can have a positive effect in the osseointegration and biomechanical fixation of implants [3-5]. Rough surfaces possess more contact area and can be more efficient in the promotion of bone anchorage and biomechanical interlocking of the implant. However, the recent developments have been focusing on a different type of roughness. The number of works studying the correlation between nanoscale roughness and biological behavior is increasing. Nanostructured surfaces can increase the surface energy and promote the adsorption of proteins and improve cell-surface interactions. The results show a beneficial effect from the nanoscale roughness, and further reveal positive outcomes from the combination of both micro and nano roughness in the same surface [4, 6-12].

Common ways to increase and control the roughness of implant surfaces are blasting or etching techniques [5]. For instance, Rosales-Leal et al. [13] tested the effect of four surface treatments on titanium (polishing, acid etching, alumina blasting and alumina blasting + acid etching). Results showed that cell adhesion and proliferation were higher on rougher surfaces, rather than on smooth titanium. Nearly similar surfaces were employed in the study of Aparicio et al. [14] which added a thermo-chemical treatment to blasted + etched samples. They analyzed the short and mid-term bone regeneration and mechanical retention using histometry and pull-out tests. The report states that osseointegration was favored in rougher surfaces, and also that the formation of a bioactive layer combined with the rough structure created the best conditions for bone regeneration around the samples. Elias et al. [15] also studied the effect of surface properties in the removal torque after implantation. Surfaces with high roughness and low contact angle were found to promote better bone ingrowth and fixation revealed by the higher removal torques. Daw et al. [16] used hydrogen peroxide solution to induce nano and micro scale roughness on titanium, resulting in enhanced osteogenic differentiation, however it also increased bacterial adhesion on micro scale roughness. Also Wu et al. [17] studied the osteoblast and bacteria response to multiple ranges of surface roughness of titanium (polished, satin-finished, blasted and plasma-sprayed). They studied the vertical and lateral length scales of each surface and found correlation with the adhesion of both bacteria and osteoblasts, concluding that a cell will tend to adhere easily on a surface with lateral roughness comparable to its size. Oliveira et al. [18] supported the theory that rougher surfaces present increased cell viability, proliferation and differentiation, when compared to smother surfaces. Although the mixed influence between roughness and chemical composition of their surfaces, they hypothesized that roughness may play a more significant role than chemical composition in determining the cell response to a surface.

The high roughness of implant surfaces started to raise the attention for additional issues other than the adhesion of osteoblasts or bacteria. Wennerberg et al. [19] thought that the increase of active surface area related to higher roughness levels would be linked to a greater metal ion release. However, their investigation proved the theory wrong, and didn't found a correlation between roughness and ion release, sufficiently relevant for the case of dental implants. On the other hand, Aparicio et al. [20] demonstrated that the increased surface area, together with the residual stresses induced by shot blasting could in fact induce changes in the electrochemical behavior. Other concerns were related to the damages in the osseous surface

during implantation of rough implants. In fact, rough implants were found to be related with increased microdamages in the bone structure [21]. In another work, it was found that during the placement of implants with high surface roughness, the amount of translocated bone fragments around the implant-bone interface can be increased. Nevertheless, these particles are thought to enhance peri-implant osteogenesis as they may act like small bone grafts [22].

As for the contribution of nanoscale roughness, Wilkinson et al. [23] decided to combine microtopographic surfaces with nanoscale features, similar to osteoresorption pits, to promote bone formation. Puckett et al. [24] produced patterned titanium surfaces with aligned nanofeatures inspired by collagen and hydroxyapatite in bones. Both studies revealed the capacity to control osteoblast response, through bioinspired nanoscaled surfaces.

Surface roughness is also directly associated with other key properties, such as surface energy. The increase in roughness is linked with higher surface energy, which will improve the wettability of the implant, and therefore favoring the interactions between the surface and the biologic environment, namely the adhesion of proteins and other biomolecules [25-27]. A good example of this concept is the SLActive® implant from Straumann Company. The processing of these implants is made by sandblasting and acid etched processes, followed by rinsing the implant in nitrogen environment, and storing in a sealed glass tube containing isotonic NaCl solution. According to the manufacturers, this prevents the exposure to air, leading to a highly hydroxylated/hydrated surface, with high surface energy, and minimizing the adsorption of contaminants [27, 28]. Some studies confirm the enhanced biological activity and tissue integration of these super hydrophilic surfaces in comparison to the previous version of the implant, which was more hydrophobic [29, 30].

Not related with topographical feature, the crystalline phases may also interfere in bone-implant interactions. Anatase phases are reported to produce good biological effects for cell adhesion, spreading, proliferation and differentiation [31]. Some works also suggest a crystallographic match between the lattices of rutile and hydroxyapatite, leading to superior apatite-forming ability [32-34]. Furthermore the presence of crystallographic phases of titanium oxide can also have a beneficial effect on the mechanical properties of the oxide [35].

Besides roughness and topography, other approaches to improve the bone-implant interface are related to the changes in the chemistry of the surface (figure 2.1), whether by incorporation of inorganic phases such as calcium phosphates or organic molecules such as proteins, enzymes or peptides involved in the cell and tissue responses [26, 36, 37].

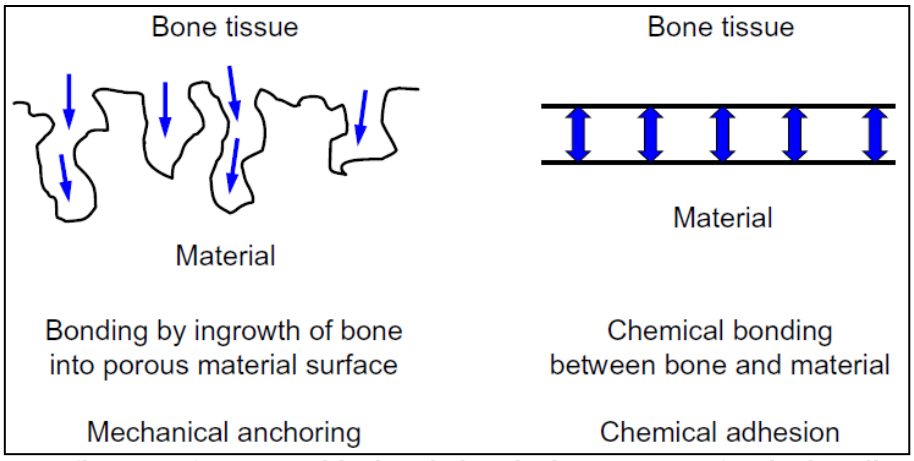

Figure 2.1 – Influence of topographical and chemical parameters for the bonding between bone and implanted material [1]

1.1.2. Chemical composition

Tailoring the chemical composition of implant surfaces is also understood as a vital process to improve the osteogenic processes and/or cause injuries to microbial cells minimizing bacterial colonization. [38, 39]

Hydroxyapatite (HAp) or calcium phosphate coatings generate a lot of reports for the improvement of biofunctions of titanium implants. It is demonstrated that calcium ions (Ca^{2+}) can induce osteogenesis of human Mesenchymal Stem Cells (hMSC) [40] and are deeply involved in the basic processes of cell signaling [41, 42]. In the first moments of contact, all biomaterials inserted in the human body, will have their behavior regulated by a layer of proteins adsorbed in the surface. Calcium is involved in the binding mechanism of some proteins, namely cell adhesion molecules (CAM's) such as cadherin or selectin. It can adsorb to the TiO_2 surface and then contribute to the adsorption of important macromolecules from the surrounding environment [43, 44].

Calcium, as well as phosphate ions has an important structural role in bone. During osseointegration, osteoblasts deposit an extracellular matrix, containing nucleation sites for mineral deposition. Ca^{2+} and PO_4^{3-} are the main constituents of that mineral, Hydroxyapatite ($Ca_{10}(PO_4)_6(OH)_2$), which is the dominant mineral phase present in bone, thus being of extreme importance in the step of mineralization, during bone formation [26, 40, 45, 46].

Based on these notions, the approaches to incorporate calcium and phosphorous in implant surfaces are widely found in literature and also in commercial implants [38, 47, 48]. Several techniques, such as Thermal Spraying [49-54], Ion Implantation [55-58], Sol-gel [59-61], Magnetron Sputtering [62-65], Electrodeposition [66-70] or Micro-Arc Oxidation [18, 71-79] are used to incorporate bioactive calcium and phosphates into titanium surfaces.

Briefly, all the mentioned references state an improvement of osteogenic behavior due to alterations in chemical composition of the surface. Better implant-tissue integration was observed due to high apatite-inducing ability and enhanced cellular adhesion, proliferation, differentiation and mineralization phenomena.

Besides calcium and phosphorous, a relevant amount of scientific works also tested the incorporation of other elements in surfaces for implantology. Some of these works are based on the principle of ionic substitution in the stable and highly flexible structure of HAp, thus allowing the incorporation of other cationic elements such as magnesium, strontium or zinc (divalent cations) in exchange for calcium atoms in the HAp lattice. Also, there is the possibility of fluorine ions to substitute hydroxyl groups, or carbonate groups to replace phosphate or hydroxyl groups [80, 81]. Incorporation of trace metal ions in the HAp lattice, may affect the stability and dissolution kinetics of bioactive elements involved in the osseointegration process into the human body, thus improving or hampering the biological properties of implantable surfaces, according to the dissolution rates and the release of metal complexes to the environment [82].

Magnesium, being the fourth most abundant cation in the human body and an important trace element in teeth and bone, is known to play a significant role in bone metabolism [83]. It is used in some surface modifications, involving the integration in HAp structures or the direct incorporation in titanium surfaces by means of electrochemical or physical methods. The replacement of calcium by magnesium in the HAp is limited by the substantial difference in the size of Mg^{2+} and Ca^{2+} cations (72 pm for Mg^{2+}; 100 pm for Ca^{2+} [84]), leading to strong distortions in the Hap lattice around the Mg—O bonds, which are much shorter than the Ca—O bonds [85]. This leads to a decrease in the degree of crystallinity, with effects on the stability, solubility and biodegradability of the substituted material in physiological conditions. The extent of Mg substitution can vary from 2 wt.% to almost 30 wt.% in several works using electrolytic depositions, sol-gel techniques or mechanochemical–hydrothermal synthesis [60, 86, 87]. These Mg-substituted Hap materials seem to promote the precipitation of new apatite phases and bone formation [60], other studies reveal no adverse effects on morphology and proliferation of osteoblasts [88]. Magnesium was also briefly referred to cause antibacterial effects through an increase in pH of the environment due to its high corrosion rates in physiological solutions [89]. However, the lower amount of magnesium in Mg-substituted HAp-based materials may not present enough ion release to cause such antibacterial phenomenon.

Strontium is also found in trace quantities in calcified tissues and in the mineral phase of bone due to its electronic configuration similar to calcium. Strontium ranelate is already commercially used as a treatment for osteoporosis and it is proved to improve the osteoblast activity and proliferation, while inhibiting differentiation and activity of osteoclasts [90]. Li et al. [91] approached the incorporation of strontium ranelate in titanium implants, with successful results on the osseointegration under osteoporotic conditions. Despite having similar chemical properties when compared with magnesium, strontium presents higher atomic radius than calcium (118 pm against 100 pm [84]), thus causing local deformations in the same sites of the structure of a Sr-substituted HAp material and an increase in lattice parameters [81, 92]. The same effects on the crystallinity and solubility are verified for strontium substitution, namely the decrease in crystallinity, and higher solubility of the material, which could contribute to a sustained release of the element with benefits in the osseointegration properties of the implants [93, 94].

Zinc is the major trace metal element found in bone composition and is essential for bone metabolism, stimulating osteoblast and inhibiting osteoclast activities. It is also a cofactor for several enzymes, particularly in alkaline phosphatase involved in bone mineralization [81, 95]. Furthermore, zinc is known to have antibacterial properties. McDevitt et al. [96] proposed a mechanism in which zinc could bind to manganese transport proteins and inhibit the uptake of manganese (an essential element for bacterial growth) by the cells. Also, some recent works highlight the role of different metals, including zinc, in causing damages to microbial cells by processes of oxidative stress, protein dysfunction or membrane damage. [39]

With ZnO nanoparticles, some authors [97-99] suggested that the antibacterial mechanism was likely to occur due to the possible accumulation or deposition of ZnO nanoparticles in the membrane or the cytoplasm of bacteria, leading to bacteriostatic and bactericidal effects. Another proposed mechanism was the production of reactive oxygen species, namely hydroxyl radicals and the increase of oxidative stresses. Additionally, the size of the nanoparticles was also found to influence the cellular internalization of the nanoparticles and bacterial damages to the cells. Ionic radius of Zn^{2+} is smaller than Ca^{2+} (74 pm against 100 pm [84]), causing changes in the geometric parameters of Zn-substituted HAp and consequently its crystalline properties and stability. The incorporation of zinc in HAp by electrochemical methods is reported to have beneficial effects on the proliferation and differentiation of osteoblasts [100] and a decrease in the number of osteoclasts and resorptive activity [101]. Other study correlated the effect of Zn

substitution and the adsorption of RGD peptides, to found that the simple substitution of Zn in the HAp structure was more effective than the combined Zn-HAp-RGD treatments in promoting osteoblastic cell adhesion and spreading in the surface [102]. The antibacterial properties of Zn-HAp are also demonstrated by the significant decrease in the number of bacteria when compared to simple HAp [103]. Hu et al. [104] have incorporated zinc into titanium oxide porous coatings by plasma electrolytic oxidation. They suggested that the increase of Zn content could effectively inhibit the growth of bacteria due to the slow and constant release from the coatings. Also the adhesion, proliferation and differentiation of bMSC's were significantly enhanced in the presence of Zn-containing coatings, without cytotoxic effects.

Silver is one of the most effective antibacterial elements used in biomedical materials. Its efficiency against a broad spectrum of bacteria (both gram-positive and -negative) is well proven. Just like zinc, silver is thought to present an antibacterial mechanism by causing damages to cellular structures, generation of reactive oxygen species or DNA damages. However, among all the elements presented before, silver presents the most contradictory reports on the cytotoxicity behavior in contact with osteoblastic cells, by affecting basic cellular metabolic functions and a possibility to be deposited and accumulated in blood and in several organs [105]. Silver coatings on titanium implants can be easily applied by well-established physical methods such as PVD or ion implantation [106, 107]. The presence of silver in HAp-based coatings reveals low or absent cytotoxic effect on the behavior of osteoblastic cells for low concentration of released Ag^{+} ions to the environment [107-109]. Other studies demonstrate that higher amounts of silver ions have a strong impact on cell differentiation and viability, with toxic effects in both osteoblast and osteoclast cells [110]. In the case of silver nanoparticles, size is reported to be a major factor affecting the activity of human cells. Smaller silver nanoparticles are more capable of entering the cell body and cause more cytotoxic effects [111].

Independently of the metallic elements used in biomaterials surfaces, their bioactive or cytotoxic properties are mostly related to the dosage or release kinetics from the implant surface into the environment and the adjacent tissues. Given the need for multifunctional activity of implant materials, the incorporation of external elements must be performed under the idea of an active compromise between biological integration and infection prevention [112].

1.1.3. Functional biomolecules

Extracellular matrix (ECM) proteins are known to regulate cell adhesion, growth and all the subsequent phenomena. ECM is composed by a mixture of structural and functional proteins that can adsorb to the surface of the implant in the first moments of contact with the body fluids [113]. Some of these are directly involved in the mechanisms of cell adhesion through the interaction with cell adhesion molecules (CAM's) present in the cell surface. For instance, integrins are a CAM responsible for connecting the ECM to the intracellular environment, activating the cellular signaling pathways that eventually lead to adhesion of cells. Cell adhesion molecules, such as integrins are receptors that can recognize specific motifs, related to particular amino acid sequences in the proteins of the ECM, acting as binding sites for the attachment of cells. The most established peptide for mediation of cell attachment in biomaterials is the RGD sequence (arginine-glycine-aspartate). RGD is the main integrin-binding domain present in ECM proteins. Synthesis of RGD is quite simple and cheap, and it can be attached to the surface of biomaterials under controlled conditions of density and orientation, thus being extensively studied for the guidance of cell behavior in biomaterials for regenerative medicine and tissue engineering [114-119].

The biofunctionalization of dental materials with functional molecules has therefore two main approaches: the adsorption of native ECM proteins, such as fibronectin, vitronectin or collagens, and the incorporation of synthetic peptides directly involved in the integrin-binding mechanisms. These molecules can be incorporated into titanium surfaces by methods of adsorption, covalent binding, nanomechanical incorporation or self-organizing layers. Functionalization with organic biomolecules can represent, thus, a shortcut in the process of adsorption of proteins and even tailor the implant surface according to specific need of patients creating surfaces with more attractive potential for osteogenic cells [26, 115].

Fibronectin is one of the most used ECM proteins to functionalize titanium. Petrie et al. [120] studied fibronectin-inspired coatings on titanium by simple physical adsorption and found that recombinant fragments of the protein could enhance osteoblastic differentiation and mineralization in BMSC cultures as well as increased osseointegration in rat cortical bone model. Rapuano et al. [121] analyzed the effects of different physico-chemical properties of titanium oxides modified with a fibronectin coating adsorbed in the surface. Their findings stated a positive influence of negatively charged complexes in the oxide surface, in modulating fibronectin activity, possibly through changes in conformation of the molecule. Gorbahn et al. [122] confirmed the

good adhesion, proliferation and differentiation response of osteoblasts to fibronectin modified titanium oxide surfaces, by self-assembly immobilization. Ren et al. [123] conjugated fibronectin and rhBMP-2 in previously polymerized titanium surfaces and demonstrated that the treatment could induce higher levels of adhesion of MC3T3-E1 cells. Some other reports highlight the better osteogenic properties of titanium surfaces functionalized with different ECM molecules, such as Fibrinogen [124, 125], Laminin [126, 127] or Vitronectin [128, 129].

But despite, the success demonstrated in the literature, the possible bacterial adherence and biofilm formation in titanium coated with ECM proteins [130, 131] together with high extraction and purification costs represent disadvantages for their use [114]. In 2011, the functionalization of surfaces with ECM proteins or synthetic adhesion peptides was the motion for a series of papers discussing the better approach to control cell behavior [117, 118, 132-134]. One of the main arguments in favor of synthetic adhesion peptides is their chemical definition, in opposition to ECM proteins. Synthetic peptides such as RGD can also maintain their functionality through processing and sterilization steps that may cause protein denaturation. Unlike ECM proteins, the synthesis of peptidic sequences is relatively simple and cheap, making it easier to translate for industrial and clinical use. The small peptide sequences also allow more precise and controlled immobilization into biomedical surfaces than large ECM molecules. The opinions opposing the use of synthetic peptides were related to their reduced length and specificity which can hamper the tissue response in such a complex and dynamic environment, in contrast with the more widespread functions of the ECM proteins which can better modulate intricate cellular phenomena.

Independently of the discussion, the immobilization of synthetic peptides, with a great emphasis on RGD sequences, is widely studied in the literature. One specific strategy is the immobilization of RGD peptide sequences in non-fouling materials. Substrates that inhibit the adhesion of other proteins can immobilize RGD peptides through specific functional groups and allow for a controlled definition of the RGD activity. The drawback of this technique is that any required physiological reactions must be specifically engineered in the surface, which represents a great technical and scientific challenge [117]. The selective behavior of non-fouling surfaces may also present good perspectives for the inhibition of bacterial adhesion in the surface of implantable materials.

RGD peptides have successfully been introduced to titanium surfaces by several methods such as simple immersion [135, 136] or silanization techniques [137-142], via physiologically

stable phosphonate anchor groups [143-145] or combined with nanoparticles for assessment of nanospacing and nanopatterning of RGD molecules in the behavior of mesenchymal stem cells and the adhesion of osteoblasts [146-148]. PEG-based coatings seem to be a popular approach in the literature presenting good biological results [149-152], however some works also state that no significant improvements in cell behavior or bone-implant contact were observed [153-155].

Other works on RGD biofunctionalization via PEG-based coatings also address the issue of bacterial adhesion and bioselective surfaces [156-158]. PEG-RGD coatings may allow the attachment and proliferation of fibroblasts and osteoblasts, while reducing the bacterial adhesion, when compared to common biomaterial surfaces. Lin et al. [140] functionalized the surface of titanium with a mixture of RGD and antimicrobial peptides achieving cell selective surfaces with bioactive properties and antimicrobial activity.

Functionalization of surfaces with bone morphogenetic proteins (BMP's) is still another technique used to improve bone integration with implant materials. BMP's are multi-functional growth factors secreted by cells, with osteoinductive properties, stimulating osteoblast precursor cells to differentiate into osteoblasts and promote bone repair [159, 160].

Some polysaccharides have been used for grafting BMP's on titanium surfaces. Hyaluronic acid [161, 162], dextran [163, 164], chitosan [165] and more widely spread heparin [166-168] can potentiate the immobilization of BMP's to titanium surfaces, improving osteoblast functions and bone regeneration. Some results even evoke the inhibition of inflammation on BMP-Heparin-Ti surfaces [169], while other combine the immobilization of BMP's and gentamicin antibiotics to achieve dual functions on the implant surface [170]. Alternative methods also refer the possibility of direct immobilization of BMP's into titanium oxide, calcium phosphates or hydroxyapatite [171-173] with the same osteoinductive properties and improved biological behavior.

1.2. Improvement of corrosion resistance

"*It is important to understand that the corrosion of orthopaedic biomaterials is not just an exercise in physics and chemistry. There are real problems related to the corrosion of implants that are in current clinical use.*"

J. Jacobs, J. Gilbert, R. Urban; (1998) [174]

1.2.1. Understanding corrosion

Corrosion can be defined as reaction of a metal with its surrounding environment, resulting in a subsequent deterioration of its properties [175]. This degradation of metallic biomedical

materials represents a concern for two main reasons: it can decrease the structural integrity of the implant materials and it may release corrosion products that are harmful for the surrounding tissues and can cause adverse reactions in the host [174].

However, despite the detrimental connotation of the term corrosion, some electrochemical reactions can be regarded as positive for the outcome of a material, depending on the nature of the reaction products (protective or non-protective) and on the speed and extent of the reaction [175]. For instance, in contact with atmospheric air or aerated aqueous solutions, titanium instantaneously forms a thin nanometric oxide layer on its surface, which acts as a protection from the surrounding environment, and slows the active corrosion of the metal in several orders of magnitude. This is commonly referred to as passive film and presents a stable and compact structure (mostly comprised of TiO_2), being responsible for the high corrosion resistance of titanium and its relative inertness and good biocompatibility in dental implant applications. The protective character of the passive film is determined by the rate of ion release through the film, and also its stability against dissolution [176].

A metallic implant inserted into the human body will find itself in extreme corrosive conditions, in contact with the physiological fluids of varying pH's, temperatures and complex chemical compositions. Particularly, the chemical environment of blood plasma is very hostile for many metals and alloys, due to the high concentration of chloride ions and their ability to induce localized corrosion [176]. Also, in the presence of high concentrations of fluoride ions or acidic fluoride solutions, titanium may suffer from localized corrosion which may cause the nucleation of fatigue cracks, hampering the mechanical stability and eventually leading to failures of dental prosthesis [177-179]. Oral hygiene methods, such as the prevention of caries and bleaching treatments, use some fluoride-based products, and therefore may eventually induce the degradation of titanium implants by the dissolution of the passive oxide layer. (Fluoride-based acid solutions are also regularly used to modify the surface of titanium materials, by etching the surface, precisely due to their corrosion inducing properties).

One of the main factors affecting corrosion of titanium in physiological environments is pH. Generally it is known that lower pH values will account for higher corrosion of titanium, as may be concluded from the observation of figure 2.2, presenting thermodynamic information for titanium electrochemical reactions in the pure titanium-water system at 25 °C.

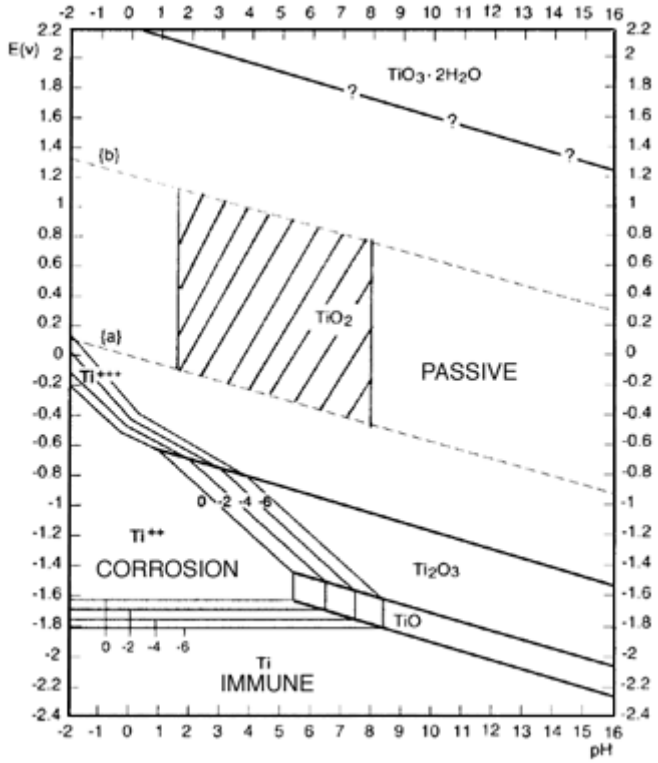

Figure 2.2 – The Pourbaix (potential-pH) diagram for titanium-water system at 25 °C. [180]

Although the information taken from the Pourbaix diagrams doesn't include any kinetic information and is limited to specific environments, it could be a legitimate indication of the electrochemical behavior of titanium in biological environments. Several studies confirm the fact that corrosion of titanium and alloys is enhanced in the presence of acidic environments. For instance, Barão et al. [181] published results confirming the increase of corrosion rates of pure titanium and Ti6Al4V, in acidic artificial saliva. Robin and Carvalho [182] found the same tendency in titanium and alloys of the Ti-Nb-Zr system in Ringer solution. Rodrigues et al. [183] suggested that acidic environments can trigger corrosive processes leading to breakdown of the passive film and the release of metal ions and metal oxide corrosion products. The mechanism of dissolution rate of titanium at low pH environments is associated with the high H^+ concentration, which promotes the formation of hydrated Ti oxides such as $Ti(OH)_3^+$ and a further release of Ti ions and TiO_2 to the surrounding environment [184].

1.2.2. Corrosion in biomedical applications

The harsh corrosive environment found in the human body can be enlarged, for instance, by the presence of bacterial biofilms producing lactic acid and H_2O_2 during inflammatory responses. These two chemical agents, together with fluoride ions from oral hygiene products were found to increase the chemical attack of titanium surfaces, resulting in higher corrosion

extent evidenced by some roughness increase over time [185, 186]. Also the effects of lower pH can be increased in patients with medically compromising systemic conditions such as diabetes, as confirmed by Messer at al. [187] and Taman and Turkyilmaz [188], highlighting the higher possibility of corrosion related problems for devices implanted in persons with hyperglycemia.

Souza et al. [184, 189] devoted some work studying the role of bacterial biofilms on the corrosion behavior of commercially pure titanium. Considering the tendency for a lower pH in presence of bacterial biofilms and measured in the growth medium after experiments, they hypothesized that the pH values localized within the biofilms and in the close vicinity of the surface could be much lower than those measured in the medium due to gradual diffusion of acidic substances.

As previously stated, corrosion of implant materials can result in loosening of the implant and compromise the surrounding tissues with dangerous metal traces. Olmedo et al. [190] evaluated histologically the biological effects of pitting corrosion in titanium implants. Corrosion processes were responsible for a scarce bone-implant contact that only occurred in non-corroded areas. Corrosion products containing titanium were also found in the peri-implant area around blood vessels and bone marrow. Another study by Olmedo et al.[191] showed the presence of macrophages in the peri-implant adjacent area, loaded with titanium particles originated from corrosion processes.

Corrosion phenomena represent primarily a special concern for the development of local bone-implant integration. However the overall effects may not be limited to the peri-implant area, because ions or particles can enter the blood stream and migrate for other organs.

Due to the size difference between oral and orthopedic devices, effects of metal release are less prone to occur in dental implants. Still, some reports underline that metal traces generated from dental implants have been found in several human organs such as blood, liver, lungs and lymph nodes [192-195]. Berglund and Calmark [196] even found titanium in nail clippings of patients with dental implants.

The fact that corrosion products in the form of metal ions or nanoparticles can generate from implantable devices is well known in dental and orthopedic fields. However there is still controversy on the acceptable amounts of these products that can be tolerable in the human body. Furthermore, metallic-based particles are not only due to corrosion processes but also can originate from frictional wear or a synergistic combination of both processes.

In dental implants, some surface treatments used to improve bioactivity rely on the increase of surface area for contact with bone, achieved normally by shot blasting the surfaces with nano or micro-sized particles. Aparicio et al. [20] stated that the increased surface area could be responsible for differences in the electrochemical behavior and corrosion resistance of shot blasted materials. Furthermore, the compressive residual stresses induced by the process could also influence the corrosion of titanium implants.

The most common approach to improve the corrosion resistance of titanium materials for dental implants, takes advantage of the protective properties of the oxide film that is naturally formed on the surface. Thermal oxidation or electrochemical methods such as anodization can promote the growth of thick and adherent oxide films on the surface and enhance its corrosion resistance. These oxide films tend to be more protective due to the higher thickness and also more resistant to degradation by frictional stresses.

Kumar et al. [197] used thermal oxidation at 650 °C to create oxide films on titanium surfaces. The corrosion resistance was found to increase with the higher oxide thickness, since it provided more effective protection in Ringer solution, evaluated by potentiodynamic polarization and EIS analysis. Jamesh et al. [198] also correlated the improvement of corrosion properties of the same treatments to the uniform coverage and good compactness of the oxide layer, which provided an effective barrier and hindered the corrosion of titanium.

As for the electrochemical modifications of titanium induced by surface modifications, the amount of works in the literature is wide. For instance Cigada et al. [199] studied the corrosion resistance and passivity currents of anodized Ti6Al4V in physiological solution, and found that anodized samples showed reduced passivity current and a wider range of potentials presenting passive protection. Souza et al. [200] grew oxide films on titanium by anodization in a hydrofluoric acid solution. The surfaces were studied by electrochemical impedance spectroscopy and concluded that the treatment created a double layer oxide film composed of inner barrier and outer porous layers and an increase in corrosion properties. Mohsen et al. [201] produced a dual treatment for titanium materials, consisting of anodization in nickel sulfate solution and sealing the anodized film to enhance its corrosion resistance. Cui et al. [202] also performed a dual treatment in a β titanium alloy, consisting of pre-anodization and Micro-Arc Oxidation and evaluated the corrosion properties of the resulting surfaces. Pre-anodization before Micro-Arc Oxidation was found to improve the density and quality of the final oxide, effectively inhibiting the penetration of the electrolyte and decreasing the corrosion rate. The same tendencies for greater

protection of anodically grown oxide films were also recently confirmed by other authors, whether on pure titanium or titanium alloys [203, 204]. Using a commercial brand of titanium implants with an anodic phosphate-enriched oxide layer, Messer et al. [205] compared its corrosion behavior against a machined titanium implant. Under inflammatory and hyperglycemic conditions, commercial implants presented lower corrosion rates than untreated titanium implants in all simulated environments and a significantly lower corrosion rate after a simulated implantation into bone.

1.3. Improvement of tribocorrosion behavior

Due to the release of metal ions and the possibility for detachment of wear particles from titanium that can cause harmful reactions in human tissues and compromise the success of the implant, the tribocorrosion behavior of implant surfaces has been increasingly studied over the last years.

1.3.1. Understanding tribocorrosion

Tribocorrosion concerns the behavior of materials under combined conditions of corrosion and mechanical loading, and perhaps the most well-known characteristic of tribocorrosion processes it's the synergistic relation between both mechanisms. This synergism sometimes can bring benefits to the system, as in the case of formation of self-lubricating or self-healing layers; however, in general the combination of wear and corrosion causes an amplified degradation of the surface. In simple terms, the synergy effects of tribocorrosion processes are sometimes described by a simple relation: [206]

$$W_{total} = W_{corr} + W_{wear} + W_{syn}$$

The total degradation of a surface under tribocorrosion conditions is given as the sum of the contributions from corrosion (in the absence of wear) and wear (in the absence of corrosion) separately, plus a synergy parcel due to the combined effects of both processes. The presence of a corrosive environment can amplify the wear mechanisms, just like the wear processes can increase the corrosion rate of a material, for instance by removing the protective passive film from the surface [207]. To a great extent, synergism can be explained by the presence of surface reaction layers. Furthermore, other factors namely the formation of wear debris, the galvanic coupling established between worn and non-worn areas, the possible accumulation of dissolved species in the electrolyte surrounding the contact zone or the work hardening of the material by the mechanical solicitations can also contribute to synergistic mechanisms [208]. The presence

of surface reactions layers such as the passive oxide films exerts a great influence in the process, since it provides a stable protection that can be easily disrupted by mechanical actions. This will cause a great change in the equilibrium of the system. The removal of the passive film will cause itself the release of debris to the surrounding environment. Furthermore, a galvanic coupling effect between the newly exposed metal and the still protected surface can cause a significant increase in the corrosion rate and the release of metal ions. The rapid regeneration of the passive film in contact with the dissolved oxygen of the medium (repassivation) [209] will restore the protection, but also will be again prone to the mechanical loads, possibly leading to more wear debris [208]. Although the complex oral environment is difficult to simulate, the tribocorrosion behavior of a system can be investigated in situ by coupled tribological and electrochemical apparatus, monitoring the evolution of mechanical properties of the contact (coefficient of friction) and the corrosion parameters (open circuit potential, current density) [210, 211].

The outcomes of a tribocorrosion system are dependent on several parameters as seen in figure 2.3.

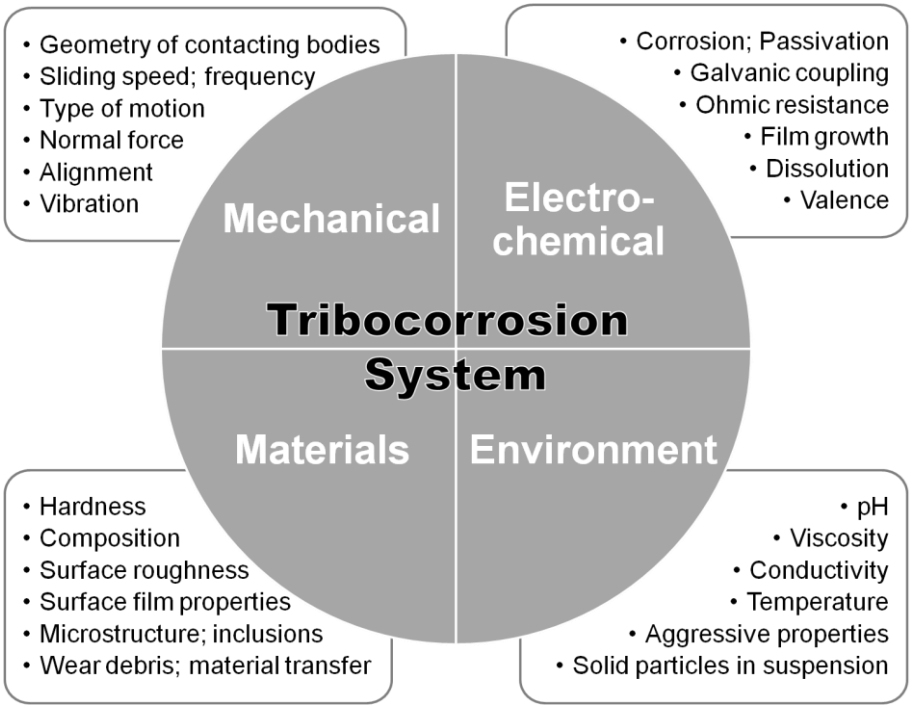

Figure 2.3 - Parameters influencing tribocorrosion phenomena (adapted from [212])

First and naturally, the materials are the major factor. Mechanical properties such as hardness and ductility govern a great deal of the surface deterioration and even structural transformations of the material [213]. Also the topography of the surfaces is of extreme importance. For instance, rougher topographies promote an uneven distribution of loads, which are concentrated in the higher asperities of the material and result in elevated contact pressures

[214]. Other issue is the mechanics of the tribological contact. Applied load, geometry of the contact, speed and type of motion can influence the total worn area and also the properties of depassivation/repassivation processes. These last phenomena are also correlated with environmental parameters and electrochemistry of the contact. Essentially the properties of the solution/environment will determine not only the corrosive properties of the system but also the possible adsorption of species that will influence the contact [211].

Additionally to these parameters, tribocorrosion processes occurring in a biological environment (bio-tribocorrosion) such as the conditions found in dental implants, should also take into account the effects of proteins, bone cells and microorganisms. [214]

All these aspects will, at some extent, influence the type of wear mechanism and the release of wear products. The most common tribological configurations occurring in implant materials are sliding or fretting [211, 215]. While sliding refers to high amplitude motions (for instance during insertion of an implant), fretting concerns very small amplitude movements in the order of a few dozens or hundreds of micrometers (micromovements caused by the transmission of mastication loads). The mechanisms that these contacts can promote can essentially be divided in two groups: 2-body wear and 3-body wear. Furthermore, one can distinguish abrasion and adhesion wear mechanisms as seen in figure 2.4.

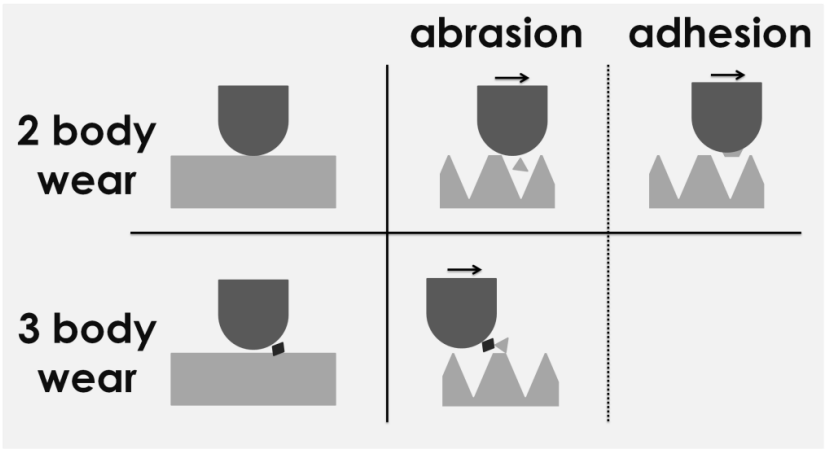

Figure 2.4 – Possible contact modes and wear mechanisms in sliding and fretting regimes.

The appearance of third bodies in the contact zone has a great importance for the behavior of the system. These can arise from the surrounding environment, or be produced during the contact and released from the material due to mechanical actions. The presence of solid debris in the contact zone alters the wear mechanism, since the particles can act as abrasives and promote increased degradation from the mechanical point of view (abrasive wear mechanisms). Electrochemically speaking the release of solid particles from the material also has

its negative aspects, because the removal of surface particles will expose unprotected metal to corrosion. Furthermore, the debris themselves also possess an electrochemically active area with high surface-to-volume ratio from where corrosion can occur. In the case of flat surfaces, the generation of wear debris can spread through the whole surface, whereas in rough surfaces, there is the possibility for the debris to be accumulated in the recesses of the structure, without causing further mechanical degradation. Another particularity of contacting surfaces with high roughness is that in the case of very small amplitude movements (fretting), the asperities of each surface can interlock and adsorb the stresses to the material through some elastic deformation of the asperities [214]. Being a complex subject for monolithic materials, tribocorrosion could be even more challenging in the case of coated materials [216].

1.3.2. Tribocorrosion in biomedical applications

In the biomedical field, tribocorrosion can be identified in two major areas of study: orthopedics and dentistry. In the case of dental implants, which is the subject of this work, the mastication/chewing process can be understood as a tribocorrosion cycle, as it causes the occurrence of micro-movements ate the bone-implant interface and the subsequent mechanic-electrochemical phenomena schematically shown in figure 2.5.

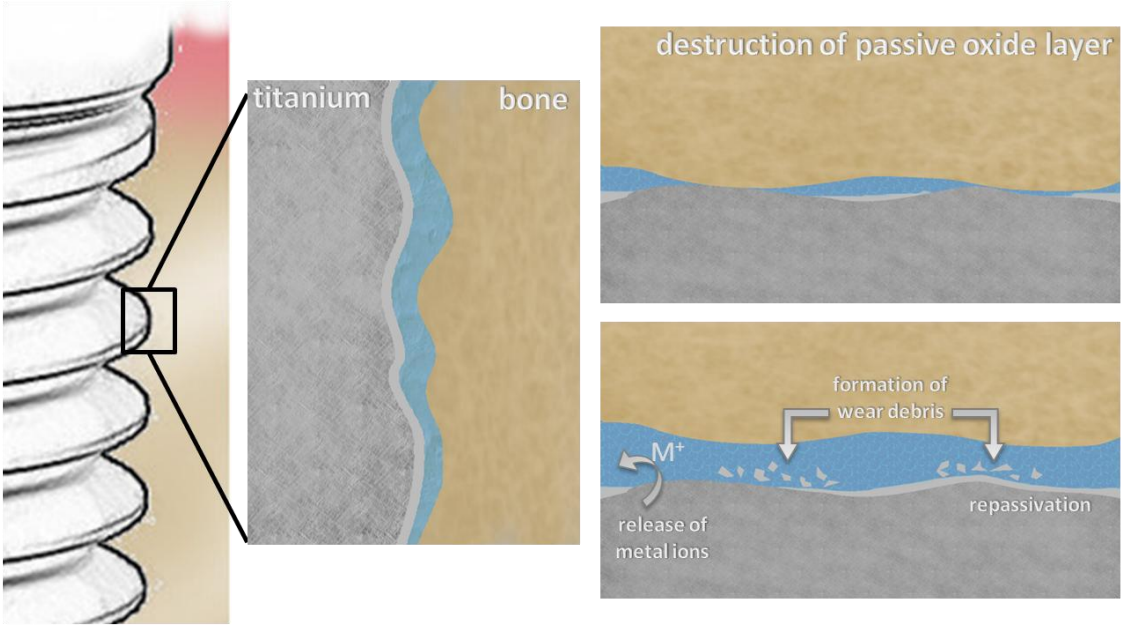

Figure 2.5 – Schematic representation of the occurrence of micro-movements at the bone-implant interface and the tribocorrosion phenomena arising from such event

Recent works have measured mastication forces in a range of 20 to 140 N, for a single molar [217]. Generally, the degradation of the material will result in the release of metal ions and solid wear debris to the surrounding tissues; fact that can induce peri-implant inflammatory

reactions and ultimately lead to the peri-implant bone loss and loosening of the implant (which will cause even more micro-motions) and ultimately to the failure of the prosthesis [207]. Therefore, dental implant materials must present a natural aptitude to resist the physiological loads transmitted by mastication processes [218].

If released from implant surfaces, wear particles are known to affect osteoblast properties as a function of the amount of particles in contact with the medium. For particle sizes below 5 μm, these can undergo phagocytosis by macrophages or other local cells, with potential adverse effects on cell's viability, proliferation and function [219-221]. These interactions will result in the release of pro-inflammatory substances such as cytokines or reactive oxygen species and create a chronic inflammation scenario leading to the upregulation of pathways of bone destruction (inducing osteoclast differentiation [222]) and downregulation of bone formation. Eventually this will all converge to painful symptoms, decreased functionality, instability and loosening of the implant [223, 224]. Besides implant-asociated issues, wear can also be the reason for dissemination of particles to the liver, spleen or abdominal lymph nodes as reported by Urban et al [225].

The phenomenon of tribocorrosion in biomedical applications is often called bio-tribocorrosion due to the influence of complex biological conditions, involving cellular and bacterial interactions with the surface, together with the mechanical and corrosive aspects [214]. The literature on bio-tribocorrosion aims to characterize and quantify the degradation of implant materials whether using different simulated physiological and biological conditions, or using different implantable materials.

Fretting-corrosion phenomena have been given plenty of attention in several works. Kumar et al. [226] found that commercially pure titanium materials present difficulties to instantaneously reform the passive oxide layer after fretting induced damages, which could lead to continuous dissolution of metal from damaged areas. In the case of Ti6Al4V alloy, Sivakumar et al. [227] revealed a strong dependence of the fretting behavior over the fluoride content in artificial saliva. Instantaneous repassivation of damaged areas was found in the absence of fluorides, while the addition of fluorides contributed for a slower and more ineffective repassivation.

The study of environmental conditions on tribocorrosion behavior of titanium has been approached since 2006, when Vieira et al. [228] studied the environmental effects of pH and corrosion inhibitors in tribocorrosion properties of pure titanium. Results obtained after the

addition of citric acid and anodic inhibitors revealed an improvement of the tribocorrosion behavior, attributed to the nature of oxidation and reduction reactions during the test, which promoted the formation of stable tribolayers and a reduction in friction coefficient and corrosion currents. More recently, Mathew et al. [229] found high degradation rates of titanium under tribocorrosion conditions up to near neutral pH values. Results obtained at pH of 6.0 (near the oral cavity pH of 6.3), showed that the passive layer on titanium was not effectively reformed, which might represent a concern for dental implant applications. Another studies by Licausi et al. [230, 231] evaluated the same environmental conditions plus the addition of fluorides, using cast and sintered Ti6Al4V alloy. No differences were found in the tribocorrosion mechanisms of cast and sintered alloys for varying pH's, however the addition of fluorides to an acidified environment was responsible for an increased material degradation due to active dissolution of the alloys. In the work of Souza et al. [178] with commercially pure titanium, high concentrations of fluorides were related to a decrease in coefficient of friction during sliding, which was attributed to the formation of reaction layers. Nevertheless, the material loss was increased at higher fluoride concentrations, demonstrating the influence of the aggressive chemical environment. Huang et al. [232] tested the behavior of a Ti-25Nb-3Mo-3Zr-2Sn alloy in contact with physiological solutions containing hyaluronic acid and bovine serum albumin. The corrosion currents found during the sliding tests were two orders of magnitude higher than those under static corrosion, suggesting a mechanism of wear-accelerated corrosion. Mathew et al. [233] brought to this discussion the role of lipopolysaccharides, which negatively affected the tribocorrosion behavior of titanium materials. These molecules can appear in patients with oral infections, which may account for an increased degradation of the implant in those cases. Runa et al. [234] studied the effect of albumin addition and different electrochemical potentials in Ti6Al4V tribocorrosion behavior. Albumin showed no special effects in the absence of corrosion, however once the surface of the material is damaged, albumin affects the tribocorrosion properties of the system according to the state of the passive film. Dimah et al. [235] studied $\alpha+\beta$ Ti6Al4V and α cp-Ti materials and also the effect of solution chemistry by the addition of bovine serum albumin to a PBS solution. Despite the same degradation mechanisms observed for both materials, the wear debris were found to be dependent on the material and on the solution chemistry. Anyway, $\alpha+\beta$ phase material showed better wear resistance than the β phase cp-Ti material.

In the oral environment, dental implants are also exposed to microbial colonization and the formation of biofilms. The role of oral biofilms composed of *S. mutans* and *C. albicans* was

studied by Souza et al. [189, 236]. An increased tendency to corrosion was found in the presence of biofilms, however the tribocorrosion mechanism was characterized by a decrease in friction for biofilm-covered samples. Despite the apparent lubricant properties of biofilms, the accentuated pH decrease caused by biofilms can lead to severe corrosion of titanium. Furthermore the decrease in friction was hypothesized as a possible cause for the loss of mechanical stability in dental implants.

Concerning the colonization of bone cells in implant materials, Runa et al. [237] were the first to study the effect of osteoblastic layers in the tribocorrosion behavior of a Ti6Al4V alloy, and vice-versa. At low contact pressures, the presence of an osteoblast cell layer was able to form a protection for the surface, inhibiting further wear degradation of the alloy and decreasing its corrosion tendency. In opposition there was noted a possible detrimental effect in the cells, as the length of their cytoplasmatic extensions was strongly reduced after the mechanical contact.

As for the intrinsic properties of the implant material, Martin et al. [213] studied the influence of microstructure and texture in corrosion and tribocorrosion processes. Martensitic microstructure along with high hardness values were the most determinant factors contributing for lower mass loss due to smaller damaged areas and decreased amount of wear debris in the contact region. Hacisalihoglu et al. [238] also compared the effect of α- (cp-Ti), β- (Ti-15Mo, Ti-45Nb, Ti-13Nb-13Zr) and α+β- (Ti6Al4V) Ti alloys submitted to tribocorrosion in SBF solution, but found no correlation between microstructure and tribocorrosion behavior. Still, α+β Ti6Al4V alloy and β Ti-13Nb-13Zr alloy showed a decreased wear volume among all the tested materials.

A recent trend started by Vieira et al. [239] and followed by some other authors [240, 241] has proposed a mathematical model for the prediction of potential drop in cases of galvanic coupling between worn and non-worn zones of the testing samples (anodic and cathodic areas) which could be of great importance for the prediction of electrochemical behavior of implant materials implanted in the body. The cathodic kinetics of the material and the geometric properties of the wear track and its evolution during the test are greatly correlated to the evolution of corrosion potential, allowing an accurate modeling of the materials electrochemical performance. Licausi et al. [242] applied zero-resistance ammetry (ZRA) to measure the galvanic potential and current between the wear track (anodic) and the passive surface (cathodic) of Ti6Al4V alloys, thus successfully simulating the potential and current evolution during tribocorrosion tests.

The search for more tribocorrosion resistant materials to be applied in implantology has led many authors to work on surface modification to improve the poor wear properties of titanium. For use in biomedical materials, surface modifications techniques must produce coatings that are not only able to resist both chemical and mechanical solicitations, but also maintain the good biological properties of pre-existing materials.

Nitriding has been approached in several works as a potential technique to improve tribological behavior of titanium through an increased hardness associated with TiN phases [243-245].

Many other studies refer to micro-arc oxidation (MAO) or plasma electrolytic oxidation (PEO) as suitable and economical methods for improving tribocorrosion resistance, while guaranteeing also a good biological behavior.

The trend started with Ishizawa and Ogino [71] in 1995, with the production of bioactive anodic oxide films containing calcium and phosphorous. More recently, some focus has been pointing to the mechanical, corrosion and wear testing of these kinds of surfaces. Some authors [246-248] have characterized mechanical and tribological properties of anodic titanium oxide layers. A significant outcome was related to the elastic modulus of the layers, which was measured to be around 40 GPa, which is very close to the values for human bone. The lower values of elastic modulus can be attributed to the porosity of the coating. [249, 250] Such feature is extremely important for prevention of stress shielding phenomena and avoiding bone resorption around dental implants. In anodic oxide layers with similar structure, Yetim [251] found an improved wear behavior and correlated it with the possible self-lubricating properties of the mixed anatase-rutile structure, which decreased the coefficient of friction during the test. Also the presence of hard rutile phase was mentioned to improve the mechanical properties of the coatings.

Albayrak et al. [252] took advantage of previously studied nitrided materials and performed anodization in sulfuric and phosphoric acid solution to create a porous titanium oxide layer. The anodically grown layers were better from the corrosion point of view, but presented higher wear rates and friction coefficients than the nitride condition. Using the same kind of electrolyte solution, Garsivaz Jazi et al. [253] performed anodic oxidation in Ti6Al4V alloy using different voltages. The increase in applied voltage during anodization provided a more efficient protection against tribocorrosion, seen by the lower rate in potential drop during sliding and the decrease in wear volume after tribocorrosion tests. Also using Ti6Al4V alloy, de Viteri et al. [254] performed

an anodic treatment in electrolytes containing Ca, P and I, obtaining improved tribocorrosion properties and increased antibacterial behavior due to the presence of iodine components. Alves et al. [255] produced anodic oxide layers using a commercial electrolyte and different current densities. In their work, the use of higher current densities accounted for thicker and rougher oxide layers with large sized pores when compared to lower current density treatments. Nevertheless, both situations significantly improved the tribocorrosion performance in artificial saliva, when compared to untreated samples of pure titanium. Felgueiras et al. [73] modified the surface of commercially pure titanium to form an oxide layer containing calcium and phosphorous. This enhanced cell attachment and differentiation, proving the good biological behavior of the coatings. Biotribocorrosion studies demonstrated that anodic treated samples had better resistance to mechanical solicitations and proved an important aptitude to induce cell attachment even after surface degradation with verified biomaterial-cell bond strength.

In conclusion, the tribocorrosion of anodic oxide layers for biomedical applications have met an increase in number of publications in the last couple of years, acknowledging the important contribute of both MAO treatments and tribocorrosion testing for the improvement of biomedical materials performance.

2. Micro-Arc Oxidation

Micro-Arc Oxidation (MAO) is an electrochemical method for the surface modification of materials. In the field of implant dentistry, it is already used for some time in commercial products with reported success. For instance, Jungner et al. [256] compared the performance of anodized and turned commercial implants in patients. Following a minimum of five months of loading, all anodized implants were functional, while 3.6% of turned implants have failed. A five year follow-up on the patients revealed the continued success of oxidized implants [257].

The popularity of this surface treatment arises from its simplicity and economical viability. Briefly, the electrochemical process relies on the installation of an electrical circuit, in which the titanium material is immersed in a conductive electrolyte solution, and will act as anode undergoing oxidation reactions on its surface after the application of a predetermined current or potential. Commonly, the result is an oxide film with variable properties, according to the treatment parameters and type of electrolyte.

From literature, one can distinguish two main types of structures, which can be obtained from anodic treatments in titanium. One of the trending topics over the last years is the

production of a nanotubular titanium oxide structure, at very well defined conditions of low voltage and high processing times, using fluoride-rich electrolytes. In this case, a simultaneous process of electrochemical oxidation (film formation) and dissolution caused by the fluoride ions, gives rise to the ordered growth of nanotubes [258]. These structures have been widely studied for their potentialities in drug delivery systems of biomedical materials [259-261].

Unlike the previous case, MAO process in titanium is characterized by the application of high voltages during shorter periods of time. The result is commonly a thick, rough and porous oxide layer, with the possibility for incorporation of chemical elements present in the electrolyte. The anodic polarization induces the growth of an oxide film in the surface of a titanium anode. Due to the resistor properties of the forming oxide, the resistivity of the circuit will increase to a point that it will become a barrier to the flow of electrical current in the circuit. To guarantee the continuous flow of current, the high applied voltages will cause the local rupture of the oxide, in a phenomenon known by dielectric breakdown of the oxide. The flow of current through the system will happen by means of powerful micro electrical discharges (micro-arcs) in the surface of the anode, creating very localized increases in temperature able to locally and instantaneously melt and re-solidify the oxide, and giving rise to a porous structure. During the occurrence of these phenomena the chemical elements present in the electrolyte can mix with the melted oxide and be incorporated in the structure after solidification. Another particularity of the high temperature process is the modification of the oxide crystalline structure, resulting in the formation of anatase or rutile crystalline phases [262-264].

Both the incorporation of foreign chemical species and the formation of crystalline structures of anatase and rutile have been used to promote biological improvements to titanium materials. The use of electrolytes containing bioactive elements, such as calcium and phosphorous can produce oxides with improved bioactivity and chemical affinity with the biological tissues as mentioned in section 1.1.2. On the other hand, the appearance of crystalline phases of anatase and rutile can have a two-fold advantage in biological properties and mechanical behavior as explained in section 1.1.1.

Despite being a well established method for surface modification of implantable materials, some authors are suggesting coupled techniques to improve the performance of electrochemical methods. The role of ultrasound was referred by Huang et al. [265] as a method to alter the equilibrium between the reactions of oxidation and dissolution, leading to the formation of titanium dioxide nanotubes with different morphologies. The application of ultrasound was

associated with a great enhancement of the diffusion of chemical species in the electrolyte and lead to acceleration of the processes of film formation. The same was found by Zhang et al. [266] during the formation of nanotubes of aluminum oxide. Recenlty, Neupane et al. [267] compared the effect of magnetic stirring and ultrasound in Micro-Arc Oxidation of titanium. The oxide formation was promoted by the ultrasonic application and also the properties of the film were dependent on the ultrasound parameters. The pore size, surface roughness and Ca/P ratio were increased by higher ultrasonic powers applied during Micro-Arc Oxidation. Ultrasound has been applied as an energy source for enhancing the rate of chemical reactions, diffusion and mass transfer processes leading to the formation of the oxide film. Furthermore, it can also be an efficient method to incorporate functional micro or nano particles in the structure of electrochemically grown oxide films [268].

References

[1] T. Hanawa. Research and development of metals for medical devices based on clinical needs. *Science and Technology of Advanced Materials*, 13(6): 64102-64116, **2012**.

[2] M. Niinomi, M. Nakai, and J. Hieda. Development of new metallic alloys for biomedical applications. *Acta Biomaterialia*, 8(11): 3888-3903, **2012**.

[3] Y.T. Sul, C. Johansson, A. Wennerberg, L.R. Cho, B.S. Chang, and T. Albrektsson. Optimum surface properties of oxidized implants for reinforcement of osseointegration: surface chemistry, oxide thickness, porosity, roughness, and crystal structure. *The International Journal of Oral and Maxillofacial Implants*, 20(3): 349-359, **2005**.

[4] A. Wennerberg and T. Albrektsson. On implant surfaces: A review of current knowledge and opinions. *The International Journal of Oral and Maxillofacial Implants*, 25(1): 63-74, **2010**.

[5] L. Le Guéhennec, A. Soueidan, P. Layrolle, and Y. Amouriq. Surface treatments of titanium dental implants for rapid osseointegration. *Dental Materials*, 23(7): 844-854, **2007**.

[6] G. Mendonça, D.B.S. Mendonça, F.J.L. Aragão, and L.F. Cooper. Advancing dental implant surface technology: From micron- to nanotopography. *Biomaterials*, 29(28): 3822-3835, **2008**.

[7] L. Lin, H. Wang, M. Ni, Y. Rui, T.-Y. Cheng, C.-K. Cheng, X. Pan, G. Li, and C. Lin. Enhanced osteointegration of medical titanium implant with surface modifications in micro/nanoscale structures. *Journal of Orthopaedic Translation*, 2(1): 35-42, **2014**.

[8] G. Zhao, O. Zinger, Z. Schwartz, M. Wieland, D. Landolt, and B.D. Boyan. Osteoblast-like cells are sensitive to submicron-scale surface structure. *Clinical Oral Implants Research*, 17(3): 258-264, **2006**.

[9] R.A. Gittens, R. Olivares-Navarrete, Z. Schwartz, and B.D. Boyan. Implant osseointegration and the role of microroughness and nanostructures: Lessons for spine implants. *Acta Biomaterialia*, 10(8): 3363-3371, **2014**.

[10] L. Salou, A. Hoornaert, G. Louarn, and P. Layrolle. Enhanced osseointegration of titanium implants with nanostructured surfaces: An experimental study in rabbits. *Acta Biomaterialia*, 11: 494-502, **2015**.

[11] F. Gentile, L. Tirinato, E. Battista, F. Causa, C. Liberale, E.M. di Fabrizio, and P. Decuzzi. Cells preferentially grow on rough substrates. *Biomaterials*, 31(28): 7205-7212, **2010**.

[12] A. Bruinink, M. Bitar, M. Pleskova, P. Wick, H.F. Krug, and K. Maniura-Weber. Addition of nanoscaled bioinspired surface features: A revolution for bone related implants and scaffolds? *Journal of Biomedical Materials Research Part A*, 102(1): 275-294, **2014**.

[13] J.I. Rosales-Leal, M.A. Rodríguez-Valverde, G. Mazzaglia, P.J. Ramón-Torregrosa, L. Díaz-Rodríguez, O. García-Martínez, M. Vallecillo-Capilla, C. Ruiz, and M.A. Cabrerizo-Vílchez. Effect of roughness, wettability and morphology of engineered titanium surfaces on osteoblast-like cell adhesion. *Colloids and Surfaces A: Physicochemical and Engineering Aspects*, 365(1–3): 222-229, **2010**.

[14] C. Aparicio, A. Padrós, and F.-J. Gil. *In vivo* evaluation of micro-rough and bioactive titanium dental implants using histometry and pull-out tests. *Journal of the Mechanical Behavior of Biomedical Materials*, 4(8): 1672-1682, **2011**.

[15] C.N. Elias, Y. Oshida, J.H.C. Lima, and C.A. Muller. Relationship between surface properties (roughness, wettability and morphology) of titanium and dental implant removal torque. *Journal of the Mechanical Behavior of Biomedical Materials*, 1(3): 234-242, **2008**.

[16] A.E. Daw, H.A. Kazi, J.S. Colombo, W.G. Rowe, D.W. Williams, R.J. Waddington, D.W. Thomas, and R. Moseley. Differential cellular and microbial responses to nano-/micron-scale titanium surface roughness induced by hydrogen peroxide treatment. *Journal of Biomaterials Applications*, 28(1): 144-160, **2013**.

[17] Y. Wu, J.P. Zitelli, K.S. TenHuisen, X. Yu, and M.R. Libera. Differential response of Staphylococci and osteoblasts to varying titanium surface roughness. *Biomaterials*, 32(4): 951-960, **2011**.

[18] N.C.M. Oliveira, C.C.G. Moura, D. Zanetta-Barbosa, D.B.S. Mendonça, L. Cooper, G. Mendonça, and P. Dechichi. Effects of titanium surface anodization with CaP incorporation on human osteoblastic response. *Materials Science and Engineering: C*, 33(4): 1958-1962, **2013**.

[19] A. Wennerberg, A. Ide-Ektessabi, S. Hatkamata, T. Sawase, C. Johansson, T. Albrektsson, A. Martinelli, U. Södervall, and H. Odelius. Titanium release from implants prepared with different surface roughness. *Clinical Oral Implants Research*, 15(5): 505-512, **2004**.

[20] C. Aparicio, F. Javier Gil, C. Fonseca, M. Barbosa, and J.A. Planell. Corrosion behaviour of commercially pure titanium shot blasted with different materials and sizes of shot particles for dental implant applications. *Biomaterials*, 24(2): 263-273, **2003**.

[21] P.M. Bartold, J.S. Kuliwaba, V. Lee, S. Shah, V. Marino, and N.L. Fazzalari. Influence of surface roughness and shape on microdamage of the osseous surface adjacent to titanium dental implants. *Clinical Oral Implants Research*, 22(6): 613-618, **2011**.

[22] A. Tabassum, F. Walboomers, J.G.C. Wolke, G.J. Meijer, and J.A. Jansen. The influence of surface roughness on the displacement of osteogenic bone particles during placement of titanium screw-type implants. *Clinical Implant Dentistry and Related Research*, 13(4): 269-278, **2011**.

[23] A. Wilkinson, R.N. Hewitt, L.E. McNamara, D. McCloy, R.M. Dominic Meek, and M.J. Dalby. Biomimetic microtopography to enhance osteogenesis *in vitro*. *Acta Biomaterialia*, 7(7): 2919-2925, **2011**.

[24] S. Puckett, R. Pareta, and T.J. Webster. Nano rough micron patterned titanium for directing osteoblast morphology and adhesion. *International Journal of Nanomedicine*, 3(2): 229-241, **2008**.

[25] D.V. Kilpadi and J.E. Lemons. Surface energy characterization of unalloyed titanium implants. *Journal of Biomedical Materials Research*, 28(12): 1419-1425, **1994**.

[26] H. Schliephake and D. Scharnweber. Chemical and biological functionalization of titanium for dental implants. *Journal of Materials Chemistry*, 18(21): 2404-2414, **2008**.

[27] G. Zhao, Z. Schwartz, M. Wieland, F. Rupp, J. Geis-Gerstorfer, D.L. Cochran, and B.D. Boyan. High surface energy enhances cell response to titanium substrate microstructure. *Journal of Biomedical Materials Research Part A*, 74A(1): 49-58, **2005**.

[28] A. Wennerberg, S. Galli, and T. Albrektsson. Current knowledge about the hydrophilic and nanostructured SLActive surface. *Clinical, Cosmetic and Investigational Dentistry*, 3: 59-67, **2011**.

[29] F. Schwarz, M. Wieland, Z. Schwartz, G. Zhao, F. Rupp, J. Geis-Gerstorfer, A. Schedle, N. Broggini, M.M. Bornstein, D. Buser, S.J. Ferguson, J. Becker, B.D. Boyan, and D.L. Cochran. Potential of chemically modified hydrophilic surface characteristics to support tissue integration of titanium dental implants. *Journal of Biomedical Materials Research Part B: Applied Biomaterials*, 88B(2): 544-557, **2009**.

[30] S. Zinelis, N. Silikas, A. Thomas, K. Syres, and G. Eliades. Surface characterization of SLActive dental implants. *The European Journal of Esthetic Dentistry*, 7(1): 72-92, **2012**.

[31] J. He, W. Zhou, X. Zhou, X. Zhong, X. Zhang, P. Wan, B. Zhu, and W. Chen. The anatase phase of nanotopography titania plays an important role on osteoblast cell morphology and proliferation. *Journal of Materials Science: Materials in Medicine*, 19(11): 3465-3472, **2008**.

[32] B. Yang, M. Uchida, H.-M. Kim, X. Zhang, and T. Kokubo. Preparation of bioactive titanium metal via anodic oxidation treatment. *Biomaterials*, 25(6): 1003-1010, **2004**.

[33] H.-T. Chen, C.-J. Chung, T.-C. Yang, C.-H. Tang, and J.-L. He. Microscopic observations of osteoblast growth on micro-arc oxidized β titanium. *Applied Surface Science*, 266: 73-80, **2013**.

[34] X. Cui, H.M. Kim, M. Kawashita, L. Wang, T. Xiong, T. Kokubo, and T. Nakamura. Preparation of bioactive titania films on titanium metal via anodic oxidation. *Dental Materials*, 25(1): 80-86, **2009**.

[35] O. Zywitzki, T. Modes, H. Sahm, P. Frach, K. Goedicke, and D. Glöß. Structure and properties of crystalline titanium oxide layers deposited by reactive pulse magnetron sputtering. *Surface and Coatings Technology*, 180–181: 538-543, **2004**.

[36] D.M. Dohan Ehrenfest, P.G. Coelho, B.-S. Kang, Y.-T. Sul, and T. Albrektsson. Classification of osseointegrated implant surfaces: materials, chemistry and topography. *Trends in Biotechnology*, 28(4): 198-206, **2010**.

[37] K. Anselme. Biomaterials and interface with bone. *Osteoporosis International*, 22(6): 2037-2042, **2011**.

[38] C.N. Elias. Factors affecting the success of dental implants. in *Implant Dentistry - A Rapidly Evolving Practice*. InTech, **2011**.

[39] J.A. Lemire, J.J. Harrison, and R.J. Turner. Antimicrobial activity of metals: mechanisms, molecular targets and applications. *Nature Reviews Microbiology*, 11(6): 371-384, **2013**.

[40] A.M.C. Barradas, H.A.M. Fernandes, N. Groen, Y.C. Chai, J. Schrooten, J. van de Peppel, J.P.T.M. van Leeuwen, C.A. van Blitterswijk, and J. de Boer. A calcium-induced signaling cascade leading to osteogenic differentiation of human bone marrow-derived mesenchymal stromal cells. *Biomaterials*, 33(11): 3205-3215, **2012**.

[41] D.E. Clapham. Calcium Signaling. *Cell*, 131(6): 1047-1058, **2007**.

[42] W.R. Thompson, C.T. Rubin, and J. Rubin. Mechanical regulation of signaling pathways in bone. *Gene*, 503(2): 179-193, **2012**.

[43] J.E. Ellingsen. A study on the mechanism of protein adsorption to TiO_2. *Biomaterials*, 12(6): 593-596, **1991**.

[44] B. Nagar, M. Overduin, M. Ikura, and J.M. Rini. Structural basis of calcium-induced E-cadherin rigidification and dimerization. *Nature*, 380(6572): 360-364, **1996**.

[45] M.J. Olszta, X. Cheng, S.S. Jee, R. Kumar, Y.-Y. Kim, M.J. Kaufman, E.P. Douglas, and L.B. Gower. Bone structure and formation: A new perspective. *Materials Science and Engineering: R: Reports*, 58(3–5): 77-116, **2007**.

[46] R.A. Surmenev, M.A. Surmeneva, and A.A. Ivanova. Significance of calcium phosphate coatings for the enhancement of new bone osteogenesis: A review. *Acta Biomaterialia*, 10(2): 557-579, **2014**.

[47] R. Narayanan, S.K. Seshadri, T.Y. Kwon, and K.H. Kim. Calcium phosphate-based coatings on titanium and its alloys. *Journal of Biomedical Materials Research Part B: Applied Biomaterials*, 85B(1): 279-299, **2008**.

[48] S.R. Paital and N.B. Dahotre. Calcium phosphate coatings for bio-implant applications: Materials, performance factors, and methodologies. *Materials Science and Engineering: R: Reports*, 66(1–3): 1-70, **2009**.

[49] P.S. Gomes, C. Botelho, M.A. Lopes, J.D. Santos, and M.H. Fernandes. Evaluation of human osteoblastic cell response to plasma-sprayed silicon-substituted hydroxyapatite coatings over titanium substrates. *Journal of Biomedical Materials Research Part B: Applied Biomaterials*, 94B(2): 337-346, **2010**.

[50] M. Roy, A. Bandyopadhyay, and S. Bose. Induction plasma sprayed nano hydroxyapatite coatings on titanium for orthopaedic and dental implants. *Surface and Coatings Technology*, 205(8–9): 2785-2792, **2011**.

[51] R.A. Surmenev. A review of plasma-assisted methods for calcium phosphate-based coatings fabrication. *Surface and Coatings Technology*, 206(8–9): 2035-2056, **2012**.

[52] S. Take, K. Kikuchi, S. Suda, S. Izawa, and Y. Itoi. Preparation and evaluation of Zn doped HAp plasma spray biocombatible coatings on titanium. *ECS Transactions*, 58(38): 17-22, **2014**.

[53] W. Zhang, G. Wang, Y. Liu, X. Zhao, D. Zou, C. Zhu, Y. Jin, Q. Huang, J. Sun, X. Liu, X. Jiang, and H. Zreiqat. The synergistic effect of hierarchical micro/nano-topography and bioactive ions for enhanced osseointegration. *Biomaterials*, 34(13): 3184-3195, **2013**.

[54] H. Cao and X. Liu. Plasma-sprayed ceramic coatings for osseointegration. *International Journal of Applied Ceramic Technology*, 10(1): 1-10, **2013**.

[55] X.-B. Chen, Y.-C. Li, J.D. Plessis, P.D. Hodgson, and C. Wen. Influence of calcium ion deposition on apatite-inducing ability of porous titanium for biomedical applications. *Acta Biomaterialia*, 5(5): 1808-1820, **2009**.

[56] T. Hanawa, Y. Kamiura, S. Yamamoto, T. Kohgo, A. Amemiya, H. Ukai, K. Murakami, and K. Asaoka. Early bone formation around calcium-ion-implanted titanium inserted into rat tibia. *Journal of Biomedical Materials Research*, 36(1): 131-136, **1997**.

[57] I. Braceras, J.I. Alava, L. Goikoetxea, M.A. de Maeztu, and J.I. Onate. Interaction of engineered surfaces with the living world: Ion implantation vs. osseointegration. *Surface and Coatings Technology*, 201(19–20): 8091-8098, **2007**.

[58] T.R. Rautray, R. Narayanan, T.-Y. Kwon, and K.-H. Kim. Surface modification of titanium and titanium alloys by ion implantation. *Journal of Biomedical Materials Research Part B: Applied Biomaterials*, 93B(2): 581-591, **2010**.

[59] P. Choudhury and D.C. Agrawal. Sol–gel derived hydroxyapatite coatings on titanium substrates. *Surface and Coatings Technology*, 206(2–3): 360-365, **2011**.

[60] Y. Cai, S. Zhang, X. Zeng, Y. Wang, M. Qian, and W. Weng. Improvement of bioactivity with magnesium and fluorine ions incorporated hydroxyapatite coatings via sol–gel deposition on Ti6Al4V alloys. *Thin Solid Films*, 517(17): 5347-5351, **2009**.

[61] S. Ziani, S. Meski, and H. Khireddine. Characterization of magnesium-doped hydroxyapatite prepared by sol-gel process. *International Journal of Applied Ceramic Technology*, 11(1): 83-91, **2014**.

[62] S. Yokota, N. Nishiwaki, K. Ueda, T. Narushima, H. Kawamura, and T. Takahashi. Evaluation of thin amorphous calcium phosphate coatings on titanium dental implants deposited using magnetron sputtering. *Implant Dentistry*, 23(3): 343-350, **2014**.

[63] R.A. Surmenev, M.A. Surmeneva, K.E. Evdokimov, V.F. Pichugin, T. Peitsch, and M. Epple. The influence of the deposition parameters on the properties of an RF-magnetron-deposited nanostructured calcium phosphate coating and a possible growth mechanism. *Surface and Coatings Technology*, 205(12): 3600-3606, **2011**.

[64] F. Alexander, U. Christian, T. Stefan, V. Christoph, G. Reinhard, and W. Georg. Long-term effects of magnetron-sputtered calcium phosphate coating on osseointegration of dental implants in non-human primates. *Clinical Oral Implants Research*, 20(2): 183-188, **2009**.

[65] M.M. McCafferty, G.A. Burke, and B.J. Meenan. Mesenchymal stem cell response to conformal sputter deposited calcium phosphate thin films on nanostructured titanium surfaces. *Journal of Biomedical Materials Research Part A*, 102(10): 3585-3597, **2014**.

[66] Y. Huang, S. Han, X. Pang, Q. Ding, and Y. Yan. Electrodeposition of porous hydroxyapatite/calcium silicate composite coating on titanium for biomedical applications. *Applied Surface Science*, 271: 299-302, **2013**.

[67] R. Drevet, A. Viteaux, J.C. Maurin, and H. Benhayoune. Human osteoblast-like cells response to pulsed electrodeposited calcium phosphate coatings. *RSC Advances*, 3(28): 11148-11154, **2013**.

[68] D. Gopi, A. Karthika, S. Nithiya, and L. Kavitha. *In vitro* biological performance of minerals substituted hydroxyapatite coating by pulsed electrodeposition method. *Materials Chemistry and Physics*, 144(1–2): 75-85, **2014**.

[69] D. Lakstein, W. Kopelovitch, Z. Barkay, M. Bahaa, D. Hendel, and N. Eliaz. Enhanced osseointegration of grit-blasted, NaOH-treated and electrochemically hydroxyapatite-coated Ti–6Al–4V implants in rabbits. *Acta Biomaterialia*, 5(6): 2258-2269, **2009**.

[70] Y. Parcharoen, P. Kajitvichyanukul, S. Sirivisoot, and P. Termsuksawad. Hydroxyapatite electrodeposition on anodized titanium nanotubes for orthopedic applications. *Applied Surface Science*, 311: 54-61, **2014**.

[71] H. Ishizawa and M. Ogino. Formation and characterization of anodic titanium oxide films containing Ca and P. *Journal of Biomedical Materials Research*, 29(1): 65-72, **1995**.

[72] J.M. Lee, J.I. Lee, and Y.J. Lim. *In vitro* investigation of anodization and CaP deposited titanium surface using MG63 osteoblast-like cells. *Applied Surface Science*, 256(10): 3086-3092, **2010**.

[73] H.P. Felgueiras, L. Castanheira, S. Changotade, F. Poirier, S. Oughlis, M. Henriques, C. Chakar, N. Naaman, R. Younes, V. Migonney, J.P. Celis, P. Ponthiaux, L.A. Rocha, and D. Lutomski. Biotribocorrosion (tribo-electrochemical) characterization of anodized titanium biomaterial containing calcium and phosphorus before and after osteoblastic cell culture. *Journal of Biomedical Materials Research Part B: Applied Biomaterials*, doi:10.1002/jbm.b.33236: **2014**.

[74] H. Cimenoglu, M. Gunyuz, G.T. Kose, M. Baydogan, F. Uğurlu, and C. Sener. Micro-arc oxidation of Ti6Al4V and Ti6Al7Nb alloys for biomedical applications. *Materials Characterization*, 62(3): 304-311, **2011**.

[75] T.-C. Yang, H.-Y. Shu, H.-T. Chen, C.-J. Chung, and J.-L. He. Interface between grown osteoblast and micro-arc oxidized bioactive layers. *Surface and Coatings Technology*, 259, Part B: 185-192, **2014**.

[76] A. dos Santos, J. Araujo, S. Landi, A. Kuznetsov, J. Granjeiro, L. de Sena, and C. Achete. A study of the physical, chemical and biological properties of TiO_2 coatings produced by micro-arc oxidation in a Ca–P-based electrolyte. *Journal of Materials Science: Materials in Medicine*, 25(7): 1769-1780, **2014**.

[77] Y. Tsutsumi, M. Niinomi, M. Nakai, H. Tsutsumi, H. Doi, N. Nomura, and T. Hanawa. Micro-arc oxidation treatment to improve the hard-tissue compatibility of Ti–29Nb–13Ta–4.6Zr alloy. *Applied Surface Science*, 262: 34-38, **2012**.

[78] X. Zhu, K.-H. Kim, and Y. Jeong. Anodic oxide films containing Ca and P of titanium biomaterial. *Biomaterials*, 22(16): 2199-2206, **2001**.

[79] P. Schlegel, J.S. Hayes, V.M. Frauchiger, B. Gasser, R. Wieling, M. Textor, and R.G. Richards. An *in vivo* evaluation of the biocompatibility of anodic plasma chemical (APC) treatment of titanium with calcium phosphate. *Journal of Biomedical Materials Research Part B: Applied Biomaterials*, 90B(1): 26-34, **2009**.

[80] S.C. Cox, P. Jamshidi, L.M. Grover, and K.K. Mallick. Preparation and characterisation of nanophase Sr, Mg, and Zn substituted hydroxyapatite by aqueous precipitation. *Materials Science and Engineering: C*, 35: 106-114, **2014**.

[81] J. Shepherd, D. Shepherd, and S. Best. Substituted hydroxyapatites for bone repair. *Journal of Materials Science: Materials in Medicine*, 23(10): 2335-2347, **2012**.

[82] I.R. de Lima, G.G. Alves, C.A. Soriano, A.P. Campaneli, T.H. Gasparoto, E. Schnaider Ramos, L.Á. de Sena, A.M. Rossi, and J.M. Granjeiro. Understanding the impact of divalent cation substitution on hydroxyapatite: An *in vitro* multiparametric study on biocompatibility. *Journal of Biomedical Materials Research Part A*, 98A(3): 351-358, **2011**.

[83] M.M. Belluci, T. Schoenmaker, C. Rossa-Junior, S.R. Orrico, T.J. de Vries, and V. Everts. Magnesium deficiency results in an increased formation of osteoclasts. *The Journal of Nutritional Biochemistry*, 24(8): 1488-1498, **2013**.

[84] A. Earnshaw and N. Greenwood. Effective ionic radii in pm for various oxidation states - Appendix 5. in *Chemistry of the Elements (Second Edition)*. Elsevier Butterworth-Heinemann, **1997**.

[85] D. Laurencin, N. Almora-Barrios, N.H. de Leeuw, C. Gervais, C. Bonhomme, F. Mauri, W. Chrzanowski, J.C. Knowles, R.J. Newport, A. Wong, Z. Gan, and M.E. Smith. Magnesium incorporation into hydroxyapatite. *Biomaterials*, 32(7): 1826-1837, **2011**.

[86] M.-J. Jiao and X.-X. Wang. Electrolytic deposition of magnesium-substituted hydroxyapatite crystals on titanium substrate. *Materials Letters*, 63(27): 2286-2289, **2009**.

[87] W.L. Suchanek, K. Byrappa, P. Shuk, R.E. Riman, V.F. Janas, and K.S. TenHuisen. Preparation of magnesium-substituted hydroxyapatite powders by the mechanochemical–hydrothermal method. *Biomaterials*, 25(19): 4647-4657, **2004**.

[88] G. Qi, S. Zhang, K.A. Khor, S.W. Lye, X. Zeng, W. Weng, C. Liu, S.S. Venkatraman, and L.L. Ma. Osteoblastic cell response on magnesium-incorporated apatite coatings. *Applied Surface Science*, 255(2): 304-307, **2008**.

[89] D.A. Robinson, R.W. Griffith, D. Shechtman, R.B. Evans, and M.G. Conzemius. *In vitro* antibacterial properties of magnesium metal against *Escherichia coli, Pseudomonas aeruginosa* and *Staphylococcus aureus*. *Acta Biomaterialia*, 6(5): 1869-1877, **2010**.

[90] P.J. Marie, D. Felsenberg, and M.L. Brandi. How strontium ranelate, via opposite effects on bone resorption and formation, prevents osteoporosis. *Osteoporosis International*, 22(6): 1659-1667, **2011**.

[91] Y. Li, X. Li, G. Song, K. Chen, G. Yin, and J. Hu. Effects of strontium ranelate on osseointegration of titanium implant in osteoporotic rats. *Clinical Oral Implants Research*, 23(9): 1038-1044, **2012**.

[92] J. Terra, E.R. Dourado, J.-G. Eon, D.E. Ellis, G. Gonzalez, and A.M. Rossi. The structure of strontium-doped hydroxyapatite: an experimental and theoretical study. *Physical Chemistry Chemical Physics*, 11(3): 568-577, **2009**.

[93] R. Drevet and H. Benhayoune. Pulsed electrodeposition for the synthesis of strontium-substituted calcium phosphate coatings with improved dissolution properties. *Materials Science and Engineering: C*, 33(7): 4260-4265, **2013**.

[94] V. Offermanns, O.Z. Andersen, G. Falkensammer, I.H. Andersen, K.P. Almtoft, S. Sørensen, M. Sillassen, C.S. Jeppesen, M. Rasse, M. Foss, and F. Kloss. Enhanced osseointegration of endosseous implants by predictable sustained release properties of strontium. *Journal of Biomedical Materials Research Part B: Applied Biomaterials*, doi:10.1002/jbm.b.33279: **2014**.

[95] M.O. Li, X. Xiao, R. Liu, C. Chen, and L. Huang. Structural characterization of zinc-substituted hydroxyapatite prepared by hydrothermal method. *Journal of Materials Science: Materials in Medicine*, 19(2): 797-803, **2008**.

[96] C.A. McDevitt, A.D. Ogunniyi, E. Valkov, M.C. Lawrence, B. Kobe, A.G. McEwan, and J.C. Paton. A molecular mechanism for bacterial susceptibility to zinc. *PLoS Pathogens*, 7(11): e1002357, **2011**.

[97] Y. Xie, Y. He, P.L. Irwin, T. Jin, and X. Shi. Antibacterial activity and mechanism of action of zinc oxide nanoparticles against *Campylobacter jejuni*. *Applied and Environmental Microbiology*, 77(7): 2325-2331, **2011**.

[98] K.R. Raghupathi, R.T. Koodali, and A.C. Manna. Size-dependent bacterial growth inhibition and mechanism of antibacterial activity of zinc oxide nanoparticles. *Langmuir*, 27(7): 4020-4028, **2011**.

[99] G. Applerot, A. Lipovsky, R. Dror, N. Perkas, Y. Nitzan, R. Lubart, and A. Gedanken. Enhanced antibacterial activity of nanocrystalline ZnO due to increased ROS-mediated cell injury. *Advanced Functional Materials*, 19(6): 842-852, **2009**.

[100] F. Yang, W.-J. Dong, F.-M. He, X.-X. Wang, S.-F. Zhao, and G.-L. Yang. Osteoblast response to porous titanium surfaces coated with zinc-substituted hydroxyapatite. *Oral Surgery, Oral Medicine, Oral Pathology and Oral Radiology*, 113(3): 313-318, **2012**.

[101] D.V. Shepherd, K. Kauppinen, R.A. Brooks, and S.M. Best. An *in vitro* study into the effect of zinc substituted hydroxyapatite on osteoclast number and activity. *Journal of Biomedical Materials Research Part A*, 102(11): 4136-4141, **2014**.

[102] E. Mavropoulos, M. Hausen, A.M. Costa, G. Alves, A. Mello, C.A. Ospina, M. Mir, J.M. Granjeiro, and A.M. Rossi. The impact of the RGD peptide on osteoblast adhesion and spreading on zinc-substituted hydroxyapatite surface. *Journal of Materials Science: Materials in Medicine*, 24(5): 1271-1283, **2013**.

[103] E.S. Thian, T. Konishi, Y. Kawanobe, P.N. Lim, C. Choong, B. Ho, and M. Aizawa. Zinc-substituted hydroxyapatite: a biomaterial with enhanced bioactivity and antibacterial properties. *Journal of Materials Science: Materials in Medicine*, 24(2): 437-445, **2013**.

[104] H. Hu, W. Zhang, Y. Qiao, X. Jiang, X. Liu, and C. Ding. Antibacterial activity and increased bone marrow stem cell functions of Zn-incorporated TiO_2 coatings on titanium. *Acta Biomaterialia*, 8(2): 904-915, **2012**.

[105] C. You, C. Han, X. Wang, Y. Zheng, Q. Li, X. Hu, and H. Sun. The progress of silver nanoparticles in the antibacterial mechanism, clinical application and cytotoxicity. *Molecular Biology Reports*, 39(9): 9193-9201, **2012**.

[106] S.B. Goodman, Z. Yao, M. Keeney, and F. Yang. The future of biologic coatings for orthopaedic implants. *Biomaterials*, 34(13): 3174-3183, **2013**.

[107] W. Chen, Y. Liu, H.S. Courtney, M. Bettenga, C.M. Agrawal, J.D. Bumgardner, and J.L. Ong. *In vitro* anti-bacterial and biological properties of magnetron co-sputtered silver-containing hydroxyapatite coating. *Biomaterials*, 27(32): 5512-5517, **2006**.

[108] S. Sandukas, A. Yamamoto, and A. Rabiei. Osteoblast adhesion to functionally graded hydroxyapatite coatings doped with silver. *Journal of Biomedical Materials Research Part A*, 97A(4): 490-497, **2011**.

[109] N. Rameshbabu, T.S. Sampath Kumar, T.G. Prabhakar, V.S. Sastry, K.V.G.K. Murty, and K. Prasad Rao. Antibacterial nanosized silver substituted hydroxyapatite: Synthesis and characterization. *Journal of Biomedical Materials Research Part A*, 80A(3): 581-591, **2007**.

[110] C.E. Albers, W. Hofstetter, K.A. Siebenrock, R. Landmann, and F.M. Klenke. *In vitro* cytotoxicity of silver nanoparticles on osteoblasts and osteoclasts at antibacterial concentrations. *Nanotoxicology*, 7(1): 30-36, **2013**.

[111] W. Liu, Y. Wu, C. Wang, H.C. Li, T. Wang, C.Y. Liao, L. Cui, Q.F. Zhou, B. Yan, and G.B. Jiang. Impact of silver nanoparticles on human cells: Effect of particle size. *Nanotoxicology*, 4(3): 319-330, **2010**.

[112] K.G. Neoh, X. Hu, D. Zheng, and E.T. Kang. Balancing osteoblast functions and bacterial adhesion on functionalized titanium surfaces. *Biomaterials*, 33(10): 2813-2822, **2012**.

[113] C.J. Wilson, R.E. Clegg, D.I. Leavesley, and M.J. Pearcy. Mediation of biomaterial-cell interactions by adsorbed proteins: A review. *Tissue Engineering*, 11(1-2): 1-18, **2005**.

[114] A. Shekaran and A.J. García. Extracellular matrix-mimetic adhesive biomaterials for bone repair. *Journal of Biomedical Materials Research Part A*, 96A(1): 261-272, **2011**.

[115] M.B. Rahmany and M. Van Dyke. Biomimetic approaches to modulate cellular adhesion in biomaterials: A review. *Acta Biomaterialia*, 9(3): 5431-5437, **2013**.

[116] P. Schaffner and M.M. Dard. Structure and function of RGD peptides involved in bone biology. *Cellular and Molecular Life Sciences*, 60(1): 119-132, **2003**.

[117] S.L. Bellis. Advantages of RGD peptides for directing cell association with biomaterials. *Biomaterials*, 32(18): 4205-4210, **2011**.

[118] T.H. Barker. The role of ECM proteins and protein fragments in guiding cell behavior in regenerative medicine. *Biomaterials*, 32(18): 4211-4214, **2011**.

[119] K. von der Mark, J. Park, S. Bauer, and P. Schmuki. Nanoscale engineering of biomimetic surfaces: cues from the extracellular matrix. *Cell and Tissue Research*, 339(1): 131-153, **2010**.

[120] T.A. Petrie, C.D. Reyes, K.L. Burns, and A.J. García. Simple application of fibronectin–mimetic coating enhances osseointegration of titanium implants. *Journal of Cellular and Molecular Medicine*, 13(8b): 2602-2612, **2009**.

[121] B.E. Rapuano and D.E. MacDonald. Surface oxide net charge of a titanium alloy: Modulation of fibronectin-activated attachment and spreading of osteogenic cells. *Colloids and Surfaces B: Biointerfaces*, 82(1): 95-103, **2011**.

[122] M. Gorbahn, M.O. Klein, M. Lehnert, T. Ziebart, D. Brüllmann, I. Köper, W. Wagner, B. Al-Nawas, and M. Veith. Promotion of osteogenic cell response using quasicovalent immobilized fibronectin on titanium surfaces: Introduction of a novel biomimetic layer system. *Journal of Oral and Maxillofacial Surgery*, 70(8): 1827-1834, **2012**.

[123] X. Ren, Y. Wu, Y. Cheng, H. Ma, and S. Wei. Fibronectin and bone morphogenetic protein-2-decorated Poly(OEGMA-r-HEMA) brushes promote osseointegration of titanium surfaces. *Langmuir*, 27(19): 12069-12073, **2011**.

[124] N. Horasawa, T. Yamashita, S. Uehara, and N. Udagawa. High-performance scaffolds on titanium surfaces: Osteoblast differentiation and mineralization promoted by a globular fibrinogen layer through cell-autonomous BMP signaling. *Materials Science and Engineering: C*, 46: 86-96, **2015**.

[125] A. Arvidsson, F. Currie, P. Kjellin, Y.-T. Sul, and V. Stenport. Nucleation and growth of calcium phosphates in the presence of fibrinogen on titanium implants with four potentially bioactive surface preparations. An *in vitro* study. *Journal of Materials Science: Materials in Medicine*, 20(9): 1869-1879, **2009**.

[126] K. Bougas, V.F. Stenport, F. Currie, and A. Wennerberg. Laminin coating promotes calcium phosphate precipitation on titanium discs *in vitro*. *Journal of Oral & Maxillofacial Research*, 2(4): e5, **2011**.

[127] S. Werner, O. Huck, B. Frisch, D. Vautier, R. Elkaim, J.-C. Voegel, G. Brunel, and H. Tenenbaum. The effect of microstructured surfaces and laminin-derived peptide coatings on soft tissue interactions with titanium dental implants. *Biomaterials*, 30(12): 2291-2301, **2009**.

[128] A. Cacchioli, F. Ravanetti, A. Bagno, M. Dettin, and C. Gabbi. Human vitronectin–derived peptide covalently grafted onto titanium surface improves osteogenic activity: A pilot *in vivo* study on rabbits. *Tissue Engineering Part A*, 15(10): 2917-2926, **2009**.

[129] D.M. Rivera-Chacon, M. Alvarado-Velez, C.Y. Acevedo-Morantes, S.P. Singh, E. Gultepe, D. Nagesha, S. Sridhar, and J.E. Ramirez-Vick. Fibronectin and vitronectin promote human fetal osteoblast cell attachment and proliferation on nanoporous titanium surfaces. *Journal of Biomedical Nanotechnology*, 9(6): 1092-1097, **2013**.

[130] H. Mahmoud, D.W. Williams, A. Hannigan, and C.D. Lynch. Influence of extracellular matrix proteins in enhancing bacterial adhesion to titanium surfaces. *Journal of Biomedical Materials Research Part B: Applied Biomaterials*, 100B(5): 1319-1327, **2012**.

[131] L.B. Hauslich, M.N. Sela, D. Steinberg, G. Rosen, and D. Kohavi. The adhesion of oral bacteria to modified titanium surfaces: Role of plasma proteins and electrostatic forces. *Clinical Oral Implants Research*, 24: 49-56, **2013**.

[132] J.H. Collier and T. Segura. Evolving the use of peptides as components of biomaterials. *Biomaterials*, 32(18): 4198-4204, **2011**.

[133] A. Ratcliffe. Difficulties in the translation of functionalized biomaterials into regenerative medicine clinical products. *Biomaterials*, 32(18): 4215-4217, **2011**.

[134] D.F. Williams. The role of short synthetic adhesion peptides in regenerative medicine; The debate. *Biomaterials*, 32(18): 4195-4197, **2011**.

[135] C.-Y. Chien, T.-Y. Liu, W.-H. Kuo, M.-J. Wang, and W.-B. Tsai. Dopamine-assisted immobilization of hydroxyapatite nanoparticles and RGD peptides to improve the osteoconductivity of titanium. *Journal of Biomedical Materials Research Part A*, 101A(3): 740-747, **2013**.

[136] B. Elmengaard, J.E. Bechtold, and K. Søballe. *In vivo* effects of RGD-coated titanium implants inserted in two bone-gap models. *Journal of Biomedical Materials Research Part A*, 75A(2): 249-255, **2005**.

[137] S.-Y. Park, H.-S. Kim, J.-H. Kim, J.-H. Shim, M.-J. Yun, Y.-C. Jeon, J.-B. Huh, and C.-M. Jeong. Effects of anodized titanium implant coated with RGD peptides via chemical fixation on osseointegration and bone regeneration. *Tissue Engineering and Regenerative Medicine*, 9(4): 194-202, **2012**.

[138] M. Dettin, A. Bagno, R. Gambaretto, G. Iucci, M.T. Conconi, N. Tuccitto, A.M. Menti, C. Grandi, C. Di Bello, A. Licciardello, and G. Polzonetti. Covalent surface modification of titanium oxide with different adhesive peptides: Surface characterization and osteoblast-like cell adhesion. *Journal of Biomedical Materials Research Part A*, 90A(1): 35-45, **2009**.

[139] P.W. Kammerer, M. Heller, J. Brieger, M.O. Klein, B. Al-Nawas, and M. Gabriel. Immobilisation of linear and cyclic RGD-peptides on titanium surfaces and their impact on endothelial cell adhesion and proliferation. *European Cells and Materials*, 21: 364-372, **2011**.

[140] W. Lin, C. Junjian, C. Chengzhi, S. Lin, L. Sa, R. Li, and W. Yingjun. Multi-biofunctionalization of a titanium surface with a mixture of peptides to achieve excellent antimicrobial activity and biocompatibility. *Journal of Materials Chemistry B*, 3(1): 30-33, **2015**.

[141] X. Cao, W.-Q. Yu, J. Qiu, Y.-F. Zhao, Y.-L. Zhang, and F.-Q. Zhang. RGD peptide immobilized on TiO_2 nanotubes for increased bone marrow stromal cells adhesion and osteogenic gene expression. *Journal of Materials Science: Materials in Medicine*, 23(2): 527-536, **2012**.

[142] W.-C. Chen and C.-L. Ko. Roughened titanium surfaces with silane and further RGD peptide modification *in vitro*. *Materials Science and Engineering: C*, 33(5): 2713-2722, **2013**.

[143] J. Chen, R.A. Bly, M.M. Saad, M.A. AlKhodary, R.M. El-Backly, D.J. Cohen, N. Kattamis, M.M. Fatta, W.A. Moore, C.B. Arnold, M.K. Marei, and W.O. Soboyejo. In-vivo study of adhesion and bone growth around implanted laser groove/RGD-functionalized Ti-6Al-4V pins in rabbit femurs. *Materials Science and Engineering: C*, 31(5): 826-832, **2011**.

[144] J. Auernheimer, D. Zukowski, C. Dahmen, M. Kantlehner, A. Enderle, S.L. Goodman, and H. Kessler. Titanium implant materials with improved biocompatibility through coating with phosphonate-anchored cyclic RGD peptides. *ChemBioChem*, 6(11): 2034-2040, **2005**.

[145] H.C. Kroese-Deutman, J. van den Dolder, P.H. Spauwen, and J.A. Jansen. Influence of RGD-loaded titanium implants on bone formation *in vivo*. *Tissue Engineering*, 11(11-12): 1867-1875, **2005**.

[146] X. Wang, C. Yan, K. Ye, Y. He, Z. Li, and J. Ding. Effect of RGD nanospacing on differentiation of stem cells. *Biomaterials*, 34(12): 2865-2874, **2013**.

[147] X. Wang, K. Ye, Z. Li, C. Yan, and J. Ding. Adhesion, proliferation, and differentiation of mesenchymal stem cells on RGD nanopatterns of varied nanospacings. *Organogenesis*, 9(4): 280-286, **2013**.

[148] M.N. Nguyen, T. Lebarbe, O.F. Zouani, L. Pichavant, M.-C. Durrieu, and V. Héroguez. Impact of RGD nanopatterns grafted onto titanium on osteoblastic cell adhesion. *Biomacromolecules*, 13(3): 896-904, **2012**.

[149] B.F. Bell, M. Schuler, S. Tosatti, M. Textor, Z. Schwartz, and B.D. Boyan. Osteoblast response to titanium surfaces functionalized with extracellular matrix peptide biomimetics. *Clinical Oral Implants Research*, 22(8): 865-872, **2011**.

[150] K. Oya, Y. Tanaka, H. Saito, K. Kurashima, K. Nogi, H. Tsutsumi, Y. Tsutsumi, H. Doi, N. Nomura, and T. Hanawa. Calcification by MC3T3-E1 cells on RGD peptide immobilized on titanium through electrodeposited PEG. *Biomaterials*, 30(7): 1281-1286, **2009**.

[151] J.-W. Park, K. Kurashima, Y. Tustusmi, C.-H. An, J.-Y. Suh, H. Doi, N. Nomura, K. Noda, and T. Hanawa. Bone healing of commercial oral implants with RGD immobilization through electrodeposited poly(ethylene glycol) in rabbit cancellous bone. *Acta Biomaterialia*, 7(8): 3222-3229, **2011**.

[152] M. Schuler, G.R. Owen, D.W. Hamilton, M. de Wild, M. Textor, D.M. Brunette, and S.G.P. Tosatti. Biomimetic modification of titanium dental implant model surfaces using the RGDSP-peptide sequence: A cell morphology study. *Biomaterials*, 27(21): 4003-4015, **2006**.

[153] N. Broggini, S. Tosatti, S.J. Ferguson, M. Schuler, M. Textor, M.M. Bornstein, D.D. Bosshardt, and D. Buser. Evaluation of chemically modified SLA implants (modSLA) biofunctionalized with integrin (RGD)- and heparin (KRSR)-binding peptides. *Journal of Biomedical Materials Research Part A*, 100A(3): 703-711, **2012**.

[154] M. Jäger, C. Böge, R. Janissen, D. Rohrbeck, T. Hülsen, S. Lensing-Höhn, R. Krauspe, and M. Herten. Osteoblastic potency of bone marrow cells cultivated on functionalized biometals with cyclic RGD-peptide. *Journal of Biomedical Materials Research Part A*, 101(10): 2905-2914, **2013**.

[155] S. Tosatti, Z. Schwartz, C. Campbell, D.L. Cochran, S. VandeVondele, J.A. Hubbell, A. Denzer, J. Simpson, M. Wieland, C.H. Lohmann, M. Textor, and B.D. Boyan. RGD-containing peptide GCRGYGRGDSPG reduces enhancement of osteoblast differentiation by poly(L-lysine)-graft-poly(ethylene glycol)-coated titanium surfaces. *Journal of Biomedical Materials Research Part A*, 68A(3): 458-472, **2004**.

[156] R.R. Maddikeri, S. Tosatti, M. Schuler, S. Chessari, M. Textor, R.G. Richards, and L.G. Harris. Reduced medical infection related bacterial strains adhesion on bioactive RGD modified titanium surfaces: A first step toward cell selective surfaces. *Journal of Biomedical Materials Research Part A*, 84A(2): 425-435, **2008**.

[157] L.G. Harris, S. Tosatti, M. Wieland, M. Textor, and R.G. Richards. *Staphylococcus aureus* adhesion to titanium oxide surfaces coated with non-functionalized and peptide-functionalized poly(l-lysine)-grafted-poly(ethylene glycol) copolymers. *Biomaterials*, 25(18): 4135-4148, **2004**.

[158] G. Subbiahdoss, B. Pidhatika, G. Coullerez, M. Charnley, R. Kuijer, H.C. van der Mei, M. Textor, and H.J. Busscher. Bacterial biofilm formation versus mammalian cell growth on titanium-based mono- and bi-functional coating. *European Cells and Materials*, 19: 205-213, **2010**.

[159] J.M. Granjeiro, R.C. Oliveira, J.C. Bustos-Valenzuela, M.C. Sogayar, and R. Taga. Bone morphogenetic proteins: from structure to clinical use. *Brazilian Journal of Medical and Biological Research*, 38: 1463-1473, **2005**.

[160] B. Bragdon, O. Moseychuk, S. Saldanha, D. King, J. Julian, and A. Nohe. Bone morphogenetic proteins: A critical review. *Cellular Signalling*, 23(4): 609-620, **2011**.

[161] Q.-H. Jiang, L. Liu, S. Peel, G.-L. Yang, S.-F. Zhao, and F.-M. He. Bone response to the multilayer BMP-2 gene coated porous titanium implant surface. *Clinical Oral Implants Research*, 24(8): 853-861, **2013**.

[162] R. Guillot, F. Gilde, P. Becquart, F. Sailhan, A. Lapeyrere, D. Logeart-Avramoglou, and C. Picart. The stability of BMP loaded polyelectrolyte multilayer coatings on titanium. *Biomaterials*, 34(23): 5737-5746, **2013**.

[163] Z. Shi, K.G. Neoh, E.-T. Kang, C. Poh, and W. Wang. Titanium with surface-grafted dextran and immobilized bone morphogenetic protein-2 for inhibition of bacterial adhesion and enhancement of osteoblast functions. *Tissue Engineering Part A*, 15(2): 417-426, **2008**.

[164] M.-C. Degat, G. Dubreucq, A. Meunier, L. Dahri-Correia, L. Sedel, H. Petite, and D. Logeart-Avramoglou. Enhancement of the biological activity of BMP-2 by synthetic dextran derivatives. *Journal of Biomedical Materials Research Part A*, 88A(1): 174-183, **2009**.

[165] T. Lim, W. Wang, Z. Shi, C. Poh, and K.G. Neoh. Human bone marrow-derived mesenchymal stem cells and osteoblast differentiation on titanium with surface-grafted chitosan and immobilized bone morphogenetic protein-2. *Journal of Materials Science: Materials in Medicine*, 20(1): 1-10, **2009**.

[166] S.E. Kim, C.-S. Kim, Y.-P. Yun, D.H. Yang, K. Park, S.E. Kim, C.-M. Jeong, and J.-B. Huh. Improving osteoblast functions and bone formation upon BMP-2 immobilization on titanium modified with heparin. *Carbohydrate Polymers*, 114: 123-132, **2014**.

[167] T. Ishibe, T. Goto, T. Kodama, T. Miyazaki, S. Kobayashi, and T. Takahashi. Bone formation on apatite-coated titanium with incorporated BMP-2/heparin *in vivo*. *Oral Surgery, Oral Medicine, Oral Pathology, Oral Radiology, and Endodontology*, 108(6): 867-875, **2009**.

[168] D.H. Yang, D.-W. Lee, Y.-D. Kwon, H.J. Kim, H.J. Chun, J.W. Jang, and G. Khang. Surface modification of titanium with hydroxyapatite–heparin–BMP-2 enhances the efficacy of bone formation and osseointegration *in vitro* and *in vivo*. *Journal of Tissue Engineering and Regenerative Medicine*, doi:10.1002/term.1973: **2014**.

[169] S.E. Kim, S.-H. Song, Y.P. Yun, B.-J. Choi, I.K. Kwon, M.S. Bae, H.-J. Moon, and Y.-D. Kwon. The effect of immobilization of heparin and bone morphogenic protein-2 (BMP-2) to titanium surfaces on inflammation and osteoblast function. *Biomaterials*, 32(2): 366-373, **2011**.

[170] D.-W. Lee, Y.-P. Yun, K. Park, and S.E. Kim. Gentamicin and bone morphogenic protein-2 (BMP-2)-delivering heparinized-titanium implant with enhanced antibacterial activity and osteointegration. *Bone*, 50(4): 974-982, **2012**.

[171] J. Hall, R.G. Sorensen, J.M. Wozney, and U.M.E. Wikesjö. Bone formation at rhBMP-2-coated titanium implants in the rat ectopic model. *Journal of Clinical Periodontology*, 34(5): 444-451, **2007**.

[172] D. Yoo, N. Tovar, R. Jimbo, C. Marin, R.B. Anchieta, L.S. Machado, J. Montclare, F.P.S. Guastaldi, M.N. Janal, and P.G. Coelho. Increased osseointegration effect of bone morphogenetic protein 2 on dental implants: An *in vivo* study. *Journal of Biomedical Materials Research Part A*, 102(6): 1921-1927, **2014**.

[173] Y. Cai, X. Wang, C.K. Poh, H.C. Tan, M.T. Soe, S. Zhang, and W. Wang. Accelerated bone growth *in vitro* by the conjugation of BMP2 peptide with hydroxyapatite on titanium alloy. *Colloids and Surfaces B: Biointerfaces*, 116: 681-686, **2014**.

[174] J.J. Jacobs, J.L. Gilbert, and R.M. Urban. Current concepts review - Corrosion of metal orthopaedic implants. *The Journal of Bone & Joint Surgery*, 80(2): 268-282, **1998**.

[175] L.L. Shreir. Basic concepts of corrosion. in *Shreir's Corrosion*. Elsevier, **2010**.

[176] S. Virtanen, I. Milošev, E. Gomez-Barrena, R. Trebše, J. Salo, and Y.T. Konttinen. Special modes of corrosion under physiological and simulated physiological conditions. *Acta Biomaterialia*, 4(3): 468-476, **2008**.

[177] N. Schiff, B. Grosgogeat, M. Lissac, and F. Dalard. Influence of fluoride content and pH on the corrosion resistance of titanium and its alloys. *Biomaterials*, 23(9): 1995-2002, **2002**.

[178] J.C.M. Souza, S.L. Barbosa, E. Ariza, J.P. Celis, and L.A. Rocha. Simultaneous degradation by corrosion and wear of titanium in artificial saliva containing fluorides. *Wear*, 292–293: 82-88, **2012**.

[179] J.C.M. Souza, S.L. Barbosa, E.A. Ariza, M. Henriques, W. Teughels, P. Ponthiaux, J.-P. Celis, and L.A. Rocha. How do titanium and Ti6Al4V corrode in fluoridated medium as found in the oral cavity? An *in vitro* study. *Materials Science and Engineering: C*, 47: 384-393, **2015**.

[180] M. Pourbaix. Atlas of electrochemical equilibria in aqueous solutions. **1966**.

[181] V.A.R. Barão, M.T. Mathew, W.G. Assunção, J.C.-C. Yuan, M.A. Wimmer, and C. Sukotjo. Stability of cp-Ti and Ti-6Al-4V alloy for dental implants as a function of saliva pH – an electrochemical study. *Clinical Oral Implants Research*, 23(9): 1055-1062, **2012**.

[182] A. Robin and O.A.S. Carvalho. Influence of pH and Fluoride Species on the Corrosion Behavior of Ti-xNb-13Zr Alloys in Ringer's Solution. *Advances in Materials Science and Engineering*, 2013: 434975, **2013**.

[183] D. Rodrigues, P. Valderrama, T. Wilson, K. Palmer, A. Thomas, S. Sridhar, A. Adapalli, M. Burbano, and C. Wadhwani. Titanium corrosion mechanisms in the oral environment: A retrieval study. *Materials*, 6(11): 5258-5274, **2013**.

[184] J.C.M. Souza, P. Ponthiaux, M. Henriques, R. Oliveira, W. Teughels, J.-P. Celis, and L.A. Rocha. Corrosion behaviour of titanium in the presence of *Streptococcus mutans*. *Journal of Dentistry*, 41(6): 528-534, **2013**.

[185] G. Mabilleau, S. Bourdon, M.L. Joly-Guillou, R. Filmon, M.F. Baslé, and D. Chappard. Influence of fluoride, hydrogen peroxide and lactic acid on the corrosion resistance of commercially pure titanium. *Acta Biomaterialia*, 2(1): 121-129, **2006**.

[186] C. Fonseca and M.A. Barbosa. Corrosion behaviour of titanium in biofluids containing H_2O_2 studied by electrochemical impedance spectroscopy. *Corrosion Science*, 43(3): 547-559, **2001**.

[187] R.L.W. Messer, G. Tackas, J. Mickalonis, Y. Brown, J.B. Lewis, and J.C. Wataha. Corrosion of machined titanium dental implants under inflammatory conditions. *Journal of Biomedical Materials Research Part B: Applied Biomaterials*, 88B(2): 474-481, **2009**.

[188] E. Tamam and I. Turkyilmaz. Effects of pH and elevated glucose levels on the electrochemical behavior of dental implants. *Journal of Oral Implantology*, 40(2): 153-159, **2014**.

[189] J.C.M. Souza, M. Henriques, R. Oliveira, W. Teughels, J.P. Celis, and L.A. Rocha. Do oral biofilms influence the wear and corrosion behavior of titanium? *Biofouling*, 26(4): 471-478, **2010**.

[190] D.G. Olmedo, G. Duffó, R.L. Cabrini, and M.B. Guglielmotti. Local effect of titanium implant corrosion: an experimental study in rats. *International Journal of Oral and Maxillofacial Surgery*, 37(11): 1032-1038, **2008**.

[191] D. Olmedo, M.M. Fernández, M.B. Guglielmotti, and R.L. Cabrini. Macrophages related to dental implant failure. *Implant Dentistry*, 12(1): 75-80, **2003**.

[192] M. Mohedano, E. Matykina, R. Arrabal, A. Pardo, and M.C. Merino. Metal release from ceramic coatings for dental implants. *Dental Materials*, 30(3): e28-e40, **2014**.

[193] B. Finet, G. Weber, and R. Cloots. Titanium release from dental implants: an *in vivo* study on sheep. *Materials Letters*, 43(4): 159-165, **2000**.

[194] S.J. Lugowski, D.C. Smith, A.D. McHugh, and J.C. Van Loon. Release of metal ions from dental implant materials *in vivo*: Determination of Al, Co, Cr, Mo, Ni, V, and Ti in organ tissue. *Journal of Biomedical Materials Research*, 25(12): 1443-1458, **1991**.

[195] V. Sansone, D. Pagani, and M. Melato. The effects on bone cells of metal ions released from orthopaedic implants. A review. *Clinical Cases in Mineral and Bone Metabolism*, 10(1): 34-40, **2013**.

[196] F. Berglund and B. Carlmark. Titanium, sinusitis, and the yellow nail syndrome. *Biological Trace Element Research*, 143(1): 1-7, **2011**.

[197] S. Kumar, T.S.N.S. Narayanan, S.G.S. Raman, and S.K. Seshadri. Thermal oxidation of CP-Ti: Evaluation of characteristics and corrosion resistance as a function of treatment time. *Materials Science and Engineering: C*, 29(6): 1942-1949, **2009**.

[198] M. Jamesh, S. Kumar, and T.S.N.S. Narayanan. Effect of thermal oxidation on corrosion resistance of commercially pure titanium in acid medium. *Journal of Materials Engineering and Performance*, 21(6): 900-906, **2012**.

[199] A. Cigada, M. Cabrini, and P. Pedeferri. Increasing of the corrosion resistance of the Ti6Al4V alloy by high thickness anodic oxidation. *Journal of Materials Science: Materials in Medicine*, 3(6): 408-412, **1992**.

[200] M.E.P. Souza, M. Ballester, and C.M.A. Freire. EIS characterisation of Ti anodic oxide porous films formed using modulated potential. *Surface and Coatings Technology*, 201(18): 7775-7780, **2007**.

[201] Q. Mohsen and S.A. Fadl-Allah. Improvement in corrosion resistance of commercial pure titanium for the enhancement of its biocompatibility. *Materials and Corrosion*, 62(4): 310-319, **2011**.

[202] W.F. Cui, L. Jin, and L. Zhou. Surface characteristics and electrochemical corrosion behavior of a pre-anodized microarc oxidation coating on titanium alloy. *Materials Science and Engineering: C*, 33(7): 3775-3779, **2013**.

[203] Z. Liu, X. Liu, U. Donatus, G.E. Thompson, and P. Skeldon. Corrosion behaviour of the anodic oxide film on commercially pure titanium in NaCl environment. *International Journal of Electrochemical Science*, 9: 3558-3573, **2014**.

[204] M.L. Vera, E. Linardi, L. Lanzani, C. Mendez, C.E. Schvezov, and A.E. Ares. Corrosion resistance of titanium dioxide anodic coatings on Ti–6Al–4V. *Materials and Corrosion*, doi:10.1002/maco.201407988: **2014**.

[205] R.L.W. Messer, F. Seta, J. Mickalonis, Y. Brown, J.B. Lewis, and J.C. Wataha. Corrosion of phosphate-enriched titanium oxide surface dental implants (TiUnite®) under *in vitro* inflammatory and hyperglycemic conditions. *Journal of Biomedical Materials Research Part B: Applied Biomaterials*, 92B(2): 525-534, **2010**.

[206] J.P. Celis, P. Ponthiaux, and F. Wenger. Tribo-corrosion of materials: Interplay between chemical, electrochemical, and mechanical reactivity of surfaces. *Wear*, 261(9): 939-946, **2006**.

[207] H.V. Cruz, J.C.M. Souza, M. Henriques, and L.A. Rocha. Tribocorrosion and bio-tribocorrosion in the oral environment: The case of dental implants. in *Biomedical Tribology*. Nova Science Publishers, **2011**.

[208] P. Ponthiaux, F. Wenger, and J.-P. Celis. Tribocorrosion: Material behavior under combined conditions of corrosion and mechanical loading. in *Corrosion Resistance*. InTech, **2012**.

[209] T. Hanawa, K. Asami, and K. Asaoka. Repassivation of titanium and surface oxide film regenerated in simulated bioliquid. *Journal of Biomedical Materials Research*, 40(4): 530-538, **1998**.

[210] P. Ponthiaux, F. Wenger, D. Drees, and J.P. Celis. Electrochemical techniques for studying tribocorrosion processes. *Wear*, 256(5): 459-468, **2004**.

[211] M.T. Mathew, P. Srinivasa Pai, R. Pourzal, A. Fischer, and M.A. Wimmer. Significance of tribocorrosion in biomedical applications: Overview and current status. *Advances in Tribology*, 2009: 250986, **2009**.

[212] J.-P. Celis and P. Ponthiaux. Testing tribocorrosion of passivating materials supporting research and industrial innovation: Handbook. Maney Publishing, **2012**.

[213] É. Martin, M. Azzi, G.A. Salishchev, and J. Szpunar. Influence of microstructure and texture on the corrosion and tribocorrosion behavior of Ti–6Al–4V. *Tribology International*, 43(5–6): 918-924, **2010**.

[214] L.A. Rocha, F. Oliveira, H.V. Cruz, C. Sukotjo, and M.T. Mathew. Bio-tribocorrosion in dental applications. in *Bio-Tribocorrosion in Biomaterials and Medical Implants*. Woodhead Publishing, **2013**.

[215] J. Geringer, B. Forest, and P. Combrade. Fretting-corrosion of materials used as orthopaedic implants. *Wear*, 259(7–12): 943-951, **2005**.

[216] R.J.K. Wood. Tribo-corrosion of coatings: A review. *Journal of Physics D: Applied Physics*, 40(18): 5502, **2007**.

[217] C.L. Nathaniel, J. Sridhar, C. Deniz, and O.B. John. An analysis of the physiologic parameters of intraoral wear: A review. *Journal of Physics D: Applied Physics*, 46(40): 404007, **2013**.

[218] J. Geringer, N. Demanget, and J. Pellier. From acid etching treatments to tribocorrosive properties of dental implants: Do some experimental results on surface treatments have an influence on the tribocorrosion behaviour of dental implants? *Journal of Physics D: Applied Physics*, 46(40): 404005, **2013**.

[219] S.B. Goodman, T. Ma, R. Chiu, R. Ramachandran, and R.L. Smith. Effects of orthopaedic wear particles on osteoprogenitor cells. *Biomaterials*, 27(36): 6096-6101, **2006**.

[220] C. Vermes, R. Chandrasekaran, J.J. Jacobs, J.O. Galante, K.A. Roebuck, and T.T. Glant. The effects of particulate wear debris, cytokines, and growth factors on the functions of MG-63 osteoblasts. *The Journal of Bone & Joint Surgery*, 83(2): 201-201, **2001**.

[221] J. Yao, G. Cs-Szabó, J.J. Jacobs, K.E. Kuettner, and T.T. Glant. Suppression of osteoblast function by titanium particles. *The Journal of Bone & Joint Surgery*, 79(1): 107-112, **1997**.

[222] Y. Bi, R.R. VanDeMotter, A.A. Ragab, V.M. Goldberg, J.M. Anderson, and E.M. Greenfield. Titanium particles stimulate bone resorption by inducing differentiation of murine osteoclasts. *The Journal of Bone & Joint Surgery*, 83(4): 501-501, **2001**.

[223] S.B. Goodman, E. Gibon, J. Pajarinen, T.-H. Lin, M. Keeney, P.-G. Ren, C. Nich, Z. Yao, K. Egashira, F. Yang, and Y.T. Konttinen. Novel biological strategies for treatment of wear particle-induced periprosthetic osteolysis of orthopaedic implants for joint replacement. *Journal of the Royal Society Interface*, 11(93): 20130962, **2014**.

[224] N.J. Hallab and J.J. Jacobs. Biologic effects of implant debris. *Bulletin of the NYU Hospital for Joint Diseases*, 67(2): 182-188, **2009**.

[225] R.M. Urban, J.J. Jacobs, M.J. Tomlinson, J. Gavrilovic, J. Black, and M. Peoc'h. Dissemination of wear particles to the liver, spleen, and abdominal lymph nodes of patients with hip or knee replacement. *The Journal of Bone & Joint Surgery*, 82(4): 457-457, **2000**.

[226] S. Kumar, T.S.N.S. Narayanan, S.G.S. Raman, and S.K. Seshadri. Evaluation of fretting corrosion behaviour of CP-Ti for orthopaedic implant applications. *Tribology International*, 43(7): 1245-1252, **2010**.

[227] B. Sivakumar, S. Kumar, and T.S.N.S. Narayanan. Fretting corrosion behaviour of Ti–6Al–4V alloy in artificial saliva containing varying concentrations of fluoride ions. *Wear*, 270(3–4): 317-324, **2011**.

[228] A.C. Vieira, A.R. Ribeiro, L.A. Rocha, and J.P. Celis. Influence of pH and corrosion inhibitors on the tribocorrosion of titanium in artificial saliva. *Wear*, 261(9): 994-1001, **2006**.

[229] M.T. Mathew, S. Abbey, N.J. Hallab, D.J. Hall, C. Sukotjo, and M.A. Wimmer. Influence of pH on the tribocorrosion behavior of CpTi in the oral environment: Synergistic interactions of wear and corrosion. *Journal of Biomedical Materials Research Part B: Applied Biomaterials*, 100B(6): 1662-1671, **2012**.

[230] M.P. Licausi, A.I. Muñoz, and V.A. Borrás. Tribocorrosion mechanisms of Ti6Al4V biomedical alloys in artificial saliva with different pHs. *Journal of Physics D: Applied Physics*, 46(40): 404003, **2013**.

[231] M.P. Licausi, A. Igual Muñoz, and V. Amigó Borrás. Influence of the fabrication process and fluoride content on the tribocorrosion behaviour of Ti6Al4V biomedical alloy in artificial saliva. *Journal of the Mechanical Behavior of Biomedical Materials*, 20: 137-148, **2013**.

[232] W. Huang, Z. Wang, C. Liu, and Y. Yu. Wear and electrochemical corrosion behavior of biomedical Ti–25Nb–3Mo–3Zr–2Sn alloy in simulated physiological solutions. *Journal of Bio and Tribo-Corrosion*, 1(1): doi:10.1007/s40735-40014-40001-40739, **2014**.

[233] M.T. Mathew, V.A. Barão, J.C.-C. Yuan, W.G. Assunção, C. Sukotjo, and M.A. Wimmer. What is the role of lipopolysaccharide on the tribocorrosive behavior of titanium? *Journal of the Mechanical Behavior of Biomedical Materials*, 8: 71-85, **2012**.

[234] M.J. Runa, M.T. Mathew, and L.A. Rocha. Tribocorrosion response of the Ti6Al4V alloys commonly used in femoral stems. *Tribology International*, 68: 85-93, **2013**.

[235] M.K. Dimah, F.D. Albeza, V.A. Borrás, and A.I. Muñoz. Study of the biotribocorrosion behaviour of titanium biomedical alloys in simulated body fluids by electrochemical techniques. *Wear*, 294–295: 409-418, **2012**.

[236] J.C.M. Souza, M. Henriques, R. Oliveira, W. Teughels, J.-P. Celis, and L.A. Rocha. Biofilms inducing ultra-low friction on titanium. *Journal of Dental Research*, 89(12): 1470-1475, **2010**.

[237] M.J. Runa, M.T. Mathew, M.H. Fernandes, and L.A. Rocha. First insight on the impact of an osteoblastic layer on the bio-tribocorrosion performance of Ti6Al4V hip implants. *Acta Biomaterialia*, 12: 341-351, **2015**.

[238] I. Hacisalihoglu, A. Samancioglu, F. Yildiz, G. Purcek, and A. Alsaran. Tribocorrosion properties of different type titanium alloys in simulated body fluid. *Wear*, doi:10.1016/j.wear.2014.12.017: **2014**.

[239] A.C. Vieira, L.A. Rocha, N. Papageorgiou, and S. Mischler. Mechanical and electrochemical deterioration mechanisms in the tribocorrosion of Al alloys in NaCl and in $NaNO_3$ solutions. *Corrosion Science*, 54: 26-35, **2012**.

[240] N. Papageorgiou. The relevance of cathode kinetics to the interpretation of triboelectrochemical corrosion. *Tribology International*, 66: 60-71, **2013**.

[241] N. Espallargas, R. Johnsen, C. Torres, and A.I. Muñoz. A new experimental technique for quantifying the galvanic coupling effects on stainless steel during tribocorrosion under equilibrium conditions. *Wear*, 307(1–2): 190-197, **2013**.

[242] M.P. Licausi, A.I. Muñoz, V.A. Borrás, and N. Espallargas. Tribocorrosion mechanisms of Ti6Al4V in artificial saliva by Zero-Resistance Ammetry (ZRA) technique. *Journal of Bio and Tribo-Corrosion*, 1(1): doi:10.1007/s40735-40015-40008-x, **2015**.

[243] F. Galliano, E. Galvanetto, S. Mischler, and D. Landolt. Tribocorrosion behavior of plasma nitrided Ti–6Al–4V alloy in neutral NaCl solution. *Surface and Coatings Technology*, 145(1–3): 121-131, **2001**.

[244] A.C. Fernandes, F. Vaz, E. Ariza, L.A. Rocha, A.R.L. Ribeiro, A.C. Vieira, J.P. Rivière, and L. Pichon. Tribocorrosion behaviour of plasma nitrided and plasma nitrided + oxidised Ti6Al4V alloy. *Surface and Coatings Technology*, 200(22–23): 6218-6224, **2006**.

[245] T.M. Manhabosco, S.M. Tamborim, C.B. dos Santos, and I.L. Müller. Tribological, electrochemical and tribo-electrochemical characterization of bare and nitrided Ti6Al4V in simulated body fluid solution. *Corrosion Science*, 53(5): 1786-1793, **2011**.

[246] G.B. de Souza, G.G. de Lima, N.K. Kuromoto, P. Soares, C.M. Lepienski, C.E. Foerster, and A. Mikowski. Tribo-mechanical characterization of rough porous and bioactive Ti anodic layers. *Journal of the Mechanical Behavior of Biomedical Materials*, 4(5): 796-806, **2011**.

[247] Y. Han, S.H. Hong, and K.W. Xu. Porous nanocrystalline titania films by plasma electrolytic oxidation. *Surface and Coatings Technology*, 154(2–3): 314-318, **2002**.

[248] E. Szesz, G. de Souza, G. de Lima, B. da Silva, N. Kuromoto, and C. Lepienski. Improved tribo-mechanical behavior of CaP-containing TiO_2 layers produced on titanium by shot

blasting and micro-arc oxidation. *Journal of Materials Science: Materials in Medicine*, 25(10): 2265-2275, **2014**.

[249] P. Soares, A. Mikowski, C.M. Lepienski, E. Santos, G.A. Soares, V.S. Filho, and N.K. Kuromoto. Hardness and elastic modulus of TiO_2 anodic films measured by instrumented indentation. *Journal of Biomedical Materials Research Part B: Applied Biomaterials*, 84B(2): 524-530, **2008**.

[250] R.L. Coble and W.D. Kingery. Effect of porosity on physical properties of sintered alumina. *Journal of the American Ceramic Society*, 39(11): 377-385, **1956**.

[251] A.F. Yetim. Investigation of wear behavior of titanium oxide films, produced by anodic oxidation, on commercially pure titanium in vacuum conditions. *Surface and Coatings Technology*, 205(6): 1757-1763, **2010**.

[252] Ç. Albayrak, İ. Hacısalihoğlu, S.Y. vangölü, and A. Alsaran. Tribocorrosion behavior of duplex treated pure titanium in simulated body fluid. *Wear*, 302(1–2): 1642-1648, **2013**.

[253] M.R. Garsivaz Jazi, M.A. Golozar, K. Raeissi, and M. Fazel. Evaluation of corrosion and tribocorrosion of plasma electrolytic oxidation treated Ti–6Al–4V alloy. *Surface and Coatings Technology*, 244: 29-36, **2014**.

[254] V.S. de Viteri, A. Igartua, R. Bayon, G. Barandika, C. Perez-Jorge, J. Esteban, and M. Martinez. Tribocorrosion and antibacterial behaviour of TiO_2 coatings obtained by PEO technique. in IEEE International Symposium on Medical Measurements and Applications (MeMeA). Lisbon, **2014**.

[255] S.A. Alves, R. Bayón, A. Igartua, V. Saénz de Viteri, and L.A. Rocha. Tribocorrosion behaviour of anodic titanium oxide films produced by plasma electrolytic oxidation for dental implants. *Lubrication Science*, 26(7-8): 500-513, **2014**.

[256] M. Jungner, P. Lundqvist, and S. Lundgren. Oxidized titanium implants (Nobel Biocare® TiUnite™) compared with turned titanium implants (Nobel Biocare® mark III™) with respect to implant failure in a group of consecutive patients treated with early functional loading and two-stage protocol. *Clinical Oral Implants Research*, 16(3): 308-312, **2005**.

[257] M. Jungner, P. Lundqvist, and S. Lundgren. A retrospective comparison of oxidized and turned implants with respect to implant survival, marginal bone level and peri-implant soft tissue conditions after at least 5 years in function. *Clinical Implant Dentistry and Related Research*, 16(2): 230-237, **2014**.

[258] X. Zhou, N.T. Nguyen, S. Özkan, and P. Schmuki. Anodic TiO_2 nanotube layers: Why does self-organized growth occur: A mini review. *Electrochemistry Communications*, 46: 157-162, **2014**.

[259] D. Losic, M.S. Aw, A. Santos, K. Gulati, and M. Bariana. Titania nanotube arrays for local drug delivery: Recent advances and perspectives. *Expert Opinion on Drug Delivery*, 12(1): 103-127, **2015**.

[260] T. Shokuhfar, S. Sinha-Ray, C. Sukotjo, and A.L. Yarin. Intercalation of anti-inflammatory drug molecules within TiO_2 nanotubes. *RSC Advances*, 3(38): 17380-17386, **2013**.

[261] C. Moseke, F. Hage, E. Vorndran, and U. Gbureck. TiO_2 nanotube arrays deposited on Ti substrate by anodic oxidation and their potential as a long-term drug delivery system for antimicrobial agents. *Applied Surface Science*, 258(14): 5399-5404, **2012**.

[262] N.K. Kuromoto, R.A. Simão, and G.A. Soares. Titanium oxide films produced on commercially pure titanium by anodic oxidation with different voltages. *Materials Characterization*, 58(2): 114-121, **2007**.

[263] A.L. Yerokhin, X. Nie, A. Leyland, A. Matthews, and S.J. Dowey. Plasma electrolysis for surface engineering. *Surface and Coatings Technology*, 122(2–3): 73-93, **1999**.

[264] H. Ishizawa and M. Ogino. Thin hydroxyapatite layers formed on porous titanium using electrochemical and hydrothermal reaction. *Journal of Materials Science*, 31(23): 6279-6284, **1996**.

[265] L. Huang, F. Peng, H. Yu, H. Wang, J. Yang, and Z. Li. The influence of ultrasound on the formation of TiO_2 nanotube arrays. *Materials Research Bulletin*, 45(2): 200-204, **2010**.

[266] R. Zhang, K. Jiang, Y. Zhu, H. Qi, and G. Ding. Ultrasound-assisted anodization of aluminum in oxalic acid. *Applied Surface Science*, 258(1): 586-589, **2011**.

[267] M.P. Neupane, I.S. Park, T.S. Bae, and M.H. Lee. Sonochemical assisted synthesis of nano-structured titanium oxide by anodic oxidation. *Journal of Alloys and Compounds*, 581: 418-422, **2013**.

[268] I. Tudela, Y. Zhang, M. Pal, I. Kerr, and A.J. Cobley. Ultrasound-assisted electrodeposition of composite coatings with particles. *Surface and Coatings Technology*, 259, Part C: 363-373, **2014**.

Biofunctionalization of titanium surfaces for dental implants

Chapter 3

Tribocorrosion behavior of anodic treated titanium surfaces intended for dental implants

Chapter 3

Published in Journal of Physics D: Applied Physics, 46: 404001. 2013

Tribocorrosion behavior of anodic treated titanium surfaces intended for dental implants

A C Alves[1], **F Oliveira**[1], F Wenger[2], P Ponthiaux[2], J-P Celis[3], L A Rocha[1,4]

1 - Centre for Mechanics and Materials Technologies (CT2M), Department of Mechanical Engineering, University of Minho, Campus de Azurém, 4800-058 Guimarães, Portugal

2 - Laboratoire de Génie des Procédés et Matériaux-LGPM, École Centrale de Paris, Grande Voie des Vignes, 92290 Chatenây-Malabry, France

3 - Dept. MTM-KU Leuven, Kasteelpark Arenberg 44, 3001 Leuven, Belgium

4 - Dep. Physics, Faculdade de Ciências de Bauru, Unesp - Universidade Estadual Paulista, 17033-360 Bauru, SP, Brazil

Abstract

Tribocorrosion plays an important role in the lifetime of metallic implants. Once implanted, biomaterials are subjected to micro-movements in aggressive biological fluids. Titanium is widely used as an implant material because it spontaneously forms a compact and protective nanometric thick oxide layer, mainly TiO_2, in ambient air. That layer provides good corrosion resistance, and very low toxicity, but its low wear resistance is a concern.

In this work, an anodizing treatment was performed on commercial pure titanium to form a homogeneous thick oxide surface layer in order to provide bioactivity and improve the biological, chemical and mechanical properties. Anodizing was performed in an electrolyte containing β-glycerophosphate and calcium acetate. The influence of the calcium acetate content on the tribocorrosion behavior of the anodized material was studied. The concentration of calcium acetate in the electrolyte was found to largely affect the crystallographic structure of the resulting oxide layer. Better tribocorrosion behavior was noticed on increasing the calcium acetate concentration.

1. Introduction

Titanium and its alloys are widely used in dental implants due to their mechanical properties, high corrosion resistance and adequate biocompatibility. The good biological response

and corrosion resistance result from the characteristics of the passive titanium oxide surface film that spontaneously forms on the surface of the material [1]. However, dental implants undergo complex physiological loads essentially due to mastication [2], and are always exposed to an intricate mechanical, (electro)chemical [3-5] and biological aggressive environment [6-8]. Consequently, an accelerated degradation of the material by tribocorrosion may occur. Such an interplay of a mechanical loading between surfaces and a corrosive environment results frequently in a synergistic effect [9, 10]. In most cases, wear leads to an increase in the corrosion rate of a metallic material due to the mechanical destruction of the passive film, while corrosion can also affect the friction and wear behavior. In fact, the nature of the tribological contact may change, as corrosion products become part of the contact region. Actually, due to the intrinsic low wear resistance of titanium and titanium alloys, their native passive film can be easily damaged under mechanical solicitations, and the resulting unprotected surface exposed to the corrosive environment experiences an increase in corrosion rate [3, 11]. This degradation process can result in the release of wear debris that may act as abrasive particles increasing the mechanical damage, and in the case of implants they can also be harmful for the human body [12]. Depassivation/repassivation phenomena occurring on metallic surfaces in between mechanical contact events can result in an acceleration of the overall degradation process [9, 10, 13, 14].

Surface properties play an essential role in the success of an implant [15-17]. In recent years, much effort has been made to improve the surface properties of titanium and titanium alloys in dental applications. Many surface modification techniques have been tried to achieve titanium surfaces with better biological properties, enhancing the osseointegration rate and the success of implant materials [18-23], and improving the mechanical properties to better withstand micro-movements between implants and bone in the oral cavity [24-26].

It is very important to tailor the properties of the surface, such as roughness, porosity, structure and composition, as well as to predict the tribocorrosion behavior [27]. Chemical, thermal and anodic treatments are some surface modification techniques applied to improve the surface properties of titanium and titanium alloys [17, 19].

Ishizawa and Ogino [28] were among the first authors to document the anodic treatment to produce titanium oxide films doped with bioactive elements. In their work, a mixture of β-glycerophosphate and calcium acetate was used as an anodizing electrolyte to incorporate Ca and P in the anodic oxide film, with a Ca/P ratio similar to that found in hydroxyapatite.

Precipitation of hydroxyapatite crystals was observed after a hydrothermal treatment, confirming the bioactivity of the surfaces.

Although the biological activity of modified titanium surfaces has attracted considerable attention over the past few years, there is still a lack of information on the tribocorrosion mechanisms acting in dental implants. The possibility of creating a bioactive surface film with good mechanical properties, resistant to tribocorrosive environments and interacting correctly with human tissues would be a significant progress in this field.

Recently, Yetim [29] studied the dry wear behavior of titanium oxide films produced by anodic processes on commercially pure titanium. The anodizing of titanium resulted in porous oxide films composed mainly of anatase and small amounts of rutile. Such thick oxide films improved the wear resistance of the material due to their self-lubricant properties.

Also, Henry et al [30] studied the tribocorrosion properties of 316L stainless steel and Ti6Al4V alloy in sulfuric acid. They concluded that the characteristics of the passive films formed on the surface of these materials, controlled by potentiostatic polarization, significantly influenced the coefficient of friction. In turn, repassivation kinetics during sliding was found to be strongly dependent on the sliding speed and applied load.

The tribocorrosion behavior of pure titanium in artificial saliva was investigated by Vieira et al [3]. They focused on the influence of pH and corrosion inhibitors. The addition of citric acid or anodic inhibitors improved the tribocorrosion behavior due to the nature of the electrochemical reactions in the contact area, allowing the formation of tribolayers, which lowered the coefficient of friction as well as the corrosion current.

Avoiding wear is necessary for guaranteeing a successful integration of implant materials. The production of micrometric wear particles and their influence on the osteoblast attachment and cytoskeleton architecture were recently studied by Saldaña and Vilaboa [31]. They observed that micrometric debris could negatively affect the mechanisms that regulate the osteoblast–substrate anchorage by reducing the ability of cells to interact with the surface.

In this work, anodic treatments were used to modify the surface state of commercially pure titanium (grade 2). Bioactive elements, namely Ca and P, were incorporated into the oxide film. Tribocorrosion mechanisms taking place on titanium and anodized titanium containing different Ca/P ratio are discussed.

2. Materials and Methods

2.1. Materials

Commercially pure titanium (cp-Ti grade 2) (Goodfellow Cambridge Limited, UK) samples were cut into square shape of 20x20x2mm. The samples were ultrasonically cleaned in acetone for 3 min and then etched in Kroll's reagent (2ml HF, 10ml HNO_3, 88ml H_2O) for 10 min. After chemical etching the cp-Ti samples were again ultrasonically cleaned for 15 min successively in propanol and water, and then dried with warm air.

2.2. Anodizing

The electrolyte used for the anodic treatment was a solution containing β-glycerophosphate disodium salt pentahydrate (β-GP) (supplied by Fluka-BioChemika) and calcium acetate monohydrate (CA) (supplied by Sigma-Aldrich). β-GP and CA were used as P and Ca suppliers, respectively, for the incorporation of these bioactive species in the oxide film. Concentrations of 0.15 M and 0.35 M CA were used while the β-GP concentration was kept constant at 0.02 M. The anodic treatment was performed at room temperature using a dc power supply (GPR-30H10D). This treatment was carried out for 1 min at a constant voltage of 300 V. The surface area of the titanium sample (anode) exposed to the electrolyte solution was 1.33 cm^2. A platinum plate was used as the cathode with an exposed area of 7.79 cm^2. The distance between the cathode and the anode was 8 cm. All the anodic treatments were carried out under magnetic stirring at 200 rpm.

2.3. Tribocorrosion Experiments

For tribocorrosion experiments, the anodized test samples were fixed in an electrochemical cell. The cell was mounted on a pin-on-disc tribometer (CETR– UMT-2), with the anodized surface facing upwards. In a three-electrode setup, the cp-Ti or anodized test samples were used as the working electrode, the counter electrode was a platinum electrode, and a saturated calomel electrode (Hg/Hg_2Cl_2/saturated KCl solution; SCE = +244 mV/NHE) was used as the reference electrode. The tribocorrosion tests were carried out in a 8 g/l sodium chloride solution. An alumina ball (diameter: 10 mm) was used as the counterbody, and was positioned on top of the test samples. Tribocorrosion tests were carried out under reciprocating sliding at an applied normal load of 1.5 N. The displacement amplitude was 10 mm, and the sliding frequency was 2 Hz. The time of testing was determined by the number of contact events (1000 and 7256) corresponding to testing times of 250 s and 1814 s, respectively.

During the sliding tests the tangential force was measured and the coefficient of friction was calculated by the following equation 3.1:

$$COF = \frac{Ft}{Fn} \quad (3.1)$$

where Ft (N) is the tangential force and Fn (N) is the normal load.

The open-circuit potential was measured before, during and after sliding, using a Gamry Instruments potentiostat/galvanostat (Reference 600). Before starting the sliding tests, all samples were immersed in the electrolyte for 1 h in order to allow the open-circuit potential to stabilize. To guarantee the reproducibility of the results, at least three samples for each condition were tested.

The surface roughness of the test samples was measured before anodizing using a high-resolution optical sensor STIL (model CHR150-N). The structure of the anodized films was analyzed by x-ray diffraction (XRD, Bruker D8 Discover) with Cu Kα radiation in the scan range (2θ) from 20° to 60°. The morphological microstructure and the chemical composition of the anodized layers on cp-Ti and in the wear tracks after the tribocorrosion tests were investigated by scanning electron microscopy (SEM, Model FEI Nova 200 (FEG/SEM)) and energy dispersive x-ray spectroscopy (EDAX, Pegasus X4M (EDS/EBSD)) attached to the SEM.

3. Results and Discussion

3.1. Surface Characterization

Representative SEM images of the etched cp-Ti surfaces and anodized titanium samples are shown in figure 3.1. Samples referred to as 015CA were anodized in the electrolyte containing 0.15 M calcium acetate monohydrate, while those denoted as 035CA were produced in the 0.35 M calcium acetate monohydrate solution.

Etched cp-Ti (figure 3.1(a)) shows a typical surface on which the granular structure of the material is visible. The surface roughness, Ra, of the etched samples was 0.40±0.06 μm.

Porous surfaces are obtained on titanium after anodizing (figures 3.1(b) and (c)). In fact, as soon as the cell voltage applied during anodizing reaches the dielectric breakdown voltage of the oxide film already formed, a porous structure is expected due to the very high local temperatures attained at the electrolyte/surface interface and the vigorous release of oxygen and/or water vapor [32]. The pore size and the amount of cracks in the anodic film increase when the calcium acetate concentration increases in the anodizing solution (see the inset in figure 3.1(c)). This is in accordance with the findings of Ishizawa and Ogino [28].

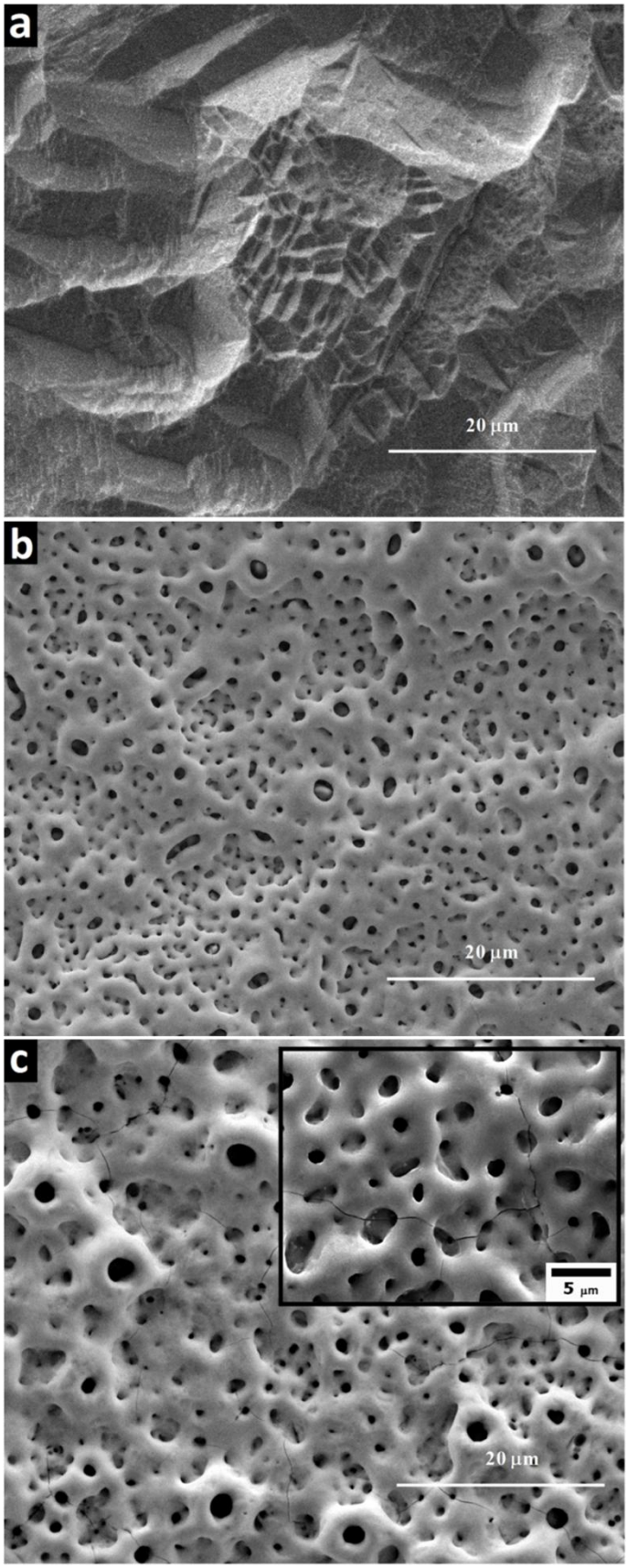

Figure 3.1 - SEM morphology of (a) etched cp-Ti, (b) anodized Ti sample 015CA, and c) anodized Ti sample 035CA

The amount of Ca incorporated into the oxide layers increases with increasing calcium acetate concentration in the electrolyte, as can be deduced from the Ca/P ratios presented in table 3.1. In both types of anodized samples, the Ca/P ratio in the oxide layer is approximately 8.5% of the Ca/P ratio in the electrolyte.

Table 3.1 - Ca/P ratio in the electrolyte and incorporated in the two types of anodized Ti-layers produced in this work

	015CA	**035CA**
Ca/P ratio (electrolyte)	18.68	39.34
Ca/P ratio (oxide film)	1.57 ± 0.14	3.53 ± 0.14

Representative XRD patterns obtained on the samples considered in this study are presented in figure 3.2. As can be observed, different structures are observed on the 015CA and 035CA samples: rutile appears at a higher calcium acetate monohydrate concentration in the electrolyte.

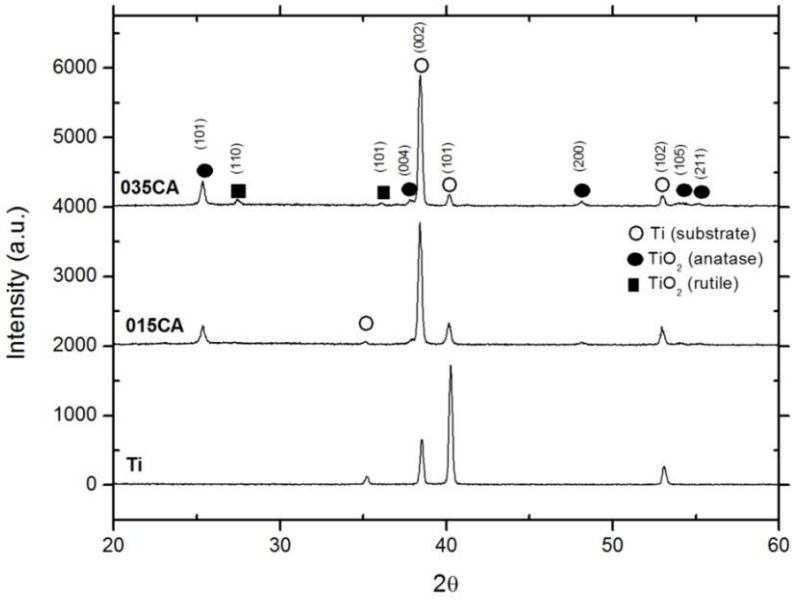

Figure 3.2 - X-ray diffraction patterns obtained on etched cp-Ti, anodized 015CA and 035CA samples

The thicknesses of the anodized layers are 3.42±0.97 μm and 4.39±1.14 μm on the 015CA and 035CA samples, respectively. A cross-section of the anodic layer on the 035CA samples reveals that it consists of three layers as seen in the image of figure 3.3(a) and in more detail in figure 3.3(b). A compact and uniform oxide layer (A) is formed at the interface with the bulk cp-Ti material, followed towards the surface of the anodized layer by two porous sub-layers.

The inner porous layer (B) is more compact and contains smaller pores compared with the outer porous layer (C). The structure of the 015CA samples was found to be similar.

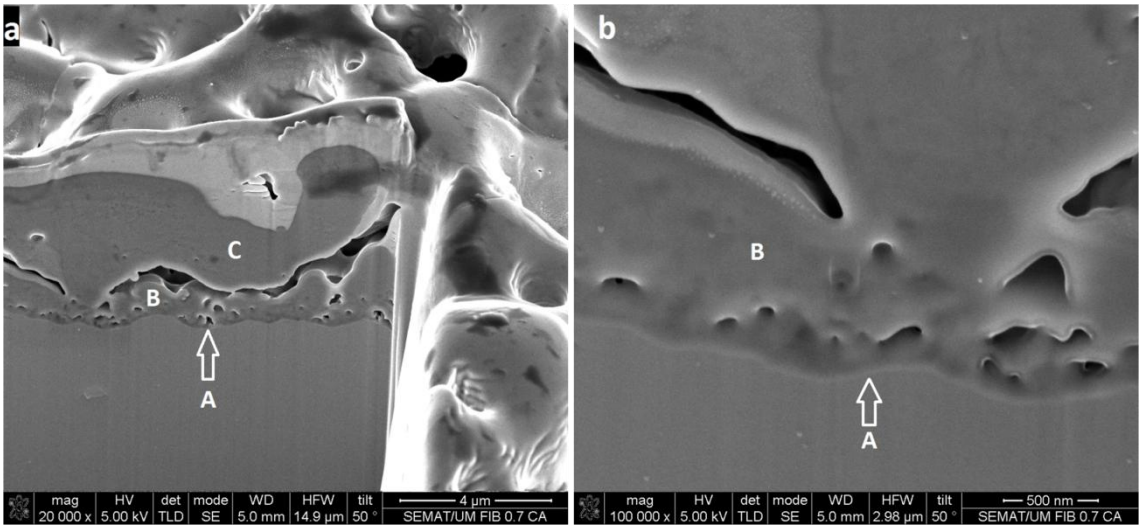

Figure 3.3 - FIB/SEM micrograph of the cross-section of the 035CA sample; a) overview of the cross-section; b) detail of the cross section focusing on the inner layers of the oxide film

3.2. Tribocorrosion results

3.2.1. Electrochemical behavior during sliding

The evolution of the open-circuit potential of the cp-Ti, 015CA and 035CA samples before, during and after sliding is shown in figure 3.4. In the case of figure 3.4(a) the duration of the sliding test corresponded to 1000 contact events, while in figure 3.4(b) 7256 sliding contact events took place.

On etched cp-Ti a significant potential drop from -0.3 V down to about -0.9 V occurred immediately after starting the sliding tests, suggesting a rapid destruction of the native passive oxide film due to the rubbing action of the alumina counterbody. Consequently, in the sliding track fresh active titanium becomes exposed to the solution, which causes the drop in the open-circuit potential. During sliding, the open-circuit potential shows small oscillations attributed to depassivation/repassivation phenomena during the successive contact events.

The open-circuit potentials recorded for the 015CA and 035CA samples before sliding are significantly higher than those observed on the etched cp-Ti (figure 3.4), indicating a decrease in the tendency to corrosion due to the presence of the anodic film.

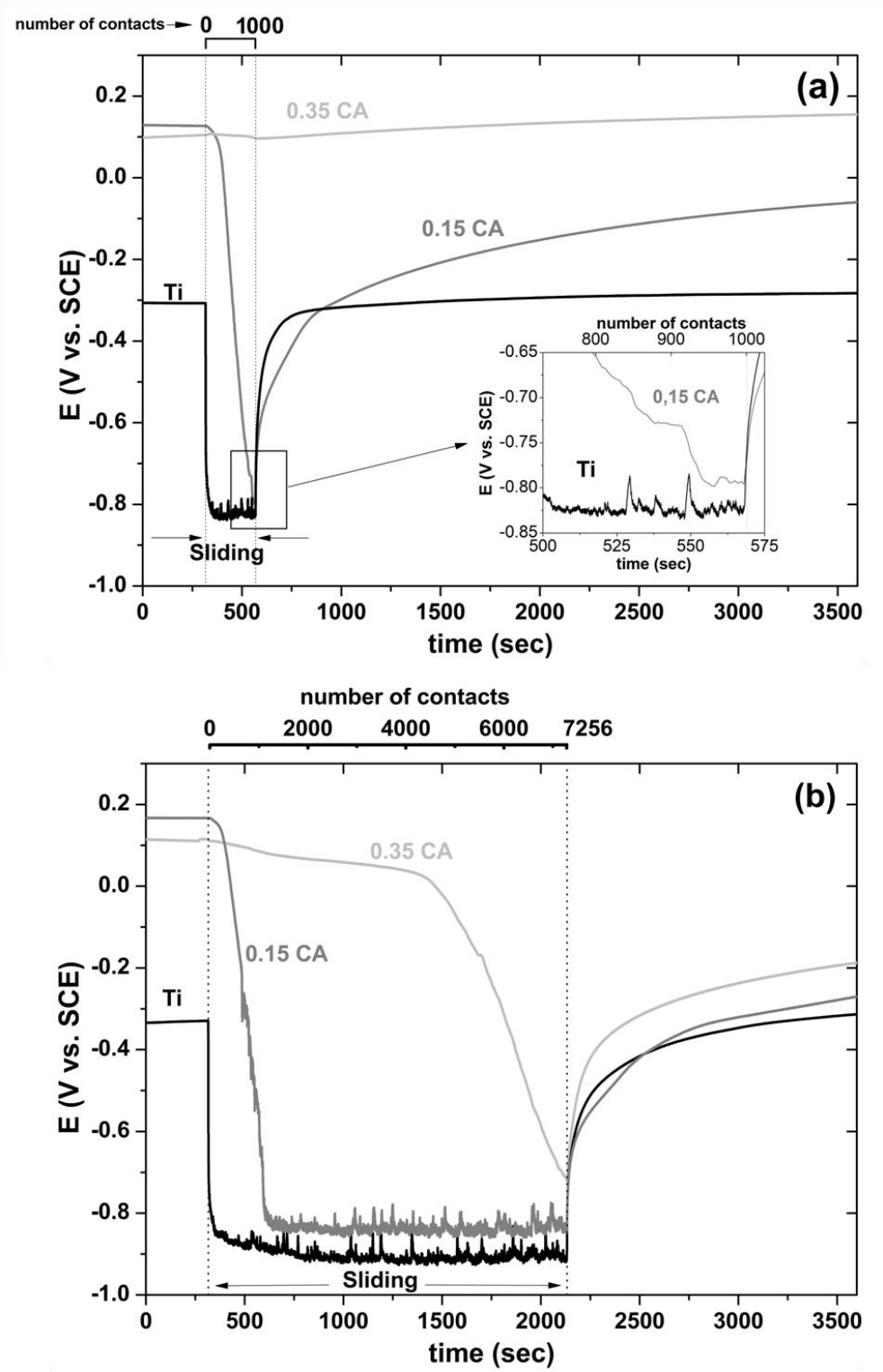

Figure 3.4 - Potential evolution recorded before, during and after reciprocating sliding tests against alumina ball on cp-Ti, 015CA, and 035CA samples immersed in 8 g/l NaCl for a) 1000 and b) 7256 contact events performed at 1.5 N and 2 Hz

Considering sample 015CA, as soon as sliding starts a monotonic decrease in the open-circuit potential is observed, at a rate much slower than that registered for cp-Ti. As can be observed in figures 3.4(a) and (b), after approximately 950 contact events, the open-circuit

potential reaches a low value of around -0.8 V, nearly similar to the one of etched cp- Ti. However, as shown in the inset in figure 3.4(a), before reaching the lowest electrochemical potential value, a short stabilization period is detected (around 10 s), after which the potential drops to about -0.8 V. As discussed above, a compact oxide layer is present between the porous film structure and the base titanium material (label A in figure 3.3). While sliding occurs in the porous layers (labels B and C in figure 3.3) a monotonic decrease in potential is recorded. Apparently, as soon as those porous layers are removed the counterbody starts sliding in the compact layer, which offers some additional resistance to be destroyed, in comparison with the porous layers. Consequently, while this compact layer is not damaged, it continues providing some corrosion protection, and a short stabilization of the open-circuit values is observed. Regarding the 035CA samples, distinctive behavior was observed. As seen in figure 3.4(a), no significant variation of the electrochemical potential is detected during sliding after 1000 contact events. Nevertheless, as observed in figure 3.4(b), when the number of contact events increases the open-circuit potential of the 035CA sample starts to decrease very slowly. In a second stage (from about 4500 contact events onwards) a faster decrease in potential occurs. Nevertheless, even after 7256 contact events, the open-circuit potential of the 035CA sample did not reach the one recorded on the 015CA sample and etched cp-Ti.

Once sliding is stopped, the open-circuit potential progressively increases to higher values for all samples. This reveals a progressive repassivation of the wear track area. It is evident from figure 3.4 that after some time of repassivation the open-circuit potential of etched cp-Ti reaches the value initially recorded before the start of the sliding test. The same is not verified for the anodized samples indicating that the oxide layers suffered significant damage during the sliding tests. Despite the fact that the potential of the anodized 015CA and 035CA samples never reaches the values recorded before the start of the sliding tests, the open-circuit potential of these samples once repassivated is still higher than that observed on etched cp-Ti.

According to Hanawa et al. [13] the evolution of the repassivation potential can be calculated using the following equation:

$$\Delta E = k_1 \cdot \log(t) + k_2 , \qquad (3.2)$$

where t is the time after interrupting the sliding, k_1 is the slope and k_2 is a constant. These parameters are determined by fitting measured values to the equation 3.2. In this way the evolution of the repassivation potential with time can be calculated by determining k_1, the slope of the curve. The values of k_1 and k_2 estimated in this work are summarized in table 3.2.

Table 3.2 - Parameters ΔE, k_1, and k_2, calculated from equation (3.2) as a function of the sliding contacts events

		Etched cp-Ti	015CA	035CA
1000 sliding contact events	**k_1(V/s)**	0.078 ± 0.037	0.233 ± 0.028	-
	k_2	-0.026 ± 0.070	-0.246 ± 0.108	-
	ΔE(V)	0.222 ± 0.062	0.493 ± 0.057	-
7256 sliding contact events	**k_1(V/s)**	0.122 ± 0.042	0.241 ± 0.012	0.240 ± 0.022
	k_2	0.080 ± 0.015	-0.238 ± 0.038	-0.188 ± 0.044
	ΔE(V)	0.467 ± 0.133	0.526 ± 0.031	0.572 ± 0.133

For both anodized samples, the k_1 values are substantially higher than that calculated for the etched cp-Ti, meaning that the overall repassivation process proceeds to a stronger extent on the anodized samples. The values of ΔE calculated through equation (3.2) also confirm this. The increase in potential after the end of the sliding tests was significantly higher on the anodized samples.

3.2.2. Coefficient of friction versus open-circuit potential

The evolution of the open-circuit potential and of the coefficient of friction with sliding time is shown in figures 3.5(a-c) for the etched cp-Ti, 015CA and 035CA samples, respectively.

As can be observed in figure 3.5(a), after a short running-in period, the coefficient of friction of the cp-Ti samples is kept relatively constant throughout sliding (around 0.45), as expected for this tribological pair. However, for the anodized samples distinctive behavior is observed. As seen in figure 3.5(b) (sample 015CA), the initial decrease in electrochemical potential, till about 950 contact events, is accompanied by an increase in the coefficient of friction that stabilizes at a value around 0.65 after an initial running-in period. However, as soon as the open circuit potential reaches the minimum value, similar to that recorded for the cp-Ti samples (figure 3.5(a)), an abrupt decrease in the coefficient of friction to around 0.45 is observed, indicating that sliding is now mainly occurring between the alumina sphere and pure titanium. In fact, as will be shown below (section 3.2.3), the anodic film is totally removed from the 015CA samples after 900 contact events, explaining the evolution of both the electrochemical potential and the coefficient of friction of these samples.

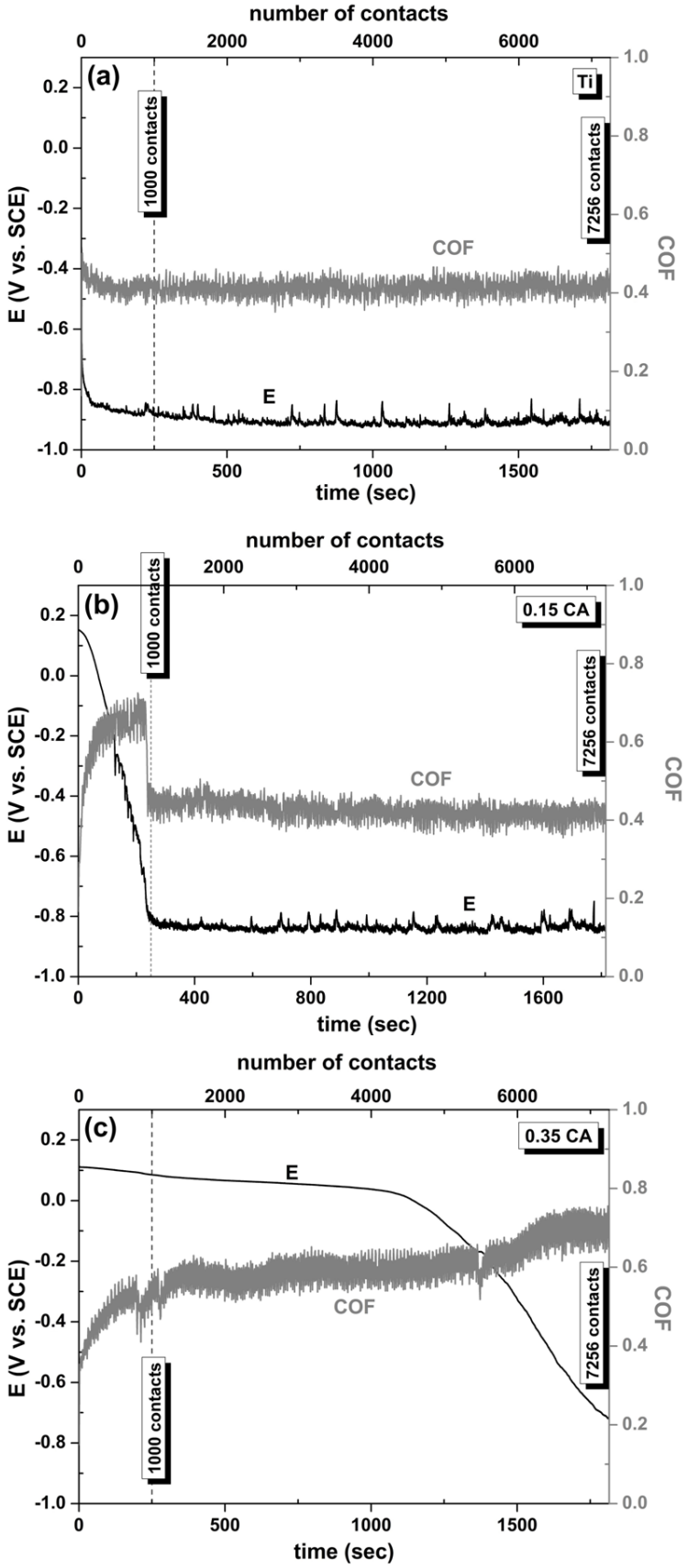

Figure 3.5 - Evolution of the open-circuit potential and coefficient of friction during sliding on a) cp-Ti, b) 015CA and c) 035CA samples up to 7256 contact events

On the 035CA samples (figure 3.5(c)), a very gradual decrease in potential is noticed at the early sliding stages while at the same time a slow increase in the coefficient of friction takes place, after the initial running-in period. After 4500 contact events, the damage caused by sliding leads to a faster drop in the open-circuit potential and to a small increase in the coefficient of friction to approximately 0.7. As will be shown below (section 3.2.3), after 7256 contacts sliding still occurs on the anodic film, as also indicated by the evolution of the electrochemical potential. These differences in coefficient of friction between the 015 and 035CA samples can also eventually result from the different surface structure. It should be mentioned that a higher coefficient of friction can be useful when considering implant dentistry, as the retention of the implant in contact with bone may be improved [33]. Additionally, crestal bone stress state around implants with porous surfaces was shown to be lower in comparison with machined surfaces, increasing the success of the osseointegration process [34].

3.2.3. Wear track characterization

Representative wear track profiles are shown in figure 3.6. Wear track depths (h), calculated from the wear track profiles, are also included in the figure. The wear track depth for the cp-Ti sample is 12.42±1.74 μm after 7256 contact events. As can be observed in figure 3.7, which presents representative micrographs of the central region of the wear track of the cp-Ti samples, adhesive wear along with some limited ploughing was the main mechanism identified in these samples.

As predicted from the results presented above, the wear track depth of the 015CA sample (13.82±0.65 μm) is larger than the initial oxide film thickness (3.42±0.97 μm) created in these samples after the anodic treatment. However, even if the removal of the oxide film occurs at a relatively low rate (see figure 3.4), the final wear depth for the 015CA samples is higher than that observed in the cp-Ti samples.

In figure 3.8, representative micrographs of the wear track region after different number of contact events is presented. As observed in the micrographs referring to the 015CA samples, wear debris (identified as titanium oxides) can be observed in the wear track (darker particles). A more pronounced ploughing might have occurred due to third-body abrasive mechanisms caused by wear debris produced during sliding on the anodic oxide film.

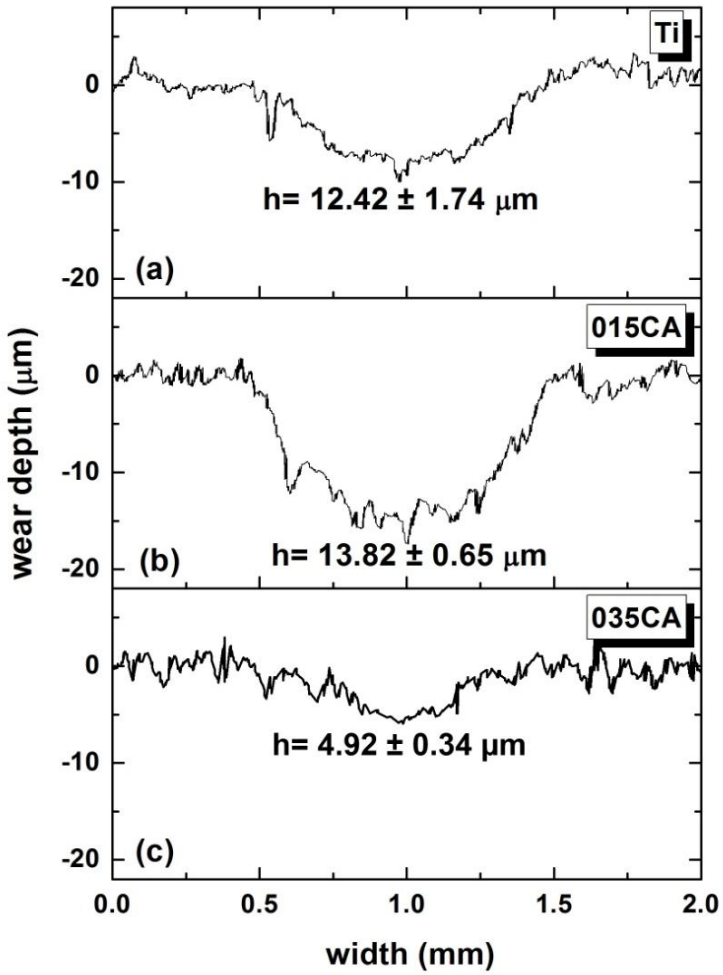

Figure 3.6 - Profilometry results of the three groups of samples after sliding tests for 7256 sliding contact events; a)etched titanium, b) 015CA , and c) 035CA samples

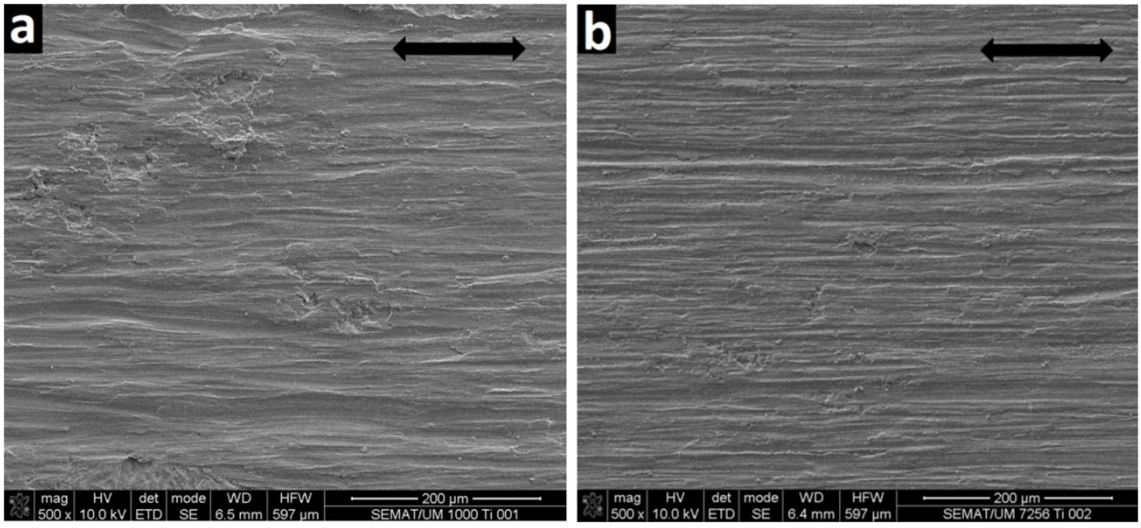

Figure 3.7 - SEM micrographs of the central part of wear tracks on etched titanium samples after a) 1000 and b) 7256 sliding contact events

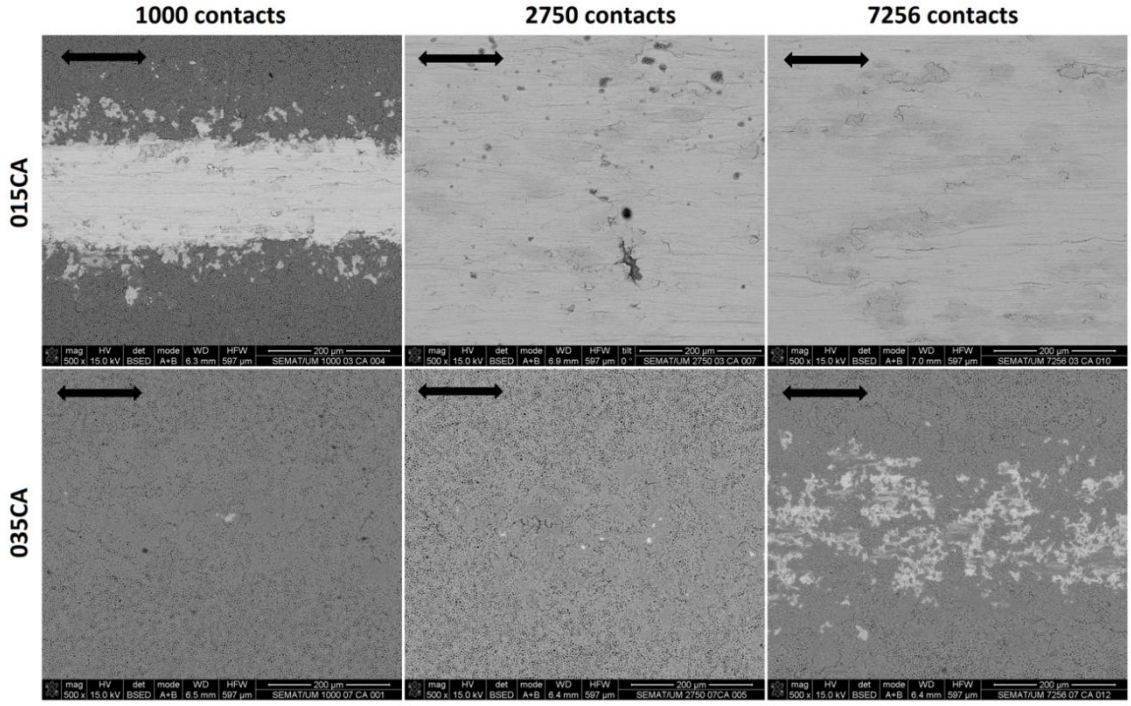

Figure 3.8 - SEM micrographs of wear tracks on anodized samples for 015CA and 035CA after tribocorrosion tests for different number of contact events

In the case of the 035CA samples, the wear track depth (4.92±0.34 μm) is of the same order of magnitude as the initial oxide film thickness (4.39±1.14 μm). As can be seen in figure 3.8, after 7256 contact events brighter areas (bulk titanium) start to appear indicating that the oxide film is almost worn out from the centre area of the wear track, in accordance with the results presented in figure 3.4.

As seen, the anodic oxide film on the 035CA samples showed much better tribocorrosion behavior when compared with the 015CA samples. The differences in the crystalline structure between the 015CA and 035CA samples may be hypothesized as a possible explanation for this dissimilar behavior. In fact, as shown above, rutile appears together with anatase on the 035CA samples, while the 015CA samples are composed mainly of anatase. According to Zywitzki et al. [35] the hardness of anatase is 8GPa, while rutile is associated with an increase in hardness up to 17 GPa. Hardness measurements were not performed in this work due to the porous and irregular structure of the surface.

Also the increased calcium content in the anodized surface film can be responsible for the observed differences, but the incorporation of calcium and phosphorous in the structure of the surface film is not yet fully understood, and the effects that these elements might have on the mechanical behavior of the surface films are still unknown.

In any case, an eventual increase in the hardness of the 035CA anodic film did not result in a dramatic augmentation of brittleness. In fact, as observed in more detail in figure 3.9, signs of some plastic deformation of the surface of the 035CA sample can be observed, but wear debris are generated and accumulated in the lower topographic planes and pores. Further investigations will try to understand this behavior in more detail.

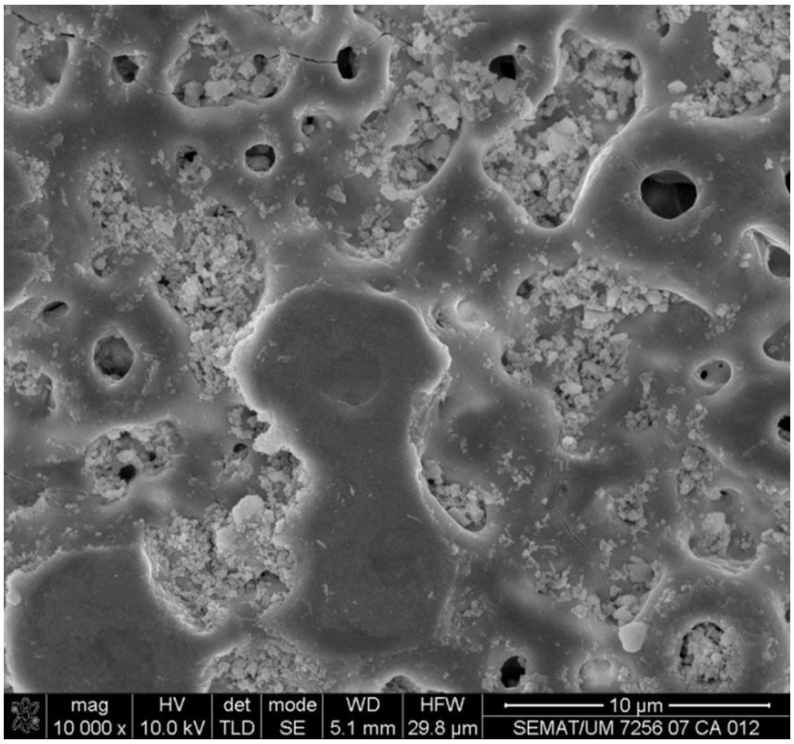

Figure 3.9 - SEM micrographs showing evidence of plastic deformation on the wear track of 035CA samples tested for 7256 sliding contact events

4. Conclusions

The effect of the amount of calcium acetate in the electrolyte used to anodize commercial pure titanium on the composition, structure and tribocorrosion behavior of the anodic films was investigated. The main outcomes of this work are the following:

- By changing the amount of calcium acetate of the electrolyte different surface states, in terms of topography, chemical composition and structure, can be obtained.
- The crystalline structure of the anodized films appears to play an important role in the tribocorrosion behavior once the presence of rutile results in a significant decrease in the mechanical damage after sliding.

- Nevertheless, once the anodic oxide film is worn out, the wear volume becomes higher, in comparison with that measured in cp-titanium under the same testing conditions, probably due to third-body mechanisms resulting from abrasive oxide wear debris that remains in the contact area.

Still, this work brings new insights into the tribocorrosion mechanisms of titanium surfaces used in dental implants, opening new perspectives for the improvement of their tribocorrosion behavior.

References

[1] X. Liu, P.K. Chu, and C. Ding. Surface modification of titanium, titanium alloys, and related materials for biomedical applications. *Materials Science and Engineering: R: Reports*, 47(3–4): 49-121, **2004**.

[2] M. Barry, D. Kennedy, K. Keating, and Z. Schauperl. Design of dynamic test equipment for the testing of dental implants. *Materials & Design*, 26(3): 209-216, **2005**.

[3] A.C. Vieira, A.R. Ribeiro, L.A. Rocha, and J.P. Celis. Influence of pH and corrosion inhibitors on the tribocorrosion of titanium in artificial saliva. *Wear*, 261(9): 994-1001, **2006**.

[4] V.A.R. Barão, M.T. Mathew, W.G. Assunção, J.C.-C. Yuan, M.A. Wimmer, and C. Sukotjo. Stability of cp-Ti and Ti-6Al-4V alloy for dental implants as a function of saliva pH – an electrochemical study. *Clinical Oral Implants Research*, 23(9): 1055-1062, **2012**.

[5] J.C.M. Souza, S.L. Barbosa, E. Ariza, J.P. Celis, and L.A. Rocha. Simultaneous degradation by corrosion and wear of titanium in artificial saliva containing fluorides. *Wear*, 292–293: 82-88, **2012**.

[6] P.E. Kolenbrander and J. London. Adhere today, here tomorrow: Oral bacterial adherence. *Journal of Bacteriology*, 175(11): 3247-3252, **1993**.

[7] J.C.M. Souza, M. Henriques, R. Oliveira, W. Teughels, J.P. Celis, and L.A. Rocha. Do oral biofilms influence the wear and corrosion behavior of titanium? *Biofouling*, 26(4): 471-478, **2010**.

[8] K.G. Neoh, X. Hu, D. Zheng, and E.T. Kang. Balancing osteoblast functions and bacterial adhesion on functionalized titanium surfaces. *Biomaterials*, 33(10): 2813-2822, **2012**.

[9] P. Ponthiaux, F. Wenger, D. Drees, and J.P. Celis. Electrochemical techniques for studying tribocorrosion processes. *Wear*, 256(5): 459-468, **2004**.

[10] S. Mischler. Triboelectrochemical techniques and interpretation methods in tribocorrosion: A comparative evaluation. *Tribology International*, 41(7): 573-583, **2008**.

[11] M. Niinomi. Mechanical biocompatibilities of titanium alloys for biomedical applications. *Journal of the Mechanical Behavior of Biomedical Materials*, 1(1): 30-42, **2008**.

[12] A. Sargeant and T. Goswami. Hip implants: Paper V. Physiological effects. *Materials & Design*, 27(4): 287-307, **2006**.

[13] T. Hanawa, K. Asami, and K. Asaoka. Repassivation of titanium and surface oxide film regenerated in simulated bioliquid. *Journal of Biomedical Materials Research*, 40(4): 530-538, **1998**.

[14] N. Diomidis, J.P. Celis, P. Ponthiaux, and F. Wenger. Tribocorrosion of stainless steel in sulfuric acid: Identification of corrosion–wear components and effect of contact area. *Wear*, 269(1–2): 93-103, **2010**.

[15] L. Le Guéhennec, A. Soueidan, P. Layrolle, and Y. Amouriq. Surface treatments of titanium dental implants for rapid osseointegration. *Dental Materials*, 23(7): 844-854, **2007**.

[16] K.-H. Kim and N. Ramaswamy. Electrochemical surface modification of titanium in dentistry. *Dental Materials Journal*, 28(1): 20-36, **2009**.

[17] M.B. Rosa, T. Albrektsson, C.E. Francischone, H.O. Schwartz Filho, and A. Wennerberg. The influence of surface treatment on the implant roughness pattern. *Journal of Applied Oral Science*, 20: 550-555, **2012**.

[18] X. Zhu, K.-H. Kim, and Y. Jeong. Anodic oxide films containing Ca and P of titanium biomaterial. *Biomaterials*, 22(16): 2199-2206, **2001**.

[19] T. Hanawa. Biofunctionalization of titanium for dental implant. *Japanese Dental Science Review*, 46(2): 93-101, **2010**.

[20] C. Rungsiyakull, Q. Li, G. Sun, W. Li, and M.V. Swain. Surface morphology optimization for osseointegration of coated implants. *Biomaterials*, 31(27): 7196-7204, **2010**.

[21] Y. Tsutsumi, M. Niinomi, M. Nakai, H. Tsutsumi, H. Doi, N. Nomura, and T. Hanawa. Micro-arc oxidation treatment to improve the hard-tissue compatibility of Ti–29Nb–13Ta–4.6Zr alloy. *Applied Surface Science*, 262: 34-38, **2012**.

[22] F.P.S. Guastaldi, D. Yoo, C. Marin, R. Jimbo, N. Tovar, D. Zanetta-Barbosa, and P.G. Coelho. Plasma treatment maintains surface energy of the implant surface and enhances osseointegration. *International Journal of Biomaterials*, 2013: 354125, **2013**.

[23] N.C.M. Oliveira, C.C.G. Moura, D. Zanetta-Barbosa, D.B.S. Mendonça, L. Cooper, G. Mendonça, and P. Dechichi. Effects of titanium surface anodization with CaP incorporation on human osteoblastic response. *Materials Science and Engineering: C*, 33(4): 1958-1962, **2013**.

[24] A. Bloyce, P.Y. Qi, H. Dong, and T. Bell. Surface modification of titanium alloys for combined improvements in corrosion and wear resistance. *Surface and Coatings Technology*, 107(2–3): 125-132, **1998**.

[25] S. Kumar, T.S.N.S. Narayanan, S.G.S. Raman, and S.K. Seshadri. Surface modification of CP-Ti to improve the fretting-corrosion resistance: Thermal oxidation vs. anodizing. *Materials Science and Engineering: C*, 30(6): 921-927, **2010**.

[26] C.R. Ramos-Saenz, P.A. Sundaram, and N. Diffoot-Carlo. Tribological properties of Ti-based alloys in a simulated bone–implant interface with Ringer's solution at fretting contacts. *Journal of the Mechanical Behavior of Biomedical Materials*, 3(8): 549-558, **2010**.

[27] Y. Yan, A. Neville, D. Dowson, and S. Williams. Tribocorrosion in implants - assessing high carbon and low carbon Co–Cr–Mo alloys by in situ electrochemical measurements. *Tribology International*, 39(12): 1509-1517, **2006**.

[28] H. Ishizawa and M. Ogino. Formation and characterization of anodic titanium oxide films containing Ca and P. *Journal of Biomedical Materials Research*, 29(1): 65-72, **1995**.

[29] A.F. Yetim. Investigation of wear behavior of titanium oxide films, produced by anodic oxidation, on commercially pure titanium in vacuum conditions. *Surface and Coatings Technology*, 205(6): 1757-1763, **2010**.

[30] P. Henry, J. Takadoum, and P. Berçot. Tribocorrosion of 316L stainless steel and TA6V4 alloy in H_2SO_4 media. *Corrosion Science*, 51(6): 1308-1314, **2009**.

[31] L. Saldaña and N. Vilaboa. Effects of micrometric titanium particles on osteoblast attachment and cytoskeleton architecture. *Acta Biomaterialia*, 6(4): 1649-1660, **2010**.

[32] N.K. Kuromoto, R.A. Simão, and G.A. Soares. Titanium oxide films produced on commercially pure titanium by anodic oxidation with different voltages. *Materials Characterization*, 58(2): 114-121, **2007**.

[33] Y.-T. Sul, B.-S. Kang, C. Johansson, H.-S. Um, C.-J. Park, and T. Albrektsson. The roles of surface chemistry and topography in the strength and rate of osseointegration of titanium implants in bone. *Journal of Biomedical Materials Research Part A*, 89A(4): 942-950, **2009**.

[34] R.M. Pilliar, G. Sagals, S.A. Meguid, R. Oyonarte, and D.A. Deporter. Threaded versus porous-surfaced implants as anchorage units for orthodontic treatment: Three-dimensional finite element analysis of peri-implant bone tissue stresses. *The International Journal of Oral & Maxillofacial Implants*, 21(6): 879-889, **2006**.

[35] O. Zywitzki, T. Modes, H. Sahm, P. Frach, K. Goedicke, and D. Glöß. Structure and properties of crystalline titanium oxide layers deposited by reactive pulse magnetron sputtering. *Surface and Coatings Technology*, 180–181: 538-543, **2004**.

Biofunctionalization of titanium surfaces for dental implants

Chapter 4

Micro-arc oxidation as a tool to develop multifunctional calcium-rich surfaces for dental implants applications

Chapter 4

For publication in Materials Science and Engineering: C

Micro-arc oxidation as a tool to develop multifunctional calcium-rich surfaces for dental implants applications

AR Ribeiro[1, 2,3], **F Oliveira**[3, 4], LC Boldrini[2], PE Leite[2], P Falagan-Lotsch[2], WF Zambuzzi[5], B Fragneaud[6], APC Campos[7], CP Gouvêa[7], BS Archanjo[7], CA Achete[7], E Marcantonio Jr[1], LA Rocha[3,8], JM Granjeiro[2,3,9]

1 - Department of Periodontology, Araraquara Dental School, University Estadual Paulista, Rua Humaitá 1680, 14801-903 Araraquara São Paulo, Brazil

2 - Directory of Metrology Applied to Life Science, National Institute of Metrology Quality and Technology, Av. N. S. das Graças 50, Xerém - Duque de Caxias, Rio de Janeiro, Brazil

3 - Brazilian Branch of Institute of Biomaterials, Tribocorrosion and Nanomedicine (IBTN/Br)

4 - Centre for Mechanical and Materials Technologies, University of Minho, Campus de Azurém, 4800-058 Guimarães, Portugal

5 - Departamento de Química e Bioquímica, Universidade Estadual Paulista – UNESP, Distrito de Rubião Junior S/N 18618-970, Botucatu, São Paulo, Brazil

6 - Physics Department, Federal University of Juiz de Fora (UFJF), Rua José Lourenço Kelmer, 36036-900, Minas Gerais, Brazil

7 - Metrology Materials Division, National Institute of Metrology Quality and Technology, Av. N. S. das Graças 50, - Xerém - Duque de Caxias, Rio de Janeiro, Brazil

8 - Departamento de Física, Universidade Estadual Paulista – UNESP, Av. Eng. Luiz Edmundo Carrijo Coube, 14-01, Bauru, São Paulo, Brazil

9 - Dental School, Fluminense Federal University, Niterói, Brazil

Abstract

Titanium (Ti) is commonly used in dental implants applications. Surface modification strategies are being followed in last years in order to build Ti oxide-based surfaces that can fulfill, simultaneously, the following requirements: induce cell attachment and adhesion, while providing a superior corrosion and tribocorrosion performance. In this work micro-arc oxidation (MAO) was used as a tool for the growth of a nanostructured bioactive titanium oxide layer aimed to enhance cell attachment and adhesion for dental implant applications. Characterization of the surfaces was performed, in terms of morphology, topography, chemical composition and crystalline structure. Primary human osteoblast adhesion to the developed surfaces was investigated in

detail by electronic and atomic force microscopy as well as immunocytochemistry. Also an investigation on the early cytokine production was performed. Results show that a relatively thick hybrid and graded oxide layer was produced on the Ti surface, being constituted by a mixture of anatase, rutile and amorphous phases where calcium (Ca) and phosphorous (P) were incorporated. An outermost nanometric-thick amorphous oxide layer rich in Ca was present in the film. This Ca-rich amorphous layer improved fibroblasts viability and metabolic activity as well as osteoblasts adhesion. High-resolution characterization techniques allowed to understand that osteoblasts adhered less in the crystalline-rich regions and preferentially attach and spread over the Ca-rich amorphous oxide layer. Also, these surfaces induce higher amounts of IFN-γ cytokine secretion, which is known to regulate inflammatory responses, bone microarchitecture as well as cytoskeleton reorganization and cellular spreading. These surfaces are promising in the context of dental implants, since they might lead to faster osseointegration.

1. Introduction

Titanium based materials are successfully used in dental implants due to their excellent biocompatibility and mechanical properties when implanted in the jaw. Despite the high success of titanium implants, the shortening of the oral rehabilitation time, without compromising osseointegration, still is a topic of particular interest in dentistry, due to its influence on the quality of life of patients. "Active" surfaces have been developed, aiming to accelerate osteogenesis in order to allow implant loading within 1 week subsequent to implant placement [1]. It has been reported that osseointegration rate is dependent on surface composition and roughness, where rough implants favor both bone anchoring and biomechanical stability. Also, osteoconductive calcium phosphate coatings stimulate bone healing, leading to the rapid fixation of the implants [2-6]. However, the bonding between the implant and bone tissue is not always satisfactory, while the adhesion of those coatings to the titanium substrate is a matter of concern [7, 8]. Surface modifications able to change surface energy, chemistry or topography to improve the early bone-to-implant response and guarantee a favorable outcome of the implant are being reported in the recent literature [2-4]. Among different surface functionalization techniques, special attention has been given to micro-arc oxidation which may promote an increase of surface bioactivity through the manipulation of the chemistry of the native TiO_2 layer by the incorporation of ionic species, such as calcium (Ca), phosphorus (P) and magnesium (Mg), elements natively present in bone [9-17]. It is already known that anodized titanium doped with

Ca and P ions interacts better with the surrounding bone and directly affects cellular responses such as osteoblast proliferation, differentiation, gene expression as well as the overall osseointegration process [15, 16, 18-24]. Dos Santos et al. [18] developed and characterized porous titanium oxide layers produced by anodic treatments and observed that those surfaces were hydrophilic without revealing any kind of cytotoxicity. Felgueiras et al. [16] recently demonstrated that these anodic surfaces enhance osteoblast attachment, differentiation (ALP production and mineralization) as well as osteointegration. In fact also clinical observations have shown that oxidized implants demonstrate stronger bone anchorage comparing to machined implants in both animal and human experiments [6, 8, 25].

Cell–surface interactions are also mediated at a molecular level. It has been shown that pre-osteoblast and fibroblast adhesion is influenced by the atomic structure of the titanium oxide surface due to the interaction between the functional groups of extracellular matrix proteins and the atomic order of these surface crystals [26-30]. Although several theories have been proposed, evidence of the effect of TiO_2 crystal structure on its biocompatibility remains inconclusive. While some works indicate an enhanced cell behavior to anatase [31-33], others refer that rutile promotes a better osseointegration [28, 29, 34]. Rutile has also a higher chemical stability comparing to anatase, exhibiting a superior apatite-forming ability, i.e. bioactivity [29, 34]. The successful interaction of hepatocytes and osteoblasts with rutile was already reported by some authors [26, 29]. On rutile-rich films produced on β-Ti alloys by micro-arc oxidation technique it was observed an improved osteogenesis performance [29, 34]. The crystallographic lattice matching of rutile with that of apatite was referred as a possible mechanism for this behavior, resulting in an excellent apatite-forming ability of rutile surfaces [34]. Differential affinities of macromolecules and proteins to the different TiO_2 crystallographic phases were also reported as possible mechanisms for that behavior [35]. Still regarding the crystalline structure, some works highlight the role of anodic treatments, as a method to obtain rutile-rich surfaces for better tribocorrosion behavior, thus minimizing the degradation of the material [13, 17, 36-38]. In fact, Alves et al. [13] demonstrated the important role of rutile in the improvement of the tribocorrosion behavior of the surfaces being used in this work.

In this work MAO was used as a tool to develop a new multiphasic nanostructured titanium oxide film with graded structure (anatase, rutile and amorphous phases) and chemical composition (essentially Ca). The main aim of this paper was to investigate bone derived cell attachment and adhesion to those surfaces. These initial cell events occurring on implant

surfaces are prerequisites for the success of osseointegration and bone regeneration process. As a proof of concept the *in vitro* adhesion mechanisms of primary human osteoblasts on these surfaces were investigated using electronic microscopy (SEM and TEM), coupled atomic force/Raman microscopy and immunofluorescence techniques. A study of the early gene and cytokines expression was also carried-out, since not much research has been focused on gene and cytokines regulation by anodic treated surfaces.

2. Experimental Section

2.1. Preparation and characterization of multifunctional titanium surfaces

A sheet of commercially pure titanium (Ti) grade 2 (Goodfellow Cambridge Ltd, UK)) with 2 mm thickness, was cut into squares of 10×10 mm and consecutively cleaned in acetone for 3 min and finally warm air-dried. Prior to anodic treatment, all the specimens were etched in a Kroll's reagent solution (2% HF, and 10% HNO_3, in 88% H_2O) for 10 min in order to remove the native oxide layer. These substrates were ultrasonically cleaned in propanol, water, and dried with warm air. The etched samples (Ti) worked as control samples.

The electrolyte used for the anodic treatment was a solution of 0.02M β-glycerophosphate disodium salt pentahydrate (β-GP) (Fluka-BioChemika) and 0.35M calcium acetate monohydrate (CA) (Sigma- Aldrich), with β-GP and CA being used as P and Ca sources, respectively. The anodic treatment was performed at room temperature using a dc power supply (GPR-30H10D). This treatment was carried out for 1 min at a constant voltage of 300 V [13].

A detailed surface characterization was performed on both surfaces (Ti and CaP). The surface morphologies and chemical composition analysis of Ti and CaP were studied with a field emission scanning electron microscope (FEI Magellan 400) equipped with an energy dispersive X-ray analysis unit (EDX). The structure and the topography of both surfaces was analyzed by the means of a coupled atomic force microscope/confocal Raman (Witec Alpha300 AR). The surface characterization was performed in 3 to 5 different specimens, depending on the characterization technique.

2.2. Biological tests

2.2.1. Cytotoxicity assay

Prior to cell culture tests, all disks were sterilized by autoclaving and by an ultraviolet light in a sterile culture hood for 2 h.

Extracts were collected for cytotoxicity assay in according to ISO 10993-12. Ti and CaP surfaces (3cm^2/mL) were immersed in culture medium Dulbecco's Modified Eagle's Medium (DMEM, Sigma) supplemented with 5% of fetal bovine serum (FBS, Gibco) at 37°C for 24 h. As a negative and positive control, it was used DMEM and sodium dodecyl sulphate (SDS 0.00005%, USB), respectively. As recommended, fibroblasts cells (L929, provided by Rio de Janeiro Cell Bank) were seeded in 96-well cell culture plate (1×10^4/well) and cultured in DMEM supplemented with 10% fetal bovine serum for 24 h at 37°C under 5% CO_2 and 95% air condition. After 24 h of cell exposure to each extract media, cytotoxicity was evaluated with a commercial kit (IN Cytotox, Xenometrix, Germany) which allows the evaluation of 3 different parameters of cell survival and integrity on the same sample: 2,3-bis[2-methyloxy-4- nitro-5-sulfophenyl]-2H-tetrazolium-5-carboxanilide (XTT), Neutral Red (NR) and Crystal Violet Dye Elution (CVDE). Mitochondrial dehydrogenase activity was measured by the XTT assay using a UV–Vis microplate reader with an absorbance of 480nm (Synergy II; Biotek Inst.). The same cells were washed and assayed and the lysosomal activity measured by the neutral red uptake test (NR). After 3 h of exposition to the dye, cells were fixed and the NR extracted and measured by the optical density (O.D.) of the supernatant at 540 nm. Finally fixed cells were washed and cell proliferation evaluated by crystal violet dye elution (CVDE). The dye extracted was measured at 540 nm absorbance in a UV–Vis microplate reader (Synergy II; Biotek Inst.). Each condition was tested on three replicates and three different assays. Mean values and standard deviations were submitted to one-way ANOVA.

2.2.2. Design of experiments: human bone derived cell studies

Primary human osteoblasts were isolated from human cancellous bone explants discarded in arthroplasty surgical procedures of adult healthy donors [39]. All procedures were carried out in accordance with a local Ethical Committee (Fluminense Federal University, Ethic Committee's register numbers: #232/08). Cancellous bone pieces were harvested, treated enzymatically with 0.2% collagenase (Sigma-Aldrich) for 2 h and then incubated in plastic flasks with DMEM with 10% FBS, at 37°C and 5% CO_2 atmosphere. After 7 days, the cells migrated from bone explants to plastic ground. The growth medium was changed every 2 days. Thereafter, when the cells reached 80-90% confluence, cells were detached by trypsinization (0.25% trypsin), suspended in fresh culture medium and its phenotype characterized. The osteoblast-like cells at 2-6 passages were used for *in vitro* studies. Those osteoblasts were then seeded ($5x10^3$ cells) on Ti and CaP

surfaces for 30 min, 2 h and 4 h and analyzed for estimating osteoblast behavior. Conventional culture well plates were used always as control for each set of experiments.

2.2.3. Scanning electron microscopy, focused ion beam and transmission electron microscopy

Primary human osteoblasts ($5x10^3$ cells) cultured in DMEM 10% FBS were seeded on different titanium surfaces for 30 min, 2 h and 4 h. Specimens with adhered cells were fixed at room temperature for 2 h with 2.5 % glutaraldehyde (Electron Microscopy Sciences) in 0.1 M cacodylate buffer (pH 7.4) (Electron Microscopy Sciences). After fixation, the specimens were washed several times and then postfixed for 1 h with 1% osmium tetroxide in distillate water. After washing they were subsequently dehydrated in a graded ethanol series of 30%, 50%, 70%, 80%, 90%, and 100% followed by critical point drying. Specimens were then mounted on a stub, gold coated and the morphology of osteoblasts was investigated in a field emission scanning electron microscope (FEI Magellan 400). A Nova NanoLab 600 Dual Beam instrument (FEI Company) equipped with a Focused Ion Beam (FIB) and a Scanning Electron Microscope (SEM) was used in order to analyze the interface between osteoblast and oxide layer. FIB cross-sections were performed on osteoblasts adhered for 2 h. Ion currents ranging from 7 nA down to 0.3 nA, and beam energy of 30 keV were used. Lower beam currents were used for the cleaning mill. SEM imaging was obtained by means of the electron column available. The cross-section was further analyzed using a SEM Magellan 400 (FEI Company) equipped with an energy dispersive X-ray spectroscopy (EDS) system. The FIB cross-sections were also analyzed by Transmission Electron Microscopy (TEM) using a probe-corrected FEI-FEG TITAN 80-300 operated at 300 kV. EDS in Scanning Transmission Electron Microscopy (STEM) mode was applied to investigate regions containing amorphous and crystalline nanostructures. Specifically, a coherent, focused probe was scanned across the specimen, and at each probe position, the resultant X-ray emission spectrum was recorded. Finally, an elemental map was constructed.

2.2.4. Immunocytochemistry

In order to verify the morphological changes of osteoblast cultured on different modified titanium surfaces, actin filaments were stained with phalloidin, as follows. Briefly, primary cells ($1x10^4$ cells) were seed on the different samples by specific culture times (30 min, 2h, and 4h), and then the cells were washed and fixed with 4% paraformaldehyde in PBS. Cells were then permeabilized with 0.5% Triton X-100 in PBS for 30 min and non-specific binding sites were blocked by incubating the samples with 5% bovine serum albumin (BSA, Sigma-Aldrich, USA) in

PBS for 30 min at room temperature. After 3x washing in PBS, cells were incubated with rhodamine TRITC-conjugated phalloidin (1:40) for 30 min and the nucleus was stained with ProLong® Gold Antifade Reagent with DAPI (Invitrogen, USA), as recommended by the manufacturer. Thereafter, stained cells were examined using a confocal microscope Leica TCS SP5. High-magnification immunofluorescence images were acquired using a 100x objective to study actin arrangement and cell nuclei using band-pass excitation (BP 488 and 405 nm respectively). Randomized images were acquired by using appropriate software.

2.2.5. Combined Atomic Force and Confocal Raman Microscopy System

The distribution and spreading of the osteoblasts cultured on different surfaces of titanium were evaluated by a coupled Atomic Force and Confocal Raman Microscopy system (Witec Alpha300 AR). For that, primary human osteoblasts ($5x10^3$ cells) were seeded on different titanium surfaces for 2 h and then were fixed and dehydrated as described above for electron microscopy evaluation. For this kind of analysis there was no need of coating. AFM/Raman imaging over areas of 40 μm^2 was performed since an area lower than that would be occupied by a spreaded osteoblast. These analyses were carried out on several cell extensions and samples.

2.2.6. Gene expression assay

In order to identify the expression of some gene related with responsive behavior of osteoblast in contact with the surfaces, 2 time points were selected: 30 min and 4 h, during which cells were properly cultivated on Ti-modified surfaces. Thereafter the only adherent osteoblasts were harvested in RNAlater solution (QIAGEN GmbH, Hilden, Germany) and stored until analysis. RNA extraction from osteoblasts was performed with RNeasy Mini Kit (Qiagen, Sweden) according to manufacturer's protocol. RNA purity and concentration were determined by spectrophotometry (Nanodrop 2000C, Thermo Scientific) at 260 nm and 280 nm using samples only with A260/A280 ratio equals or greater than 2.0. A quantitative polymerase chain reaction technique (qPCR) was applied for the evaluation of early gene expression response of osteoblasts for both surfaces, assessing the expression of two genes: peroxisome proliferator-activated receptor-gamma - PPARγ (inflammation) and Vimentin (cytoskeleton). The qPCR assays were carried out from three independent and different experiments. The reagents were purchased from Applied Biosystems, USA. The qPCR was performed using the AgPath-ID™ one step RT-PCR kit. Briefly, 1µl purified RNA (50 ng/µl) was reverse transcribed and amplified in a reaction mixture

containing 5 µl of 2x RT-PCR buffer, 0.4 µl of 25x RT-PCR enzyme mix, and 1.25 µl Yeast RNA 5 mg/mL (Ambion). mRNA of individual genes was quantified with the 7500 Real-Time PCR System (Applied Biosystems) with TaqMan Gene Expression Assays (Hs00185584-m1: Vimentin; Hs01115513-m1: PPARγ) using 0.5 µl of each assay 20x. The reference gene CASC3 (cancer susceptibility candidate gene 3) was used as an internal control to normalize the expression of target gene. Thermal cycling conditions comprised 10 min RT step at 45°C, a 10 min initial PCR activation step at 95°C (AmpliTaq Gold activation) followed by 40 cycles of 95°C for 15 s and 60°C for 45s each. Relative expression levels were calculated for each sample after normalization against the reference gene CASC3 using the ΔΔCt method for comparing relative fold expression differences.

2.2.7. Cytokine expression

The cells were cultivated during 4 h on both surfaces and supernatants collected for cytokine analysis. An 8-Plex panel was used, where the analysis includes IL-2, IL-4, IL-6, IL-8, IL-10, TNFα, INF-γ and GM-CSF. All experimental procedures were preceded by washing steps with the automated Bio-Plex Pro wash station (Biorad Laboratories Inc., Hercules, CA, USA), and the incubations done in the dark during 1 h with 350 rpm shaking at room temperature. After calibration and validation of the apparatus and reagents reconstitution, the assay was done according to the manufacturer recommendations with adjustments. Finally, magnetic beads were resuspended and read in the Bio-Plex MAGPIX apparatus (Biorad Laboratories Inc., Hercules, CA, USA).

2.3. Statistical analysis

Data from experiments characterizing the surface properties of Ti and CaP samples are presented as the mean ± one standard deviation (SD) of all the measurements performed on different specimens. Data from experiments examining cell response are presented as mean ± one standard deviation (SD) for three independent cultures. The concentration of each secreted product was quantified by the xPONENT software version 4.2 (Biorad Laboratories Inc., Hercules, CA, USA). All experiments were repeated at least twice to ensure validity of the observations and results from individual experiments are shown. GraphPad prism software was used to calculate the difference between sets of data based on analysis of variance (ANOVA). P values less than 0.05 were considered statically significant.

3. Results

3.1. Surfaces characterization

In figure 4.1, representative micrographs of the Ti and CaP surfaces are presented.

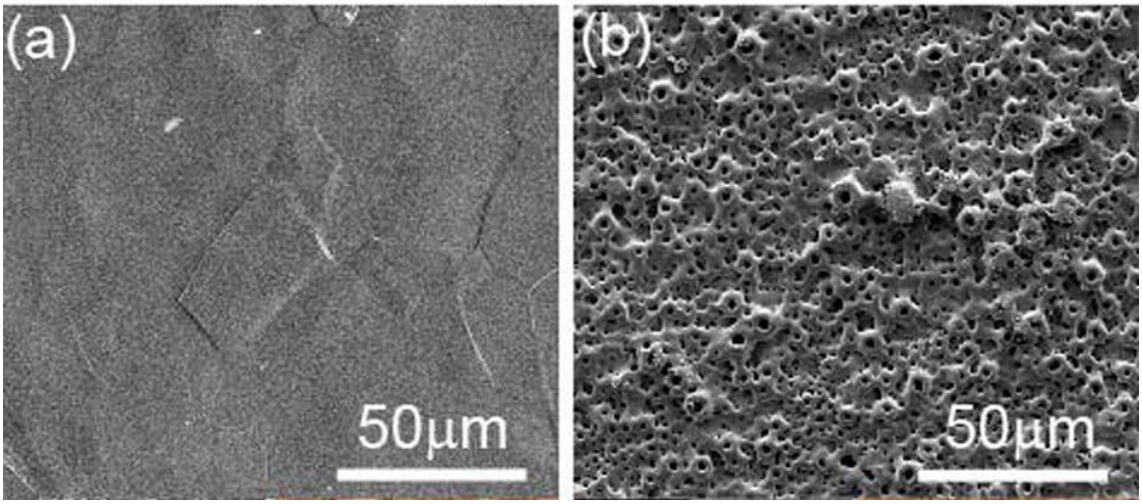

Figure 4.1 - Morphology of Ti surfaces: SEM micrographs showing a)Ti and b)CaP surface morphology.

As it can be observed Ti surfaces revealed a uniformly smooth surface with a typical granular structure revealed by the chemical etching (figure 4.1a). On the other hand, anodic oxidation demonstrates to be a suitable technique to produce a porous surface with nano/micro topographic features (figure 4.1b). Surface roughness (Ra data) at a micrometric scale measured by profilometry confirms the higher roughness for CaP surface comparing to Ti (Ti 0.4±0.06 µm; CaP 1.61±0.03 µm). However, no significant differences were observed at the nano-scale roughness evaluated by AFM (Ti 3.9±0.7 nm; CaP 4.2±0.3 nm). The distribution of the different crystallographic phases present on MAO treated surfaces was recently described [17]. It was observed that the oxide layer is made of a mixture of anatase and rutile phases where rutile is mainly located on the top of the porous structures ("volcanoes"). As for the incorporation of Ca and P on the oxide, the Ca/P ratio in the film is approximately 8.5% of the Ca/P ratio in the electrolyte [13].

3.2. Cytotoxicity of Ti and CaP surfaces

Results of the *in vitro* cytotoxicity tests evaluated by three different assays (NR, XTT, CVDE), after exposure to 24h extracts are given in figure 4.2.

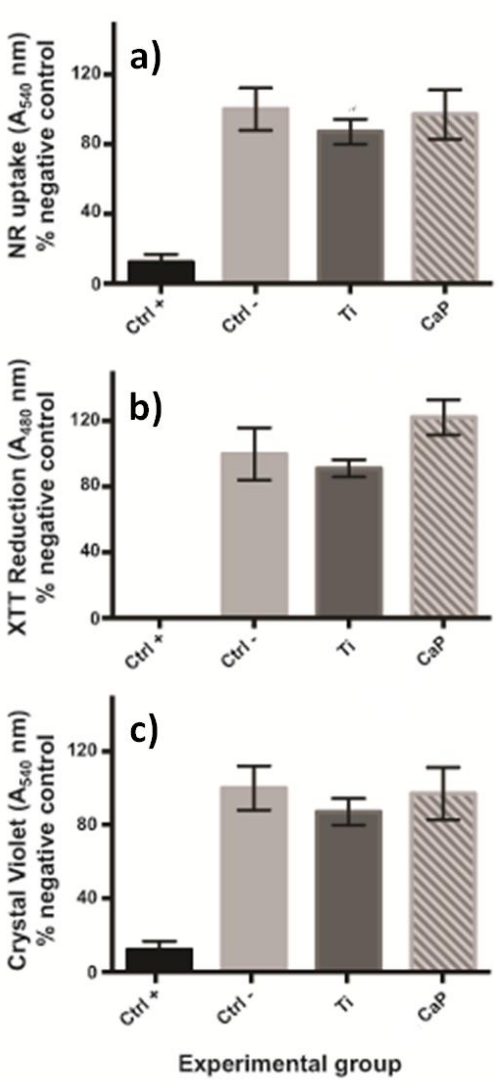

Figure 4.2 - Cytotoxic effects of Ti and CaP surfaces following ISO 10993-12. NR (a), XTT (b) and crystal violet (c), results are expressed as a percentage of the negative control (cells exposed to culture medium). Bars indicate mean±SD.

CaP surfaces improved cell viability and metabolic activity comparing to Ti. Results were always comparable or superior to the negative control condition (DMEM with 5% SFB). Neutral red stains viable cells, through the absorption of the dye, which becomes concentrated in lysosomes. Neutral red uptake of cells on CaP surfaces (figure 4.2a) was greater than the negative control and Ti. XTT is metabolically reduced by mitochondrial dehydrogenase in viable cells to a water-soluble formazan product, thus being used to evaluate cell viability. As observed in figure 4.2b, anodized titanium surfaces with Ca and P do not reduce the metabolism of fibroblasts. Crystal violet binds electrostatically to nuclear proteins and stains DNA. As shown in figure 4.2c, results indicate similar levels of CV inclusion for Ti and CaP groups when compared to the negative control.

3.3. Osteoblast early behavior on titanium surfaces

3.3.1. Osteoblast attachment, spreading, and morphology

SEM micrographs of figure 4.3 show the evolution of osteoblast morphology at 30 min, 2 h and 4 h on Ti and CaP surfaces.

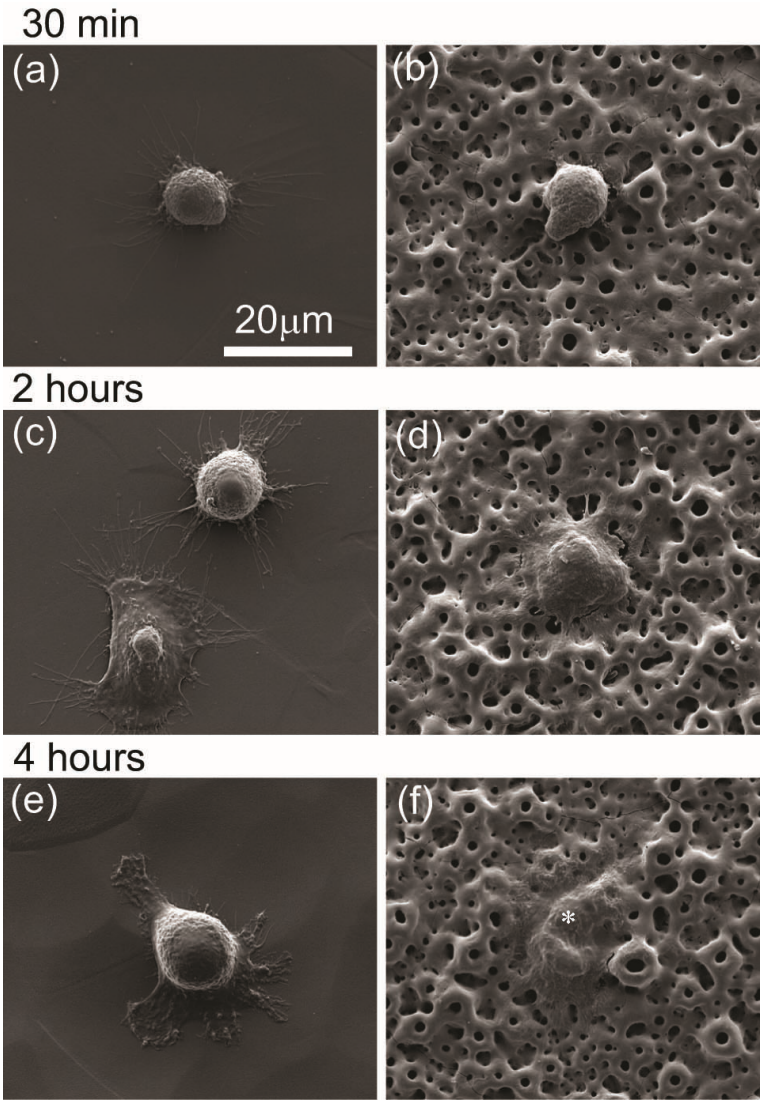

Figure 4.3 - Representative SEM images showing osteoblast morphology on Ti and CaP surfaces: osteoblast cells cultured on etched Ti (a, c, e) and CaP surfaces (b, d, f) for 30 min (a and b), 2 h (c and d) and 4 h (e and f). (*) on figure 4.3f represents the position of the osteoblast fully spread on CaP surface.

Morphological features were assessed in terms of cell adhesion and spreading on the surface. Primary human osteoblast cells grown on both Ti and CaP surfaces exhibited intact and well-defined phenotypic morphology. As shown in figure 4.3 (a and b) at 30 min, cells are initiating substrate adhesion, and their morphology remains round on both surfaces. With the increase of adhesion time, cells start to spread and well-developed lamellipodia and filopodia were formed on both surfaces (figure 4.3 c and d). These cytoplasmatic projections are

representative of the beginning of physical contact and support the cells posterior evolution. Nevertheless, osteoblasts adhered to CaP surfaces showed a more flattened cell body with a large network of cytoplasmatic extensions and substantial binding to the porous surface (see figure 4.3 d and f) while in the control group (Ti) cells kept hemispheroidal after 4 h of contact (see figure 4.3 c and e). With the exception of 30 min of cell adhesion where no significant differences were observed, osteoblasts cultured on CaP surfaces were larger, when comparing to cells grown on Ti, indicating enhanced cell spreading (figure 4.3 d and f).

Looking into detail to the interaction of osteoblasts with CaP oxide layers (figure 4.4 a and b), it is possible to observe that cells cover the porous structure accompanying surface morphology.

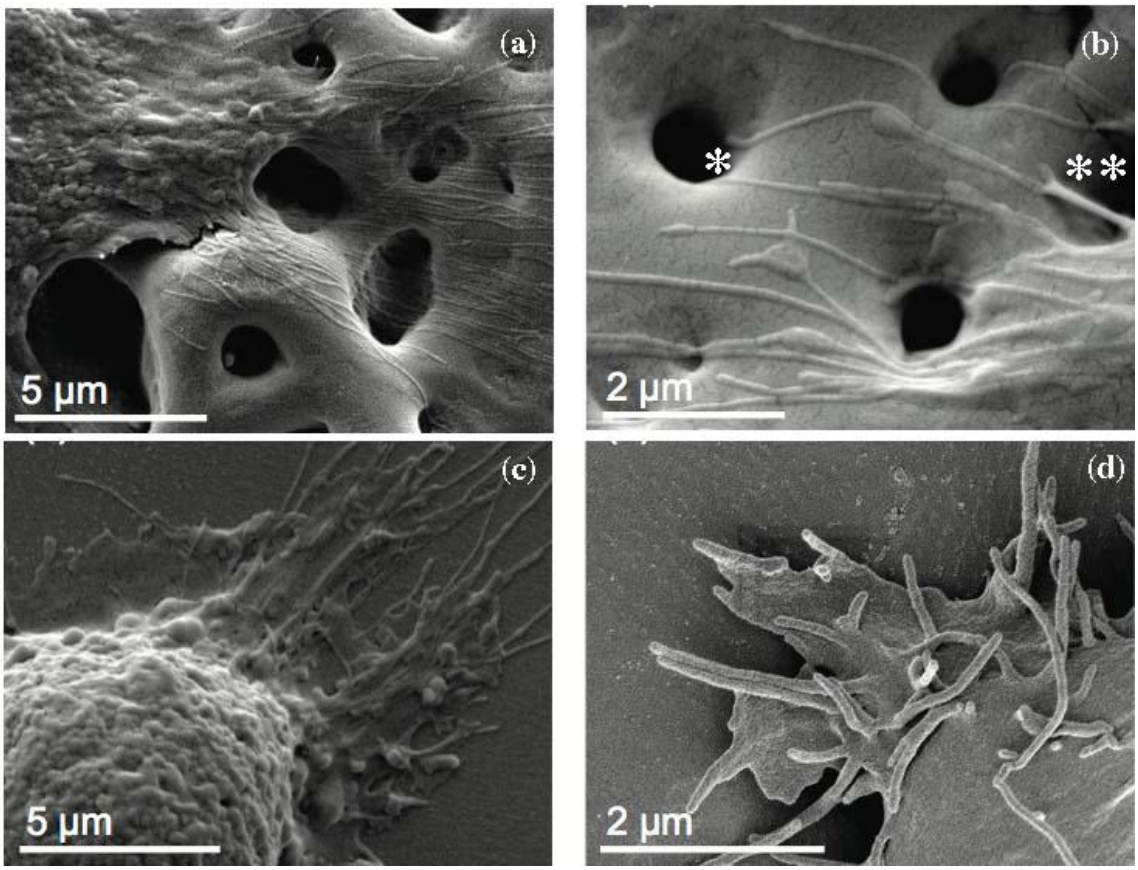

Figure 4.4 - High magnification SEM images presenting details of osteoblasts adhesion on CaP (a and b) and Ti surfaces (c and d). In figure b), mention to cytoplasmatic extensions penetrating (*) and crossing (**) the pores.

Also, as it can be observed in figure 4.4b, some cytoplasmatic extensions penetrate the pores present in the surface (*), while others tend to create bridges across them (**). Filopodia were also visualized on Ti etched surfaces (figure 4.4 c and d), however in a lower amount. In both surfaces, cells exhibited the appearance of metabolically active osteoblasts, with dorsal granules and numerous cytoplasmatic extensions.

3.3.2. Cytoskeleton organization

The actin cytoskeleton organization of primary human osteoblast cells at 30 min, 2 h and 4 h of cell adhesion was evaluated by confocal laser scanning microscopy and is presented in figure 4.5.

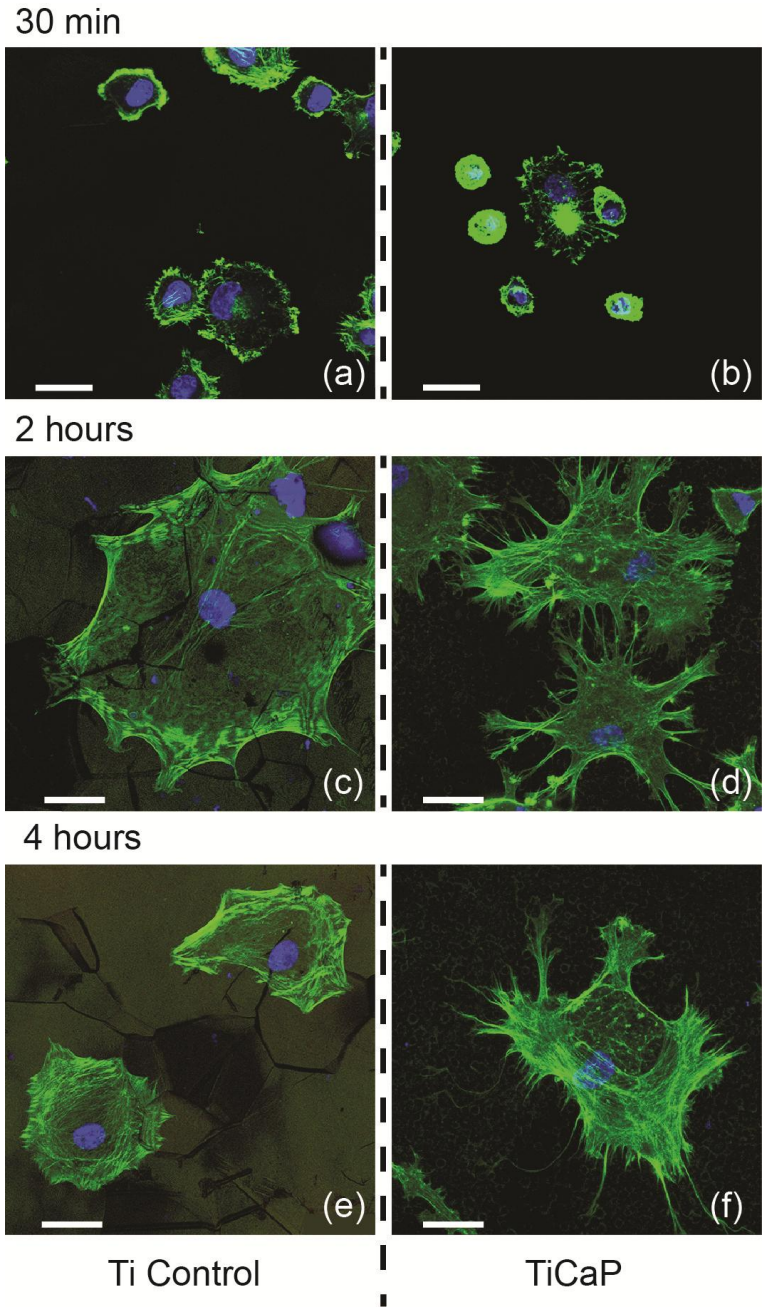

Figure 4.5 - Cytoskeleton organization: The changes in the actin cytoskeleton of primary human osteoblasts after 30 min (a and b), 2 h (c and d) and 4 h (e and f) of adhesion in Ti and CaP surfaces. Cells were stained by fluorescent phalloidin (green) and nucleus by DAPI (blue) and observed by confocal fluorescence microscopy.

As observed in figure 4.5, cells stained with TRITC-phalloidin show the presence of actin filaments on both surfaces. Images at 30 min of cell adhesion indicate that actin filaments appeared to be more concentrated at the periphery of the cells, allowing them to adhere and

properly adapt to the surfaces. At 2 h of osteoblast adhesion, there was a clear actin filament rearrangement to form actin stress fibers that were more prominent on CaP surfaces. In addition, the cells morphology on Ti surfaces at 2 h of adhesion showed a change ranging from rounded out cell form to spread and flatted cell morphology, presenting well-defined acting stress fibers distributed along of osteoblasts margins. Osteoblasts cultured on CaP with 2 h of adhesion were fully spread-out and with an extensive network of cytoplasmatic extensions extending to the underlying surface and establishing contact among neighbor cells. At 4 h of osteoblast adhesion, cells on both Ti and CaP surfaces exhibit microvillus and actin stress fibers distributed within the cytoplasm but also a peripheral actin layer (figure 4.5 e and f). Comparing both surfaces, it seems that CaP induces a more irregular distribution of actin fibers and the formation of higher content of cytoplasmatic extensions entering in direct contact with the porous surface.

3.3.3. Gene expression

A qPCR technique was applied for the evaluation of early gene expression response of osteoblasts for both surfaces. The study focused on the expression of a marker involved on the inflammatory pathway PPARγ and on cell cytoskeleton (vimentin). No significant differences on the PPARγ and vimentin expression for both Ti and Ti CaP surfaces were observed after 30 min and 4 h of osteoblast adhesion as seen in figure 4.6.

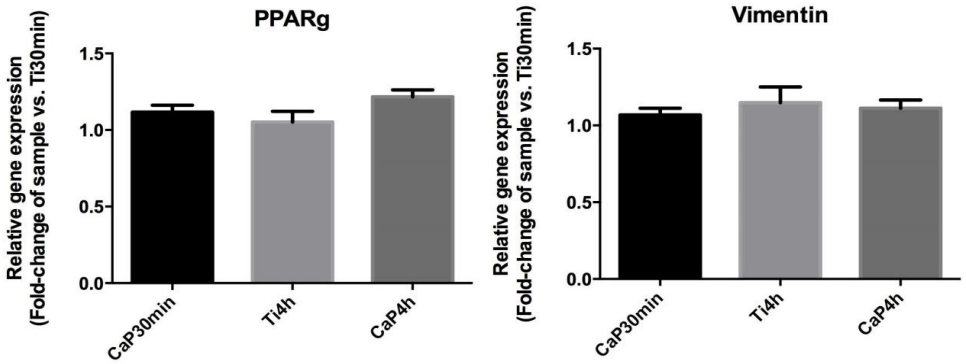

Figure 4.6 – Gene expression of PPARγ and Vimentin after 30 min and 4 h of cell adhesion. Results are expressed as a fold-change sample versus the Ti at 30 min of adhesion.

3.3.4. Cytokine expression

The supernatant of primary human osteoblasts cells cultivated on CaP surfaces during 4 h showed a higher increase of IFN-γ levels comparing to Ti control samples (figure 4.7a). No significant differences were observed on the levels of GM-CSF growth factor and IL-10 cytokine (figure 4.7 b and c).

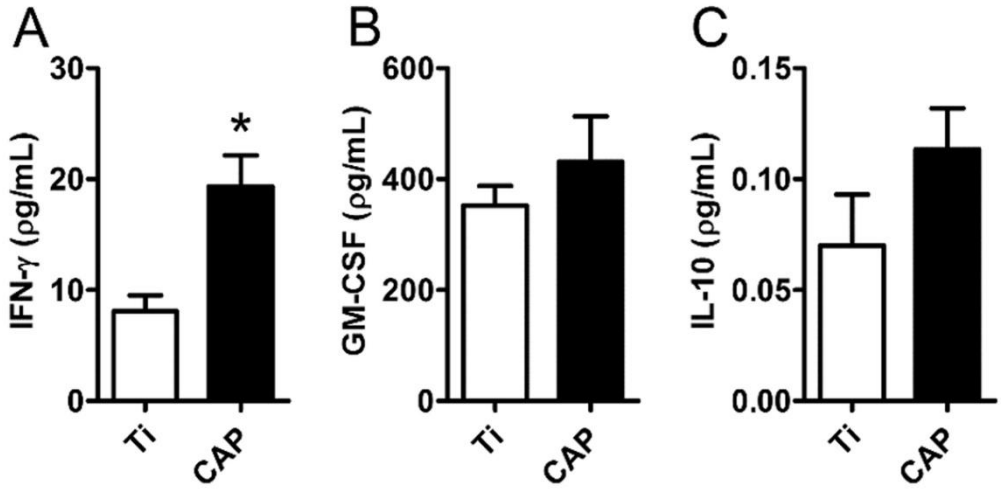

Figure 4.7 - Cytokines secreted by osteoblasts: in contact with Ti (control sample) and CaP surfaces after 4h of osteoblast adhesion.

4. Discussion

Usually, after implants are placed in the mandible or maxilla, a period of 3 to 6 months is required for enough bone/implant contact (osseointegration) to occur, allowing the implant to support masticatory loads. The reduction of the rehabilitation time after surgery will have a high impact on the quality of life of patients [1]. Evidence of successful immediate loading (i.e. immediately after surgery) arises from several clinical studies and is already in practice. However, in certain regions of the oral cavity, as in maxilla, osseointegration is still a challenge to be overcomed [40]. Over the last years, many surface functionalization strategies have been investigated in order to tailor more efficient osseointegrative surfaces while maintaining bulk material properties. It is accepted that the surface topography at the nano-micro-scale, surface chemistry, adsorbed proteins, surface energy and structure of the outermost surface layers of the implant strongly influence the interaction of implants with cells [41-47]. Nevertheless controversy still exists on the individual and joint contribution of those parameters for the complex cell/surface interactions mechanisms. The current study had two main goals: use of the MAO technique as a tool to develop a new nanocomposite graded titanium oxide structure doped with Ca and P and to investigate the role of this film on early osteoblast adhesion behavior.

4.1. Early osteoblast response to Ti surfaces

Results obtained in this work indicate that primary human osteoblastic cells adhere with different spreading characteristics on CaP surfaces comparing with the Ti used as control. Through the morphological analysis, osteoblastic cells presented a round shape and undergone relatively less cell spreading on Ti surfaces, indicating a possible lack of adhesion that is

commonly observed for non-proliferating cells. This is probably related with signaling-induced cell death by a decreasing of survival pathways [20, 48-50]. On contrast, osteoblasts on CaP surfaces were well-spread presenting a polygonal cell shape, covering more surface area and presenting a different organization of the cytoskeleton. This is an indication of a good interaction with the substrate. In fact, immunocytochemistry results revealed that CaP surfaces reorganize cell cytoskeleton with an enhanced formation of well-organized stress fibers, indicating that the cells are firmly attached to the surface. On other words, the enhanced cytoskeletal rearrangement of the cells cultured on CaP suggests that these surfaces play an active role on the events governing osteoblastic cell behavior, at least for the early stages of interaction [44, 51-53]. These outcomes are in agreement some previous reports, where it was proposed that during osteoblast adhesion there are different pathways triggering the modulation of actin-filament rearrangement [48-50]. Actin stress fibers are usually closely associated with cell maturation and its tighter adhesion to the implant surface. As well the degree of cytoskeletal organization could be related with focal contact formation [49, 50].

Some cases of early dental implant failures are related with inflammation [54]. PPARγ is a gene that modulates inflammation and also has a well-known important anti-inflammatory action in human dental pulp cells. PPARγ also plays a strong role in increasing pulp cells viability, odontoblastic differentiation, and dentin mineralization under oxidative stress [55-57]. Vimentin is known to be an intermediate cytoskeleton filament that regulates cell attachment, subcellular organization/traffic and signal transduction [58]. No significant changes were observed in the expression of PPARγ and Vimentin when comparing Ti with CaP surfaces. However, gene expression changes may occur after a few min or several hours, depending on the response to a specific stimulus. In fact, some papers report gene expression changes in cells, up to 30 min after the contact with a specific biomaterial [59, 60]. Cell adhesion is the first event that occurs during contact between a cell and a substrate. In the same way, the inflammation process can start in a very short time after the cell-biomaterial contact. Since Vimentin is related with focal adhesion and PPARγ is a transcription factor produced in early stages after inflammatory stimuli, it seems reasonable to think that 30 min and 4h exposures could be enough to affect the expression of these genes. Thus, these results suggest that both surfaces are not inducing a high inflammation process or alterations in the cell adhesion process.

Nevertheless, it was observed significant higher levels of the pleiotropic IFN-γ cytokine in the CaP samples in comparison with the Ti control. The IFN-γ cytokine is involved in the

regulation of nearly all phases of immune and inflammatory responses, including the activation, growth and differentiation of many cell types [61, 62]. Regarding the bone microenvironment, IFN-γ is produced locally and plays a crucial role on bone microarchitecture and its mechanical properties. Indeed, the activation of IFN-γ signaling pathways is an important physiologic mechanism to prevent osteoporosis; the administration of IFN-γ increases bone mass in mice through the induction of bone formation [63]. The increased levels of IFN-γ secreted by cells in contact with CaP surfaces can be associated with several functions such inflammatory regulation, osteoblast cellular differentiation as well as cytoskeleton reorganization and cellular spreading.

4.2. Influence of surface structure and chemistry on osteoblast response

In figure 4.8, is shown the distribution of crystalline phases on CaP sample with an attached osteoblast on the surface, obtained by coupled AFM/Raman.

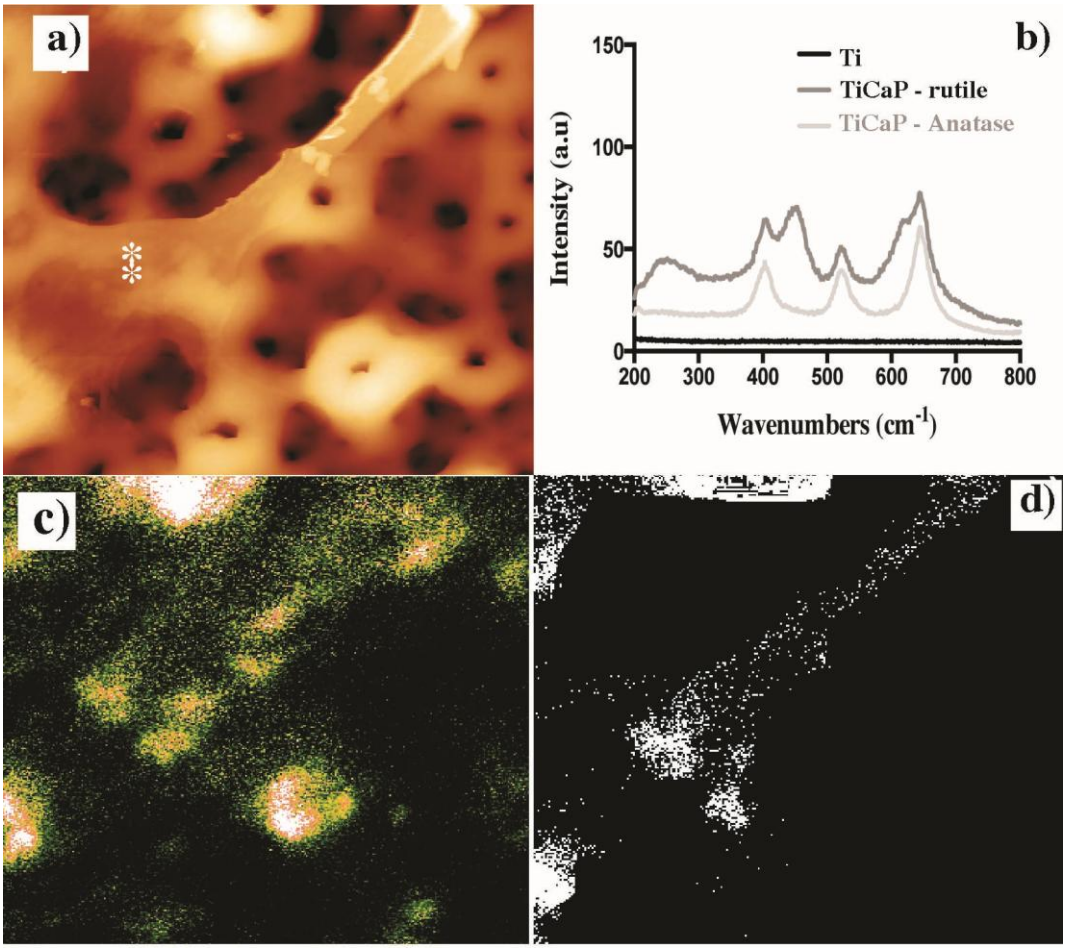

Figure 4.8 - Osteoblast spreading over CaP surface: a) Topographical image showing cytoplasmatic extension of an osteoblast (**) spreading over the porous surface. b) Raman spectra of Ti and CaP surfaces. c) Distribution of rutile (bright spots) and anatase (dark regions) in the area considered in a). d) Combination of distribution of rutile beyond osteoblast cytoplasmatic extension.

Figure 4.8a, shows the topographic image of an osteoblast cytoplasmatic extension (identified with **) laying on CaP substrate. As for figure 4.8b, a Raman spectra obtained in different points of the surface indicates the presence of anatase or anatase + rutile. In fact, the top of the volcanoes-like structures presents a mixture of rutile and anatase as seen in figure 4.8c (rutile: brighter areas; anatase: darker areas), while the valleys of the surface are mostly constituted by anatase or amorphous titanium oxide. By overlapping the image of the cytoplasmatic extension with the rutile rich areas of the surface (figure 4.8d), it was possible to observe that filopodia preferentially spread over the area of the surface in which higher amount of rutile phase was observed. These results indicate that osteoblasts appear to spread preferentially along the regions of the surface where rutile is present. This behavior could explain why filopodia sometimes penetrate well the surface pores of the oxide film, while in other cases they form bridges across the pores as shown in figure 4.4b.

To further understand the preferential spreading of osteoblasts through different areas of the surface, the osteoblasts/CaP interfaces were investigated by transmission electron microscopy (TEM).

Figure 4.9a presents a cross-section of the bio-interface, where it is possible to see the outer protective layer used for the FIB etching (platinum), an osteoblast cell, the CaP layer and the bulk Ti. In several regions of the analyzed cross-sections, a good adhesion of the osteoblast to the oxide layer was observed, essentially at the top of the volcanoes-like structures (see * in figure 4.9a). However in some locations of the surface the cells didn't adhere (marked as ** in figure 4.9a). Looking into detail to the cross-section of the oxide film (figure 4.9b), it was possible to observe that amorphous phases (not detected by AFM/Raman) are present in the constitution of the oxide film, which has a nanocomposite-graded structure. As shown in figure 4.9b, the inner part of the film is composed of a mixture of crystalline and amorphous material, while in the top of the oxide film a nanometric amorphous region covers some parts of the surface, often over the rutile-rich regions, i.e. on the top of the volcanoes-like structures. In fact, FFT patterns of the crystalline regions revealed nanocrystals of rutile in the top part of the oxide film (essentially at the volcanoes-like regions, and most of the times below the amorphous oxide film) in opposition to the inner part of the film, where only anatase phase was found.

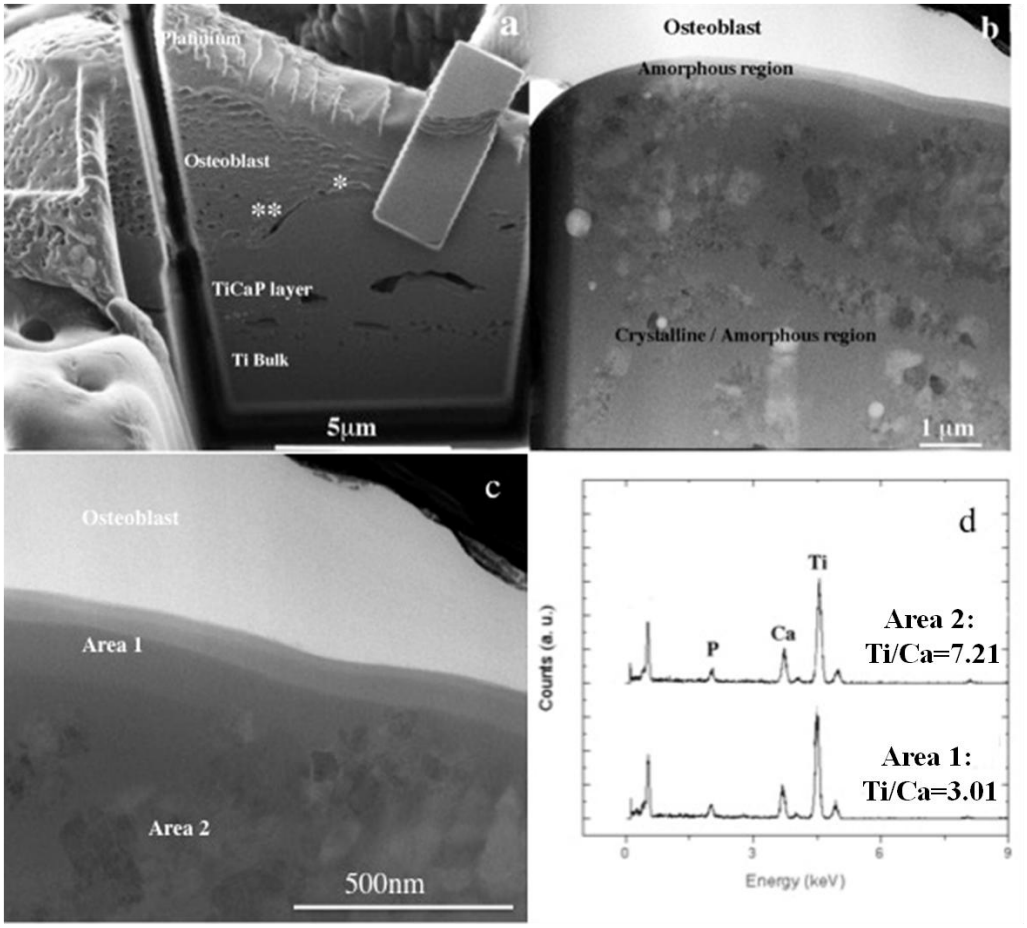

Figure 4.9 - Biointerface between osteoblast and CaP surface: a) FIB/SEM cross-sectional image of the osteoblast/CaP interface after 2 h of osteoblast adhesion (* and ** correspond respectively to osteoblast non-adhesion and adhesion regions as seen in b). b) Bright field TEM image of the cross section, showing the amorphous and crystalline regions of the thick oxide layer. c) High angle annular dark field (HAADF) TEM image of osteoblast adhered on the oxide layer. d) EDS of area 1 and 2, showing the distribution of Ca and P in the amorphous and crystalline areas.

As observed in figure 4.9b, the cell is well adhered to the surface when the amorphous nanometric film is present, but not when the surface is made of a mixture of crystalline and amorphous phases. Additionally, EDS analysis in figure 4.9d, performed in the HRTEM indicate that Ca is preferentially retained on the amorphous regions (area 1) of the oxide film in comparison to the crystalline phases (area 2). Indeed, while Ca incorporates preferentially in the amorphous regions of the oxide film, P distribution was more homogenous within the film thickness.

For clarification, in figure 4.10 a schematic representation of the mechanism of osteoblast adhesion to these surfaces is presented. As shown in this figure, the oxide film possesses a graded structure in which the amount of the Ca-rich amorphous phase increases at the places where the film thickness is higher, being in these Ca-rich surface regions that the adhesion of the cell is more effective.

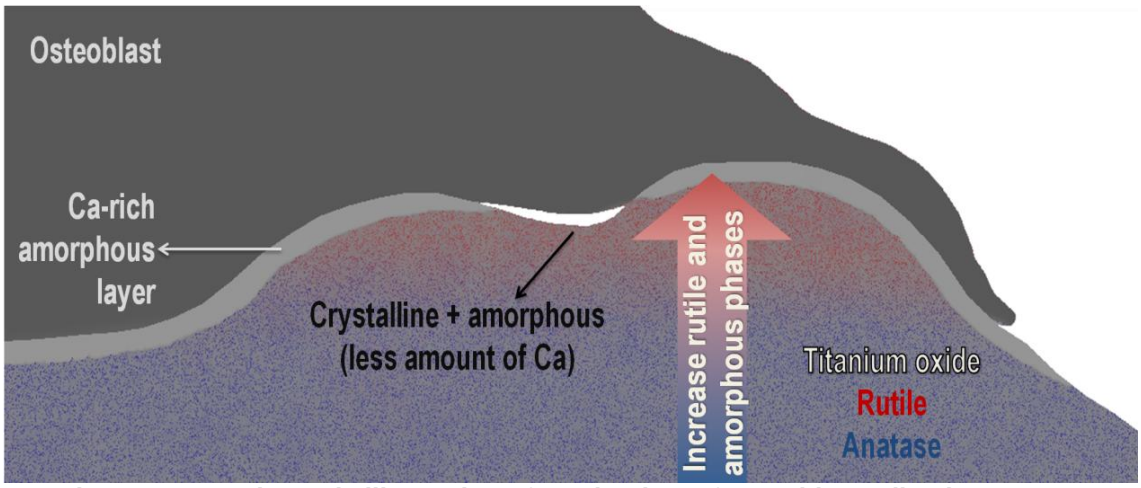

Figure 4.10 - Schematic illustration of mechanism of osteoblast adhesion to CaP surfaces: mention to chemical and crystallographic composition of the oxide layer: (rutile - red regions and anatase - blue).

It is known that the incorporation of Ca and P via MAO on titanium surfaces positively affects osteoblast attachment, viability and gene expression, encouraging osteoblast differentiation [14-16, 18, 64]. As well, it was observed *in vivo*, that surfaces containing both Ca and P (via anodic oxidation) had enhanced bone apposition on the surface [5, 25, 65, 66]. The release of Ca and P from those surfaces, penetrate or activate cell membrane bound receptors. This was referred as a possible mechanism for the enhancement of the osteoblast response because it creates an environment compatible with osteogenesis [19, 65]. In fact, Ca ions provide initial signaling in processes such as cell proliferation, mitosis and differentiation but also they can modulate bone cell cycle and enhance cell adhesion. High levels of Ca ions improve osteoblasts spreading, formation of focal adhesion contacts, expression of integrins and an enhanced fibrillar network [20-24]. In summary, Ca and P-containing oxide films with poor crystallinity and high solubility are more favorable for initial cell attachment and proliferation, and can induce higher osteoconduction. Nevertheless, the role of Ca, P and different crystalline phases on the complex mechanisms of protein adsorption cannot be disregarded. A detailed investigation on these aspects will be done in future works, because although an increase in the Ca and P dissolution rate from surfaces, results in an enhanced protein adsorption, the mechanisms behind the selective protein adsorption and respective conformation are still largely unknown.

5. Conclusions

In this work, titanium oxide films doped with calcium and phosphorous were grown on titanium surfaces by micro-arc oxidation (MAO). The main conclusions are as follows:

- A nanometric-thick calcium-rich amorphous layer is formed on the top surface of the oxide film;
- This amorphous Ca-rich layer was shown to be the main factor leading to a faster osteoblast adhesion and spreading, promoting also higher amounts of IFN-γ cytokine secretion, which is known to regulate inflammatory responses, bone microarchitecture (preventing osteoporosis) as well as cytoskeleton reorganization and cellular spreading.

Micro-arc oxidation is a process already in use by several dental implant companies. The control of the structure and composition of the titanium oxide films produced by this technique together with the understanding of the interactions of these surfaces with osteoblasts opens new opportunities for the production of a new generation of dental implants with faster osseointegration and less rehabilitation time, contributing for the well-being of patients.

References

[1] H.P. Weber, D. Morton, G.O. Gallucci, M. Roccuzzo, L. Cordaro, and L. Grutter. Consensus statements and recommended clinical procedures regarding loading protocols. *The International Journal of Oral & Maxillofacial Implants*, 24: 180-183, **2009**.

[2] U. Diebold. The surface science of titanium dioxide. *Surface Science Reports*, 48(5–8): 53-229, **2003**.

[3] L. Le Guéhennec, A. Soueidan, P. Layrolle, and Y. Amouriq. Surface treatments of titanium dental implants for rapid osseointegration. *Dental Materials*, 23(7): 844-854, **2007**.

[4] L. Treccani, T.Y. Klein, F. Meder, K. Pardun, and K. Rezwan. Functionalized ceramics for biomedical, biotechnological and environmental applications. *Acta Biomaterialia*, 9(7): 7115-7150, **2013**.

[5] Y.-T. Sul, C. Johansson, E. Byon, and T. Albrektsson. The bone response of oxidized bioactive and non-bioactive titanium implants. *Biomaterials*, 26(33): 6720-6730, **2005**.

[6] A. Wennerberg and T. Albrektsson. Effects of titanium surface topography on bone integration: A systematic review. *Clinical Oral Implants Research*, 20: 172-184, **2009**.

[7] P. Schüpbach, R. Glauser, A. Rocci, M. Martignoni, L. Sennerby, A. Lundgren, and J. Gottlow. The human bone-oxidized titanium implant interface: A light microscopic, scanning electron microscopic, back-scatter scanning electron microscopic, and energy-dispersive X-ray study of clinically retrieved dental implants. *Clinical Implant Dentistry and Related Research*, 7: s36-s43, **2005**.

[8] A. Palmquist, O.M. Omar, M. Esposito, J. Lausmaa, and P. Thomsen. Titanium oral implants: Surface characteristics, interface biology and clinical outcome. *Journal of The Royal Society Interface*, doi:10.1098/rsif.2010.0118.focus: **2010**.

[9] H. Ishizawa and M. Ogino. Formation and characterization of anodic titanium oxide films containing Ca and P. *Journal of Biomedical Materials Research*, 29(1): 65-72, **1995**.

[10] X. Zhu, K.-H. Kim, and Y. Jeong. Anodic oxide films containing Ca and P of titanium biomaterial. *Biomaterials*, 22(16): 2199-2206, **2001**.

[11] N.K. Kuromoto, R.A. Simão, and G.A. Soares. Titanium oxide films produced on commercially pure titanium by anodic oxidation with different voltages. *Materials Characterization*, 58(2): 114-121, **2007**.

[12] M.V. Diamanti and M.P. Pedeferri. Effect of anodic oxidation parameters on the titanium oxides formation. *Corrosion Science*, 49(2): 939-948, **2007**.

[13] A.C. Alves, F. Oliveira, F. Wenger, P. Ponthiaux, J.P. Celis, and L.A. Rocha. Tribocorrosion behaviour of anodic treated titanium surfaces intended for dental implants. *Journal of Physics D: Applied Physics*, 46(40): 404001, **2013**.

[14] Y. Wang, L. Wang, H. Zheng, C. Du, ChengyunNing, Z. Shi, and C. Xu. Effect of frequency on the structure and cell response of Ca- and P-containing MAO films. *Applied Surface Science*, 256(7): 2018-2024, **2010**.

[15] N.C.M. Oliveira, C.C.G. Moura, D. Zanetta-Barbosa, D.B.S. Mendonça, L. Cooper, G. Mendonça, and P. Dechichi. Effects of titanium surface anodization with CaP incorporation on human osteoblastic response. *Materials Science and Engineering: C*, 33(4): 1958-1962, **2013**.

[16] H.P. Felgueiras, L. Castanheira, S. Changotade, F. Poirier, S. Oughlis, M. Henriques, C. Chakar, N. Naaman, R. Younes, V. Migonney, J.P. Celis, P. Ponthiaux, L.A. Rocha, and D. Lutomski. Biotribocorrosion (tribo-electrochemical) characterization of anodized

titanium biomaterial containing calcium and phosphorus before and after osteoblastic cell culture. *Journal of Biomedical Materials Research Part B: Applied Biomaterials*, doi:10.1002/jbm.b.33236: **2014**.

[17] F.G. Oliveira, A.R. Ribeiro, G. Perez, B.S. Archanjo, C.P. Gouvea, J.R. Araújo, A.P.C. Campos, A. Kuznetsov, C.M. Almeida, M.M. Maru, C.A. Achete, P. Ponthiaux, J.-P. Celis, and L.A. Rocha. Understanding growth mechanisms and tribocorrosion behaviour of porous TiO_2 anodic films containing calcium, phosphorous and magnesium. *Applied Surface Science*, 341: 1-12, **2015**.

[18] A. dos Santos, J. Araujo, S. Landi, A. Kuznetsov, J. Granjeiro, L. de Sena, and C. Achete. A study of the physical, chemical and biological properties of TiO_2 coatings produced by micro-arc oxidation in a Ca–P-based electrolyte. *Journal of Materials Science: Materials in Medicine*, 25(7): 1769-1780, **2014**.

[19] H.S. Alghamdi, R. Bosco, J.J.J.P. van den Beucken, X.F. Walboomers, and J.A. Jansen. Osteogenicity of titanium implants coated with calcium phosphate or collagen type-I in osteoporotic rats. *Biomaterials*, 34(15): 3747-3757, **2013**.

[20] B.-S. Kang, Y.-T. Sul, C.B. Johansson, S.-J. Oh, H.-J. Lee, and T. Albrektsson. The effect of calcium ion concentration on the bone response to oxidized titanium implants. *Clinical Oral Implants Research*, 23(6): 690-697, **2012**.

[21] R. Narayanan, S.K. Seshadri, T.Y. Kwon, and K.H. Kim. Calcium phosphate-based coatings on titanium and its alloys. *Journal of Biomedical Materials Research Part B: Applied Biomaterials*, 85B(1): 279-299, **2008**.

[22] S.N. Nayab, F.H. Jones, and I. Olsen. Modulation of the human bone cell cycle by calcium ion-implantation of titanium. *Biomaterials*, 28(1): 38-44, **2007**.

[23] S.N. Nayab, F.H. Jones, and I. Olsen. Effects of calcium ion implantation on human bone cell interaction with titanium. *Biomaterials*, 26(23): 4717-4727, **2005**.

[24] R. Sawada, K. Kono, K. Isama, Y. Haishima, and A. Matsuoka. Calcium-incorporated titanium surfaces influence the osteogenic differentiation of human mesenchymal stem cells. *Journal of Biomedical Materials Research Part A*, 101A(9): 2573-2585, **2013**.

[25] M. Fini, A. Cigada, G. Rondelli, R. Chiesa, R. Giardino, G. Giavaresi, N. Nicoli Aldini, P. Torricelli, and B. Vicentini. *In vitro* and *in vivo* behaviour of Ca- and P-enriched anodized titanium. *Biomaterials*, 20(17): 1587-1594, **1999**.

[26] S. Buchloh, B. Stieger, P.J. Meier, and L. Gauckler. Hepatocyte performance on different crystallographic faces of rutile. *Biomaterials*, 24(15): 2605-2610, **2003**.

[27] S. Faghihi, F. Azari, J.A. Szpunar, H. Vali, and M. Tabrizian. Titanium crystal orientation as a tool for the improved and regulated cell attachment. *Journal of Biomedical Materials Research Part A*, 91A(3): 656-662, **2009**.

[28] H.-K. Tsou, P.-Y. Hsieh, M.-H. Chi, C.-J. Chung, and J.-L. He. Improved osteoblast compatibility of medical-grade polyetheretherketone using arc ionplated rutile/anatase titanium dioxide films for spinal implants. *Journal of Biomedical Materials Research Part A*, 100A(10): 2787-2792, **2012**.

[29] H.-T. Chen, C.-J. Chung, T.-C. Yang, C.-H. Tang, and J.-L. He. Microscopic observations of osteoblast growth on micro-arc oxidized β titanium. *Applied Surface Science*, 266: 73-80, **2013**.

[30] A. Verket, H. Tiainen, H.J. Haugen, S.P. Lyngstadaas, O. Nilsen, and J.E. Reseland. Enhanced osteoblast differentiation on scaffolds coated with TiO_2 compared to SiO_2 and CaP coatings. *Biointerphases*, 7(1): 36, **2012**.

[31] M.-C. Bernier, K. El Kirat, M. Besse, S. Morandat, and M. Vayssade. Preosteoblasts and fibroblasts respond differently to anatase titanium dioxide nanoparticles: A cytotoxicity and inflammation study. *Colloids and Surfaces B: Biointerfaces*, 90: 68-74, **2012**.

[32] V. Sollazzo, A. Palmieri, F. Pezzetti, A. Scarano, M. Martinelli, L. Scapoli, L. Massari, G. Brunelli, E. Caramelli, and F. Carinci. Genetic effect of anatase on osteoblast-like cells. *Journal of Biomedical Materials Research Part B: Applied Biomaterials*, 85B(1): 29-36, **2008**.

[33] J. He, W. Zhou, X. Zhou, X. Zhong, X. Zhang, P. Wan, B. Zhu, and W. Chen. The anatase phase of nanotopography titania plays an important role on osteoblast cell morphology and proliferation. *Journal of Materials Science: Materials in Medicine*, 19(11): 3465-3472, **2008**.

[34] X. Cui, H.M. Kim, M. Kawashita, L. Wang, T. Xiong, T. Kokubo, and T. Nakamura. Preparation of bioactive titania films on titanium metal via anodic oxidation. *Dental Materials*, 25(1): 80-86, **2009**.

[35] G. Raffaini and F. Ganazzoli. Molecular modelling of protein adsorption on the surface of titanium dioxide polymorphs. *Philosophical Transactions of the Royal Society A: Mathematical,* , 370(1963): 1444-1462, **2012**.

[36] Ç. Albayrak, İ. Hacısalihoğlu, S.Y. vangölü, and A. Alsaran. Tribocorrosion behavior of duplex treated pure titanium in simulated body fluid. *Wear*, 302(1–2): 1642-1648, **2013**.

[37] A.F. Yetim. Investigation of wear behavior of titanium oxide films, produced by anodic oxidation, on commercially pure titanium in vacuum conditions. *Surface and Coatings Technology*, 205(6): 1757-1763, **2010**.

[38] M.R. Garsivaz Jazi, M.A. Golozar, K. Raeissi, and M. Fazel. Evaluation of corrosion and tribocorrosion of plasma electrolytic oxidation treated Ti–6Al–4V alloy. *Surface and Coatings Technology*, 244: 29-36, **2014**.

[39] C. Gray, A. Boyde, and S.J. Jones. The isolation, culture and functional assay of osteoclasts and osteoblasts. in *Cell Biology: A Laboratory Handbook,*. Academic Press, **1998**

[40] P. Barndt, H. Zhang, and F. Liu. Immediate loading: From biology to biomechanics. Report of the Committee on Research in Fixed Prosthodontics of the American Academy of Fixed Prosthodontics. *Journal of Prosthetic Dentistry*, 113(2): 96-107,

[41] K. Anselme. Biomaterials and interface with bone. *Osteoporosis International*, 22(6): 2037-2042, **2011**.

[42] K. Anselme and M. Bigerelle. On the relation between surface roughness of metallic substrates and adhesion of human primary bone cells. *Scanning*, 36(1): 11-20, **2014**.

[43] K. Anselme, A. Ponche, and M. Bigerelle. Relative influence of surface topography and surface chemistry on cell response to bone implant materials. Part 2: Biological aspects. *Proceedings of the Institution of Mechanical Engineers, Part H: Journal of Engineering in Medicine*, 224(12): 1487-1507, **2010**.

[44] X. Zhu, J. Chen, L. Scheideler, R. Reichl, and J. Geis-Gerstorfer. Effects of topography and composition of titanium surface oxides on osteoblast responses. *Biomaterials*, 25(18): 4087-4103, **2004**.

[45] T.J. Webster, C. Ergun, R.H. Doremus, R.W. Siegel, and R. Bizios. Specific proteins mediate enhanced osteoblast adhesion on nanophase ceramics. *Journal of Biomedical Materials Research*, 51(3): 475-483, **2000**.

[46] A. Bruinink, M. Bitar, M. Pleskova, P. Wick, H.F. Krug, and K. Maniura-Weber. Addition of nanoscaled bioinspired surface features: A revolution for bone related implants and scaffolds? *Journal of Biomedical Materials Research Part A*, 102(1): 275-294, **2014**.

[47] W. Zhang, G. Wang, Y. Liu, X. Zhao, D. Zou, C. Zhu, Y. Jin, Q. Huang, J. Sun, X. Liu, X. Jiang, and H. Zreiqat. The synergistic effect of hierarchical micro/nano-topography and bioactive ions for enhanced osseointegration. *Biomaterials*, 34(13): 3184-3195, **2013**.

[48] W.F. Zambuzzi, A. Bruni-Cardoso, J.M. Granjeiro, M.P. Peppelenbosch, H.F. de Carvalho, H. Aoyama, and C.V. Ferreira. On the road to understanding of the osteoblast adhesion: Cytoskeleton organization is rearranged by distinct signaling pathways. *Journal of Cellular Biochemistry*, 108(1): 134-144, **2009**.

[49] W.F. Zambuzzi, P.G. Coelho, G.G. Alves, and J.M. Granjeiro. Intracellular signal transduction as a factor in the development of "Smart" biomaterials for bone tissue engineering. *Biotechnology and Bioengineering*, 108(6): 1246-1250, **2011**.

[50] W.F. Zambuzzi, C.V. Ferreira, J.M. Granjeiro, and H. Aoyama. Biological behavior of pre-osteoblasts on natural hydroxyapatite: A study of signaling molecules from attachment to differentiation. *Journal of Biomedical Materials Research Part A*, 97A(2): 193-200, **2011**.

[51] S. Miura and J. Takebe. Biological behavior of fibroblast-like cells cultured on anodized-hydrothermally treated titanium with a nanotopographic surface structure. *Journal of Prosthodontic Research*, 56(3): 178-186, **2012**.

[52] J.M. Lee, J.I. Lee, and Y.J. Lim. *In vitro* investigation of anodization and CaP deposited titanium surface using MG63 osteoblast-like cells. *Applied Surface Science*, 256(10): 3086-3092, **2010**.

[53] F. Badique, D.R. Stamov, P.M. Davidson, M. Veuillet, G. Reiter, J.-N. Freund, C.M. Franz, and K. Anselme. Directing nuclear deformation on micropillared surfaces by substrate geometry and cytoskeleton organization. *Biomaterials*, 34(12): 2991-3001, **2013**.

[54] M. Quirynen, M. De Soete, and D. Van Steenberghe. Infectious risks for oral implants: A review of the literature. *Clinical Oral Implants Research*, 13(1): 1-19, **2002**.

[55] Y.-H. Lee, Y.-M. Kang, M.-J. Heo, G.-E. Kim, G. Bhattarai, N.-H. Lee, M.-K. Yu, and H.-K. Yi. The survival role of peroxisome proliferator-activated receptor gamma induces odontoblast differentiation against oxidative stress in human dental pulp cells. *Journal of Endodontics*, 39(2): 236-241, **2013**.

[56] G. Bhattarai, Y.-H. Lee, N.-H. Lee, I.L.S. Park, M.-H. Lee, and H.-K. Yi. PPARγ delivered by Ch-GNPs onto titanium surfaces inhibits implant-induced inflammation and induces bone mineralization of MC3T3 E1 osteoblast-like cells. *Clinical Oral Implants Research*, 24(10): 1101-1109, **2013**.

[57] T.-G. Kim, Y.-H. Lee, G. Bhattari, N.-H. Lee, K.-W. Lee, H.-K. Yi, and M.-K. Yu. PPARγ inhibits inflammation and RANKL expression in epoxy resin-based sealer-induced osteoblast precursor cells E1 cells. *Archives of Oral Biology*, 58(1): 28-34,

[58] J. Ivaska, H.-M. Pallari, J. Nevo, and J.E. Eriksson. Novel functions of vimentin in cell adhesion, migration, and signaling. *Experimental Cell Research*, 313(10): 2050-2062, **2007**.

[59] M. Pegueroles, A. Aguirre, E. Engel, G. Pavon, F.J. Gil, J.A. Planell, V. Migonney, and C. Aparicio. Effect of blasting treatment and Fn coating on MG63 adhesion and differentiation on titanium: A gene expression study using real-time RT-PCR. *Journal of Materials Science: Materials in Medicine*, 22(3): 617-627, **2011**.

[60] Y. Hashimoto, A. Ueda, and M. Nakamura. Evidence that HSP70 gene expression may be useful for assessing the cytocompatibility of dental biomaterials. *Dental Materials Journal*, 23(2): 184-189, **2004**.

[61] P. Spyrou, S. Papaioannou, G. Hampson, K. Brady, R.M. Palmer, and F. McDonald. Cytokine release by osteoblast-like cells cultured on implant discs of varying alloy compositions. *Clinical Oral Implants Research*, 13(6): 623-630, **2002**.

[62] F.-C. Lin and H.A. Young. The talented interferon-gamma. *Advances in Bioscience and Biotechnology*, 4: 6-13, **2013**.

[63] G. Duque, D.C. Huang, N. Dion, M. Macoritto, D. Rivas, W. Li, X.F. Yang, J. Li, J. Lian, F.T. Marino, J. Barralet, V. Lascau, C. Deschênes, L.-G. Ste-Marie, and R. Kremer. Interferon-γ plays a role in bone formation *in vivo* and rescues osteoporosis in ovariectomized mice. *Journal of Bone and Mineral Research*, 26(7): 1472-1483, **2011**.

[64] C.-S. Chen, Y.-L. Tsao, D.-J. Wang, S.-F. Ou, H.-Y. Cheng, Y.-C. Chiang, and K.-L. Ou. Research on cell behavior related to anodized and hydrothermally treated titanium surface. *Applied Surface Science*, 271: 1-6, **2013**.

[65] R.A. Surmenev, M.A. Surmeneva, and A.A. Ivanova. Significance of calcium phosphate coatings for the enhancement of new bone osteogenesis: A review. *Acta Biomaterialia*, 10(2): 557-579, **2014**.

[66] Y.-T. Sul. The significance of the surface properties of oxidized titanium to the bone response: special emphasis on potential biochemical bonding of oxidized titanium implant. *Biomaterials*, 24(22): 3893-3907, **2003**.

Biofunctionalization of titanium surfaces for dental implants

Chapter 5

Understanding Growth Mechanisms and Tribocorrosion Behaviour of Porous TiO_2 Anodic Films Containing Calcium, Phosphorous and Magnesium

Chapter 5

Published in Applied Surface Science, 341: 1-12. 2013

Understanding growth mechanisms and tribocorrosion behaviour of porous TiO_2 anodic films containing calcium, phosphorous and magnesium

FG Oliveira[1,2], AR Ribeiro[2,3], G Perez[4], BS Archanjo[4], CP Gouvea[4], JR Araújo[4], APC Campos[4], A Kuznetsov[4], CM Almeida[4], MM Maru[4], CA Achete[4], P Ponthiaux[5], JP Celis[6], LA Rocha[1,2,7]

1 - Center MicroElectroMechanical Systems (MEMS-UMinho), Department of Mechanical Engineering, University of Minho, Campus de Azurém, 4800-058 Guimarães, Portugal

2 - IBTN/Br – Brazilian Branch of the Institute of Biomaterials, Tribocorrosion and Nanomedicine, Universidade Estadual Paulista – UNESP, Av. Eng. Luiz Edmundo Carrijo Coube, 17033-360 Bauru, São Paulo, Brazil

3 - Diretoria de Metrologia Aplicada às Ciências da Vida, Grupo de Bioengenharia, Instituto Nacional de Metrologia, Qualidade e Tecnologia, Av. Nossa Senhora das Graças 50, 25250-020 Duque de Caxias, Rio de Janeiro, Brazil

4 - Divisão de Metrologia de Materiais, Instituto Nacional de Metrologia, Qualidade e Tecnologia, Av. Nossa Senhora das Graças 50, 25250-020 Duque de Caxias, Rio de Janeiro, Brazil

5 - Laboratoire Génie des Procédés et Matériaux, École Centrale de Paris, Grande Voie des Vignes, 92290 Chatenây- Malabry, France

6 - Department of Materials Engineering, KU Leuven, Kasteelpark Arenberg 44, 3001 Leuven, Belgium

7 - Faculdade de Ciências, Departamento de Física, Universidade Estadual Paulista - UNESP, Av. Eng. Luiz Edmundo Carrijo Coube, 17033-360 Bauru, São Paulo, Brasil

Abstract

The growth of the dental implant market increases the concern regarding the quality, efficiency, and lifetime of dental implants. Titanium and its alloys are dominant materials in this field thanks to their high biocompatibility and corrosion resistance, but they possess a very low wear resistance. Besides problems related to osteointegration and bacterial infections, tribocorrosion phenomena being the simultaneous action between corrosion and wear, are likely to occur during the lifetime of the implant. Therefore, tribocorrosion resistant surfaces are needed to guarantee the preservation of dental implants.

This work focused on the incorporation of magnesium, together with calcium and phosphorous, in the structure of titanium oxide films produced by micro-arc oxidation (MAO). The characterization of morphology, chemical composition, and crystalline structure of the surfaces provided important insights leading to 1) a better understanding of the oxide film growth mechanisms during the MAO treatment; and 2) a better awareness on the degradation process during tribocorrosion tests. The addition of magnesium was shown to support the formation of rutile which improves the tribocorrosion properties of the surfaces.

1. Introduction

Over the last decades, the worldwide dental implant market has been on the rise. This trend is expected to continue over the next years with a global yearly growth rate of 10 % from US$ 3.4 billion in 2011, to reach values around US$ 6.6 billion in 2018 [1]. The driving force for this evolution has been the constant increase in life expectancy, as well as an increased concern over the oral hygiene. Also, the advances in dental technology are producing more attractive and efficient solutions to convince patients to opt for a dental implant.

Despite the high overall success rate of dental implants, some failures still occur. In a recent analysis by Hujoel et al. [2], failures of two dental implant brands were reported to range between 4.3 % (porous oxidized surface) and 8.2 % (chemically altered surface). Implant dentistry is a complex field, and the success/failure ratio will always be dependent on the patient host conditions, surgery procedures and material properties [3, 4].

From the beginning of modern implantology by Branemark in the 1960´s [5] to modern days, titanium-based materials have been used for the production of dental implants, being in commercial use nowadays [6, 7]. The evolution of dental implants went from the use of simply machined titanium surfaces (still in use), to highly modified and functionalized surfaces, with a wide range of surface properties [6, 8]. However, most studies found in literature regarding surfaces for dental implants, only show concern about the osteointegration process, while other significant aspects, such as tribocorrosion have been left aside [9]. Actually, titanium-based materials, represent the vast majority of the materials used in implant dentistry, due to their good mechanical properties, high corrosion resistance and excellent biocompatibility resulting from the spontaneous formation of a stable and inert oxide layer on its surface [10]. Nevertheless, tribological/tribocorrosive conditions may easily wear out this passive layer, leading to an increased corrosion, an accelerated wear and the ejection of wear debris to the surrounding environment, [11] with its deleterious effects reported in literature [12, 13].

In fact, tribocorrosion (simultaneous wear and corrosion) is a concern in this kind of applications. Avoiding tribocorrosion damages is a target in today's dental implant practice, as the implants are submitted to tribological contacts with the bone during the implantation [14] and to physiological loads during mastication [15]. Also the complex biological environment accounts for intricate corrosion processes that synergistically enlarge and are enhanced by wear phenomena [16, 17].

A possible way to overcome this problem is to modify the surface of titanium to create new tribocorrosion resistant surfaces, while maintaining/improving the adequate biological properties. Presumptions adopted in this work for the development of new surfaces were based on the abundant literature about surface properties and biological behavior of titanium alloys for biomedical implants. The performance of these devices is mainly driven by changes in either topography (roughness, porosity) or chemical composition (incorporation of bioactive elements) [8].

Surface modifications of titanium are widely reported in literature, can be achieved by using different techniques [18-24]. In this paper, micro-arc oxidation (MAO) was used to create thick, adherent, and porous titanium oxide films on titanium which are known to possess good biological properties. Regarding this technique, the work developed by Ishizawa and Ogino [25] is a major landmark. They successfully obtained a bioactive anodic titanium oxide film, containing bioactive elements with a Ca/P ratio similar to the one found in hydroxyapatite. The mechanism of titanium oxide growth under micro-arc oxidation conditions is well known and explained in previous works [26-28]. Briefly, the anodic polarization induces the growth of a titanium oxide film. At weak spots in the oxide (cracks, locals of high tension concentrations), highly energetic micro arcs start to appear, causing a localized melting of the oxide, and leaving a hole for each occurrence. The melted oxide, in contact with the electrolyte, solidifies rapidly, allowing some elements from the electrolyte to be incorporated in the new oxide structure. The high temperatures and pressures achieved during the process, contribute to the formation of crystalline phases, such as anatase and rutile, or even amorphous titania. Furthermore, the frequent micro arcs through the oxide, can have a calcination effect on the underlying layers, which become heated due to the low thermal conductivity of the oxide, and this facilitates the transformation of anatase into rutile. According to Wang et al. [28] this transformation becomes more noticeable at extended film growth duration in opposition to shorter times.

Recently, dos Santos et al. [29] produced and characterized porous titanium oxide anodic layers. Further analysis revealed an hydrophilic surface and the absence of cytotoxic effects during *in vitro* experiments.

The introduction of magnesium in bioactive coatings has been shown to increase osteoblast adhesion and differentiation through an integrin mediated mechanism, resulting in higher percentage of bone-to-implant contact [30-32].

But, regardless of the amount of works on this subject, the tribocorrosion behavior and mechanisms are still not properly characterized. Regarding titanium without any specific surface treatment, Barril et al. [33] studied the fretting behaviour and the electrochemical responses of titanium as a passivating material. More recently, Doni et al. [34] have shown that the wear rate of Ti6Al4V alloy is about 45 times higher than for CoCrMo alloy (another material used in implantology, mainly in orthopaedics) under similar tribocorrosion conditions. Some authors [35-37] have tested the tribocorrosion behavior of titanium and titanium alloy in artificial saliva solutions of different pH's and fluoride contents. Souza et al. [38] were the first to investigate the role of biofilms in the tribocorrosion behavior of titanium surfaces. They concluded that biofilms are responsible for a reduction in the coefficient of friction, although a localized decreasing of the pH is responsible for a decrease in the corrosion resistance of the surface. Ramos-Saenz et al. [39] studied bone-implant contacts in thermally oxidized titanium alloys, which resulted in abrasion and adhesion wear mechanisms of these materials.

Some authors have already tried to characterize the tribocorrosion behavior of anodic titanium oxide films. E.g., Albayrak et al. [40] proposed a dual treatment consisting of nitriding followed by an anodizing to improve the tribocorrosion resistance of titanium, They showed that titanium nitride phases contributed for a better wear behavior, while duplex treated samples showed better corrosion properties thanks to the anodic TiO_2 layer. Alves et al. [41] studied several Plasma Electrolytic Oxidation (PEO) parameters and anodic film characteristics, such as thickness and roughness, and their influence on the tribocorrosion of titanium surfaces. Garsivaz Jazi et al. [42] verified the improvement of tribocorrosion properties of anodic treated titanium alloy on using higher anodizing voltages. Yetim [43] used anodic oxidation in vacuum. He improved the wear behavior of titanium which was supposedly to be due to the lubricating properties of the oxide and the presence of rutile.

In a previous work by Alves et al. [44], the important role of rutile in the improvement of tribocorrosion behavior was also referred.

This work attempts to achieve highly tribocorrosion resistant surfaces without compromising the biological properties. A detailed surface characterization was performed, and the discussion section emphasizes two important topics: firstly, the better understanding of the oxide film growth mechanism under MAO conditions, and secondly the better understanding of the degradation of these surfaces due to tribocorrosion.

2. Materials and Methods

2.1. Materials

Commercially pure titanium (grade 2) sheet (Goodfellow) was cut into square shape 20x20x2 mm samples. Cleaning was performed in acetone during 5 min in ultrasonic bath. After drying, samples were chemically etched in highly concentrated acid solution containing HNO_3 and HF, for 5 seconds. Again, cleaning process was made by ultrasound in propanol (10 min) and water (5 min).

2.2. Surface modification

Micro-arc oxidation was performed in an aqueous electrolyte containing β-glycerol phosphate disodium salt pentahydrate (β-GP) ($C_3H_7Na_2O_6P{\cdot}5H_2O$), calcium acetate monohydrate (CaA) ($Ca(CH_3CO_2)_2{\cdot}H_2O$) and magnesium acetate tetrahydrate (MgA) ($(CH_3COO)_2Mg{\cdot}4H_2O$) from Sigma-Aldrich. Concentrations of β-GP and CaA were established according to the experimental procedure followed in a previous work [44].

Addition of magnesium was followed according to the concentration of Mg^{2+} and Ca^{2+} ions in the solution, based on some works referring the substitution role of magnesium for calcium in the Hydroxyapatite structure [45-47]. The ionic ratio $Mg^{2+}/(Mg^{2+}+Ca^{2+})$ in the electrolyte was controlled, varying from 0 to 12.5 %. Three different groups of MAO treated samples were tested, according to the molar concentration of magnesium acetate (MgA) in the electrolyte: 0 M (0MgA group), 0.01 M (0.01MgA group) and 0.1 M (0.1MgA group).

For the MAO treatment, a DC power supply (Agilent N5772A) was set at 300 V with a limiting current of 2.5 A. Samples (anode) were completely immersed in the electrolyte (surface area: 9.6 cm^2) and a platinum foil was used as cathode (surface area: 7.8 cm^2). Distance between electrodes was fixed in 8 cm. The treatment was performed for 1 min at room temperature and under magnetic agitation.

2.3. Tribocorrosion experiments

Experimental design for the tribocorrosion tests was similar to the one presented in previous work by Alves et al. [44].

Samples were placed in an electrochemical cell and mounted on a pin-on-disk reciprocating sliding tribometer (CETR-UMT 2). Cp-Ti samples and anodized samples acted as working electrodes in a three electrode configuration completed with a saturated calomel electrode (SCE) (Hg/Hg_2Cl_2/saturated KCl solution; SCE = +244 mV/NHE) and a platinum electrode as reference and counter electrodes respectively. The electrolyte consisted of SBF solution [48] (NaCl 6,213 g/L; $NaHCO_3$ 2.974 g/L; KCl 0.225 g/L; $K_2HPO_4.3H_2O$ 0.231 g/L; $MgCl_2.6H_2O$ 0.311 g/L; $CaCl_2$ 0.292 g/L; Na_2SO_4 0.072 g/L; HCl $0.85x10^{-3}$ M) used at 37 °C to simulate oral environment.

Alumina balls (**ø** = 10 mm) were used as counterbody, sliding on the surface of the samples in a reciprocating way, with a displacement amplitude of 10 mm, a frequency of 2 Hz, and on applying a normal load of 1.5 N. Sliding time was 1,814 s corresponding to 7,256 contact events in each point of the wear track.

During the tribocorrosion tests, the variation of open circuit potential was measured before, during, and after the sliding using a Gamry Instruments potentiostat/galvanostat Reference 600.

Prior to sliding, samples were rested in the electrolyte for 1 h to allow stabilization of OCP. At least three samples were tested for each set of testing conditions in order to guarantee the repeatability of the test.

2.4. Characterization

Surface morphology before and after the tribocorrosion tests was analyzed by scanning electron microscopy (SEM) with a FEI Quanta 200 equipped with a Genesis EDAX for energy dispersive spectroscopy (EDS) elemental analysis. Chemical composition of the oxide was measured in five different regions of each sample (2 samples per condition) using an acceleration voltage of 10 kV.

Roughness of the samples was assessed via 2D profilometry using a Dektak 6M profilometer from Veeco instruments (stylus radius = 0.7 μm). Wear profiles and topography of tribocorrosion tested surfaces were obtained by 3D profilometry with a Taylor Hobson profilometer (stylus radius = 2 μm) and the software TalyMapGold.

A WITec confocal AFM/Raman microscope with 532 nm wavelength laser light was used to perform combined AFM/Raman analyses. WSxM software was used for AFM image processing and analysis [49].

X-ray diffraction to evaluate crystalline structures was performed with a Bruker D8 Focus diffractometer. Analyses were made with Co Kα radiation (Fe filter) in the scan range 2θ from 10° to 60°, with step size of 0.02° and step time of 50 s. Data retrieved from diffractometer was treated with Rietveld refinement method using software Topas-Academic.

Cross-sections of the wear track area were observed in order to determine sub-surface deformation of the bulk material. Images were recorded using a Helios NanoLab 650 dual-beam instrument with a gallium ion source for focused-ion beam (FIB) milling and a field emission gun scanning electron microscope for imaging.

Samples were prepared for transmission electron microscopy (TEM) analysis in the same dual-beam Helios Nanolab 650. TEM observation was made in a transmission electron microscope using a probe-corrected FEI TITAN 80-300 operated at 300 kV, equipped with a 2k×2k Gatan UltraScan 1000 CCD camera. Fast Fourier Transform was obtained from magnification-calibrated high resolution images with the Digital Micrograph software (Gatan Inc.).

Electrochemical behavior was evaluated with a Gamry Reference 600 Potentiostat by potentiodynamic polarizations in a similar three-electrode configuration as used in the tribocorrosion tests. Samples were immersed in SBF at 37 °C, for 1 h to allow stabilization of corrosion potential and the polarization curves were acquired from cathodic to anodic domain at a scan rate of 1mV/s.

3. Results

3.1. Surface Characterization

The initial state of the cp-Ti reference samples was achieved by chemical etching of titanium as described in the experimental section. This treatment allowed the formation of a rough topography, evidencing the granular structure of titanium, while guaranteeing equal initial conditions for all samples, through the elimination of previous passive oxide films, and the growth of a new native oxide under controlled conditions. This initial surface state is shown in figure 5.1(a), while the morphology of the anodized surface is shown in figure 5.1(b).

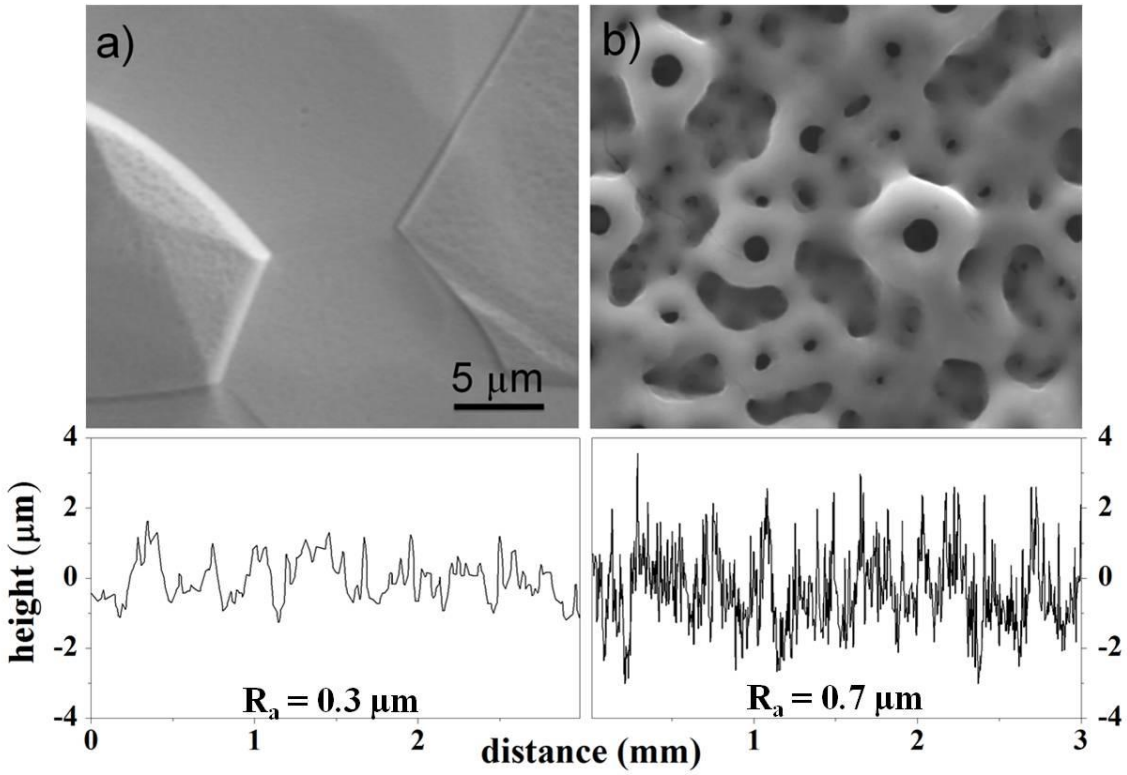

Figure 5.1 - SEM micrographs and surface profiles of etched titanium (a) and MAO treated surface (b). Microstructure of MAO treated sample (figure 5.1(b)) is representative of all three anodized conditions tested in this work.

The MAO treatment ended up in a porous anodic oxide film with similar structure, independently of the concentration of MgA added to the electrolyte. No differences in morphology or porosity (pore size, pore density, data not shown) were observed. Some cracks originated during the growth of the film are visible throughout the surface. Also the roughness values measured by profilometry were similar for all the MAO treatment conditions and furthermore evidenced an increase in roughness from c.a. Ra 0.3 µm for Ti reference samples, to c.a. Ra 0.7 µm for MAO treated samples as perceived in the surface profiles of figure 5.1, for untreated titanium and MAO treated samples. The waved topography of the oxide layers are responsible for a large variation in thickness ranging from 3 to 6 µm in different zones of surfaces regardless of the processing conditions, as it will be discussed ahead.

The chemical composition analysis of the oxide film (figure 5.2) revealed that the amount of Mg incorporated in the film increased as the MgA concentration in the electrolyte rose from 0M to 0.1M. At the same time the amount of calcium and phosphorous present in the oxide, decreased. Therefore, the total incorporation of bioactive ions (Ca+P+Mg) in the anodic film was not significantly altered by the addition of MgA.

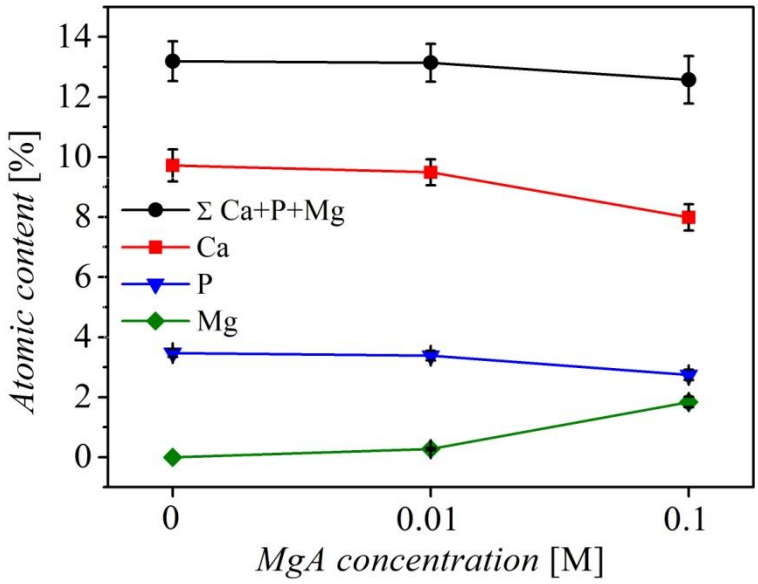

Figure 5.2 - Atomic percentage of bioactive ions incorporated into the anodic film measured by EDS

The titanium oxide created during the MAO treatment consisted of anatase and rutile, as revealed by the X-Ray Diffraction (XRD) spectra of figure 5.3. Peaks related to the bulk titanium also present in the graphic. Moreover, the addition of MgA to the electrolyte was responsible for an increase of rutile relative to anatase, despite anatase was still the dominant phase.

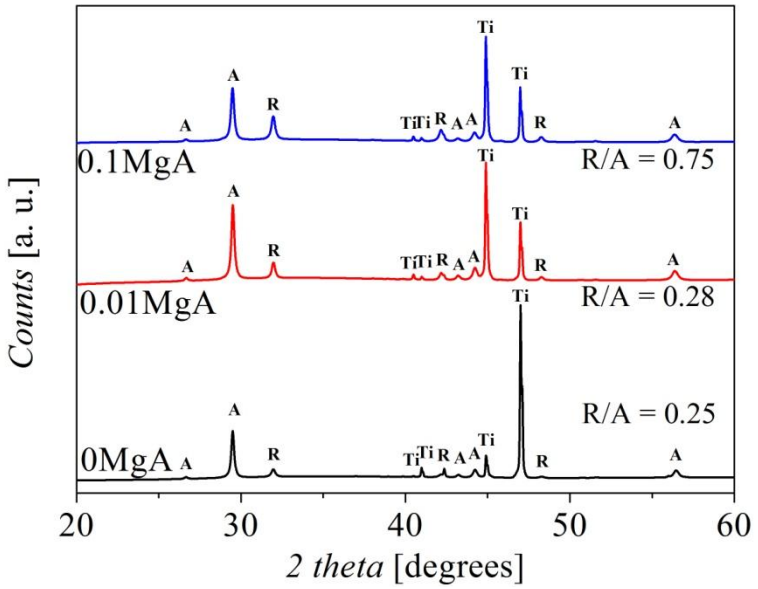

Figure 5.3 - XRD spectra of titanium oxides obtained by MAO treatment and reference to Rutile/Anatase ratio, measured by Rietveld method for each processing condition. Identification of crystalline phases: Ti) titanium; A) anatase; R) rutile

The quantitative analysis of the titanium oxide phases based on Rietveld refinement method, revealed an increase in the Rutile to Anatase ratio (R/A) at higher contents of MgA. The group with no addition of magnesium had R/A value of 0.25 (80 % anatase; 20 % rutile). In the

samples 0.01MgA a slight increase in R/A value up to 0.28 (78 % anatase; 22 % rutile) was noticed. In samples 0.1MgA, the R/A value raised up to 0.75 (57 % anatase; 43 % rutile).

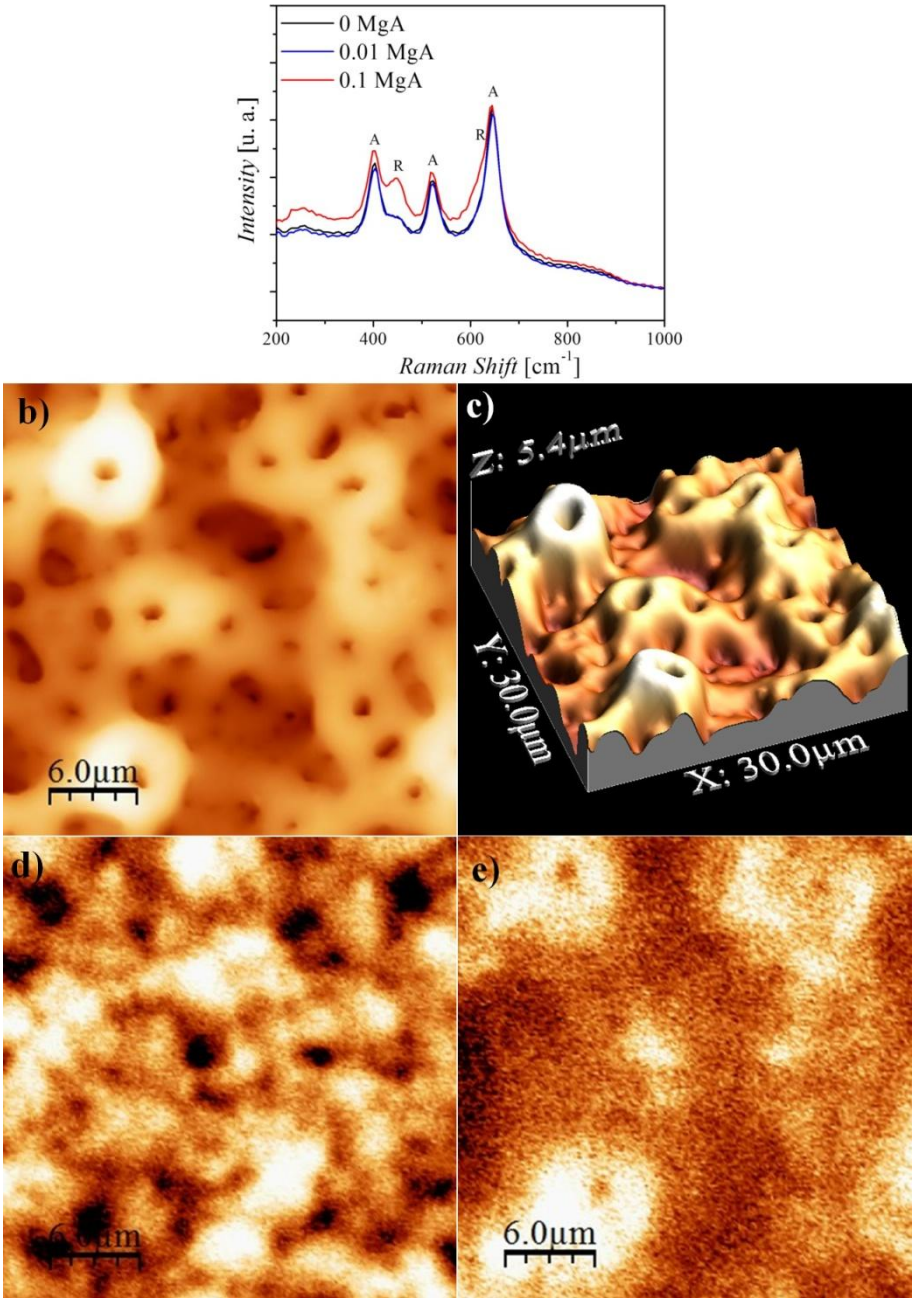

Figure 5.4 - Raman spectra of MAO treated samples with indication of Anatase (A) and Rutile (R) raman bands (a); Topographical analysis of MAO treated sample by AFM (b); 3D view of area shown in b) (c); Anatase (d) and Rutile (e) distribution relative to the area shown in 5.4b

Complementary to XRD experiments, coupled AFM-Raman analyses provided additional structural information at the microscopic scale that allowed one to infer about spatial distribution of anatase and rutile in the surface. As shown in figure 5.4(a), the samples containing higher amount of MgA present a more prominent Raman band corresponding to rutile at c.a. 450 cm^{-1},

confirming the XRD data. Figure 5.4(b) represents an AFM topographical analysis (30x30 μm) of the surface of a MAO treated sample, and figure 5.4(c) presents a 3D view of that region. Figure 5.4(d) and 5.4(e) represent, respectively, the anatase and rutile distribution (bright areas) in the same region shown in figure 5.4(b). From the correlation of the four images (5.4(b), 5.4(c), 5.4(d) and 5.4(e)), one can conclude that anatase is evenly distributed through all the surface film, while rutile seems to be preferentially located in the higher zones around the major pores ("volcanoes"). Surface characteristics of the oxide layers did not allow for a proper measurement of the mechanical properties in different points of the oxide structure.

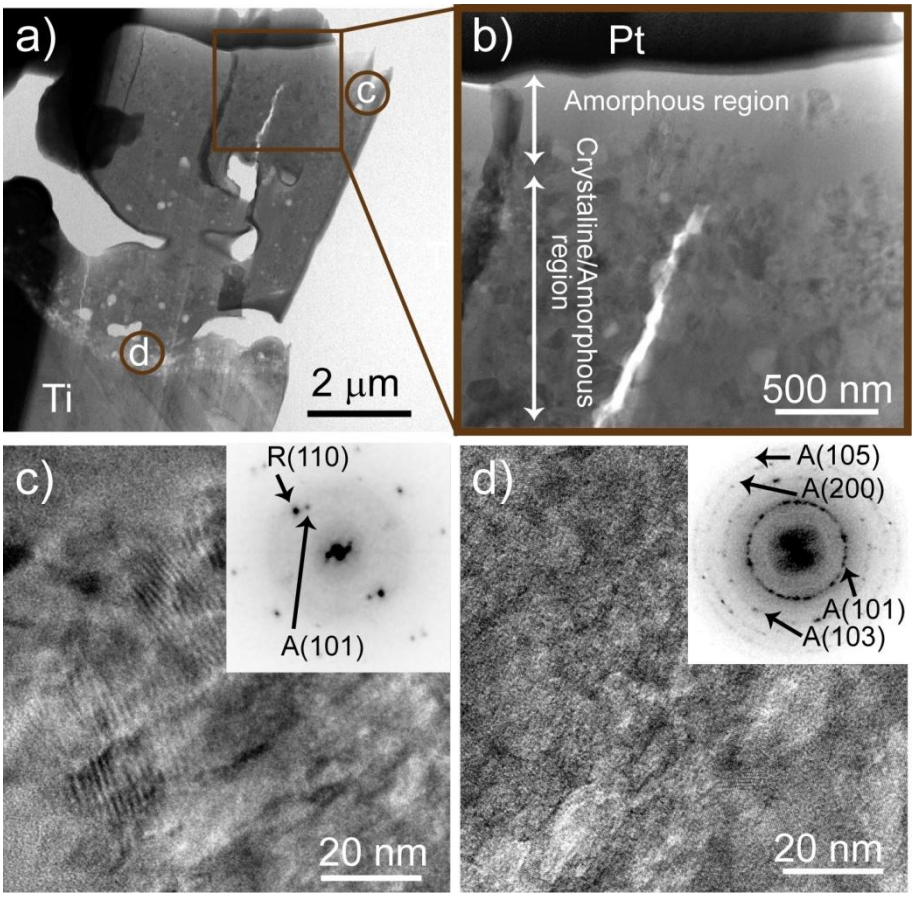

Figure 5.5 - Bright field TEM images of a cross section of MAO treated sample (0.1MgA) showing two distinct structural regions along the thickness of the oxide film (a and b). HRTEM images of the region near the top of the oxide presenting a mixture of anatase and rutile (c) and near the interface with pure Ti, presenting only anatase (d). Insets in c) and d) show the FFT patterns of the respective images

Figure 5.5(a) and 5.5(b) are Transmission Electron Microscopy (TEM) images of the cross section of the oxide film, and show two main regions concerning the structural arrangement of the oxide in a zone where the thickness was around 5 to 6 μm. This represented the highest value of oxide thickness recorded in different cross sections of MAO treated samples. Due to the irregular topography of the oxide, thickness was noted to vary from c.a. 3 to 6 μm, as already

referred. The inner part of the oxide, is composed of a mixture of crystalline and amorphous material, while on top of the oxide, an amorphous region of varying thickness (200-500 nm) covers the entire surface of the oxide. The phase identification by HRTEM and Fast Fourier Transform (FFT) patterns of crystalline regions matched the findings obtained in the coupled AFM/Raman analysis. Small nanocrystals of rutile were observed near the top region of the oxide (figure 5.5(c)), in opposition to the bottom part of the film (figure 5.5(d)), where only anatase was found.

3.2. Electrochemical and Tribocorrosion behavior

Representative potentiodynamic polarizations curves in SBF solution are presented in figure 5.6, showing the variation of current density versus the applied potential for titanium and MAO treated samples. Two curves for each surface are presented, representing the range of variation of all the tests performed in each surface. All anodized samples presented good reproducibility in the cathodic domain and E_{corr}. Also, a well-defined passivation plateau is visible for all anodized samples with i_{pass}. However, for each condition, the range of variation of the passive current density is of the order of half decade, with a relatively higher reproducibility observed for the samples not containing Mg. Anyway, when compared with pure titanium, MAO treatment caused a small increase in E_{corr} and significantly lower current densities in the passive domain.

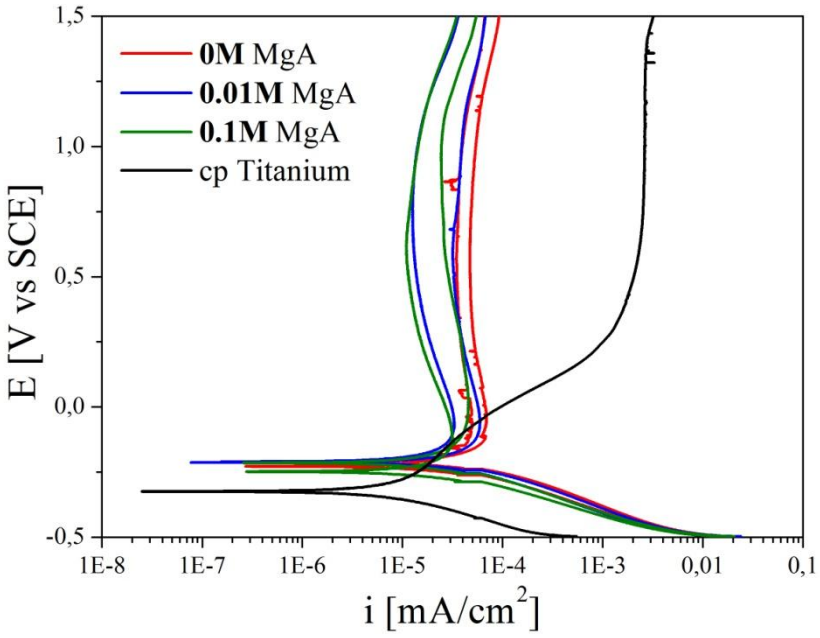

Figure 5.6 - Potentiodynamic plots of the variation of current density versus the applied potential for titanium and MAO treated samples

Figure 5.7 shows representative curves of the evolution of the open circuit potential (OCP) before, during, and after tribocorrosion tests.

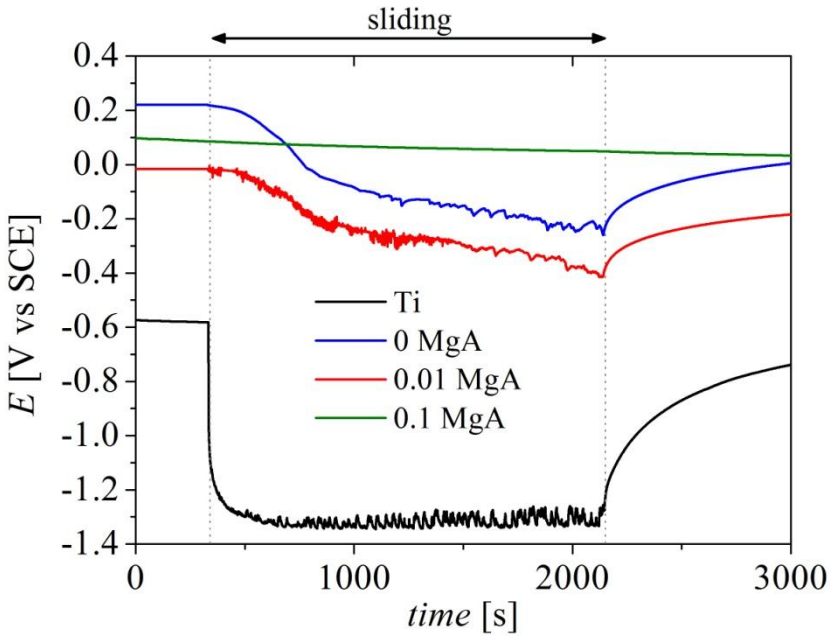

Figure 5.7 - Evolution of open circuit potential (OCP vs SCE) values before, during and after the tribocorrosion tests

Before the start of the mechanical solicitations there is a distinctive behavior between MAO-treated samples and non-treated samples. In the absence of wear, the pure Ti has a lower OCP value, indicating a higher corrosion tendency, while all the MAO groups showed significantly higher OCP values (between c.a. 0 V/SCE and 0.2 V/SCE), due to the presence of a protective anodic film.

As soon as sliding starts, the OCP of the pure titanium samples undergo an abrupt decline, due to the destruction of the fragile passive film at the surface, therefore exposing bare titanium to the corrosive effects of the physiological solution [17]. For these samples, the OCP values during sliding stabilize around -1.3 V/SCE, presenting some oscillations usually attributed to the continuous mechanical depassivation and electrochemical repassivation, occurring simultaneously in the wear track [50]. After sliding, an uninterrupted repassivation process occurs in the wear track which eventually may lead to the complete recovery of the passive film and the return of the OCP values almost back to the level before the sliding test [51].

For the MAO groups, two distinct behaviors are detected. Once sliding is started, a small and slow decrease in OCP values is noticed in the 0MgA and 0.01MgA groups. The ΔE being the difference in potential between the start of sliding and the end of sliding, is approximately -0.4 V.

Also, all curves recorded for the 0.1MgA group reveal a slight linear decrease of OCP values throughout the entire sliding test. Nevertheless, the electrochemical behavior of all MAO treated samples is undoubtedly better than the Ti group, from the point of view of both corrosion and tribocorrosion.

In figure 5.8, scanning electron microscopy (SEM) micrographs of the wear tracks of the four groups tested in this work illustrate the wear behavior of the surfaces. Wear tracks on reference Ti have well defined contours (detail in figure 5.8(a)), and reveal a high level of wear by abrasion and adhesion. In figure 5.8(a), the micrograph shows that the area inside the wear track has been mostly damaged by abrasion revealed by abrasion grooves caused by third body wear caused by detached particles. Despite the clearly visible abrasion mechanism, adhesion phenomena did also occur during the test, since a material transfer from the sample to the counterbody was observed after the sliding test.

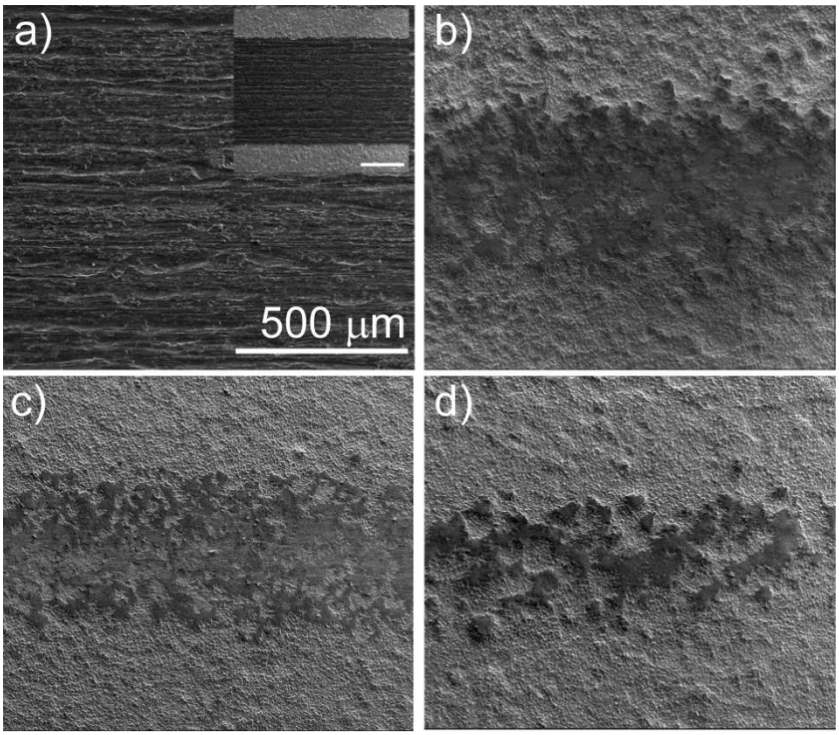

Figure 5.8 - Wear tracks of Ti group (inset shows a wider view of all wear track width, scale bar 500 um) (a); and MAO treated groups: 0M MgA (b); 0.01M MgA (c); 0.1M MgA (d). All images at the same scale

For the three MAO treated groups, the same wear mechanisms took place independently of the treatment conditions. Figures 5.8(b), 5.8(c) and 5.8(d) show that only the outer part of the anodic film was damaged during sliding. Furthermore, the group with a higher content of MgA, presented the less damages at the surface.

In figure 5.9 the wear mechanisms of MAO treated groups submitted to tribocorrosion tests are considered. Despite the better behavior of 0.1MgA group, all the wear tracks presented the same characteristics; therefore it is reasonable to state that the same wear mechanisms were active on all treated groups.

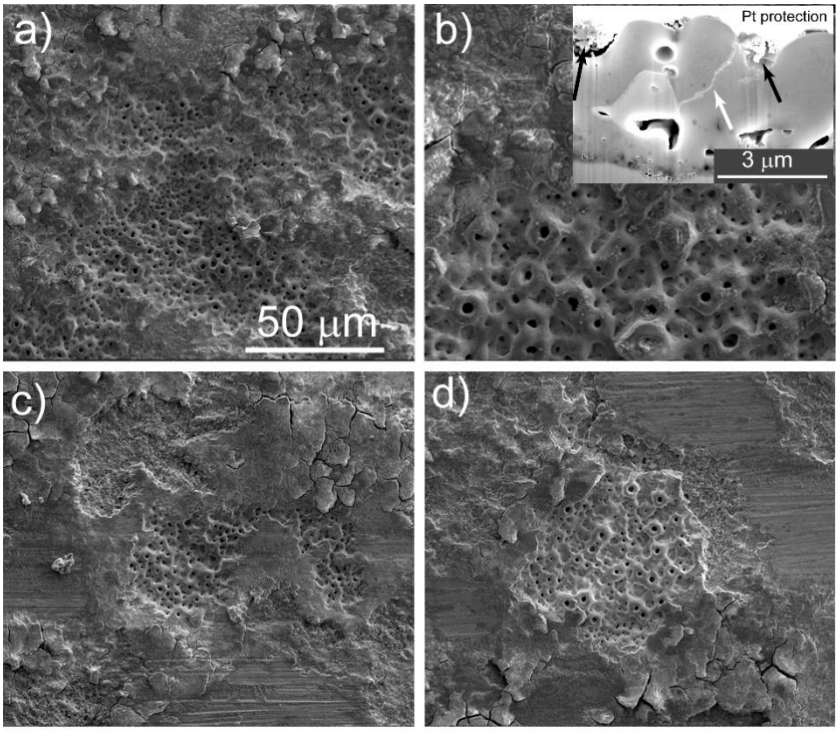

Figure 5.9 - Detailed SEM micrographs on wear mechanisms of MAO treated groups. Inset in figure 5.9(b) presents a cross section inside the wear track area prepared and imaged by FIB, with identification of wear debris (black arrows) and structural defects of the film (white arrow)

Figures 5.8(b), 5.8(c), and 5.8(d) show that the sliding test only affected the top part of the anodic film. In figure 5.9(a) this assumption is confirmed since the top peaks of the film were erased, while the bottom part of the porous structure remained undamaged. Moreover, the material removed from the higher peaks of the rough surface remains entrapped in the recesses of the surface, filling up, and finally covering the porous structure as can be seen in figure 5.9(b). The inset image in 5.9(b) presents a cross section of the wear track area prepared and imaged by FIB, where the black arrows point to the wear debris deposited in the recesses of the porous structure and the white arrow signals some structural defects of the oxide (e.g. cracks).

Figures 5.9(c) and 5.9(d) reveal that the material erased from the top peaks can be sometimes smashed and pressed against the porous surface creating an accumulation of material that can be easily worn out. Furthermore, some sharp failures of the film are observed (figure 5.9(d)) which might be associated with the cracks referred to in figure 5.1(b) and the inset in figure 5.9(b).

In some zones of the wear track (figure 5.9(c) and 5.9(d)), the counterbody caused a flattening of the wear track through the elimination of the higher peaks. This effect was also visible in the profilometry of the wear tracks on MAO treated sample (0MgA group) (see figure 5.10(a)) and etched titanium sample (Ti group) (see figure 5.10(b)).

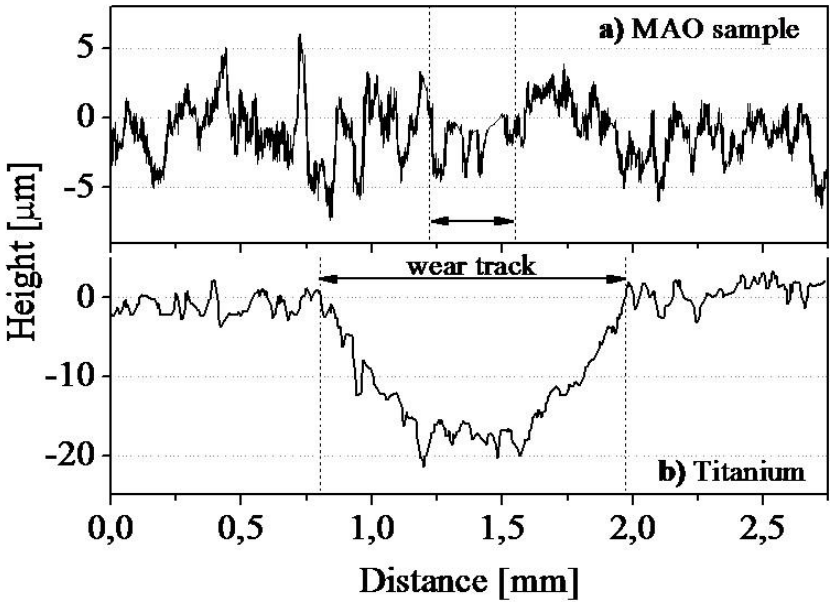

Figure 5.10 - 2D profiles of the wear tracks of MAO treated surface (0MgA) (a) and etched titanium surface (b)

The wear tracks on the reference Ti presented well defined contours and a significant depression after the tribocorrosion tests. The depth of the wear track reached a maximum of around 20 μm and its wear volume calculated by 3D profilometry was $96{,}5x10^6 \pm 2{,}1x10^6$ μm^3.

On the other hand, all groups of MAO treated samples presented wear profiles similar to figure 5.10(a). The wear track was barely visible so that the wear volume could not be calculated due to the high initial roughness of the anodic film. Anyway figure 5.10(a) shows that the counterbody interacted on the surface, and caused the leveling off of the higher peaks, and decreased the roughness inside the wear track area (Sa = 1,15 ± 0,05 μm), when compared to the initial surface conditions, outside the wear track (Sa = 1,55 ± 0,10 μm).

Recently, the study by Perret et al. [52] gathered some attention to the subsurface deformation of materials under tribocorrosion solicitations. Besides the synergism between wear and corrosion, the deformation of the subsurface material could affect both the mechanical properties and the electrochemical responses. In figure 5.11, cross sections of the wear tracks of untreated titanium and MAO treated sample (0.1MgA group) prepared and imaged by FIB are shown. The channeling effect, observed in FIB (Focused Ion Beam) images when collecting secondary electrons in crystalline samples, creates an orientation contrast, allowing an easy

observation of grains at the microscale range. For untreated titanium (figure 5.11(a)), the deformation of near surface region is clearly visible, showing a gradient in the grain deformation from the surface down to the bulk material. On the other hand, on MAO treated samples (figure 5.11(b)) the crystal structure of the bulk titanium remained unaltered, guaranteeing the mechanical integrity of the sample.

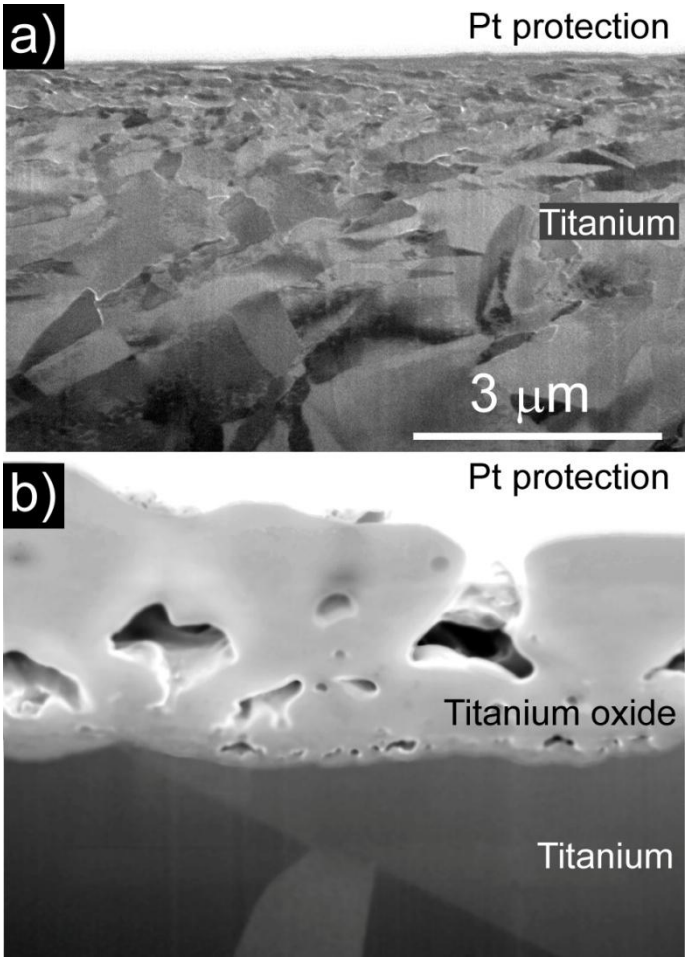

Figure 5.11 - Subsurface deformation evaluated on cross sections of wear tracks prepared and imaged by FIB on untreated titanium (a) and MAO treated 0.1MgA (b)

4. Discussion

This work aimed at the surface modification of titanium to produce highly wear/corrosion resistant surfaces for biomedical applications, without compromising the intrinsic biocompatibility of the material. The understanding of growth mechanisms and the tribocorrosion behavior of the surfaces are the two main outputs of this work, and are addressed in the following subsections.

4.1. Growth mechanisms of titanium oxide films by MAO

MAO treated samples containing magnesium or not were produced and compared with acid etched surfaces, which provided an improved surface morphology comparable to the one on

some commercial dental implants, and also allowing an increase in surface roughness, known to be suitable for cell adhesion [53]. Also the incorporation of bioactive elements such as calcium and phosphorous was achieved successfully. This incorporation has been reported to improve the biological performance of implant materials since they are elements natively present in bones [54].

The study of the crystalline structure of the samples showed that anatase and rutile were present in the oxide, forming a nanocomposite. Their relative distribution varies as a function of film thickness and distance to surface, thus creating a graded structure. Based on the work of Wang et al. [28], the transformation of anatase to rutile is more prone to happen at longer processing durations. However, results presented here show that the addition of magnesium to the electrolyte can have the same effect, namely increasing the percentage of crystalline rutile. To explain this behavior, current vs. time plots during the MAO treatment were considered (figure 5.12). Two main stages during the film growth can be identified. The first half of the graph shows a limiting current of 2.5 A (≈0.26 $A.cm^{-2}$), meaning that in the first moments of the process, a high current contributes to the fast growth of the oxide film, and to a great extent of micro arcs appearing at the surface. As the oxide becomes thicker, its resistivity increases, therefore a more powerful driven voltage is needed to keep the high current. Eventually, the applied voltage reaches the equipment limit of 300 V (moment indicated by "$t_{gal/pot}$" in the graph of figure 5.12) resulting in the decrease of current and reducing the number of micro arcs at the surface, even though the remaining sparks could be more energetic than the previous ones, and be the reason for the appearance of large sized pores.

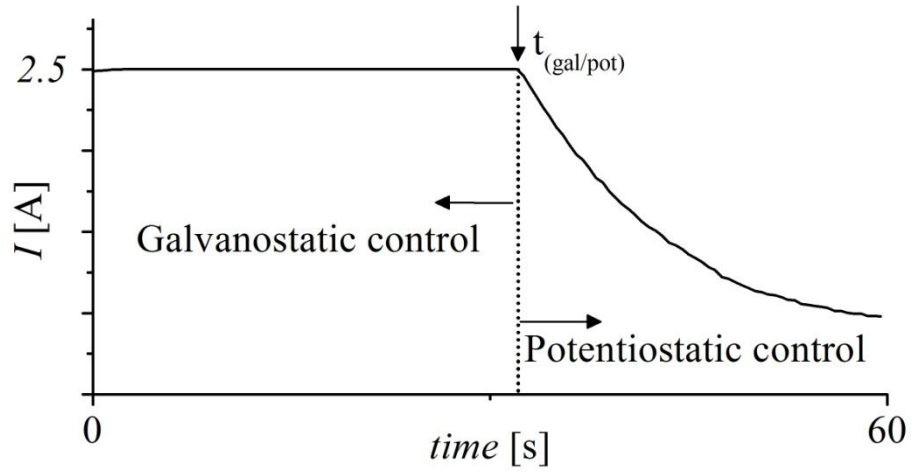

Figure 5.12 - Representative current vs. time curve from a micro arc oxidation process

In figure 5.12, the parameter $t_{gal/pot}$ corresponds to the time at which the current remains at its maximum value. Higher magnesium acetate additions cause $t_{gal/pot}$ to increase significantly (36 % increase from 0 MgA to 0.1 MgA. See Table 5.1), probably due to the increase in the conductivity of the electrolyte, causing a gradual increase in the rutile to anatase ratio, as higher currents remain for longer processing times [28]. This increase of the $t_{gal/pot}$ parameter is also related to an increase of the total charge ($Q = I \cdot t$) in the system, which is given by the integration of the curve seen in figure 5.12. Theoretically, this would influence the total amount of oxide formed during the process, with effects on the measured thickness and/or the compactness of the oxide layers. However, the increase of total charge did not account for a significant variation in the thickness of the oxide film as it ranges between 3 to 6 μm, independently of the different MAO treatment condition. Also, from the cross sections obtained in the samples from each group, it was not possible to conclude any visible effects in the compactness of the oxide.

Table 5.1 - Electrochemical parameters of the MAO process for the different groups of samples

MgA concentration [M]	Tgal/pot [s]
0	27.54 ± 2.81
0.01	28.62 ± 2.38
0.1	37.41 ± 2.40

The appearance of very high energetic discharges, could contribute to the formation of large and elongated pores, while the high temperatures and pressures generated by each spark could contribute to the preferential formation of rutile around these pores, in the higher zones of the oxide film as schematically shown in figure 5.13(a). The local melting of the oxide undergoes, in contact with the electrolyte, an almost instantaneous re-solidification of the material at a very high cooling rate. The top part of the film is expected to re-solidify at first so quickly that an atomic rearrangement could not take place, what ends up in an amorphous layer. The cooling rate is expected to slow down as the distance from the interface film/electrolyte solution increases, meaning that conditions are created for the nucleation of small nanocrystals of anatase and rutile, as explained in figure 5.13(a), which end up in a nanocomposite gradient structure.

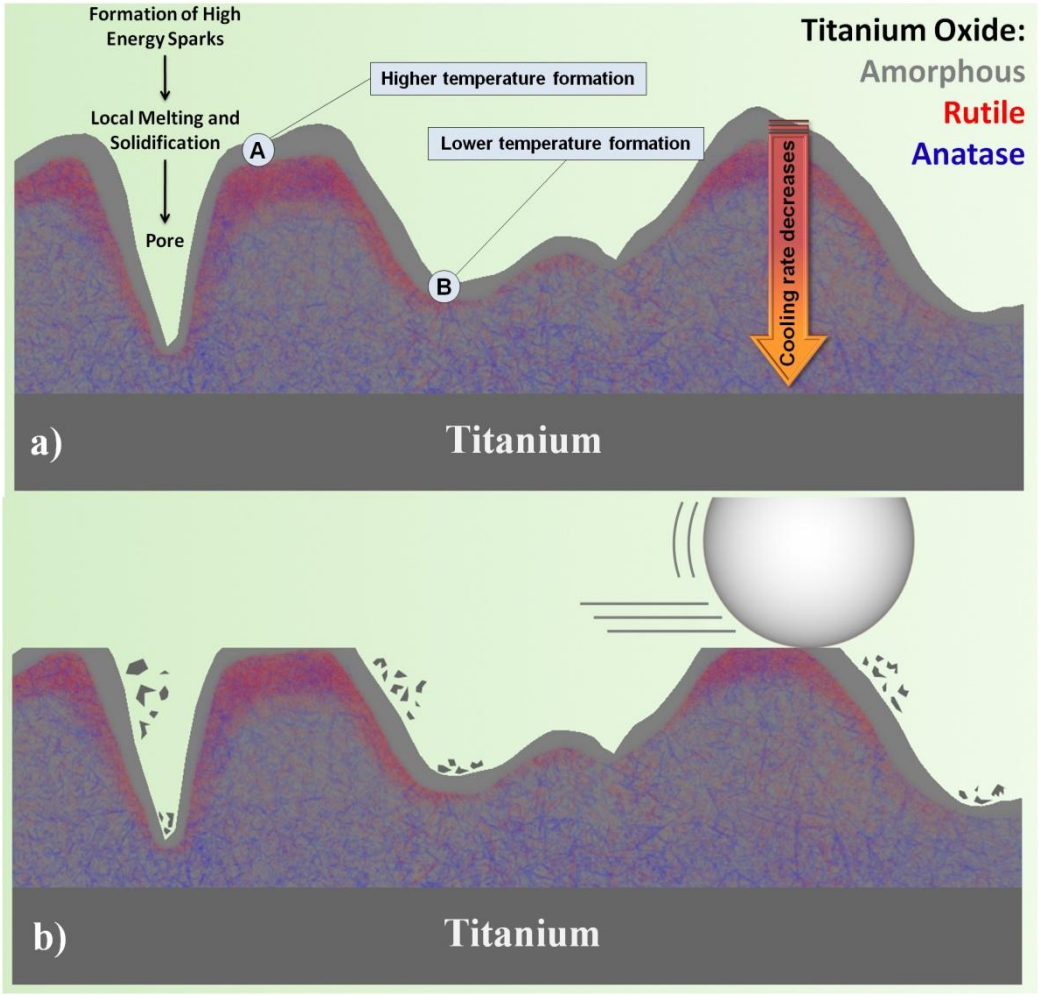

Figure 5.13 - a) Schematic illustration of the mechanisms involved in the growth of the porous layer. b) Tribocorrosion mechanism acting on the surface

4.2. Tribocorrosion mechanisms in MAO treated surfaces

In the tribocorrosion tests, all MAO treated samples exhibit higher OCP values due to the protective effect of the oxide film. In the absence of wear an improved electrochemical behavior of MAO treated samples was confirmed by potentiodynamic polarizations (figure 5.6). According to recent works [55, 56], the analysis of these plots, and particularly the cathodic domains, can help on the interpretation of tribo-electrochemical results. It is known that the decrease of OCP during a tribocorrosion test is due to a galvanic coupling, established between the wear track (anodic) and the surrounding non-worn zone (cathodic area). Vieira et al. [55] highligted two distinct situations: 1) galvanic coupling between the completely depassivated wear track and the surrounding area, or 2) a short range galvanic coupling between the depassivated areas and still passive zones (non-worn areas) within the wear track. Concerning the analysis of figures 5.8 and 5.9, one can conclude that etched titanium samples fall into the first category, while the MAO treated samples belong to the latter case. Papageorgiou [56] summarized the parameters

influencing OCP evolution during tribo-electrochemical tests, as being: the evolution of anodic/cathodic areas; the amount of anodic current density (which is considered to be constant over time; and the kinetic properties of the test sample cathode (normally obtained by cathodic polarization of the sample in the absence of sliding). Therefore, the kinetic parameters of the cathodic areas during tribocorrosion tests, can be deduced from the cathodic part of the plots presented in figure 5.6 through the calculation of Tafel constants and relation of anodic/cathodic areas. The plots for MAO treated samples, present a significant overlapping of the different curves in the cathodic domain, thus not allowing any direct inference on whether the cathodic kinetics are different for each group. Furthermore, the previous works by Vieira et al.[55], Papageorgiou [56] or Espallargas et al. [57] relied on several geometric correlations to estimate the evolution of the wear track area, considering a linear association between wear volume and sliding time, which is not applicable for the MAO treated samples studied in this work, as the graded composition of the oxide seen in figure 5.5, may account for different removal rates, according to the zone where the sliding is occurring.

As the electrochemical behavior was similar for all MAO treated conditions, the wear of the surface and the evolution of OCP decay during the tribocorrosion test can be related, to a great extent, to the mechanical properties of the oxide. For this assumption, the nanocrystalline gradient structure of the titanium oxide appears to be very important. From figures 5.7 and 5.8, one can conclude that rutile-rich oxides (0.1M MgA group) present a better tribocorrosion behavior, validated by either electrochemical measures or the evaluation of wear track damages. The good tribological properties of rutile-based titanium oxides was previously demonstrated in some works, [58, 59] and more recently applied to this same purpose [43, 44].

The wear mechanisms on titanium oxides obtained by electrochemical methods were already reported [43, 44]. In the first moments of contact, the roughness of the oxide surface causes the contact to proceed only through the higher asperities. That generates elevated contact pressures due to the small contact area. This contact takes place at the amorphous superficial layer seen in figure 5.5(b), and schematically shown in figure 5.13(b). However these contact areas cannot withstand the high contact pressures, and are easily worn out, flattening of the contact, accommodating the opposing surfaces, increasing the contact area, and consequently decreasing the contact pressure. Once this amorphous layer is worn out, the rutile preferentially located around the higher pores, in the form of a nanocomposite (rutile (harder and more resistant) + anatase (softer and more ductile) + amorphous), represents the first effective

barrier against wear due to the better mechanical properties of the crystalline phase, specially the higher hardness of rutile. This rutile-rich layer slows down the degradation rate of the film, and contributes to the leveling off of the wear track profiles (figure 5.10). Besides the role of rutile, the presence of this nanocomposite layer can avoid the brittleness and cracking phenomena associated with harder materials (rutile) under loading conditions. During the wear of the upper rutile-rich layer, the inner zone of the oxide, containing amorphous and anatase phases can contribute to the accommodation of the stresses applied and preserve the mechanical stability of the film due to its softer nature caused by the decrease of rutile content in the inner zone. The excellent wear properties of the oxide can thus be linked not only to the presence of harder rutile, but also on the crystalline gradient structure, working as a cushion for the stresses applied during tribocorrosion tests.

Both bare titanium and MAO treated groups showed some signs of abrasive wear. However the contribution of this phenomenon was much more significant in the Ti group. Wear tracks on bare titanium samples presents very distinguishable grooves even at small magnification, originated by large third body particles detached from the surface. This effect is not so noticeable in the MAO treated groups mostly due to limited wear damages in the subsurface zones and also inside the porous structure.

The defects visible in figure 5.9(c) and (d), are still a concern due to the risk of detachment of micrometer-sized portions of material and brittle failure of the oxide, endangering the full integrity of the surface oxide. However, despite the increased brittleness associated with harder materials, significant wear improvements of rutile-rich titanium oxides are definitely worth to be considered in bio-tribocorrosion applications.

5. Conclusion

The addition of magnesium to titanium oxides containing calcium and phosphorous was successfully achieved using micro-arc oxidation. The mechanisms of film growth were addressed and explained in detail. The MAO treatment induced the formation of a nanocomposite gradient crystalline structure, and revealed a localized increase in rutile due to the addition of magnesium ions in the electrolyte.

Also, the presence of rutile and the shock absorbing properties of the nanocomposite gradient structure are thought to be determining factors for achieving an improved tribocorrosion behavior of the surfaces. Thus, guaranteeing good prospects for the application of MAO rutile-based titanium oxide coatings on dental implant surfaces.

References

[1] Global boom in dental implants. *British Dental Journal*, 214(5): 219-219, **2013**. doi:10.1038/sj.bdj.2013.232

[2] P. Hujoel, W. Becker, and B. Becker. Monitoring failure rates of commercial implant brands; Substantial equivalence in question? *Clinical Oral Implants Research*, 24(7): 725-729, **2013**.

[3] T. Albrektsson, P.I. Brånemark, H.A. Hansson, and J. Lindström. Osseointegrated titanium implants: Requirements for ensuring a long-lasting, direct bone-to-implant anchorage in man. *Acta Orthopaedica*, 52(2): 155-170, **1981**.

[4] A.D. Pye, D.E.A. Lockhart, M.P. Dawson, C.A. Murray, and A.J. Smith. A review of dental implants and infection. *Journal of Hospital Infection*, 72(2): 104-110, **2009**.

[5] P.I. Branemark. Osseointegration and its experimental background. *The Journal of Prosthetic Dentistry*, 50(3): 399-410, **1983**.

[6] A. Palmquist, H. Engqvist, J. Lausmaa, and P. Thomsen. Commercially available dental implants: Review of their surface characteristics. *Journal of Biomaterials and Tissue Engineering*, 2(2): 112-124, **2012**.

[7] C. Massaro, P. Rotolo, F. De Riccardis, E. Milella, A. Napoli, M. Wieland, M. Textor, N.D. Spencer, and D.M. Brunette. Comparative investigation of the surface properties of commercial titanium dental implants. Part I: chemical composition. *Journal of Materials Science: Materials in Medicine*, 13(6): 535-548, **2002**.

[8] P.G. Coelho, J.M. Granjeiro, G.E. Romanos, M. Suzuki, N.R.F. Silva, G. Cardaropoli, V.P. Thompson, and J.E. Lemons. Basic research methods and current trends of dental implant surfaces. *Journal of Biomedical Materials Research Part B: Applied Biomaterials*, 88B(2): 579-596, **2009**.

[9] M.T. Mathew, P. Srinivasa Pai, R. Pourzal, A. Fischer, and M.A. Wimmer. Significance of tribocorrosion in biomedical applications: Overview and current status. *Advances in Tribology*, 2009: 250986, **2009**.

[10] C.N. Elias, J.H.C. Lima, R. Valiev, and M.A. Meyers. Biomedical applications of titanium and its alloys. *JOM*, 60(3): 46-49, **2008**.

[11] M.A. Khan, R.L. Williams, and D.F. Williams. Conjoint corrosion and wear in titanium alloys. *Biomaterials*, 20(8): 765-772, **1999**.

[12] N.J. Hallab and J.J. Jacobs. Biologic effects of implant debris. *Bulletin of the NYU Hospital for Joint Diseases*, 67(2): 182-188, **2009**.

[13] L. Saldaña and N. Vilaboa. Effects of micrometric titanium particles on osteoblast attachment and cytoskeleton architecture. *Acta Biomaterialia*, 6(4): 1649-1660, **2010**.

[14] P. Senna, A. Antoninha Del Bel Cury, S. Kates, and L. Meirelles. Surface damage on dental implants with release of loose particles after insertion into bone. *Clinical Implant Dentistry and Related Research*, doi:10.1111/cid.12167: **2013**.

[15] J. Geringer, N. Demanget, and J. Pellier. From acid etching treatments to tribocorrosive properties of dental implants: Do some experimental results on surface treatments have an influence on the tribocorrosion behaviour of dental implants? *Journal of Physics D: Applied Physics*, 46(40): 404005, **2013**.

[16] D. Landolt, S. Mischler, and M. Stemp. Electrochemical methods in tribocorrosion: A critical appraisal. *Electrochimica Acta*, 46(24–25): 3913-3929, **2001**.

[17] N. Diomidis, J.P. Celis, P. Ponthiaux, and F. Wenger. A methodology for the assessment of the tribocorrosion of passivating metallic materials. *Lubrication Science*, 21(2): 53-67, **2009**.

[18] V.M. Frauchiger, F. Schlottig, B. Gasser, and M. Textor. Anodic plasma-chemical treatment of CP titanium surfaces for biomedical applications. *Biomaterials*, 25(4): 593-606, **2004**.

[19] A.M. Ballo, D. Bjöörn, M. Åstrand, A. Palmquist, J. Lausmaa, and P. Thomsen. Bone response to physical-vapour-deposited titanium dioxide coatings on titanium implants. *Clinical Oral Implants Research*, 24(9): 1009-1017, **2013**.

[20] T. Hanawa. Biofunctionalization of titanium for dental implant. *Japanese Dental Science Review*, 46(2): 93-101, **2010**.

[21] Y.-T. Sul, C. Johansson, A. Wennerberg, L.-R. Cho, B.-S. Chang, and T. Albrektsson. Optimum surface properties of oxidized implants for reinforcement of osseointegration: surface chemistry, oxide thickness, porosity, roughness, and crystal structure. *The International Journal of Oral & Maxillofacial Implants*, 20(3): 349-359, **2005**.

[22] S. Kumar, T.S.N.S. Narayanan, S.G.S. Raman, and S.K. Seshadri. Thermal oxidation of CP Ti - An electrochemical and structural characterization. *Materials Characterization*, 61(6): 589-597, **2010**.

[23] C. Aparicio, F. Javier Gil, C. Fonseca, M. Barbosa, and J.A. Planell. Corrosion behaviour of commercially pure titanium shot blasted with different materials and sizes of shot particles for dental implant applications. *Biomaterials*, 24(2): 263-273, **2003**.

[24] D.P. Oliveira, A. Palmieri, F. Carinci, and C. Bolfarini. Osteoblasts behavior on chemically treated commercially pure titanium surfaces. *Journal of Biomedical Materials Research Part A*, 102(6): 1816-1822, **2014**.

[25] H. Ishizawa and M. Ogino. Formation and characterization of anodic titanium oxide films containing Ca and P. *Journal of Biomedical Materials Research*, 29(1): 65-72, **1995**.

[26] N.K. Kuromoto, R.A. Simão, and G.A. Soares. Titanium oxide films produced on commercially pure titanium by anodic oxidation with different voltages. *Materials Characterization*, 58(2): 114-121, **2007**.

[27] M.V. Diamanti and M.P. Pedeferri. Effect of anodic oxidation parameters on the titanium oxides formation. *Corrosion Science*, 49(2): 939-948, **2007**.

[28] Y. Wang, T. Lei, B. Jiang, and L. Guo. Growth, microstructure and mechanical properties of microarc oxidation coatings on titanium alloy in phosphate-containing solution. *Applied Surface Science*, 233(1–4): 258-267, **2004**.

[29] A. dos Santos, J. Araujo, S. Landi, A. Kuznetsov, J. Granjeiro, L. de Sena, and C. Achete. A study of the physical, chemical and biological properties of TiO_2 coatings produced by micro-arc oxidation in a Ca–P-based electrolyte. *Journal of Materials Science: Materials in Medicine*, 25(7): 1769-1780, **2014**.

[30] H. Zreiqat, C.R. Howlett, A. Zannettino, P. Evans, G. Schulze-Tanzil, C. Knabe, and M. Shakibaei. Mechanisms of magnesium-stimulated adhesion of osteoblastic cells to commonly used orthopaedic implants. *Journal of Biomedical Materials Research*, 62(2): 175-184, **2002**.

[31] J.-W. Park, C.-H. An, S.-H. Jeong, and J.-Y. Suh. Osseointegration of commercial microstructured titanium implants incorporating magnesium: A histomorphometric study in rabbit cancellous bone. *Clinical Oral Implants Research*, 23(3): 294-300, **2012**.

[32] J.-W. Park, Y.-J. Kim, J.-H. Jang, and H. Song. Osteoblast response to magnesium ion-incorporated nanoporous titanium oxide surfaces. *Clinical Oral Implants Research*, 21(11): 1278-1287, **2010**.

[33] S. Barril, S. Mischler, and D. Landolt. Influence of fretting regimes on the tribocorrosion behaviour of Ti6Al4V in 0.9 wt.% sodium chloride solution. *Wear*, 256(9–10): 963-972, **2004**.

[34] Z. Doni, A.C. Alves, F. Toptan, J.R. Gomes, A. Ramalho, M. Buciumeanu, L. Palaghian, and F.S. Silva. Dry sliding and tribocorrosion behaviour of hot pressed CoCrMo biomedical alloy as compared with the cast CoCrMo and Ti6Al4V alloys. *Materials & Design*, 52: 47-57, **2013**.

[35] A.C. Vieira, A.R. Ribeiro, L.A. Rocha, and J.P. Celis. Influence of pH and corrosion inhibitors on the tribocorrosion of titanium in artificial saliva. *Wear*, 261(9): 994-1001, **2006**.

[36] M.P. Licausi, A.I. Muñoz, and V.A. Borrás. Tribocorrosion mechanisms of Ti6Al4V biomedical alloys in artificial saliva with different pHs. *Journal of Physics D: Applied Physics*, 46(40): 404003, **2013**.

[37] J.C.M. Souza, S.L. Barbosa, E. Ariza, J.P. Celis, and L.A. Rocha. Simultaneous degradation by corrosion and wear of titanium in artificial saliva containing fluorides. *Wear*, 292–293: 82-88, **2012**.

[38] J.C.M. Souza, M. Henriques, R. Oliveira, W. Teughels, J.P. Celis, and L.A. Rocha. Do oral biofilms influence the wear and corrosion behavior of titanium? *Biofouling*, 26(4): 471-478, **2010**.

[39] C.R. Ramos-Saenz, P.A. Sundaram, and N. Diffoot-Carlo. Tribological properties of Ti-based alloys in a simulated bone–implant interface with Ringer's solution at fretting contacts. *Journal of the Mechanical Behavior of Biomedical Materials*, 3(8): 549-558, **2010**.

[40] Ç. Albayrak, İ. Hacısalihoğlu, S.Y. vangölü, and A. Alsaran. Tribocorrosion behavior of duplex treated pure titanium in simulated body fluid. *Wear*, 302(1–2): 1642-1648, **2013**.

[41] S.A. Alves, R. Bayón, A. Igartua, V. Saénz de Viteri, and L.A. Rocha. Tribocorrosion behaviour of anodic titanium oxide films produced by plasma electrolytic oxidation for dental implants. *Lubrication Science*, 26(7-8): 500-513, **2014**.

[42] M.R. Garsivaz Jazi, M.A. Golozar, K. Raeissi, and M. Fazel. Evaluation of corrosion and tribocorrosion of plasma electrolytic oxidation treated Ti–6Al–4V alloy. *Surface and Coatings Technology*, 244: 29-36, **2014**.

[43] A.F. Yetim. Investigation of wear behavior of titanium oxide films, produced by anodic oxidation, on commercially pure titanium in vacuum conditions. *Surface and Coatings Technology*, 205(6): 1757-1763, **2010**.

[44] A.C. Alves, F. Oliveira, F. Wenger, P. Ponthiaux, J.P. Celis, and L.A. Rocha. Tribocorrosion behaviour of anodic treated titanium surfaces intended for dental implants. *Journal of Physics D: Applied Physics*, 46(40): 404001, **2013**.

[45] E. Landi, G. Logroscino, L. Proietti, A. Tampieri, M. Sandri, and S. Sprio. Biomimetic Mg-substituted hydroxyapatite: From synthesis to *in vivo* behaviour. *Journal of Materials Science: Materials in Medicine*, 19(1): 239-247, **2008**.

[46] D. Laurencin, N. Almora-Barrios, N.H. de Leeuw, C. Gervais, C. Bonhomme, F. Mauri, W. Chrzanowski, J.C. Knowles, R.J. Newport, A. Wong, Z. Gan, and M.E. Smith. Magnesium incorporation into hydroxyapatite. *Biomaterials*, 32(7): 1826-1837, **2011**.

[47] M.-J. Jiao and X.-X. Wang. Electrolytic deposition of magnesium-substituted hydroxyapatite crystals on titanium substrate. *Materials Letters*, 63(27): 2286-2289, **2009**.

[48] M. Bohner and J. Lemaitre. Can bioactivity be tested *in vitro* with SBF solution? *Biomaterials*, 30(12): 2175-2179, **2009**.

[49] I. Horcas, R. Fernández, J.M. Gómez-Rodríguez, J. Colchero, J. Gómez-Herrero, and A.M. Baro. WSXM: A software for scanning probe microscopy and a tool for nanotechnology. *Review of Scientific Instruments*, 78(1): 013705, **2007**.

[50] P. Ponthiaux, F. Wenger, D. Drees, and J.P. Celis. Electrochemical techniques for studying tribocorrosion processes. *Wear*, 256(5): 459-468, **2004**.

[51] T. Hanawa, K. Asami, and K. Asaoka. Repassivation of titanium and surface oxide film regenerated in simulated bioliquid. *Journal of Biomedical Materials Research*, 40(4): 530-538, **1998**.

[52] J. Perret, E. Boehm-Courjault, M. Cantoni, S. Mischler, A. Beaudouin, W. Chitty, and J.P. Vernot. EBSD, SEM and FIB characterisation of subsurface deformation during tribocorrosion of stainless steel in sulphuric acid. *Wear*, 269(5–6): 383-393, **2010**.

[53] J.I. Rosales-Leal, M.A. Rodríguez-Valverde, G. Mazzaglia, P.J. Ramón-Torregrosa, L. Díaz-Rodríguez, O. García-Martínez, M. Vallecillo-Capilla, C. Ruiz, and M.A. Cabrerizo-Vílchez. Effect of roughness, wettability and morphology of engineered titanium surfaces on osteoblast-like cell adhesion. *Colloids and Surfaces A: Physicochemical and Engineering Aspects*, 365(1–3): 222-229, **2010**.

[54] L.-H. Li, Y.-M. Kong, H.-W. Kim, Y.-W. Kim, H.-E. Kim, S.-J. Heo, and J.-Y. Koak. Improved biological performance of Ti implants due to surface modification by micro-arc oxidation. *Biomaterials*, 25(14): 2867-2875, **2004**.

[55] A.C. Vieira, L.A. Rocha, N. Papageorgiou, and S. Mischler. Mechanical and electrochemical deterioration mechanisms in the tribocorrosion of Al alloys in NaCl and in $NaNO_3$ solutions. *Corrosion Science*, 54: 26-35, **2012**.

[56] N. Papageorgiou. The relevance of cathode kinetics to the interpretation of triboelectrochemical corrosion. *Tribology International*, 66: 60-71, **2013**.

[57] N. Espallargas, R. Johnsen, C. Torres, and A.I. Muñoz. A new experimental technique for quantifying the galvanic coupling effects on stainless steel during tribocorrosion under equilibrium conditions. *Wear*, 307(1–2): 190-197, **2013**.

[58] H. Dong and T. Bell. Enhanced wear resistance of titanium surfaces by a new thermal oxidation treatment. *Wear*, 238(2): 131-137, **2000**.

[59] D.S.R. Krishna, Y.L. Brama, and Y. Sun. Thick rutile layer on titanium for tribological applications. *Tribology International*, 40(2): 329-334, **2007**.

Biofunctionalization of titanium surfaces for dental implants

Chapter 6

Integrated approach combining tribocorrosion, osteogenic and antimicrobial performance of MAO treated samples and the effect of ZnO nanoparticles addition

Chapter 6

Unpublished work

Integrated approach combining tribocorrosion, osteogenic and antimicrobial performance of MAO treated samples and the effect of ZnO nanoparticles addition

FG Oliveira[1,2], BC Costa[2], CK Tokuhara[3], RC Oliveira[3], PN Lisboa-Filho[2,4], M Henriques[5], LA Rocha[1,2,4]

1 - Center MicroElectroMechanical Systems (MEMS-UMinho), Department of Mechanical Engineering, University of Minho, Campus de Azurém, 4800-058 Guimarães, Portugal
2 - IBTN/Br – Brazilian Branch of the Institute of Biomaterials, Tribocorrosion and Nanomedicine, Universidade Estadual Paulista – UNESP, Av. Eng. Luiz Edmundo Carrijo Coube, 17033-360 Bauru, São Paulo, Brazil
3 - Department of Biological Sciences, Bauru Dental School, University of São Paulo (USP), Alameda Dr. Octávio Pinheiro Brisolla 9-75, Bauru, São Paulo, SP 17012-901, Brazil
4 - Faculdade de Ciências, Departamento de Física, Universidade Estadual Paulista - UNESP, Av. Eng. Luiz Edmundo Carrijo Coube, 17033-360 Bauru, São Paulo, Brasil
5 - CEB, Centre of Biological Engineering, University of Minho, Campus de Gualtar, 4710-057 Braga, Portugal

Abstract

Titanium is a widely recognized material for production of dental implants. In this field, the performance of a biomaterial in the human body will be essentially determined by the material properties, the complex environment in which it is placed and also the cell-material interactions taking place at the interface. This way, the improvement of dental implant performance is to a great extent related to its surface properties.

Corrosion and tribocorrosion processes can arise from the chemically aggressive physiological environment together with the loads transmitted from mastication cycles. Biologically, the implant surfaces should present bio-selective characteristics to guarantee the adhesion and proper development of bone cells, as well as inhibit the adhesion and proliferation of microbial organisms.

In this work, Micro-Arc Oxidation (MAO) and coupled ultrasound-MAO techniques were used to produce titanium oxide layers doped with bioactive elements (Ca, P, Mg, Zn). The

surfaces were characterized for their basic chemical and structural properties, and further studied as the first integrated approach including corrosion, tribocorrosion, osteogenic and antibacterial properties.

The presence of ZnO nanoparticles dispersed in the electrolyte did not influence the morphology of the surfaces, but altered the chemical and structural properties of the oxides, by the incorporation of Zn species and the consequent increase in rutile content.

Multifunctional Zn-containing samples presented good corrosion and tribocorrosion performance and a bio-selective behavior that improved osteoblast functions and inhibited bacterial adhesion.

1. Introduction

Titanium, both pure and alloyed, has played a crucial role in the worldwide development of the dental implant industry, generating billions of dollars each year [1]. Titanium is widely recognized in the field due to its attractive properties, such as good mechanical properties, good interaction with bone tissues, and resistance to corrosion. These last two factors arise from the passive oxide film instantaneously formed in the surface of titanium materials in contact with oxygen [2]. This passive layer acts as a barrier to corrosion and dissolution of titanium ions into the surrounding environment. However the complex oral environment poses a difficult challenge for the good performance of any material, and in some cases can compromise the protectiveness of this barrier. The corrosive oral environment with high pH fluctuations and presence of chloride and fluoride species can represent a threat to the integrity of dental materials [3-5]. Also the physiological loads arising from mastication cycles can cause micromovements in the bone-implant interface and easily remove the passive film from the surface of the material, exposing the bulk metal to active corrosion. From the engineering point of view, this particular situation can be understood as a tribocorrosion mechanism, i.e. mechanical and corrosion degradation acting simultaneously in the material [6, 7]. This phenomenon is known in literature to cause a synergistic effect of both processes (corrosion + wear), leading, in general, to an increased material deterioration [8, 9]. Tribocorrosion has been studied for the last years, and has been recently applied to the field of materials for implantology [8, 10-13]. In a biological environment, the results from this kind of degradation are the release of metallic ions and wear particles to the adjacent tissues and possibly to other organs in the body [14, 15]. The localized effects of these wear/corrosion products can be inflammatory reactions in the peri-implant area, leading to implant loosening and ultimately the failure of the restoration.

Recent works are focusing on the characterization of tribocorrosion mechanisms in titanium materials and also trying to improve its performance. The pH of the environment and the fluoride content were studied by several authors [8, 11, 16-18] revealing a tendency for higher tribocorrosion degradation in acidic solutions with high fluoride contents. Acidic environments [16] and even the presence of biofilms [18] can cause a small attenuation of the mechanical processes through the decrease in coefficient of friction between the materials, however the aggressiveness of the chemical environment accounted for an increased material loss. Recently Alves et al. [13] developed a MAO surface treatment that could effectively reduce the surface degradation by the formation of mixed anatase and rutile layers on titanium.

The oral cavity also has optimal characteristics for microbial development and biofilm formation. The colonization of the implant surface by microorganisms can lead to severe inflammatory reactions such as peri-implantitis [19]. The degradation of the tissues can occur in the form of bone resorption, jeopardizing the structural integrity of the implant. Furthermore, biofilms are associated with the production of acidic substances, which can greatly lower the pH values in the close vicinity of the surface and contribute to severe corrosion [20]. The incorporation of elements with known antibacterial activity like silver or zinc is regarded as an option to provide antibacterial properties, whether due to bactericidal effects or the inhibition of adhesion [21]. Antibacterial mechanisms are often associated with disruption of the cell membranes of microorganisms or the production of reactive oxygen species that result in oxidative stresses and damages to proteins, membranes or DNA [22-25]. Silver is many times regarded as a potential cytotoxic element, while additions of zinc are reported to have a beneficial effect on osteoblast behavior and reduced resorptive activity in the bone [26, 27].

Finally, osseointegration is perhaps the major event leading to implant success. Since the insertion in the bone, the surface of the implant is interacting with proteins and other biomolecules that will control the further attachment and proliferation of bone cells to colonize the surface and promote a stable fixation of the implant. Topography and chemical composition of the surfaces are crucial parameters for the good development of these phenomena. Rougher surfaces can promote higher osteoblast adhesion [28] and improve the mechanical interlocking of the implant [29, 30] resulting in higher removal torques [31]. Alterations in chemical composition, to allow the incorporation of bioactive elements guarantee a better chemical affinity between the contacting materials, leading to better implant-tissue integration due to high apatite inducing ability and enhanced cellular processes [32-36].

All the previously referred aspects are dependent on the surface characteristics of the implant: its roughness, topographical features, chemical composition, crystalline structure, etc. Methods for providing the adequate surface properties to dental implant materials have been used in the last years, with special focus on micro-arc oxidation (MAO) [12, 13, 33, 34, 37]. This technique allows the creation of thick, adherent and porous oxide films on titanium surface, providing excellent conditions for osteogenic cell adhesion and proliferation, as well as an effective protection against corrosion and tribocorrosion degradation.

In this work, MAO and coupled ultrasonic-MAO were used to create titanium oxide films containing several bioactive elements (Ca, P, Mg) and further modified using ZnO nanoparticles for additional antibacterial performance. The surfaces were characterized for their basic chemical and structural properties, and further studied as the first integrated approach including corrosion, tribocorrosion, osteogenic and antibacterial properties.

2. Materials and Methods

2.1. Surface modification

Square samples of commercially pure titanium (10x10x2 mm) were cut and etched in aqueous acid solution containing HF and HNO_3 in similar proportions (1:1:1). After etching, samples were ultrasonically cleaned in propanol and water for 15 min and dried with warm air.

For the surface treatment, samples were placed in an electrochemical cell and immersed in a conductive electrolyte. Three different types of electrolytes were used in this work and determined the experimental groups as defined in table 6.1. Electrolytes consisting of aqueous solutions containing calcium acetate monohydrate (CaA), β-glycerophosphate disodium salt pentahydrate (β -GP), magnesium acetate tetrahydrate (MgA) and zinc oxide nanoparticles (ZnO NP's) were used. Mixing of precursor reagents for Ca, P and Mg was achieved by simple magnetic stirring, while the dispersion of ZnO NP's was attained by ultrasonication during 5 min using a Sonics VCX-750 Ultrasonic processor operating at 20 kHz and 300 W of nominal power, right before the MAO treatment.

Etched titanium worked as anode, while a platinum sheet served as cathode for the electrochemical reactions. Samples were submitted to MAO treatment using a DC power supply (Agilent N5772A) for 1 min at a maximum voltage of 300 V and limiting current of 2.5 A, under magnetic stirring to assure homogeneous flow of ions in the bath.

Table 6.1 - Representation of the four test groups studied in this work (Ti, CaP, Mg, Zn). Electrolyte compositions for MAO treatments of each group (voltage (300V) and time (1 min) were kept constant for all MAO groups)

Group		**Electroyte composition**			
		CaA	β-GP	MgA	ZnO NP's
etched	**Ti**	Etched samples. Without MAO treatment			
MAO treated	**CaP**	0.35 M	0.02 M	—	—
	Mg	0.35 M	0.02 M	0.1 M	—
	Zn	0.35 M	0.02 M	0.1 M	1 gr/L

2.2. Surface Characterization

Resulting surfaces from etching and MAO treatments, as well as the wear tracks of tribocorrosion tests were investigated in a scanning electron microscope (SEM, Model FEI Nova 200 (FEG/SEM)) with chemical analysis performed by energy dispersive X-ray spectroscopy (EDAX, Pegasus X4M (EDS/EBSD)) attached to the SEM. Adhesion of MC3T3-E1cells to MAO treated surfaces after 4 and 24 h of contact was analyzed in a high-resolution SEM (FEG-SEM; JEOL 7500F).

The crystalline structure of the MAO treated samples was analyzed by grazing incidence x-ray diffraction (XRD, Bruker D8 Discover) with Cu Kα radiation in the scan range (2θ) from 20° to 60°.

Surface profiles of tribocorrosion tested samples were obtained with a Veeco Dektak 150 Profilometer to allow the calculation of wear volume caused by tribocorrosion mechanisms.

2.3. Electrochemical and Tribocorrosion testing

Potentiodynamic polarizations were obtained with a Gamry Reference 600 Potentiostat using a three-electrode configuration. Samples were immersed in Simulated Body Fluid (SBF) [38] (NaCl 6,213 g/L; $NaHCO_3$ 2.974 g/L; KCl 0.225 g/L; $K_2HPO_4.3H_2O$ 0.231 g/L; $MgCl_2.6H_2O$ 0.311 g/L; $CaCl_2$ 0.292 g/L; Na_2SO_4 0.072 g/L; HCl 0.85x10-3 M) solution at 37°C, for 2 h to allow stabilization of corrosion potential and the polarization curves were acquired from cathodic to anodic domain at a scan rate of 1mV/s.

For tribocorrosion tests, samples were mounted in a electrochemical cell and immersed in SBF solution at 37°C. The cell was mounted on a pin-on-disk reciprocating sliding tribometer (CETR-UMT 2) for the tribocorrosion test. For the electrochemical measures, etched titanium or

MAO treated samples acted as working electrode while a saturated calomel electrode (SCE) (Hg/Hg_2Cl_2/saturated KCl solution; SCE = +244 mV/NHE) was the reference electrode in a two electrode configuration used to measure open circuit potential before, during and after the sliding tests using a Radiometer Copenhagen potentiostat/galvanostat, model PGP201. The potential of the samples was measured for 2 h before the sliding, to allow complete stabilization of OCP values. Mechanical contact was performed by an alumina ball counterbody (ø = 10 mm) and the sliding parameters consisted in normal load of 2 N, amplitude of 5 mm, frequency of 2 Hz, and 30 min of sliding time.

2.4. Cell culture

MC3T3-E1 (from American Type Culture Collection - ATCC) mouse preosteoblasts were cultured in α-MEM (Gibco) supplemented with 10% fetal bovine serum, FBS (Gibco) and 1% penicillin/streptomycin (Gibco) at 37°C and 5% CO_2. Thereafter, before reaching confluence, cells were detached by trypsinization, treated with trypan blue and counted in a hemocytometer.

2.5. Cell viability assays

Extracts (pure and 1:2 dillution) were collected by immersing the samples in α-MEM, supplemented with 10% FBS at a ratio of 0.1 g/ml at 37°C and 5% CO_2 atmosphere during 24h. As a positive control α-MEM supplemented with 10% FBS was used.

For cytotoxicity tests $3x10^3$ cells were cultured in the wells of a 96 well plate at 37°C and 5% CO_2 atmosphere. After incubation for 24 h, culture medium was replaced by extracts obtained from the contact with the samples. Cell viability was assessed for 3 periods of time: 24h, 48h and 72h. After each period, the extracts were removed and cells were washed with PBS before MTT reduction and Crystal Violet staining tests. Experiments were performed in octuplicate.

For MTT reduction test, cellular activity was estimated by measuring the conversion of 3-(4,5-dimethyltiazol-2-yl)-2,5-diphenyltetrazolium bromide (MTT) to its formazan product. MTT (0.5mg/ml) was added to each well, and culture plates were incubated at 37°C for 4 h. The medium was removed and then, dimethylsulfoxide (DMSO) was added to each well. After 30 min, the optical density was measured at 550 nm with a Synergy™ H1 monochromator-based multi-mode microplate reader (Bio-Tek).

For Crystal Violet (CV) staining, cells were washed with PBS, immersed in methanol for 10 min and stained with 0.2% CV in 20% ethanol for 3 min. The excess stain was removed with two Phosphate Buffered Solution (PBS: NaCl 8 g/L; KCl 0.2 g/L; Na_2HPO_4 1.44 g/L; KH_2PO_4 0.25 g/L) washes. Finally, 0.05M sodium citrate solution in 50% ethanol was added to each well for 10 min. The optical density was measured at 540 nm with a Synergy™ H1 monochromator-based multi-mode microplate reader (Bio-Tek).

GraphPad Prism software was used to calculate the difference between sets of data based on analysis of variance (ANOVA). p values less than 0.05 were considered statically significant.

2.6. Cell adhesion and proliferation

Three samples (10x10x2 mm) of each MAO group were distributed in a 24 well plate. MC3T3-E1 cells were cultured and counted, as previously described. After, $5x10^3$ cells were seeded in the surface of each sample for 4h and 24 h at 37 °C and 5% CO_2 environment. After each period, samples were washed with PBS to remove non-adhered cells and fixed by immersion in Karnovsky's solution containing 2.5% gluteraldehyde and 2% paraformaldehyde in 0.05 M sodium cachodylate buffer and 0.001 M calcium chloride, for 72 h. After fixation, the specimens were washed several times with cacodylate buffer 0.05M and then postfixed for 1 h with 1% osmium tetroxide in distilled water followed by extensive washing in distilled water. Then, samples were sequentially dehydrated in a graded acetone series of 30%, 50%, 70%, 90% and 100%. Samples rested for 48 h in a closed container, with anhydrous silica, for complete drying. Specimens were then mounted on a stub, gold coated and the morphology of osteoblasts was investigated by scanning electron microscopy.

2.7. Antibacterial tests

S. aureus bacterial cultures originated from stock culture plates were grown in Triptic Soy Broth (TSB, Merck) at 37°C under agitation for 18 h. Cell concentration was adjusted through the determination of optical density using a spectrophotometer, to obtain a cell suspension with a concentration of $1x10^5$ cel/ml. Samples were distributed in the wells of a 24-well plate and 1 ml of the cell suspension was added to each well, covering the samples. The plate was incubated overnight at 37 °C. After 24 h of contact, samples were removed from the bacterial suspension and washed in PBS for removing unattached bacteria from the surface. Samples were immersed in 10 ml of PBS and sonicated for 1 h followed by 1 min of vigorous mechanical vortexing to facilitate the release of bacteria from the surface. The resultant bacterial suspension was diluted

in PBS, plated into Triptic Soy Agar (TSA) plates and incubated overnight at 37°C. Three samples per condition were used, and the dilutions were spread in three separate TSA plates. Colony forming units were counted in each plate to assess the amount of *S. aureus* adhered in each sample.

3. Results

3.1. Surface modification

Figure 6.1 shows topographical features of etched and MAO treated samples. Surface properties of analyzed samples are similar to the ones presented in previous works [13, 39]. Etching evidenced a granular structure on titanium surfaces (figure 6.1a), while the MAO treatment created a porous structure (figure 6.1b) which was similar in morphology and porosity for all processing conditions, independently of the addition of magnesium acetate or ZnO NP's to the electrolyte solution. For the Zn group of samples, the incorporation of chemical species into the oxide films is shown in the inset of figure 6.1b, with 0.23 % at. of zinc. The incorporation rate of Ca, P and Mg was comparable to the values presented in a previous work [39].

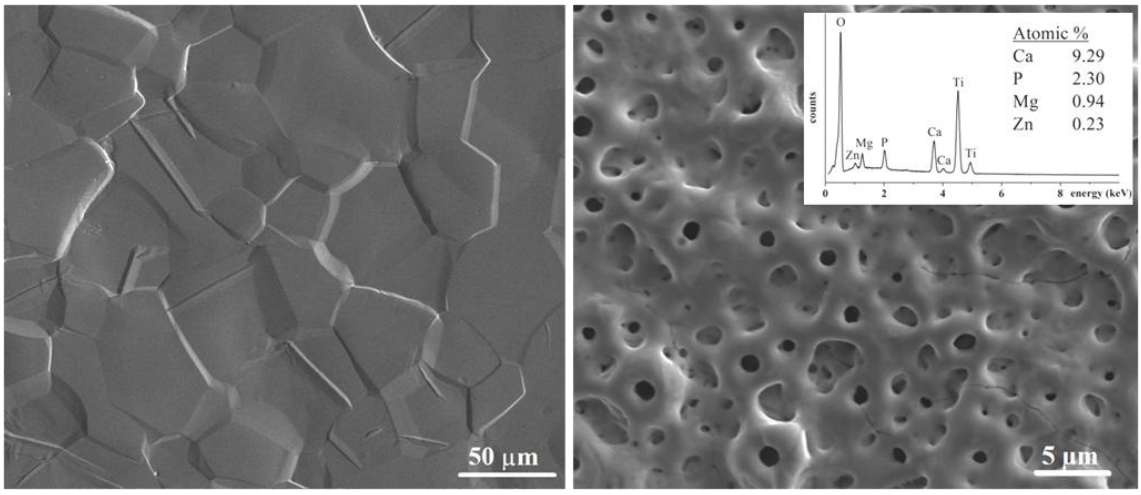

Figure 6.1 – SEM micrographs of (a) etched titanium; (b) MAO treated sample (Zn group)

The crystal structure presents the same peaks for all treated samples, with the presence of anatase and rutile. Rutile is more prone to appear in Mg and Zn samples as shown in figure 6.2. The relative intensities of anatase and rutile first two peaks (anatase at 25.28° and rutile at 27,39°) are revealing of a gradual increase in rutile content, in function of the addition of MgA and MgA + ZnONP's to the electrolyte.

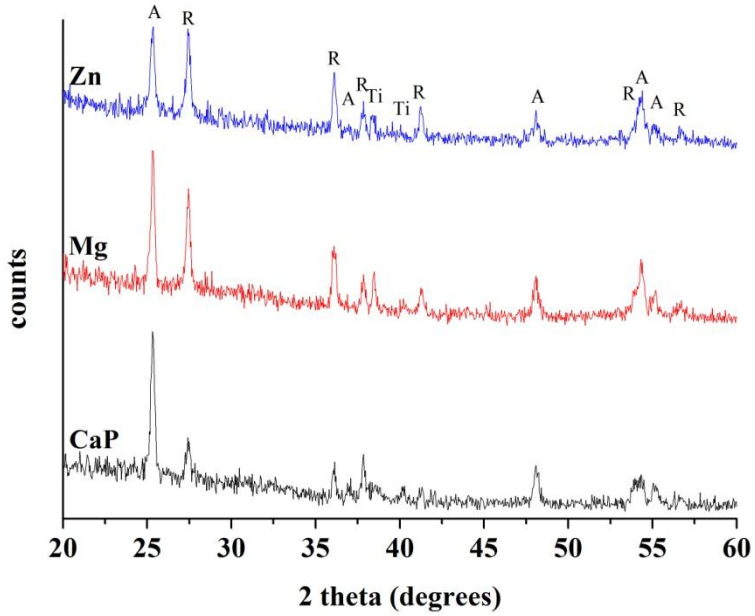

Figure 6.2 – XRD spectra for MAO treated groups with reference to peaks of titanium metal (Ti), anatase (A) and rutile (R).

3.2. Electrochemical and Tribocorrosion behavior

The corrosion behavior of all groups was evaluated by the potentiodynamic polarization curves presented in figure 6.3.

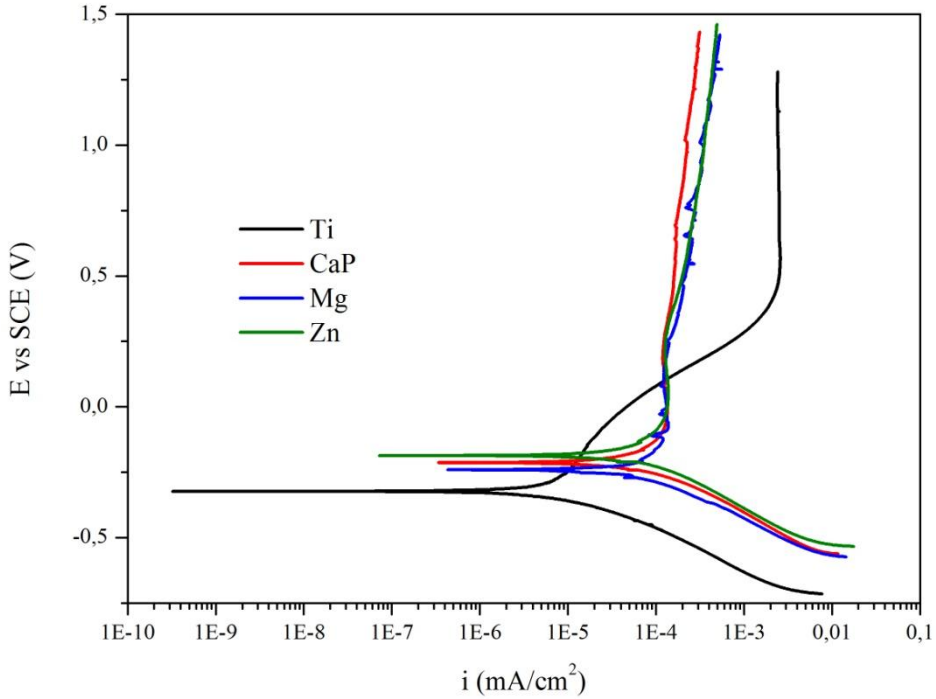

Figure 6.3 – Potentiodynamic plots of the current density versus the applied potential for etched titanium and the three groups of MAO treated samples.

Representative plots, showing the variation of current density with applied potential distinguish dissimilar behavior of titanium and MAO groups. Treated samples present higher E_{corr} and lower currents in the passive domain, confirming the better protective properties of the

oxides. Very similar behavior was found in all MAO groups, with E_{corr} values ranging between the interval -0.20 V and -0.25 V (vs. SCE), and a well-defined passive plateau with current densities around $1E^{-4}$ mA/cm^2. Among all the curves obtained in MAO treated samples the variation was short, however in the transition from cathodic to anodic domains, it was possible to distinguish a propensity for increasing E_{corr} values in the sequence Zn > CaP > Mg.

Figure 6.4 shows the curves for the evolution of OCP ad COF on the three MAO treated groups throughout tribocorrosion experiments with 2N of applied load during sliding.

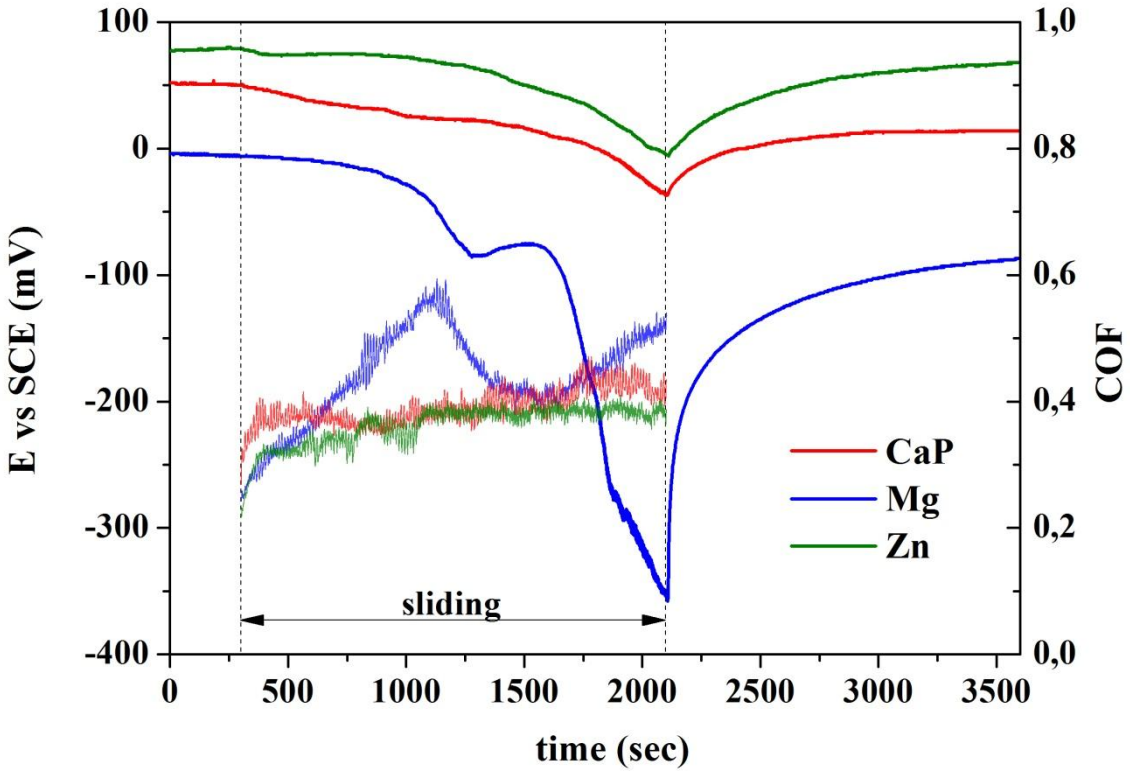

Figure 6.4 - Evolution of open circuit potential (OCP vs SCE) values before, during and after tribocorrosion tests for MAO treated groups.

Before the tribocorrosion tests, the initial potential of the groups obey the order already presented in potentiodynamic curves of figure 6.3. Zn group has the higher potential, followed by CaP and Mg groups respectively. At the beginning of sliding, there is no significant electrochemical response from the test materials, as the potential remains somehow constant, only with a small decreasing trend, for all groups in the first c.a. 10 min of test. Throughout the test, CaP and Zn groups present a very similar behavior, with a low rate of potential drop, however with a tendency for an accelerated decay in the final stage of the sliding test. For both groups, coefficient of friction (COF) values were stable around 0.4, with slightly lower values for the Zn group. Mg group showed a different behavior from half of the test onwards, with irregular potential behavior and a higher decay rate in the last moments (c.a. last 10 min) achieving -350

mV at the end of sliding. The evolution of OCP and COF values is interconnected, as can be seen at nearly half stage of the sliding test, where a decrease in COF causes a momentary stabilization and increase in OCP values. This trend is terminated, as soon as COF values start to increase again, causing then an accentuated rate of potential decay. The irregular behavior of COF can arise from the detachment of particles from the film. It can be the determinant factor for the high potential decay in the Mg group, as the surfaces are submitted to higher tangential forces that can cause increased destruction of the film. At the end of the sliding test, the potential recovers up to nobler values due to repassivation in the wear track area. Mg group samples presented the higher potential increase after the sliding, which was related to the higher drops in OCP values during sliding. However, for the repassivation time allowed in this test, Zn samples presented a very efficient recovery in potential, attaining similar OCP values to the ones presented before the sliding test.

In figure 6.5 (a-c) are presented SEM micrographs for evaluation of damages to the surface of tested groups. Figures 6.5 (d-f) present the same images obtained in backscattered electrons mode, where one can distinguish the most damaged zones of the surface in the brighter zones. In accordance with curves from figure 6.4, CaP and Zn groups showed similar wear track features with erasing of the higher peaks of the rough topography and the accumulation of densely packed oxide particles in some zones of the wear track. As for the Mg group, the analysis of the wear track can indicate the presence of a delamination effect and accumulation and compaction of oxide particles in the borders of the wear track, as seen previously in the work of Alves et al. [12]. The differences in the wear tracks seem to be mostly related to the quantity of degradation, since the wear mechanisms appear similar in all groups, just at different stages of development. It is fair to assume that a continuation of the test for CaP and Zn groups would produce the same results seen in the wear track of Mg group. Figures 6.5 (g-i) present a detailed view on the wear tracks of each group. Figures 6.5g and 6.5i, from CaP and Zn groups respectively, present detachment of large portions of the oxide film, while in 6.5e (Mg group) there is already a completely removed top layer of the film. These results led to an increased wear volume, measured in the samples of Mg group, presenting values 3 to 4 times higher than the CaP and Zn groups, as seen in figure 6.6.

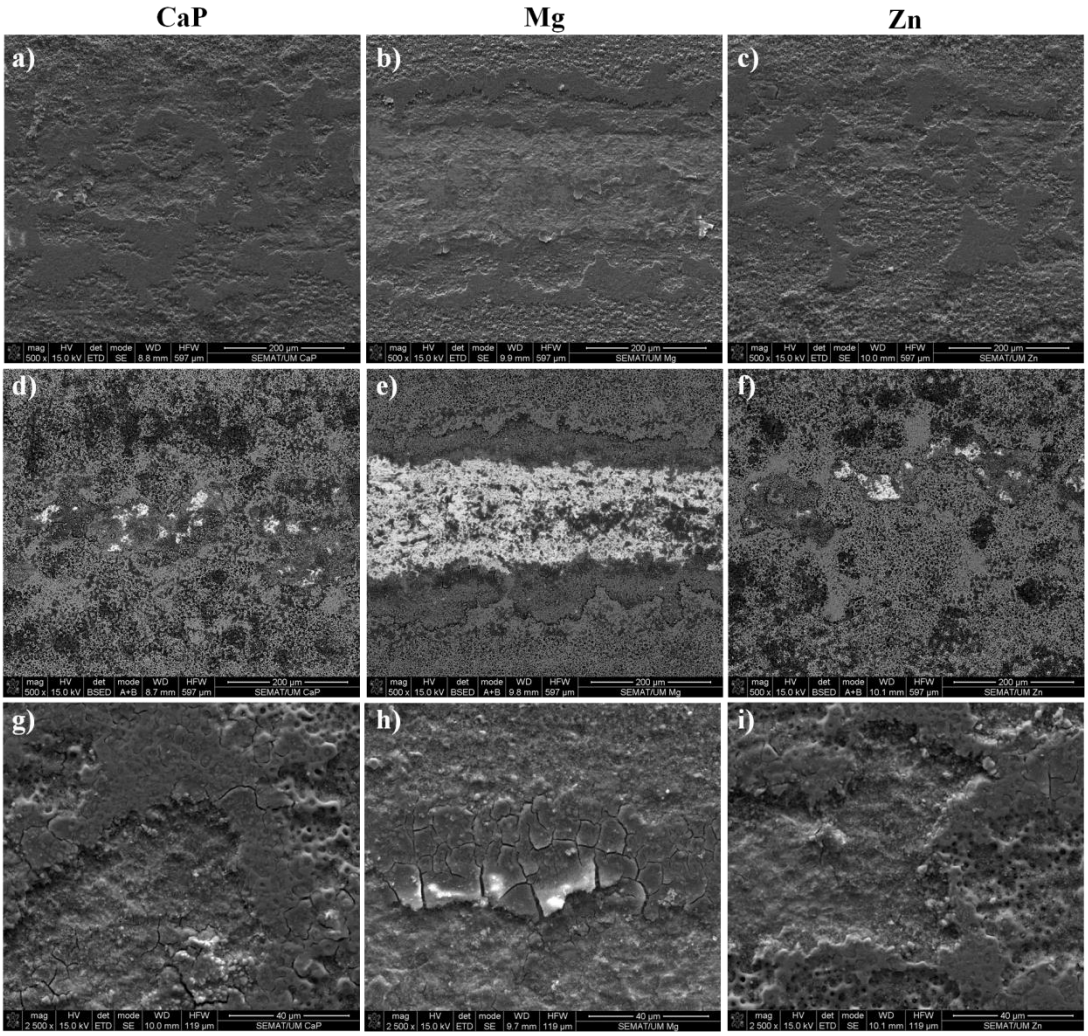

Figure 6.5 –SEM micrographs of wear tracks on MAO treated samples. Top row (a-c): general view of the wear track using secondary electrons detection mode. Middle row (d-f): general view of the wear track using backscattered electrons detection mode. Bottom row (g-i): detailed view inside the wear track using secondary electrons detection mode

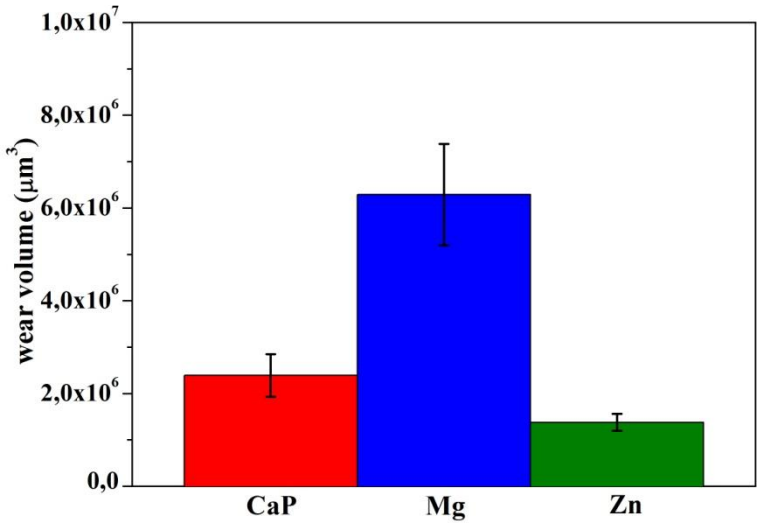

Figure 6.6 – Calculated wear volumes for MAO treated samples after tribocorrosion tests

3.3. Cell viability

Figure 6.7 represents the cell viability assays of MC3T3-E1 cells after contact with pure extracts from the four groups of samples using Crystal Violet staining and MTT reduction. Data presents the evolution of total absorbance measured after three periods of 24, 48 and 72 h of exposition. Absorbance values for diluted extracts did not provide relevant information, when compared to pure extracts and therefore are not presented in this section.

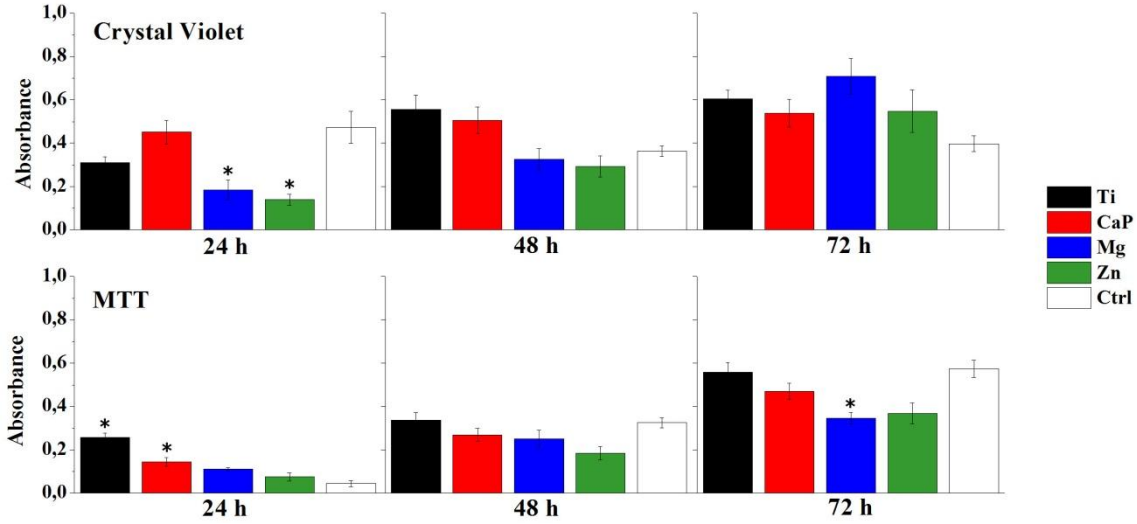

Figure 6.7 – Crystal Violet staining and MTT reduction assays of MC3T3-E1 cells in different extract media for periods of 24, 48 and 72 h (Data shown as mean ± SEM of eight experiments; statistically significant values relative to control group as p < 0.05 are presented as *)

Crystal Violet is responsible for staining cellular nucleic acids. Spectrophotometer readings of color intensity are therefore a measure of DNA content and cell number.

Absorbance values in the 24h period reveal low cell viability of all groups (except CaP) when compared to the control group. In the following periods, there is a good increase in absorbance values for all groups, and after 72 h of test, all test groups tend to present higher cell viability than the control.

The MTT assay was used to evaluate cell viability, since it is considered a sensitive assay for the determination of mitochondrial dehydrogenase activity. Viable cells with active metabolism convert MTT into a purple colored formazan product with an absorbance maximum near 570 nm.

Compared to control group, the MTT values for the test groups are higher in the first 24 h, denoting superior mitochondrial activity in this period. After this time the values from test and control groups seem to be more leveled for 48h and 72h periods. For longer times, Mg and Zn samples appear to generate lower cell viability than the Ti and CaP groups.

3.4. Cell adhesion and proliferation

Figure 6.8 presents the evolution of adhesion and morphology of MC3T3-E1 cells on surfaces of the three groups of MAO treated samples (CaP, Mg, Zn) for periods of 4 and 24 h.

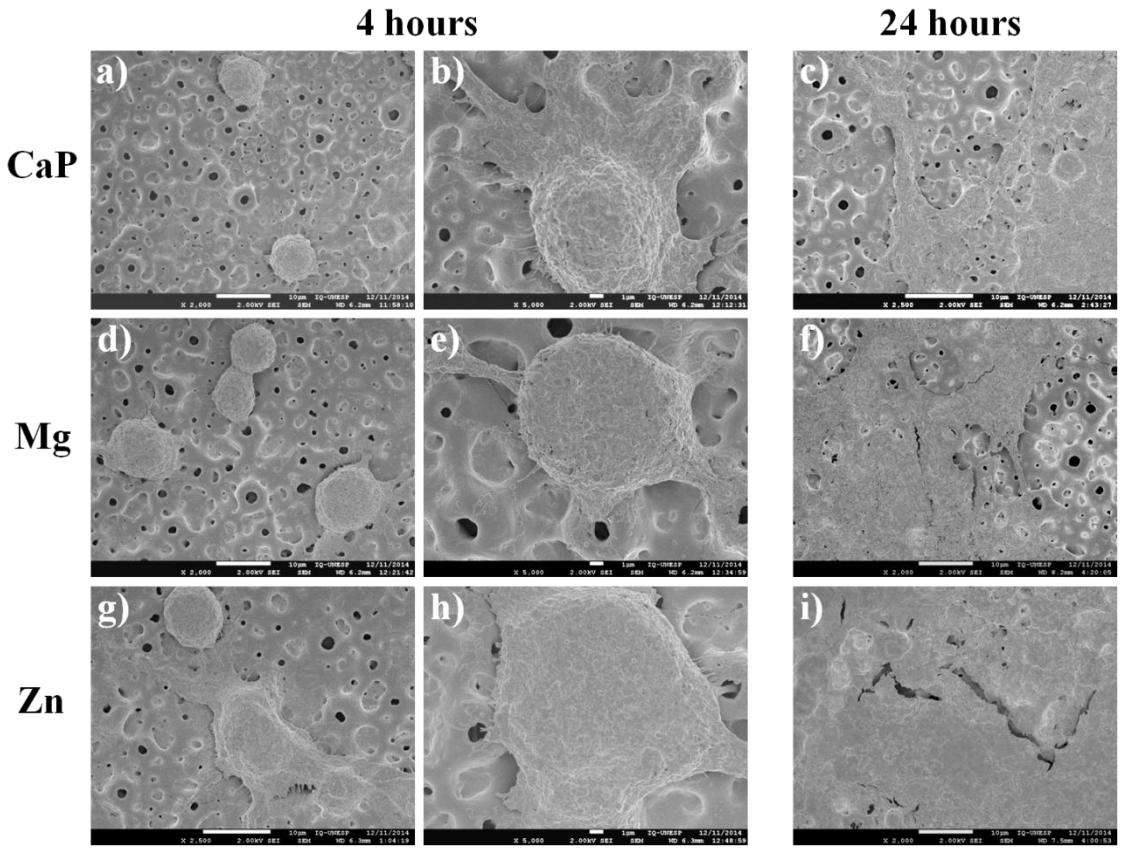

Figure 6.8 – Morphology of MC3T3-E1 cells on surfaces of MAO treated titanium after 4 and 24 h of adhesion.

At 4 h of contact (figures 6.8 a, b, d, e, g and h), cells are in the first stages of adhesion with a good phenotypic morphology of metabolically active osteoblasts, still with a round shape and sometimes starting to spread through well-developed lamellipodia and filopodia. The size of the cells was comparable in all surfaces. Cells with round shapes and cells with a good degree of spreading and more flattened cell body (well visible in images of figure 6.8 b, g and h), were found in all groups of samples and in some cases presenting already strong cytoplasmatic extensions for binding to the surface.

At 24 h of adhesion (figures 6.8 c, f and i), the cells are widely spread on the surface, presenting an interconnecting structure among them. Cells cover a large portion of the porous structure, accompanying the surface morphology, indication of a good interaction with the substrates. Zn containing samples showed the highest degree of covered surface among all the MAO treated groups.

3.5. Antibacterial properties

The antibacterial effect of test groups was assessed in contact with *S. aureus* bacterial suspension for 24 h. Results provided information about the degree of viable bacteria adhered to the surfaces of the four tested groups and reveal higher degree of microbial adhesion on MAO treated samples rather than on Ti etched surfaces. This difference is attributed to the differences in topographic properties. Nevertheless, among MAO treated groups, Zn-containing samples proved to cause a decrease in bacterial adhesion in comparison with CaP and Mg groups.

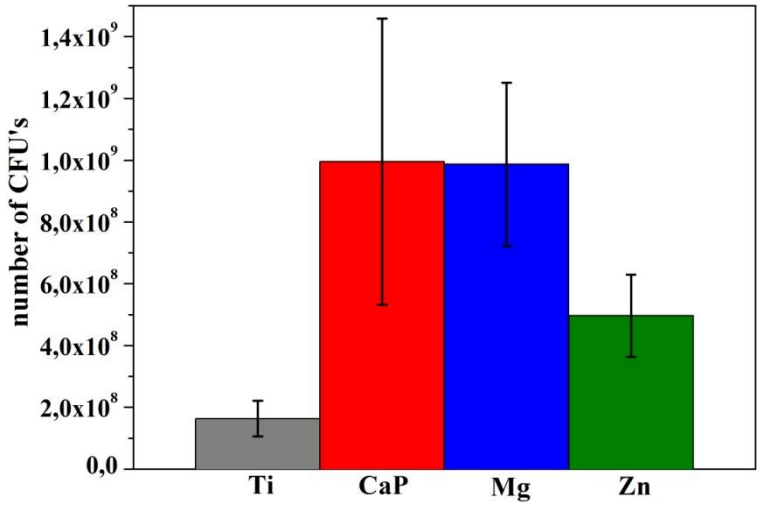

Figure 6.9 –Bacterial colony counts of S. aureus after 24 h of culture in contact with samples from Ti and MAO groups. (Data presented in terms of mean ± SEM of 3 samples per condition)

4. Discussion

For the explanation of film formation, it is assumed the previously proposed mechanism [39] to explain the oxide formation in CaP and Mg groups. Furthermore, the same mechanism can serve as basis for the understanding of film formation when zinc oxide NP's are added to the electrolyte.

Based on SEM micrographs of figure 6.1, the addition of ZnO NP's did not have an effect on the morphology of oxide film. Furthermore, the chemical composition of the oxide in the Zn group was comparable to the Mg group, with only a small appearance of Zn, as expected.

The integration of Zn in the oxide film can be explained by the same mechanism proposed elsewhere for the incorporation of other bioactive ions [39]. The highly energetic micro arcs occurring at the surface of the oxide can cause local melting of the film and bring some portions of the electrolyte in the vicinity of the surface to be mixed together with the melted oxide. Dispersed ZnO NP's can also be a part of these portions of melted material. In this case the solidification process can incorporate the Zn element, as a particle or as a part of the oxide

structure if temperatures are high enough to melt the ZnO NP's. According to the work of Dulin and Rase [40], who investigated the ZnO-TiO_2 system, two forms of zinc titanates could be formed upon the heating of zinc and titanium oxides at high temperatures: $ZnTiO_3$ and Zn_2TiO_4. Later Yang and Swisher [41] referred also the stability of $Zn_2Ti_3O_8$ compound. Upon melting of the oxide and incorporated ZnO NP's at extreme temperatures, the formation of these compounds can be possible, however in very low quantities that are not detected, for instance, in XRD analysis of figure 6.2. The one thing noticed from XRD spectra is the increase of rutile phase in the Zn group. We previously reported that the addition of Mg to the electrolyte and the associated increase in the conductivity of the solution was the reason for higher rutile formation in the oxide for Mg samples when compared to CaP samples [39]. In this work, the further addition of ZnO NP's produced similar effect as the relative rutile/anatase ratio was the highest in samples of Zn group. The sonochemical dispersion procedure could have also influenced this outcome, as the temperature of the electrolyte after the sonochemical treatment increases up to 10 °C in comparison with regular electrolytes of the CaP and Mg groups.

In a previous study [39], the formation of rutile phase, with known superior mechanical properties was considered to be a determinant factor for mechanical resistance under tribocorrosion solicitations. In this work, under higher normal loads, there was no linear relation found between the amount of rutile and tribocorrosion behavior. Samples of the CaP group with the least rutile content, presented good tribocorrosion behavior, in contrast with Mg group, which presented increased surface degradation, even in the presence of higher rutile contents. The higher loads on the surface may have caused the rutile-rich oxide of the Mg samples to crack under brittleness associated with the harder rutile. The softer oxide in CaP samples could better accommodate the stresses without cracking, and with low damages on the surface.

The tribocorrosion behavior in the Zn group was comparable to the CaP group, even with a major increase in rutile content. It could be expected that higher rutile would be more prone to brittle cracking, however both electrochemical and mechanical results proved otherwise. To explain this behavior one could assume that the possible formation of zinc titanates can influence the mechanical contact properties. There are some works referring the solid lubricant properties of zinc titanates due to low stacking fault energy in determined structural planes that can act as pathways for parallel glide of dislocations in the sliding direction, achieving low interfacial shear stresses and present a ductile behavior with decreasing friction values [42, 43]. These

mechanisms could act as attenuators of the brittle characteristics of rutile, shown in the samples of Mg group, decreasing the wear degradation of the Zn samples.

Based on micrographs from figure 6.5, related to the samples from Mg group, it is assumed that the wear of the oxide films occurs in distinctive phases. Figure 6.5b presents a dual delamination effect which can be linked to the evolution of OCP and COF of figure 6.4. The high increase in COF at the first stage of sliding can easily jeopardize the brittle characteristics of rutile and cause a higher release of oxide particles in the top zones of the oxide. To some point, these particles can accommodate in the lower recesses of the rough structure or inside the pores, creating a more compacted layer of densely packed oxide particles that can provide additional protection through a gradual decrease in friction values and subsequent OCP increase, visible at half stage of the sliding test in figure 6.5 for Mg group. With the evolution of the sliding test, this compacted layer starts also to collapse giving rise to a second increasing trend in COF and a more accentuated drop of potential.

As previously referred, the deterioration of CaP and Zn groups follows the same mechanism, however at a slower rate. At the end of the sliding test, is visible in the micrographs of figure 6.5g and 6.5i, that a first stage of material detachment is starting to occur in localized zones of the wear track and would eventually lead to a similar behavior, as verified in the Mg group.

MAO treated samples produced good results in biological tests. The cell viability assays shown in figure 6.7 proved good properties of the oxide films, with no visible cytotoxic effects in the tested MC3T3-E1 cells. In all cases was reported an increase in absorbance over time, indication of good cellular proliferation properties.

In the adhesion tests, (figure 6.8) one can perceive the spreading of cellular extensions, already with 4 h of contact, which is representative of the beginning of the process of adhesion through physical contact with the surface. Also to note, the tendency of these extensions to enter the porous structure in an attempt to get better mechanical fixation and stability to support the cell's further development. Samples from the Zn group presented stronger extensions and generally a higher tendency for spreading. After 24 h, the tendency confirms the Zn group as the most beneficial surface for the cellular development among MAO treated groups. The addition of ZnO NP's in the MAO electrolyte, and the further incorporation of Zn species in the oxide film caused the highest cell proliferation and covered sample area over a period of 24 h of contact.

These results are in accordance with several previous works from literature, reporting that the incorporation of Zn is favorable for the adhesion and proliferation of osteoblastic cells [26, 44].

Antibacterial tests revealed a dual effect of topography and chemical composition in the colonization of bacteria in the surfaces. Etched titanium presented the lowest amount of bacteria, due to the decreased surface roughness and porosity. In MAO groups the structure of the oxide film can cause the microorganisms to enter the porous structure and create suitable microenvironments for the development of biofilms and therefore increase the number of adhered bacteria. Among the MAO treated groups, the presence of Zn species caused a decrease in colony forming units after the 24 h of contact, confirming the previous reports about the antibacterial behavior of Zn [21, 44]. Although the quantitative nature of the protocol did not allow for the characterization of bactericidal or adhesion preventive properties, the results presented here confirm Zn containing oxide films as a good option for minimizing bacterial associated infections.

5. Conclusions

This work presents an integrated approach for the characterization of multifunctional behavior of MAO treated surfaces for application in dental implants. The incorporation of Zn species in the oxide film did not influenced the morphology of the oxides, but was noted to cause an increase in rutile phase. Electrochemical and tribocorrosion of Zn-containing samples have profited from the possible lubricant effect of zinc titanates causing a decrease in friction during the test. This effect balanced the brittle properties of the rutile-rich layer and led to decreased surface deterioration.

From the biological point of view, the presence of Zn species in the oxide led to improved cellular processes of adhesion and proliferation over a 24 h period. Furthermore, the presence of Zn, inhibited the adhesion of bacteria in the surface.

In conclusion, the multifunctional and bio-selective nature of Zn-containing samples makes it a promising material for application in dental implant materials.

References

[1] Global boom in dental implants. *British Dental Journal*, 214(5): 219-219, **2013**. doi:10.1038/sj.bdj.2013.232

[2] S. Virtanen, I. Milošev, E. Gomez-Barrena, R. Trebše, J. Salo, and Y.T. Konttinen. Special modes of corrosion under physiological and simulated physiological conditions. *Acta Biomaterialia*, 4(3): 468-476, **2008**.

[3] N. Schiff, B. Grosgogeat, M. Lissac, and F. Dalard. Influence of fluoride content and pH on the corrosion resistance of titanium and its alloys. *Biomaterials*, 23(9): 1995-2002, **2002**.

[4] J.C.M. Souza, S.L. Barbosa, E.A. Ariza, M. Henriques, W. Teughels, P. Ponthiaux, J.-P. Celis, and L.A. Rocha. How do titanium and Ti6Al4V corrode in fluoridated medium as found in the oral cavity? An *in vitro* study. *Materials Science and Engineering: C*, 47: 384-393, **2015**.

[5] D. Rodrigues, P. Valderrama, T. Wilson, K. Palmer, A. Thomas, S. Sridhar, A. Adapalli, M. Burbano, and C. Wadhwani. Titanium corrosion mechanisms in the oral environment: A retrieval study. *Materials*, 6(11): 5258-5274, **2013**.

[6] M.T. Mathew, P. Srinivasa Pai, R. Pourzal, A. Fischer, and M.A. Wimmer. Significance of tribocorrosion in biomedical applications: Overview and current status. *Advances in Tribology*, 2009: 250986, **2009**.

[7] L.A. Rocha, F. Oliveira, H.V. Cruz, C. Sukotjo, and M.T. Mathew. Bio-tribocorrosion in dental applications. in *Bio-Tribocorrosion in Biomaterials and Medical Implants*. Woodhead Publishing, **2013**.

[8] M.T. Mathew, S. Abbey, N.J. Hallab, D.J. Hall, C. Sukotjo, and M.A. Wimmer. Influence of pH on the tribocorrosion behavior of CpTi in the oral environment: Synergistic interactions of wear and corrosion. *Journal of Biomedical Materials Research Part B: Applied Biomaterials*, 100B(6): 1662-1671, **2012**.

[9] J.P. Celis, P. Ponthiaux, and F. Wenger. Tribo-corrosion of materials: Interplay between chemical, electrochemical, and mechanical reactivity of surfaces. *Wear*, 261(9): 939-946, **2006**.

[10] J.C.M. Souza, S.L. Barbosa, E. Ariza, J.P. Celis, and L.A. Rocha. Simultaneous degradation by corrosion and wear of titanium in artificial saliva containing fluorides. *Wear*, 292–293: 82-88, **2012**.

[11] M.P. Licausi, A.I. Muñoz, and V.A. Borrás. Tribocorrosion mechanisms of Ti6Al4V biomedical alloys in artificial saliva with different pHs. *Journal of Physics D: Applied Physics*, 46(40): 404003, **2013**.

[12] S.A. Alves, R. Bayón, A. Igartua, V. Saénz de Viteri, and L.A. Rocha. Tribocorrosion behaviour of anodic titanium oxide films produced by plasma electrolytic oxidation for dental implants. *Lubrication Science*, 26(7-8): 500-513, **2014**.

[13] A.C. Alves, F. Oliveira, F. Wenger, P. Ponthiaux, J.P. Celis, and L.A. Rocha. Tribocorrosion behaviour of anodic treated titanium surfaces intended for dental implants. *Journal of Physics D: Applied Physics*, 46(40): 404001, **2013**.

[14] N.J. Hallab and J.J. Jacobs. Biologic effects of implant debris. *Bulletin of the NYU Hospital for Joint Diseases*, 67(2): 182-188, **2009**.

[15] R.M. Urban, J.J. Jacobs, M.J. Tomlinson, J. Gavrilovic, J. Black, and M. Peoc'h. Dissemination of wear particles to the liver, spleen, and abdominal lymph nodes of patients with hip or knee replacement. *The Journal of Bone & Joint Surgery*, 82(4): 457-457, **2000**.

[16] A.C. Vieira, A.R. Ribeiro, L.A. Rocha, and J.P. Celis. Influence of pH and corrosion inhibitors on the tribocorrosion of titanium in artificial saliva. *Wear*, 261(9): 994-1001, **2006**.

[17] M.P. Licausi, A. Igual Muñoz, and V. Amigó Borrás. Influence of the fabrication process and fluoride content on the tribocorrosion behaviour of Ti6Al4V biomedical alloy in artificial saliva. *Journal of the Mechanical Behavior of Biomedical Materials*, 20: 137-148, **2013**.

[18] J.C.M. Souza, M. Henriques, R. Oliveira, W. Teughels, J.-P. Celis, and L.A. Rocha. Biofilms inducing ultra-low friction on titanium. *Journal of Dental Research*, 89(12): 1470-1475, **2010**.

[19] H. Algraffee, F. Borumandi, and L. Cascarini. Peri-implantitis. *British Journal of Oral and Maxillofacial Surgery*, 50(8): 689-694, **2012**.

[20] J.C.M. Souza, P. Ponthiaux, M. Henriques, R. Oliveira, W. Teughels, J.-P. Celis, and L.A. Rocha. Corrosion behaviour of titanium in the presence of *Streptococcus mutans*. *Journal of Dentistry*, 41(6): 528-534, **2013**.

[21] K. Huo, X. Zhang, H. Wang, L. Zhao, X. Liu, and P.K. Chu. Osteogenic activity and antibacterial effects on titanium surfaces modified with Zn-incorporated nanotube arrays. *Biomaterials*, 34(13): 3467-3478, **2013**.

[22] C.A. McDevitt, A.D. Ogunniyi, E. Valkov, M.C. Lawrence, B. Kobe, A.G. McEwan, and J.C. Paton. A molecular mechanism for bacterial susceptibility to zinc. *PLoS Pathogens*, 7(11): e1002357, **2011**.

[23] R. Pérez-Tanoira, C. Pérez-Jorge, J.L. Endrino, E. Gómez-Barrena, D. Horwat, J.F. Pierson, and J. Esteban. Bacterial adhesion on biomedical surfaces covered by micrometric silver islands. *Journal of Biomedical Materials Research Part A*, 100A(6): 1521-1528, **2012**.

[24] E.S. Thian, T. Konishi, Y. Kawanobe, P.N. Lim, C. Choong, B. Ho, and M. Aizawa. Zinc-substituted hydroxyapatite: a biomaterial with enhanced bioactivity and antibacterial properties. *Journal of Materials Science: Materials in Medicine*, 24(2): 437-445, **2013**.

[25] Y. Xie, Y. He, P.L. Irwin, T. Jin, and X. Shi. Antibacterial activity and mechanism of action of zinc oxide nanoparticles against *Campylobacter jejuni*. *Applied and Environmental Microbiology*, 77(7): 2325-2331, **2011**.

[26] F. Yang, W.-J. Dong, F.-M. He, X.-X. Wang, S.-F. Zhao, and G.-L. Yang. Osteoblast response to porous titanium surfaces coated with zinc-substituted hydroxyapatite. *Oral Surgery, Oral Medicine, Oral Pathology and Oral Radiology*, 113(3): 313-318, **2012**.

[27] D.V. Shepherd, K. Kauppinen, R.A. Brooks, and S.M. Best. An *in vitro* study into the effect of zinc substituted hydroxyapatite on osteoclast number and activity. *Journal of Biomedical Materials Research Part A*, 102(11): 4136-4141, **2014**.

[28] J.I. Rosales-Leal, M.A. Rodríguez-Valverde, G. Mazzaglia, P.J. Ramón-Torregrosa, L. Díaz-Rodríguez, O. García-Martínez, M. Vallecillo-Capilla, C. Ruiz, and M.A. Cabrerizo-Vílchez. Effect of roughness, wettability and morphology of engineered titanium surfaces on osteoblast-like cell adhesion. *Colloids and Surfaces A: Physicochemical and Engineering Aspects*, 365(1–3): 222-229, **2010**.

[29] Y.-T. Sul, C. Johansson, A. Wennerberg, L.-R. Cho, B.-S. Chang, and T. Albrektsson. Optimum surface properties of oxidized implants for reinforcement of osseointegration: surface chemistry, oxide thickness, porosity, roughness, and crystal structure. *The International Journal of Oral & Maxillofacial Implants*, 20(3): 349-359, **2005**.

[30] L. Le Guéhennec, A. Soueidan, P. Layrolle, and Y. Amouriq. Surface treatments of titanium dental implants for rapid osseointegration. *Dental Materials*, 23(7): 844-854, **2007**.

[31] C.N. Elias, Y. Oshida, J.H.C. Lima, and C.A. Muller. Relationship between surface properties (roughness, wettability and morphology) of titanium and dental implant removal torque. *Journal of the Mechanical Behavior of Biomedical Materials*, 1(3): 234-242, **2008**.

[32] H. Ishizawa and M. Ogino. Hydrothermal precipitation of hydroxyapatite on anodic titanium oxide films containing Ca and P. *Journal of Materials Science*, 34(23): 5893-5898, **1999**.

[33] H.P. Felgueiras, L. Castanheira, S. Changotade, F. Poirier, S. Oughlis, M. Henriques, C. Chakar, N. Naaman, R. Younes, V. Migonney, J.P. Celis, P. Ponthiaux, L.A. Rocha, and D. Lutomski. Biotribocorrosion (tribo-electrochemical) characterization of anodized titanium biomaterial containing calcium and phosphorus before and after osteoblastic cell culture. *Journal of Biomedical Materials Research Part B: Applied Biomaterials*, doi:10.1002/jbm.b.33236: **2014**.

[34] A. dos Santos, J. Araujo, S. Landi, A. Kuznetsov, J. Granjeiro, L. de Sena, and C. Achete. A study of the physical, chemical and biological properties of TiO_2 coatings produced by micro-arc oxidation in a Ca–P-based electrolyte. *Journal of Materials Science: Materials in Medicine*, 25(7): 1769-1780, **2014**.

[35] R. Drevet, A. Viteaux, J.C. Maurin, and H. Benhayoune. Human osteoblast-like cells response to pulsed electrodeposited calcium phosphate coatings. *RSC Advances*, 3(28): 11148-11154, **2013**.

[36] R.A. Surmenev, M.A. Surmeneva, and A.A. Ivanova. Significance of calcium phosphate coatings for the enhancement of new bone osteogenesis: A review. *Acta Biomaterialia*, 10(2): 557-579, **2014**.

[37] H. Ishizawa and M. Ogino. Formation and characterization of anodic titanium oxide films containing Ca and P. *Journal of Biomedical Materials Research*, 29(1): 65-72, **1995**.

[38] M. Bohner and J. Lemaitre. Can bioactivity be tested *in vitro* with SBF solution? *Biomaterials*, 30(12): 2175-2179, **2009**.

[39] F.G. Oliveira, A.R. Ribeiro, G. Perez, B.S. Archanjo, C.P. Gouvea, J.R. Araújo, A.P.C. Campos, A. Kuznetsov, C.M. Almeida, M.M. Maru, C.A. Achete, P. Ponthiaux, J.-P. Celis, and L.A. Rocha. Understanding growth mechanisms and tribocorrosion behaviour of porous TiO_2 anodic films containing calcium, phosphorous and magnesium. *Applied Surface Science*, 341: 1-12, **2015**.

[40] F.H. Dulin and D.E. Rase. Phase equilibria in the system ZnO-TiO_2. *Journal of the American Ceramic Society*, 43(3): 125-131, **1960**.

[41] J. Yang and J.H. Swisher. The phase stability of $Zn_2Ti_3O_8$. *Materials Characterization*, 37(2–3): 153-159, **1996**.

[42] W. Sun, V. Ageh, H. Mohseni, T.W. Scharf, and J. Du. Experimental and computational studies on stacking faults in zinc titanate. *Applied Physics Letters*, 104(24): 241903, **2014**.

[43] V. Ageh, H. Mohseni, and T.W. Scharf. Processing–structure–tribological property interrelationships of zinc titanate coatings grown by atomic layer deposition. *Surface and Coatings Technology*, 241: 112-117, **2014**.

[44] H. Hu, W. Zhang, Y. Qiao, X. Jiang, X. Liu, and C. Ding. Antibacterial activity and increased bone marrow stem cell functions of Zn-incorporated TiO_2 coatings on titanium. *Acta Biomaterialia*, 8(2): 904-915, **2012**.

Biofunctionalization of titanium surfaces for dental implants

Chapter 7

General Discussion and Conclusions

Chapter 7. General discussion and Conclusions

The main objectives of this work were to develop and characterize bio-multifunctional titanium oxide surfaces for application in dental implants. For this purpose, the knowledge about the real problems affecting dental implants *in vivo*, is of extreme importance to understand what properties need to be improved and how it can be done, in order to achieve an optimized behavior of the implant material.

The current meaning of the word Biomaterial involves a joint approach between biocompatibility and biofunctionality, therefore it cannot be defined without considering the material-host interactions (safety, absence of toxicity, corrosion resistance) and the ability to provide a positive functional response in the given application [1, 2].

From the scientific and engineering point of view, the options for the modification of biomaterials are only bounded by the human imagination and the scientific/technological advances. As of now, it is possible to tailor implant topographical features at nanoscale and to incorporate any existing chemical element which can bring some mechanical or biological benefit to the implant performance. It is also possible to identify the smallest biomolecules involved in biological processes and incorporate them into the surface of a biomaterial as well as the creation of drug delivery systems for sustained release of medicines in the so called smart biomaterials. Also, further steps are being constantly taken with the recent advent of tissue engineering and regenerative medicine approaches.

The possibilities for functionalizing biomaterials are almost unlimited. However the translation to the market represents in some cases a problem. As more complex gets the final product, more regulatory challenges will be presented for its admission in clinical use. The high cost of state-of-the-art technologies is also a drawback for implementation of highly advanced processes in industrial environment. More expensive precursor materials and processing technologies do not motivate investment as easily as simple and straightforward approaches that can bring immediate results [3].

This work used a simple, fast and inexpensive solution, already commercially used by some dental companies, with excellent results. This fact is surely an advantage that can allow an easier integration of these products in future clinical use. The process variations included along this work, besides not representing a significant increase in the production cost, were able to improve key properties of the implant surfaces.

In a more academic perspective, this work allowed a better fundamental understanding of the surface modification mechanisms and as well provided valuable information about the factors governing biological and tribocorrosion behavior.

1. Discussion

1.1. Rationale for the work progress

The use of Micro-Arc Oxidation (MAO) in titanium surfaces for biomedical applications was a trend started by Ishizawa and Ogino [4] in the mid 90's. At that time, the basic mechanisms for film formation were already described [5] as a series of powerful spark discharges across the oxide generating high local temperatures responsible for the creation of the porous structure, incorporation of chemical species (Ca and P) from the electrolyte and formation of crystalline phases.

The incorporation of calcium and phosphorous is commonly accepted to increase bioactivity and biological processes of osteoblastic cells [6, 7]. Also the roughness and porosity of the oxide layer can provide suitable biomechanical fixation with the bone [8, 9]. In the same process, the formation of a thick oxide is known to effectively protect the material from corrosion [10]. In addition to these advantages the tribocorrosion behavior of the surfaces was found to be greatly improved, when compared to the untreated titanium (see chapter 3). The better tribological properties were correlated with the formation of higher amounts of crystalline rutile, which is harder and more resistant than anatase or amorphous TiO_2 phases due to its compact structure and close packed unit cell with lower unit parameters [11]. The mechanism for preferential formation of rutile was addressed later in chapter 5, and meanwhile the prosecution of the work was done using the tribocorrosion resistance as the selection parameter. Samples with the best tribocorrosion performance were used for the characterization of biological behavior (chapter 4) and for the introduction of additional process variables in the MAO process (chapter 5).

The follow-up of the work consisted in the incorporation of magnesium into the oxide film structure. Magnesium (Mg) is an important trace element in bone and reported to promote osteoconductivity *in vitro* [12]. Mg was also briefly referred to cause antibacterial activity through a pH changing mechanism based on its high degradation rates in physiological environment [13]. The incorporation of Mg by cationic substitution in CaP-containing structures (e.g. hydroxyapatite) is known to cause lattice distortions and therefore an increased solubility and degradability of the

material [14]. This way, the rationale for use of Mg was the possibility of incorporating a bioactive element that could originate similar antibacterial properties as found by Robinson et al. [13]. The incorporation of Mg was successfully achieved by addition of several different amounts of magnesium acetate in the MAO electrolyte. Preliminary antibacterial tests were performed, but did not reveal any antimicrobial effect on *Staphylococcus aureus*. Anyhow, the Mg addition did cause an increased formation of rutile phase in the oxide film. As previously assumed, the increase of rutile could be a positive factor for the tribocorrosion resistance of the surfaces. This assumption was confirmed by new tribocorrosion experiments, and the promising performance of these newly developed surfaces led to an increased interest about its properties. A detailed characterization of the oxides topographical, chemical and structural properties was performed before and after the tribocorrosion tests, allowing the suggestion of mechanisms for oxide formation and tribocorrosion degradation.

Again, tribocorrosion performance was the selecting parameter for the continuation of the work. This time, antibacterial activity was pursued by the addition of Zn species. The antibacterial properties of Zn-based materials were previously reported by some authors [15-17]. Zinc, being also a trace metal element found in bone composition, was not anticipated to cause harmful results on the osteogenic properties of the surfaces. Furthermore, Zn was reported to positively influence adhesion, proliferation and differentiation of osteoblasts [18, 19] and decrease osteoclast resorptive activity [20].

The first approach for Zn incorporation was spin coating technique, in which a Zn-based sol gel solution was poured into a high speed rotating MAO treated sample. The synthesis procedure for the solution was based in a work from Catto et al. [21] and then some variations of process parameters included different solution viscosities, rotation speeds and processing times. The final purpose was the formation of small gelified clusters of Zn-based material, without changing the previous fundamental surface topographic features. Through microscopic observations of the resulting spin-coated surfaces, it was concluded that the process did not fulfill the previously stated requisites. Depending on the processing parameters, some samples presented significant changes to the pre-existing topographical features, with the formation of thick and uniform layers of zinc oxide. As seen in chapter 4 the surface characteristics of the oxide surface are crucial to the adhesion of bone cells. Therefore it was assumed that the zinc oxide layer on top of the porous titanium oxide film would be disadvantageous for the osteoblast behavior as they could not anymore contact with the Ca-rich surface.

Along with the previous approach the development of an adapted MAO process allowed the employment of sonochemistry technique to disperse ZnO nanoparticles in the test electrolyte, which had also the advantage of being a single step process, instead of a dual step (MAO + spincoat) method. This allowed the further incorporation of Zn species in the structure of the oxide and was the main focus of the work presented in chapter 6.

The most important surfaces produced throughout this work were tested for an integrated approach combining the characterization of surfaces performance, considering all the main problems encountered in dental implant applications.

1.2. Surface modification and mechanisms of film formation

One of the main outcomes of this work is the fundamental understanding of the mechanisms governing the formation and the final structure of anodic oxide films under MAO conditions. Several authors had already approached this subject, and had identified the basic processes leading to the formation of porous titanium oxide structures [5, 22, 23]. For the processing parameters used in this work, one can also understand the chemical incorporation of electrolyte species, as well as the controlled formation of amorphous and crystalline anatase and rutile phases in different zones of the oxide.

The evolution of this work relied on different MAO processing conditions which were mostly based on variations of the electrolyte composition. Addition of ionic species to the electrolyte can increase its conductivity and favor the electrochemical processes taking place during the growth of the oxide film. As stated in both chapters 3 and 5, the increase in the amount of dissolved ionic species promoted the formation of rutile. This relation was supported by the analysis of current vs time plots recorded during the MAO treatments. A representative shape of the curves can be observed in figure 5.12, where the introduction of parameter "$t_{gal/pot}$" allowed a better understanding of the process in different electrolytes. More conductive solutions were more dependent on galvanostatic control of the process, meaning that higher currents were allowed for more time. This increased the overall electrochemical reaction rates, including the rate of film formation and the sparking discharge phenomena throughout the surface. Furthermore, and according to Wang et al. [24] the permanence of higher current densities for longer processing times leads to more noticeable rutile formation.

The sparking discharges across the film are the key phenomena for understanding the growth mechanisms and final properties of the oxides. When highly energetic micro-arcs are

generated above breakdown potential of the oxide, there is a huge increase in temperature in small regions around the spark, causing the formation of a plasma region that incorporates chemical components from the electrolyte. Instantaneously, in contact with the electrolyte, occurs a gradual solidification of the melted material: slower in the interior regions of the film and gradually faster at the newly-formed oxide-electrolyte interface. This gives rise to a nanocomposite gradient structure consisting of amorphous and crystalline titanium oxide. For more conductive electrolytes, is verified an increase in sparking phenomena. Some of these sparks are highly energetic, which can raise even more the local temperature and incorporate more material in the plasma region, therefore creating larger pores where rutile phase will preferentially appear.

The addition of ZnO NP's and its sonochemical dispersion procedure, introduced new factors in the electrolyte properties. Conductivity became dependent on other properties such as the zeta potential, particle volume fraction and the properties of the interfacial double layer, which were not studied in detail. This way, the MAO process with solid particles in suspension in the electrolyte could not be fully understood. Changes in the crystalline structure, namely the increase in rutile content could also be induced by the increased electrolyte temperature after the sonochemical dispersion process. Despite some reports on the stability of ZnO-TiO_2 system at high temperatures [25], which highlight the formation of zinc titanates and rutile, and could explain the good tribocorrosion behavior of the zinc-containing surfaces; the structural properties and behavior of these samples is explained, based only on hypothesis from related literature.

1.3. Tribocorrosion behavior

One of the main focuses of this work was the creation of tribocorrosion resistant surfaces. The surface engineering performed on titanium samples resulted in a very much improved behavior from the point of view of both corrosion and tribocorrosion.

In comparison with untreated titanium, the mere existence of a protective oxide represents a great upgrade in terms of surface protection. Natural passive oxides in titanium are instantaneously worn out by mechanical solicitations, while even the simplest surface modification presented in this work granted a significant minimization of damaging electrochemical and mechanical aspects.

The dual layer properties of the oxides, with an inner and more compact layer and an outer layer, thicker and with a high level of porosity, combined for an excellent tribocorrosion resistance. The compact inner layer is capable of providing efficient corrosion protection. As for

the outer porous layer, its rough and porous configuration can somehow prevent the occurrence of an abrasive mechanism, as the particles released from the contact in the higher zones of the structure are accumulated in the recesses of the rough topography, or even inside the porous structure.

In most of the tribocorrosion conditions tested in this work, the wear mechanism of MAO treated samples was based in a progressive removal of the higher asperities of the rough oxide. This behavior was dictated by the structural arrangement of the nanocomposite layer with a top amorphous zone followed by a more resistant rutile-rich region that decelerated the material removal. Furthermore, it was reported that the inner region of the nanocomposite layer composed by a mixture of amorphous and crystalline titanium oxide, contributed for the absorption of mechanical stresses and the prevention of brittle fractures associated with harder phases.

In general, the presence of rutile was linked with an improved performance of the surfaces. This relation was linear for lower applied loads used in the tests presented on chapters 3 and 5, where higher relative contents of rutile minimized the amount of surface degradation. However, the application of higher mechanical loads, brought to evidence the brittle nature of rutile rich materials.

In chapter 6, rutile rich coatings that presented a successful behavior in previous tests, showed the worst tribocorrosion behavior among MAO treated samples, due to the increase of normal load and fracture of the oxide. The possibility of this behavior was already mentioned in chapter 5, based on the presence of cracks in the porous oxide that were originated during the processing of the sample. The fracture behavior of the films was found to be similar to the one already presented in the work of Alves et al. [26] and moreover can be associated to the dual layer structure of the oxide described in chapter 3, based on the two distinct fracture zones visible in the wear track observations.

Based on this behavior of the Mg group of samples, the Zn-containing surfaces which presented the most amount of rutile, were expected to present similar fragile properties under the same applied loads. However, the combination of high rutile content and a possible lubricant effect arising from the presence of zinc titanate compounds promoted again a good performance of the materials under tribocorrosion.

1.4. Biological behavior

The primary positive biological outcome of the MAO process is the rough and porous structure that is created. The osteogenic properties of these kind of surfaces are widely reported [27-30] and were confirmed in the biological experiments presented in this work. When compared to etched titanium, the rough and porous characteristics of the oxides are responsible for a wider spreading of the cells and the formation of cytoplasmatic extensions that are seeking the open porosity to promote better adhesion to the substrate in the first moments of contact. At later stages of contact, the surfaces were to a great extent covered by a uniform layer of cells, ensuring good bonding between cells and material.

Osteoblastic interactions with the oxide surface were also correlated with the nanometric amorphous layer at the top region of the oxide. As seen in chapter 4, the amorphous zones of the oxide, are also the preferential sites for the incorporation of bioactive elements from the electrolyte. Previous literature [31-34] had already defined the presence of Ca as an important reason to obtain improved cell functions. The MAO treatment developed in this work created a calcium-rich amorphous layer at the top of the oxide structure which osteoblastic cells will directly contact upon being seeded in the surface. This was assumed to promote a better adhesion and proliferation behavior of the cells, as well as an improved segregation of cytokines associated with the regulation of inflammatory processes and several cell functions.

The incorporation of Zn species in the coating revealed to be a factor for enhanced osteoblast proliferation, which led to an increased cell-covered area of the Zn-containing surfaces. Some authors reported already this behavior and attributed it to the release of Zn ions to the environment, which can up-regulate the protein and gene expression of bone cells [17].

As for antimicrobial behavior, the contribution of the surface topography was more determinant than the chemical composition. The number of microorganisms released from the surfaces after the test was much superior for all MAO treated samples, when compared to the etched titanium surfaces. The possibility of bacteria to penetrate the porous structure or be deposited in the lower regions of the oxide can create propitious microenvironments for the development of biofilm structures. Topographic features around a critical size, near the diameter of bacteria are reported to cause the entrapment of microbial organisms in the surface [35].

Nevertheless, the minimization of bacterial adhesion was achieved when Zn species were incorporated in the oxides, revealing an antibacterial behavior that can be based on some

previous mechanisms found in the literature [15-17]. Zn^{2+} cation is thought to inhibit the intracellular uptake of Mn^{2+} and increase the susceptibility to oxidative killing of bacteria [15].

2. Final considerations

This work focused in the production of titanium oxide surfaces by Micro-arc oxidation. The topographic, chemical and structural properties of the developed materials were studied and contributed for an improved tribocorrosion, osteogenic and antimicrobial performance, as follows:

- Formation of a graded nanocomposite layer with the preferential formation of rutile near the higher zones of the oxide reduces the tribocorrosion degradation;
- When the brittle characteristics of the rutile rich materials arise under higher applied loads, the introduction of Zn species and the possible formation of zinc titanates are responsible for a lubricant effect and minimization of wear;
- Introduction of bioactive elements, namely calcium in the structure of the oxide and the development of an amorphous nanometric layer at the oxide surface promotes cellular functions of adhesion, proliferation and cytokine expression;
- The introduction of zinc species in the coatings promotes a bio-selective behavior with enhanced proliferation of bone cells and a tendency for decreased bacterial adhesion among the MAO treated groups;

References

[1] D.F. Williams. There is no such thing as a biocompatible material. *Biomaterials*, 35(38): 10009-10014, **2014**.

[2] W.M. Reichert, B.D. Ratner, J. Anderson, A. Coury, A.S. Hoffman, C.T. Laurencin, and D. Tirrell. 2010 Panel on the Biomaterials Grand Challenges. *Journal of Biomedical Materials Research Part A*, 96A(2): 275-287, **2011**.

[3] A. Ratcliffe. Difficulties in the translation of functionalized biomaterials into regenerative medicine clinical products. *Biomaterials*, 32(18): 4215-4217, **2011**.

[4] H. Ishizawa and M. Ogino. Formation and characterization of anodic titanium oxide films containing Ca and P. *Journal of Biomedical Materials Research*, 29(1): 65-72, **1995**.

[5] H. Ishizawa and M. Ogino. Thin hydroxyapatite layers formed on porous titanium using electrochemical and hydrothermal reaction. *Journal of Materials Science*, 31(23): 6279-6284, **1996**.

[6] P. Schlegel, J.S. Hayes, V.M. Frauchiger, B. Gasser, R. Wieling, M. Textor, and R.G. Richards. An *in vivo* evaluation of the biocompatibility of anodic plasma chemical (APC) treatment of titanium with calcium phosphate. *Journal of Biomedical Materials Research Part B: Applied Biomaterials*, 90B(1): 26-34, **2009**.

[7] J.M. Lee, J.I. Lee, and Y.J. Lim. *In vitro* investigation of anodization and CaP deposited titanium surface using MG63 osteoblast-like cells. *Applied Surface Science*, 256(10): 3086-3092, **2010**.

[8] A. Wennerberg and T. Albrektsson. On implant surfaces: A review of current knowledge and opinions. *The International Journal of Oral and Maxillofacial Implants*, 25(1): 63-74, **2010**.

[9] L. Le Guéhennec, A. Soueidan, P. Layrolle, and Y. Amouriq. Surface treatments of titanium dental implants for rapid osseointegration. *Dental Materials*, 23(7): 844-854, **2007**.

[10] A. Cigada, M. Cabrini, and P. Pedeferri. Increasing of the corrosion resistance of the Ti6Al4V alloy by high thickness anodic oxidation. *Journal of Materials Science: Materials in Medicine*, 3(6): 408-412, **1992**.

[11] I. Gheewala, R. Smith, and S.D. Kenny. Nanoindentation and nanoscratching of rutile and anatase TiO_2 studied using molecular dynamics simulations. *Journal of Physics: Condensed Matter*, 20(35): 354010, **2008**.

[12] E. Landi, G. Logroscino, L. Proietti, A. Tampieri, M. Sandri, and S. Sprio. Biomimetic Mg-substituted hydroxyapatite: From synthesis to *in vivo* behaviour. *Journal of Materials Science: Materials in Medicine*, 19(1): 239-247, **2008**.

[13] D.A. Robinson, R.W. Griffith, D. Shechtman, R.B. Evans, and M.G. Conzemius. *In vitro* antibacterial properties of magnesium metal against *Escherichia coli, Pseudomonas aeruginosa* and *Staphylococcus aureus*. *Acta Biomaterialia*, 6(5): 1869-1877, **2010**.

[14] D. Laurencin, N. Almora-Barrios, N.H. de Leeuw, C. Gervais, C. Bonhomme, F. Mauri, W. Chrzanowski, J.C. Knowles, R.J. Newport, A. Wong, Z. Gan, and M.E. Smith. Magnesium incorporation into hydroxyapatite. *Biomaterials*, 32(7): 1826-1837, **2011**.

[15] C.A. McDevitt, A.D. Ogunniyi, E. Valkov, M.C. Lawrence, B. Kobe, A.G. McEwan, and J.C. Paton. A molecular mechanism for bacterial susceptibility to zinc. *PLoS Pathogens*, 7(11): e1002357, **2011**.

[16] E.S. Thian, T. Konishi, Y. Kawanobe, P.N. Lim, C. Choong, B. Ho, and M. Aizawa. Zinc-substituted hydroxyapatite: a biomaterial with enhanced bioactivity and antibacterial properties. *Journal of Materials Science: Materials in Medicine*, 24(2): 437-445, **2013**.

[17] H. Hu, W. Zhang, Y. Qiao, X. Jiang, X. Liu, and C. Ding. Antibacterial activity and increased bone marrow stem cell functions of Zn-incorporated TiO_2 coatings on titanium. *Acta Biomaterialia*, 8(2): 904-915, **2012**.

[18] F. Yang, W.-J. Dong, F.-M. He, X.-X. Wang, S.-F. Zhao, and G.-L. Yang. Osteoblast response to porous titanium surfaces coated with zinc-substituted hydroxyapatite. *Oral Surgery, Oral Medicine, Oral Pathology and Oral Radiology*, 113(3): 313-318, **2012**.

[19] K. Huo, X. Zhang, H. Wang, L. Zhao, X. Liu, and P.K. Chu. Osteogenic activity and antibacterial effects on titanium surfaces modified with Zn-incorporated nanotube arrays. *Biomaterials*, 34(13): 3467-3478, **2013**.

[20] D.V. Shepherd, K. Kauppinen, R.A. Brooks, and S.M. Best. An *in vitro* study into the effect of zinc substituted hydroxyapatite on osteoclast number and activity. *Journal of Biomedical Materials Research Part A*, 102(11): 4136-4141, **2014**.

[21] A.C. Catto, L.F. da Silva, M.B. Bernardi, M.S. Li, E. Longo, P.N. Lisboa-Filho, O.R. Nascimento, and V.R. Mastelaro. An investigation into the influence of zinc precursor on the microstructural, photoluminescence, and gas-sensing properties of ZnO nanoparticles. *Journal of Nanoparticle Research*, 16(12): 1-9, **2014**.

[22] A.L. Yerokhin, X. Nie, A. Leyland, A. Matthews, and S.J. Dowey. Plasma electrolysis for surface engineering. *Surface and Coatings Technology*, 122(2–3): 73-93, **1999**.

[23] S. Ikonopisov. Theory of electrical breakdown during formation of barrier anodic films. *Electrochimica Acta*, 22(10): 1077-1082, **1977**.

[24] Y. Wang, T. Lei, B. Jiang, and L. Guo. Growth, microstructure and mechanical properties of microarc oxidation coatings on titanium alloy in phosphate-containing solution. *Applied Surface Science*, 233(1–4): 258-267, **2004**.

[25] F.H. Dulin and D.E. Rase. Phase equilibria in the system ZnO-TiO_2. *Journal of the American Ceramic Society*, 43(3): 125-131, **1960**.

[26] S.A. Alves, R. Bayón, A. Igartua, V. Saénz de Viteri, and L.A. Rocha. Tribocorrosion behaviour of anodic titanium oxide films produced by plasma electrolytic oxidation for dental implants. *Lubrication Science*, 26(7-8): 500-513, **2014**.

[27] C.N. Elias, Y. Oshida, J.H.C. Lima, and C.A. Muller. Relationship between surface properties (roughness, wettability and morphology) of titanium and dental implant removal torque. *Journal of the Mechanical Behavior of Biomedical Materials*, 1(3): 234-242, **2008**.

[28] Y.T. Sul, C. Johansson, A. Wennerberg, L.R. Cho, B.S. Chang, and T. Albrektsson. Optimum surface properties of oxidized implants for reinforcement of osseointegration: surface chemistry, oxide thickness, porosity, roughness, and crystal structure. *The International Journal of Oral and Maxillofacial Implants*, 20(3): 349-359, **2005**.

[29] L.-H. Li, Y.-M. Kong, H.-W. Kim, Y.-W. Kim, H.-E. Kim, S.-J. Heo, and J.-Y. Koak. Improved biological performance of Ti implants due to surface modification by micro-arc oxidation. *Biomaterials*, 25(14): 2867-2875, **2004**.

[30] N.C.M. Oliveira, C.C.G. Moura, D. Zanetta-Barbosa, D.B.S. Mendonça, L. Cooper, G. Mendonça, and P. Dechichi. Effects of titanium surface anodization with CaP incorporation on human osteoblastic response. *Materials Science and Engineering: C*, 33(4): 1958-1962, **2013**.

[31] A.M.C. Barradas, H.A.M. Fernandes, N. Groen, Y.C. Chai, J. Schrooten, J. van de Peppel, J.P.T.M. van Leeuwen, C.A. van Blitterswijk, and J. de Boer. A calcium-induced signaling cascade leading to osteogenic differentiation of human bone marrow-derived mesenchymal stromal cells. *Biomaterials*, 33(11): 3205-3215, **2012**.

[32] R.A. Surmenev, M.A. Surmeneva, and A.A. Ivanova. Significance of calcium phosphate coatings for the enhancement of new bone osteogenesis: A review. *Acta Biomaterialia*, 10(2): 557-579, **2014**.

[33] D.E. Clapham. Calcium Signaling. *Cell*, 131(6): 1047-1058, **2007**.

[34] B. Nagar, M. Overduin, M. Ikura, and J.M. Rini. Structural basis of calcium-induced E-cadherin rigidification and dimerization. *Nature*, 380(6572): 360-364, **1996**.

[35] S.H. Flint, J.D. Brooks, and P.J. Bremer. Properties of the stainless steel substrate, influencing the adhesion of thermo-resistant streptococci. *Journal of Food Engineering*, 43(4): 235-242, **2000**.

Biofunctionalization of titanium surfaces for dental implants

Chapter 8

Future Work

Chapter 8. Future Work

In first place, the continuation of this work should focus on some less understood topics such as the characterization of Zn-containing samples. The electrolyte consisting in the colloidal dispersion of ZnO nanoparticles should be further characterized (zeta potential, size dispersion, agglomeration) to be possible to fully understand the processes taking place during the MAO treatment. Also the identification and distribution of Zn compounds across the film may allow for the more accurate definition of tribocorrosion mechanisms. Cross sectional studies by Focused Ion Beam and Transmission Electron Microscopy, and chemical analysis by X-ray Photoelectron Spectroscopy analysis would be of valuable assistance.

Biological behavior of Mg and Zn groups should be further studied, namely in what concerns the cytoskeleton organization and gene and cytokine expression for cell signaling as it was performed in chapter 4 for CaP samples. Detailed microscopic analysis on the biointerface between titanium oxide and osteoblast should be performed for assessing a possible effect of Zn in the adhesion of cells.

The possibility of carrying antibacterial tests in a more qualitative way, using microscopy or fluorescence-based techniques could help considering the interactions between microorganisms and the porous structure of the oxides.

Although not presented in this thesis, biopolymer and peptide functionalization was preliminary addressed during this work, for the further biofunctionalization of MAO treated surfaces with amine terminated polyethylene glycol and RGD peptides. The combination between excellent biological properties of PEG-RGD surfaces and tribocorrosion resistance shown by MAO treatments could be an added value for implant applications. Further tests should be performed to find the optimal conditions for electrodeposition and characterization of biopolymer-coated oxides.

The application of the surface treatments presented in this work could also be of use for the wide range of titanium alloys that are currently being developed.

Finally, the application of the methodology presented in this work for the anodic treatment of titanium surfaces will soon be put into practice using implant shaped titanium materials for *in vivo* tests in rabbits.